



**Scalable production of tissue engineered
microunits for bone regeneration using
bioactive glass microspheres and dynamic
culture conditions**

A thesis submitted to University College London in accordance with the
requirements for the degree of

Doctor of Engineering (EngD)

by

David Roshan De Silva Thompson MEng, MRes

September 2017

Department of Biochemical Engineering

University College London

Declaration of Authorship and Originality

I, David Roshan De Silva-Thompson confirm that the work presented in this thesis is my own. Where information has been derived from other sources, I confirm that this has been indicated in the thesis.

Signature

Date

15 September 2017

Acknowledgements

I would like to acknowledge all those who have assisted me in reaching this moment. The list of people who have helped me on my Doctorate journey is extensive; however, I will try my utmost to acknowledge those who have made this research possible.

First and foremost, I would like to thank my supervisor Ivan Wall for his advice, guidance, and mentorship during this project. I am grateful for the confidence you had in me and how patient you were, ensuring I remained motivated throughout. I would also like to thank my secondary supervisor Martina Micheletti for providing feedback which helped shape the direction of my research.

Sincere thanks go to Jonathan Knowles, Nilay Lakhkar and Nicola Mordan of UCL Eastman Dental Institute, for helping me learn techniques that became crucial in carrying out my research.

I would like to offer many thanks to my 'Laboratory Wife', Carlotta Peticone, who helped me grow as a researcher and for being a great lab partner. Together we have attended conferences, explored Korea, and become very good friends. Your contribution to my success is invaluable and I thank you for all the help you have provided me.

From the Department of Biochemical Engineering I would like to thank the Regenerative Medicine Laboratory Members who have been wonderful to work with. However, I would like to specifically thank Rana Khalife, who not only provided a rich supply of treats, but was always willing to impart her vast knowledge to help myself and others. Also, a big thanks to my friends Ana, Ivano, Joana, Gerry, Fatumina, Fair, Melanie, Rachael, and Mo. I am also thankful for the support from Ludmila Ruban and for her guidance with my cell culture techniques.

I would like to thank my friends for their support and encouragement. I am especially thankful to Joana Santos for being a loving and supportive girlfriend, who helped me during stressful times and always had faith in my ability.

Finally, but most importantly, I would like to thank my mother, without whom none of this would have been possible. You have been the foundation to my success throughout my life, always making sacrifices and putting me first, therefore I dedicate this thesis to you. I hope I have made you proud.

Abstract

Bone is one of the most common tissues to be transplanted, with over 2.2 million grafting procedures performed worldwide every year (Van der Stok et al., 2011). Autologous bone grafts, while considered the current gold standard, have inherent risks including limited donor tissue availability, donor site morbidity, surgical complications, and pain of procedure. Alternative approaches to treating bone tissue defects are required based on clinically effective bone graft substitutes that can be manufactured at a commercially relevant scale. Tissue engineering is an alternative strategy that uses biocompatible scaffolds in combination with cells as a bioactive implant to induce bone repair. In this thesis, microspherical bioactive glasses have been studied as a platform for scalable bone tissue engineering that has flexibility to address diverse geometric requirements with the aim of becoming a commercially available tool. Specifically, titanium-doped phosphate glass microspheres have been studied for their ability to support bone progenitor cells. Here, the microspheres (5 and 7 mol% TiO₂) were assessed in their ability to support proliferation of osteoblast-like cell (MG63) and proliferation and osteogenic differentiation of human bone-marrow derived mesenchymal stem cells (hBM-MSCs) under static and dynamic agitation culture. Scalability was assessed using scalable dimensionless Froude number to scale microwell plate cultures to 125ml Erlenmeyer flask cultures using Froude as a tool to map mixing systems at both scales. MG63 and hBM-MSC proliferation was observed on the microspheres under all conditions studied as well as extracellular matrix protein secretion, confirming the biocompatibility of the materials tested. Similar growth kinetics was observed at both scales, where moderate agitation stimulated cell proliferation, but higher agitation was damaging to cells. Upregulation of key bone expression markers (COL1A1 and SPP1) was observed also at moderate orbital agitations, while on at high agitation rates this was largely absent, except for upregulation of SPP1 on the control microsphere, Synthemax. Furthermore, biomaterial resorption was observed upon differentiating mouse-derived monocytes into osteoclasts on the titanium-phosphate glass discs. In conclusion, large-scale culture using titanium-doped phosphate glass microspheres was achieved with hBM-MSCs, with the substrate effectively supporting cell proliferation and osteogenic differentiation. This research provides a stepping stone in understanding how biomaterials processed

into microcarrier format can be utilised in a commercial environment to create clinically relevant quantities of tissue engineering bone.

Impact Statement

A Regenerative Medicine research programme carried out at the Department of Biochemical Engineering UCL has studied the potential application of bioactive phosphate glass material. There is a critical necessity for scalable and controllable technologies to manufacture bone consistently. This thesis tackles some fundamental questions by assessing whether the biomaterial processed into microspheres supports production of tissue engineered bone microunits amenable to scalable culture in bioreactors. Furthermore, the research programme has employed and validated the use of scalable mixing models to achieve effective scale up from microwell cultures to 125ml Erlenmeyer vessels. Implantable materials currently exist, however their application in large scale manufacturing has not been fully considered. This thesis has explored large scale culture techniques and the limitations when using dense biomaterials for creating tissue engineering constructs of bone. The outcomes from this thesis will allow research groups and industry to subsequently develop modified bioactive microspheres that have improved buoyancy for commercial production, using this data in addition to the existing models developed for orbital shaker culture.

Large scale culture of biomaterials commonly encounters heterogenous conditions during cell culture; however, the work carried out in this thesis provides the initial steps into establishing a standardized protocol for expanding and differentiating bone marrow-derived mesenchymal stem cells into bone tissue. This thesis has laid the foundations for further research exploring bioreactor design and culture optimization. Furthermore, the scope of this project has allowed mathematical models developed by other research groups to be applied practically, providing the foundation for future work to consider bioactive microspheres that have improved physical properties.

The outputs from this thesis have been presented in international conferences and are in the process of being disseminated through publications in journals in the areas of biomaterials and biotechnology. Having gained a better understanding of the translation of cell therapies using biomaterials, coupled with the cross-disciplinary of the project, there is opportunity for collaboration with

academics in other fields and institutions, across the broad areas of science, engineering, and medicine.

List of contents

Declaration of Authorship and Originality	2
Acknowledgements	3
Abstract	5
Impact Statement	7
List of contents	9
List of Figures	15
List of Tables	28
List of Abbreviations	29
Chapter 1 . Introduction and review of the literature	31
1.1 Introduction	31
1.2 Research Motivation	33
1.3 Organisation of review	34
1.4 Bone	34
1.4.1 Constituents of bone	34
1.4.2 Bone remodelling	35
1.4.3 Bone defects	37
1.5 Biomaterials and filling the gap	39
1.5.1 Biomaterial properties	39
1.5.2 Commercial bioactive glasses	40
1.5.3 Phosphate glasses and metallic oxides	42
1.5.3.1 Titanium dioxide	43
1.5.3.1.1 Material characterization	45
1.5.3.1.2 Biocompatibility of TiO ₂ doped phosphate glasses	47

1.6 Microcarriers for bone tissue engineering	49
1.7 Scale-up of microcarrier cultures for bone tissue engineering	51
1.7.1 Scaling orbitally shaken platforms	55
1.7.2 Bioprocess forces	59
Chapter 2 . Preliminary studies using human osteosarcoma cell line MG63 to determine efficacy of Ti-PGMs as a culture platform under static and dynamic conditions	64
2.1. Introduction	64
2.2 Materials & Methods	66
2.2.1 Formulation of glass	66
2.2.2 Preparation of Ti-PGMs	68
2.2.3 Preparation of MG63 cells	70
2.2.4 Cell culture on Ti-PGMs under static conditions in ultra-low attachment 96-well microplates	70
2.2.5 Cell culture on Ti-PGMs under dynamic conditions in ultra-low attachment 96-well microplates	71
2.2.6 Cell proliferation assay	73
2.2.7 Metabolite analysis	74
2.2.8 Phase contrast microscopy imaging	74
2.2.9 Confocal laser scanning microscopy imaging	75
2.2.10 Statistical analysis	75
2.3 Results	76
2.3.1 Cell proliferation of MG63 cells cultured on Ti-PGMs under static and dynamic conditions	77
2.3.2 Impact of agitation rates on MG63 cell metabolism	83
2.3.3 Macroscopic evaluation of MG63 cell-Ti-PGMs clustering	87
2.3.4 Matrix deposition by MG63 cells on Ti-PGMs	90
	10

2.4 Discussion	92
Chapter 3 . Critical functional responses of human bone marrow-derived mesenchymal stem cells and Ti-PGMs	97
3.1 Introduction	97
3.2 Materials & Methods	99
3.2.1 Preparation of human bone marrow derived mesenchymal stem cells	99
3.2.2 Cell characterization	99
3.2.2.1 Multilineage differentiation	99
3.2.2.2 Flow cytometry of hBM-MSCs	100
3.2.3 Interaction of hBM-MSCs on Ti-PGMs cultured under static and dynamic conditions	101
3.2.3.1 Cell culture on Ti-PGMs and Corning Synthemax II-SC microcarriers under static condition in ultra-low attachment 96-well microplates	101
3.2.3.2 Cell culture on Ti-PGMs and Corning Synthemax II-SC microcarriers under dynamic conditions in ultra-low attachment 96-well microplates	101
3.2.3.3 Cell proliferation assay	102
3.2.3.4 Phase contrast microscopy imaging	102
3.2.3.5 Confocal laser scanning microscopy	102
3.2.4 The effect of conditioned-media on cell/microsphere interaction	103
3.2.4.1 Cell culture using conditioned-media	103
3.2.4.2 Cell proliferation assay	104
3.2.4.3 Immunofluorescence imaging	104
3.2.5 Statistical analysis	104

3.3 Results	105
3.3.1 Characterization of human bone marrow mesenchymal stem cells	105
3.3.2 Interaction of hBM-MSCs on Ti-PGMs cultured under static and dynamic conditions	107
3.3.2.1 Cell proliferation of hBM-MSCs on Ti-PGMs under orbital agitation	107
3.3.2.2 Macroscopic evaluation of hBM-MSC – Ti-PGM clustering	115
3.3.2.3 Matrix deposition by hBM-MSCs on Ti-PGMs	118
3.3.3 The effect of an altered biophysical environment on cell/microsphere interaction	121
3.3.3.1 Cell proliferation of hBM-MSC cells cultured in conditioned media	121
3.3.3.2 Extracellular matrix protein immunofluorescent expression	122
3.4 Discussion	126

Chapter 4 . Scale-up of hBM-MSC culture in 125ml Erlenmeyer shake flasks using Ti-PGMs **133**

4.1 Introduction	133
4.2 Materials & Methods	135
4.2.1 Preparation of human bone marrow derived mesenchymal stem cells	135
4.2.2 Cell culture on Ti-PGMs and Corning® Synthemax in a 125ml Erlenmeyer flask under static and dynamic conditions	135
4.2.3 Metabolite analysis	136
4.2.4 Confocal laser scanning microscopy	137
4.2.5 Scanning electron microscopy	137
4.2.6 Quantitative polymerase chain reaction (qPCR)	138
4.2.7 Statistical analysis	139

4.3 Results	140
4.3.1 Expansion of hBM-MSC in scaled up culture vessels	140
4.3.2 Metabolite analysis	143
4.3.3 Cell interactions with Ti-PGMs and Synthemax cultured in 125ml Erlenmeyer flasks	147
4.3.4 Matrix deposition by hBM-MSCs on Ti-PGMs cultured at large scale	149
4.3.5 hBM-MSC osteogenic gene expression	158
4.4 Discussion	160

Chapter 5. Qualitative analysis of in vitro osteoclast resorption of Ti-PGMs and effect of modified surfaces on hBM-MSC behaviour **167**

5.1 Introduction	167
5.2 Materials and Method	170
5.2.1 Preparation of Ti-PGD	170
5.2.2 Isolation of mouse monocytes from mice and osteoclast differentiation	170
5.2.3 Seeding density study for monocyte cell culture on Ti-PGD	172
5.2.3.1 Tartrate-resistant acid phosphatase staining (TRAP)	172
5.2.3.2 Immunofluorescent staining	172
5.2.3.3 Scanning electron microscopy imaging (SEM)	173
5.2.4 Effect of RANKL concentration on osteoclastogenesis	173
5.2.4.1 Scanning electron microscopy imaging	173
5.2.5 hBM-MSCs culture on acid-etched Ti-PGDs	173
5.2.5.1 Scanning electron microscopy imaging	174
5.2.6 hBM-MSC culture on acid-etched Ti-PGMs	174

5.3 Results	175
5.3.1 Mouse bone marrow-derived monocyte culture and differentiation on Ti-PGDs	175
5.3.2 Effect of RANKL concentration on osteoclastogenesis	181
5.3.3 Evaluation of acid-etched Ti-PGDs to support hBM-MSc culture	182
5.3.4 Cell proliferation of hBM-MSCs on acid-etched Ti-PGMS	185
5.4 Discussion	187
Chapter 6. Summary: General conclusion and future work	192
6.1 Research objectives and conclusions	192
6.2 Future Work	197
Chapter 7. Bioprocess validation considerations of biomaterials used in cell therapy manufacturing	202
References	205
Appendix	234
A.1 Geometrical characteristics and calculated Fr_c and N_c (using minimum and maximum operating conditions) using 96-well microplates.	234
A.2 Geometrical characteristics and calculated Fr_c and N_c (using minimum and maximum operating conditions) using an 125ml Erlenmeyer flask.	234
A.3 Geometrical/Physical characteristics and calculated G_a and flowrate to achieve Ti-PGM suspension	235
A.4 Box-and-whisker plots required for bar charts presented in Chapter 3	235
A.5 List of conferences	238
A.6 List of publications	239

List of Figures

- Figure 1.1 Stages involved in bone repair cascade.** Copyrights of images owned by Benjamin Cummings (2004) Pearson Education. Inc 37
- Figure 1.2 Mixing zones in a cylindrical vessel.** The image highlights the change in height of mixing zone (Zone A) when fluid in a cylindrical vessel is subjected to increased agitation 57
- Figure 2.1 Standard curve of MG63 cell growth on tissue culture grade 96-well microplates.** Line graph plotted as Absorbance (nm) versus Number of viable cells after using a CCK-8 proliferation assay upon complete attachment of the cells for the experiments involving the following conditions: (A) Static (B) 150rpm and (C) 300rpm. Absorbance based on a wavelength of 450nm. Values represent mean \pm SD (n=6) 79
- Figure 2.2 MG63 proliferation on (A) Ti5 (B) Ti7 microspheres in ultra-low attachment culture plates and (C) TCP (control).** Bar charts comparing CCK-8 assay readings were at days 0, 1, 3, 5, 7, 9 and 13 under static and dynamic conditions. Values represent mean \pm SD (n=3). * indicates $p < 0.05$. 80
- Figure 2.3 MG63 proliferation under (A) 0rpm (B) 150rpm and (C) 300rpm conditions at days 0,1, 3, 5, 7, 9 and 13 cultured on the two TiO₂ compositions and TCP represented via a bar chart.** Error bars represents \pm SD (n=3). For representation purposes the significance between TCP and the phosphate glasses have not been indicated on the graph, however have been discussed further in the results. 82
- Figure 2.4 Comparison of different MG63 proliferation profiles under static conditions over 13 days.** Bar charts Exp 1, 2 and 3 denote three different static runs which were used as controls carried out in parallel with the dynamic studies (150rpm, 300rpm). Exp 1- Static only Exp 2- Static

control for 150rpm study and Exp-3 Static control for 300rpm study. Values represent mean \pm SD (n=3). 83

Figure 2.5 MG63 metabolic profiles for glucose consumption and lactate production based on agitation rate. Line graph represent glucose consumption (A, C, E) and lactate production (B, D, E) when cultured on Ti5 (A & B), Ti7 (C&D), and TCP (E & F) at days 0, 1, 3, 5, 7, 9 and 13 under ●- 0rpm ■- 150rpm and ▲-300rpm condition. Values represent mean \pm SD (n=3). 85

Figure 2.6 MG63 metabolic profiles for glucose consumption and lactate production based on culture material. Line graph represents glucose consumption (A, C, E) and lactate production (B, D, E) under 0rpm (A & B), 150rpm (C&D), and 300rpm (E & F) conditions at days 0, 1, 3, 5, 7, 9 and 13 when cells are culture on ●- Ti5 ■- Ti7 and ▲TCP. Values represent mean \pm SD (n=3). 86

Figure 2.7 Formation of networks between MG63 cells and Ti-PGMs under different agitation rates. Phase contrast images illustrating MG63 cultured on Ti-PGMs over a 13-day period. Images of phosphate glasses doped with 5 mol% (a-d) and 7 mol% (e-h) were taken on day 1 (a, c, e and g) and day 13 (b, d, f and h) cultured under static (a, b, e and f) and 150rpm (c, d, g and h) conditions. Images were taken under 20x magnifications where scale bars represent 200 μ m 89

Figure 2.8 Formation of Ti-PGM-cell clusters under different agitation rates. Phase contrast microscopy images of individual wells illustrating MG63 cells cultured on Ti5 over a 13-day period using the same well from day 3 onwards. Red markings highlight areas of clustering. Images were taken under 2x magnification. 90

Figure 2.9 MG63 cells attached to Ti5 glass microspheres on day 13 under 150rpm conditions using confocal laser scanning microscopy. Phalloidin stain was used to identify the actin filaments of the cytoskeleton

(green) while the propidium iodide (PI) stain was used for the nuclear staining (red). Image a) provides a sliced cross-section through a cluster of microspheres cultured with MG63 cells, while image b) illustrates a 3D rendered image of an individual microsphere. Scale bar is a) 50µm and b) 25 µm respectively.

91

Figure 3.1 Tri-lineage differentiation of hBM-MSC. Light microscopy (A, C, E) and immunofluorescent (B, D, F) images indicating the differentiation potential of the cells to differentiate towards adipogenic (A, B), osteogenic (C, D) and chondrogenic (E, F) lineages. hBM-MSCs cultured in adipogenic media were positively stained with Oil Red O after 21 days (A) and were positive for FABP4 (B; green signal). After 21 days in osteogenic culture media, hBM-MSCs were positively stained with Alizarin Red S (C) and were positive for osteocalcin expression (D; green signal). Chondrogenic differentiation in a cell pellet was characterised using Alcian Blue stain (e) and Aggrecan (F; green channel) after 21 days. Immunofluorescent images were counter-stained with Hoechst 33342 (blue). Images were captured at 4x (Fig 3.1 - E) and 10x magnification (Fig 3.1 – A, B, C, D and F)

106

Figure 3.2 Phenotypic analysis of hBM-MSCs and expression of pluripotency markers. A single cell suspension of hBM-MSCs was examined for the expression of mesenchymal markers A) CD90, B) CD105, C) CD73) and hematopoietic markers D) CD45, E) CD34 and F) CD11b. Matching isotype controls were used to ensure observed staining is due to specific antibody binding.

107

Figure 3.3 Standard curve of hBM-MSC's cell growth plotted as absorbance (nm) versus number of viable cells using a CCK-8 proliferation assay. Readings were taken after complete attachment of cells for (A) 70rpm (B) 100rpm and (C) 150rpm. Absorbance based on a wavelength of 450nm. Error bars represents + SD (n=3)

109

Figure 3.4 Proliferation of hBM-MSC cultured on (A) Ti5, (B) Ti7 microspheres and (C) Synthemax in ultra-low attachment well microplates under static and dynamic conditions. Readings were taken on days 0, 1, 3, 5, 7, 9 and 13. Error bars represents + SD (n=3). Significance values denoted by *= $p<0.05$, **= $p<0.01$ and ***= $p<0.001$. 110

Figure 3.5 Proliferation of hBM-MSC cultured under (A) 0rpm, (B) 70rpm, (C) 100rpm and (D) 150rpm conditions. Readings taken on days 0, 1, 3, 5, 7, 9 and 13 of cells cultured on the two TiO₂ compositions and Synthemax in ultra-low attachment well microplates. Error bars represents + SD (n=3). * = $p<0.05$ 113

Figure 3.6 Comparison of static controls used when studying hBM- MSC proliferation over 13 days where Exp 1, 2 and 3 denote three different static runs which were used as controls carried out in parallel with the dynamic studies (70rpm, 100rpm and 150rpm). Exp 1- Static control for 70rpm, Exp 2- Static control for 100rpm study and Exp-3 Static control for 150rpm study. Error bars represents + SD (n=3). 114

Figure 3.7 Formation of Ti-PGM-cell clusters under different agitation rates. Phase contrast images of an individual ultra-low attachment microwell illustrating hBM-MSCs cultured on Ti5 over a 13-day period using the same well from day 3 onwards. Red markings highlight areas of clustering. Images were taken under 2x magnification. 116

Figure 3.8 Formation of Synthemax-cell clusters under different agitation rates. Phase contrast images of an individual ultra-low attachment microwell illustrating hBM-MSCs cultured on Synthemax over a 13-day period using the same well from day 3 onwards. Red markings highlight areas of clustering. Images were taken under 2x magnification. 117

Figure 3.9 Fibronectin expression by hBM-MSCs cultured on Ti-PGMs in ultra-low attachment 96-well microplates at a range of agitation rates on days 7 and 13 post culture using confocal laser scanning microscopy. Images were acquired and converted into Z-stack images which were rendered to produce a maximum intensity projection of cross-sections up to 150µm. Images taken at 10x magnification where scale bar is 100µm.

119

Figure 3.10 Type-I collagen expression by hBM-MSCs cultured on Ti-PGMs in ultra-low attachment 96-well microplates at a range of agitation rates on days 7 and 13 post culture using confocal laser scanning microscopy. Images were acquired and converted into Z-stack images which were rendered to produce a maximum intensity projection of cross-sections up to 150µm. Images taken at 10x magnification where scale bar is 100µm.

120

Figure 3.11 Optical densities readings of hBM-MSCs proliferated in different conditioned medias. hBM-MSCs were cultured in conditioned media in Nunclon™ flat bottomed tissue culture 96-well microplates (Thermo Fisher Scientific, UK) and CCK-8 assay readings were taken at time points 1, 3, 5 and 7. Ti-conditioned media, commercially available osteogenic media (Lonza, UK) and commercially available DMEM (Gibco®, Life Technologies Ltd., Paisley, UK) were the studied conditioned media types. Error bars represent +SD and (n=3). *= $p < 0.05$, **= $p < 0.01$ and ***= $p < 0.001$. Note that the differences shown in the bar chart, while not visibly clear to be statistically significant are determined using specific models based on prerequisites of normality and variance. Box-and-whisker plots in Figure A.4 of the Appendix provide a more accurate representation of the differences observed between the different media types.

122

Figure 3.12 Type-1 collagen expression by hBM-MSCs cultured in Nunclon™ flat bottomed tissue culture 96-well microplates (Thermo Fisher Scientific, UK) after 7 days of culture in Ti-conditioned media, commercially available osteogenic differentiation media (Lonza, UK)

19

and DMEM (Gibco®, Life Technologies Ltd., Paisley, UK). Images take at 20x magnification 123

Figure 3.13 Osteopontin expression by hBM-MSCs cultured in Nunclon™ flat bottomed tissue culture 96-well microplates (Thermo Fisher Scientific, UK) after 7 days of culture in Ti-conditioned media, commercially available osteogenic differentiation media (Lonza, UK) and DMEM (Gibco®, Life Technologies Ltd., Paisley, UK). Images take at 20x magnification 124

Figure 3.14 Osteocalcin expression by hBM-MSCs cultured in Nunclon™ flat bottomed tissue culture 96-well microplates (Thermo Fisher Scientific, UK) after 7 days of culture in Ti-conditioned media, commercially available osteogenic differentiation media (Lonza, UK) and DMEM (Gibco®, Life Technologies Ltd., Paisley, UK). Images take at 20x magnification 125

Figure 4.1 Correlation between Froude number and rate of agitation. An XY scatter plot was used to scale agitation rates from (A) 96-well microplates to (B) 125 ml Erlenmeyer shake flasks. The figure highlights the speeds chosen in relation to highest agitation rate used (300rpm) at microwell scale and how the mixing dynamics have been mimicked at shake flask scale where a N_s of 320rpm was calculated. 140

Figure 4.2 Progressive changes in Ti-PGMs monolayer with increasing agitation rate. Increased orbital agitation leads to the complete suspension of Ti-PGMs (additionally doped with a minimal amount of Co^{2+} to visualize microspheres) in a 125 mL Corning® Erlenmeyer flask containing distilled water. Operating conditions are $V_L=80$ mL, $d_o=1.0$ cm, and agitation rate: $N=0$ rpm, 80rpm, 160rpm, 220rpm, 280rpm and 320rpm. Complete suspension was observed for $N_s=320$ rpm 141

Figure 4.3 Cellular/microsphere structures formed in 125ml Erlenmeyer shake flask after 21 days of culture. Different clusters formed when hBM-MSCs are cultured on Ti-PGMs under (A) 0rpm (B) 40rpm and on Synthemax under (C) 0rpm conditions. (D) Size of the Ti-PGM/cell structures formed with the largest cluster measured at 6mm in length. Image was taken at 2x magnification. Scale bar is 2000 μ m. 142

Figure 4.4 hBM-MSCs metabolic profiles when cultured on different substrates under different agitation rates. Line graphs show glucose consumption (A, C) and lactate production (B, D) when cultured on Ti-PGMs (A & B) and Syn (C&D) at days 0, 1, 4, 7, 10, 14, 17 and 21 under ● - 0rpm ■ - 40rpm ▲ - 80rpm and x - 160rpm condition. Values represent mean \pm SD (n=3). Significance values denoted by *= $p < 0.05$ indicate significant differences between 160rpm and both 0 and 40rpm while **= $p < 0.01$ indicates significant differences between 160rpm and all other conditions. 144

Figure 4.5 Glucose consumption of hBM-MSCs cultured on Ti-PGMs and Synthemax. Line graphs showing glucose levels at days 0, 1, 4, 7, 10, 14, 17 and 21 under (A) 0rpm, (B) 40rpm, (C) 80rpm, and (D) 160rpm condition. Values represent mean \pm SD (n=3). Significance values denoted by * = $p < 0.05$, ** = $p < 0.01$ and *** = $p < 0.001$. 145

Figure 4.6 Lactate production of hBM-MSCs cultured on Ti-PGM and Synthemax. Line graphs comparing lactate levels at days 0, 1, 4, 7, 10, 14, 17 and 21 under (A) 0rpm, (B) 40rpm, (C) 80rpm, and (D) 160rpm condition. Values represent mean \pm SD (n=3). Significance values denoted by * = $p < 0.05$, ** = $p < 0.01$ and *** = $p < 0.001$. 146

Figure 4.7 Glucose consumption and lactate production rates per hour of hBM-MSCs during culture. Line graphs compare the metabolic rates of hBM-MSCs cultured on Ti-PGMs (A & B) and Synthemax (C & D) at days 0, 1, 4, 7, 10, 14, 17 and 21 under 0rpm, 40rpm, 80rpm and 160rpm condition. 147

Figure 4.8 hBM-MSCs cultured on both Ti-PGMs (left column) and Synthemax (right column) after 21 days of culture under 0rpm, 40rpm and 160rpm conditions in 125ml Erlenmeyer shake flasks. Scanning electron microscopy images showing differences in microsphere size and morphology of cells cultured under different conditions. Images were taken at various magnifications

148

Figure 4.9 hBM-MSCs cultured on both Ti-PGMs (left column) and Synthemax (right column) after 21 days of culture under 0rpm and 160rpm conditions in 125ml Erlenmeyer shake flasks. Scanning electron microscopy images showing differences in thickness of tissue formed under static and high agitation conditions. Images were taken at various magnification and scale bars indicates 50µm.

149

Figure 4.10 Fibronectin and type-1 collagen expression by hBM-MSCs cultured on Ti-PGMs at days 14 and 21 of culture. Confocal laser scanning microscopy Z-stack images were rendered to produce maximum intensity projection of cross-sections up to 150µm. Staining pattern highlights fibronectin (green) and type-1 collagen (red) expressed in the extracellular matrix. Images taken at 10x magnification where scale bar is 100µm.

151

Figure 4.11 Fibronectin and type-1 collagen expression by hBM-MSCs cultured on Synthemax at days 14 and 21 of culture. Confocal laser scanning microscopy images of were acquired and converted into Z-stack images which were rendered to produce a maximum intensity projection of cross-sections up to 150µm. Staining pattern highlights fibronectin (green) and type-1 collagen (red) expressed in the extracellular matrix. Images taken at 10x magnification where scale bar is 100µm.

152

Figure 4.12 hBM-MSCs cultured on Ti-PGMs at day 21 of static culture in a 125ml Erlenmeyer flask. Confocal laser scanning microscopy images were acquired and converted into Z-stack images which were rendered to produce a maximum intensity projection of cross-sections up to 150µm.

Staining pattern highlights fibronectin (green) and type-1 collagen (red) expressed in the extracellular matrix. Nuclear staining was carried out using Hoechst 33342 (blue). Images taken at 20x magnification where scale bar is 100µm.

153

Figure 4.13 hBM-MSCs cultured on Corning® Synthemax at day 21 of culture when cultured under static conditions. Confocal laser scanning microscopy images were acquired and converted into Z-stack images which were rendered to produce a maximum intensity projection of cross-sections up to 150µm. Staining pattern highlights fibronectin (green) and type-1 collagen (red) expressed in the extracellular matrix. Nuclear staining was carried out using Hoechst 33342. Images taken at 20x magnification.

154

Figure 4.14 hBM-MSCs cultured on (A) Ti-PGMS and (B) Corning® Synthemax at day 21 of static culture. Confocal laser scanning microscopy Z-stack images were rendered to produce a maximum intensity projection of cross-sections up to 150µm. Staining pattern highlights fibronectin (green) and type-1 collagen (red) expressed in the extracellular matrix. Bright field images (far-right) show the distribution of microcarriers in the cluster. Nuclear staining was carried out using Hoechst 33342. Images were taken at 5x magnification.

155

Figure 4.15 hBM-MSCs cultured to Ti-PGMs at day 21 of static culture. Confocal laser scanning microscopy Z-stack images were rendered to produce maximum intensity projection of cross-sections up to 150µm. Staining pattern highlights osteopontin (green) and osteocalcin (red) found in the extracellular matrix. Images taken at 10x magnification where scale bar is 100µm.

156

Figure 4.16 hBM-MSCs cultured on Synthemax at day 21 of static culture. Confocal laser scanning microscopy Z-stack images were rendered to produce maximum intensity projection of cross-sections up to 150µm. Staining pattern highlights osteopontin (green) and osteocalcin (red) found

in the extracellular matrix. Images taken at 10x magnification where scale bar is 100 μ m. 157

Figure 4.17 Relative quantification of gene expression of (A) COL1A1 (B) RUNX2 and (C) SPP1 in hBM-MSCs seeded on Ti-PGMs and Synthemax after 21 days in culture. Significance values denoted by * = $p < 0.05$, ** = $p < 0.01$ and *** = $p < 0.001$ indicate highly significant gene expression compared to Synthemax. Error bars represent the mean value considered for three replicate specimens (\pm SD). 158

Figure 5.1 TRAP-staining showing monocyte distribution and osteoclast formation using different seeding densities. The different densities used were A- 2.5×10^5 cells/cm² B- 5×10^5 cells/cm² C- 1×10^6 cells/cm² and D- 2.5×10^6 cells/cm². The red arrows indicate areas of possible osteoclastogenesis. Images were taken at 20x magnification with the scale bars representing 200 μ m. 176

Figure 5.2 Cathepsin K expression from mouse monocytes cultured on Ti-PGDs. The immunofluorescent image illustrates expression of bone degrading enzyme cathepsin K (red) when 2.5×10^6 cells/cm² were seeded on Ti-PGDs. Staining of F-actin (green) and nuclear stain (blue) Hoechst 33342 were carried out to highlight actin ring formation and multi-nuclearity respectively. Scale bar indicates 400 μ m with images taken at 5x magnification. 177

Figure 5.3 Monocyte culture and differentiation into pre-osteoclasts on the Ti-PGDs. SEM images of individual monocytes are illustrated in image A after 9 days of culture, while image B shows potential pre-osteoclasts and the lateral resorption. A hollow evacuated area can be seen under the cell with a similar shape to that of the cell. The degraded edge of the Ti-PGDs can be seen detached from the cell. Images were taken at various magnifications. 179

Figure 5.4 Pre-osteoclast resorption activity of the Ti-PGDs. The SEM images show the differences between cellular material, the Ti-PGD surface and the resorption pit. The evacuated area can be seen under the cell with differing surface morphology to the Ti-PGD. Image B focuses on a section of image A to highlight the differences in textures of the modified surface. The arrows in image A indicate active (with cell processes) and inactive cells (without cell processes) adjacent to each other. Images were taken at various magnifications.

180

Figure 5.5 Mouse bone-marrow derived monocytes cultured on Ti-PGD for 9 days at different concentrations of RANKL. The different concentrations are highlighted by (A) 0 ng/ml (B) 3ng/ml and (C) 30ng/ml, with images taken at different magnifications. Scale bars represent 20µm intervals.

181

Figure 5.6 Effects of different incubation periods in 35% H₃PO₄ on the surface of Ti-PGDs. Images A-C were acquired using light microscopy technology while the images D-F were acquired using SEM. The different periods of time studied were: A/D- Untreated control, B/E- 15 minutes, and C/F- 24 hours. Scale bars for the light microscopy images indicate 400µm with images taken at 5x magnification. SEM images were taken at various magnification.

183

Figure 5.7 hBM-MSCs cultured on Ti-PGDs acid treated for 24 hours. The SEM images highlight the networks formed by hBM-MSCs within the channels created by the acid etching process of the Ti-PGDs, after 3 days of culture. The white arrow highlights a cell process passing through a horizontal valley. Images were taken at 1000x magnification with scale bars indicating 20µm.

184

Figure 5.8 Proliferation of hBM-MSCs on untreated Ti5 and acid-etched Ti5 microspheres compared to Synthemax. CCK-8 assay readings were taken at time points day 1, 4 and 7 Error bars represent +SD (n=3). **=p <0.01.

185

Fig 5.9 Scanning electron microscopy images showing the surface topography of Ti-PGMs incubated in H₃PO₄. Samples were acid-treated for 15 minutes (A, B), Synthemax microcarriers (C, D) and untreated titanium phosphate microspheres (E). Images were taken at different magnifications.

186

Figure 6.1 Glucose consumption and lactate production of hBM-MSCs cultured on Synthemax using a PBS 0.1MAG bioreactor. The magnetically driven air wheel bioreactor was run at 0, 25 and 50 rpm with samples of media taken on days 1, 4, 7, 10, 13 and 16. *= $p < 0.05$. Error bars indicate \pm SD.

199

Figure 6.2 PBS 1.0 MAG Bioreactor containing Ti-PGMs under static (A) and 50rpm (B) conditions. The image illustrates the Ti-PGMs (1g) circled in blue remaining static at the base of the reactor when the highest speed was administered. Furthermore, the location of the magnetic drive prevents extraction of the material in an effective manner. The arrow indicates the direction of wheel rotation.

199

Figure 6.3 Different perfusion devices used to study the effects of fluidization of Ti-PGMs (A - doped with 5 mol% Co²⁺ and B – Ti5). The Faculty of Engineering and Design Group at the University of Bath tested the Ti-PGMs in their in-house developed perfusion device (A), while an in-house perfusion reactor (B) developed within the UCL Biochemical Engineering Regenerative Medicine lab was used to compare different perfusion reactor dimension on fluidization of the microspheres. The perfusion devices was connected to a Watson Marlow 205U (Wolflabs, UK) peristaltic pump where various flow rates were administered from 0 to 20 ml/min. Under maximum flowrate conditions, the Ti-PGMs would momentarily fluidize however would settle immediately.

201

Figure A.1. Box-and-whisker plots representing the results of a CCK-8 assay to quantify hBM-MSC proliferation, cultured in different types of conditioned media (Ti-conditioned media (2 mg/ml,10mg/ml and 20mg/ml), DMEM and osteogenic media in Nunclon™ flat bottomed tissue culture 96-well microplates on days a) 1, b) 3 c) 5 and 7. Note that circles indicate outliers (values more than the interquartile range) while asterisks indicate extreme outliers (values more than three times the interquartile range).

237

List of Tables

Table 1.1 Bioreactor comparison	53
Table 2.1 Glass Compositions	66
Table 2.2 Fold increase values indicating the maximum cells yield achieved over the course of the experiment under the different conditions and materials used.	81
Table 3.1. Fold increase values of cultured hBM-MSCs indicating the maximum cells yield achieved over the course of the experiment under the different conditions and materials used. The time point (in days) at which the maximum yield was achieved is indicated within the parentheses.	113
Table 4.1 Critical (N_c) and suspension (N_s) agitation speeds based on models developed by Weheliye et al., (Weheliye) and Olmos et al., (Olmos)	163
Table 5.1 Different media types used during the monocyte isolation and osteoclast differentiation processes	171

List of Abbreviations

3D	Three dimensional
αMEM	Alpha Modified Eagles Medium
ALP	Alkaline phosphatase
ANOVA	Analysis of variance
ATMP	Advanced Therapy Medicinal Product
BM-MSC	Bone marrow mesenchymal stem cell
BSP	Bone sialoprotein
CCK-8	Cell counting kit 8
cDNA	Complimentary DNA
COL1A1	Collagen type I alpha subunit I
DC	Direct current
DMEM	Dulbecco's modified eagle's medium
DNA	Deoxyribonucleic acid
ECM	Extracellular matrix
EDTA	Ethylenediaminetetraacetic acid
FBS	Foetal bovine serum
FDA	Food and Drug Agency
Fr	Froude number
Fr_c	Critical Froude number
Fr_s	Suspended Froude number
GMP	Good manufacturing practice
hBM-MSC	Human bone marrow mesenchymal stem cell
HCL	Hydrochloric acid
HPLC	High performance liquid chromatography
HSPC	Haematopoietic stem and progenitor cells
IGF	Insulin growth factor
ISCT	International society for cellular therapy
M-CSF	Macrophage colony-stimulating factor
MHRA	Medicines and Healthcare Products Regulatory Agency
MMP	Matrix metalloproteinase
MSC	Mesenchymal stem cell
N	Agitation rate

N_c	Critical agitation rate
NMR	Nuclear magnetic resonance
N_s	Suspension agitation rate
OCN	Osteocalcin
OPN	Osteopontin
PBS	Phosphate buffer saline
PCL	Polycaprolactone
PCR	Polymerase chain reaction
PFA	Paraformaldehyde
PI	Propidium iodide
PLAGA	Poly lactic-co-glycolic acid
qPCR	Quantitative polymerase chain reaction
RANKL	Receptor activator of nuclear factor kappa-B ligand
RNA	Ribonucleic acid
RT-PCR	Real-time polymerase chain reaction
RUNX2	Runt-related transcription factor 2
SBF	Simulating body fluid
SD	Standard deviation
SEM	Scanning electron microscopy
SPP1	Secreted phosphoprotein 1
Syn	Corning Synthemax II
TCP	Tissue culture plastic
TGF	Transforming growth factor
Ti5	Titanium doped phosphate glass (5 mol%)
Ti7	Titanium doped phosphate glass (7 mol%)
TIMP	Tissue inhibitor of metalloproteinase
Ti-PGDs	Titanium doped phosphate glass discs
Ti-PGMs	Titanium doped phosphate glass microspheres
TRAP	Tartrate resistant acid phosphatase
V-ATPase	Vacuolar-type H ⁺ -ATPase
VEGF	Vascular endothelial growth factor
XRD	X-ray diffraction
Y_{Lac/Glc}	Lactate production to glucose consumption metabolic ratio

Chapter 1 . Introduction and review of the literature

1.1 Introduction

There has been a surge in innovative ideas used to exploit the problem of regenerating diseased and damaged tissues, resulting in the emergence of a new healthcare sector. Described as an interdisciplinary field that applies principles and methods of engineering, life sciences, material sciences, cellular and molecular biology, and surgery towards the development of biological substitutes that restore damaged tissue (Langer and Vacanti, 1993), tissue engineering has travelled a long way from its early use in diabetic patients (Chick et al., 1975). Currently, procedures involve a biopsy taken to attain an appropriate cell source, which is then expanded until enough cells have been generated for the intended purpose, and consequently transplanted back into the patient either using materials of natural sources or synthetic materials for cellular delivery.

At present, tissue can be used in either an implantation or transplantation. The latter involves harvesting cells from either the host or a donor, after which the cultured tissue sample is transplanted to the host site using surgical procedures. The former, is the development or modification of man-made materials to combine with living host tissues. The significance of tissue-engineered implants is that they provide benefits over transplantation, such as ease of availability, reliability, and reproducibility. Furthermore, stringent guidelines have been set, such as good manufacturing practise and international standards, which minimize the failure rate of such techniques. Another advantage of using tissue engineered constructs is that structures can be created to produce a product of a desired shape and size, complimentary to the defect in a three dimensional format (Lahann et al., 2003). There are concerns associated with the use of implants such as interfacial stability with host tissue, biomechanical mismatch of elastic moduli and maintaining a stable blood supply. Additionally, implants generally

don't have the ability to self-repair or modify their structure in response to environmental changes (Hench, 1998).

While progress exists in this area, no one solution has arrived to solve all issues and henceforth large bone defects remain a continuing challenge for research. The established field of tissue engineering provided the basis to develop materials around the advancing regenerative medicine, with the roles of biomaterials becoming paramount in developing bone tissue-engineered constructs. These constructs consist of any combination of bone marrow tissue, synthetic scaffolds, and various biological factors (Barrere et al., 2008).

To this date millions of individuals who have had their quality of life improved substantially with the use of the man-made implants, however the efficacy of these biomaterials has been poor due to the response illustrated not being comparable to the qualities seen of natural tissue such as their bone loading properties. Despite the conduction of many studies in tissue engineering, the field is still considered to be in its infancy, with skin grafts and cartilage repair products being the main contributors of its success. With many disciplines slowly merging together including the likes of gene therapy, stem cell research and even the nanotechnology industry, the potential for developing new effective therapies keeps increasing (Moroni and van Blitterswijk, 2006).

Stem cells provide an ideal candidate to be used in forming bone tissue engineered constructs, as they can be sourced in large amounts and differentiated under the right conditions into bone progenitor cells. To ensure that stem cell technologies are used in an efficient manner, large numbers of cells with defined characteristics need to be produced, and hence a careful systematic approach with controlled monitoring is required. Depending on the intended use of the stem cells, a suitable culture system should be used which incorporates methods to increase yields of viable cells and limit differentiation towards unwanted lineages. Owing to bioprocess engineering, successful large-scale cultures can be established and operated at the standards required for clinical application.

1.2 Research Motivation

Biomaterials have been widely studied since the development of the novel 45S5® BioGlass, reported by Larry Hench in 1969. While various iterations of this silicate-based glass have been developed and extensively studied, work with phosphate glasses is limited (Hench, 1991, Hench, 1998). Studies of phosphate glasses and their use in applications such as orthopaedic, dental and maxillofacial implants, clearly suggest that this family of glasses illustrate a new generation of biomaterials with a host of associated benefits such as their ability to be tailored and physiochemical properties (Knowles, 2003). From the range of studies focusing on the suitability and applicability of the various stoichiometric variations of phosphate glasses, limited studies have looked at the effect of scaling these exploratory studies to a clinically relevant scale. While it is important to establish the biocompatibility of these materials, a better understanding is needed of whether these novel compounds can elicit the same beneficial responses both structurally and biologically, when used in large scale culture systems.

This research focuses on understanding how commonly used bioprocessing tools, such as microcarriers and shaken culture can be used at their fullest to optimize cell yields and to gain an improved understanding of how to minimize cell variability in terms of identity and maturity. The project aims to bring together three distinct aspects of tissue engineering (cell culture, biomaterials, bioprocessing). Substantial research has been carried out in all the respective areas; however there remains a knowledge gap associated with the synergism between each of these studied areas

Therefore, it is hypothesized that spheroidized phosphate glass microspheres can support critical cell responses that enable scalable production of bone-like tissue microunits. The aim of this research was to demonstrate the potential of Titanium-doped phosphate glass to provide bone-like tissue in a manner that is transferable to scalable bioreactor-based cell culture. To establish the efficacy, the following aims were initially set out:

- 1) Assess the biocompatibility of the material with the following differentiated and primary cell types:
 - a) Osteosarcoma cell line (MG63)
 - b) Human bone marrow-derived mesenchymal stem cells (hBM-MSCs)
- 2) Determine the effects of fluid flow forces induced by dynamic culture on cell/engineered tissue quality.
- 3) Establish whether scale-up of cell culture can be achieved to create increased quantities of engineered bone-like material.

1.3 Organisation of review

This chapter aims to provide an in-depth analysis of the principles the research focuses on i.e. bone defects, the osteogenic potential of the biomaterials used in the research, focusing on phosphate glasses containing TiO₂ as a metallic oxide doping agent, the role of bioprocess forces and their influences on bioreactor development. This review aims to consolidate previously carried out studies applying similar principles to the ones of this project highlighting their relevance and main contributions to the research area.

1.4 Bone

1.4.1 Constituents of bone

Bone is responsible for protection, support and motion of the body and its vital organs. Flexibility and elasticity are key characteristic of ribs which protect the heart, lungs, and other organs whose function involves mobility. The stiffness quality of bone also allows it to provide structural support to soft tissues, such as muscle or even the lungs during expansion (Buckwalter et al., 1996a). At a cellular level, it surrounds bone marrow storage having a protective aspect in its nature. Additionally, it also plays a role in the endocrine system in regulating calcium and phosphate levels via homeostasis (Barrere et al., 2008).

The entity bone belongs to a family of tissues with varying structural motifs, each consisting of the same basic unit of collagen fibril. This structural family comprises of other materials such as dentin and cementum, the inner layer of teeth and the substance that binds teeth to the gum respectively, along with mineralized tendons (Weiner and Wagner, 1998). Collagen fibrils are composed of the protein collagen in a structural manner that is present in a variety of soft tissues. The collagen acts as the main component of a structural 3D matrix into which the mineral forms, adding strength and hardness. The primary mineral formed is known as carbonate apatite ($\text{Ca}_5(\text{PO}_4, \text{CO}_3)_3$) (Weiner and Wagner, 1998), one of the few minerals in bone. The final constituent of this structure is water. There is a need to distinguish that bone is a structure rather than a material, in that its nature is not fixed, as each of the constituents can vary in quantity present and be organized in various manners depending on the function of the bone (Weiner and Wagner, 1998).

1.4.2 Bone remodelling

Bone remodelling involves the resorption of mineralized bone by osteoclasts, followed by the formation of bone matrix through osteoblasts, and its subsequent mineralization. Adult bones are fascinating in that they constantly remodel based on the mechanical stresses exerted upon them, such as fluid flow from blood supply, which subsequently maintains bone health and its regeneration as a consequence of small injuries. Remodelling of bone occurs without any change in properties such as density or shape (Buckwalter et al., 1996b). The overall remodelling process is affected by age and can be illustrated by certain diseases which impact bone mass, hence promoting fragility of the bone, and leaving it prone to fracture. One of the key causes is the imbalance of resorption and formation of bone due to oestrogen deprivation (Vaananen and Harkonen, 1996, Marie, 2005). Further examples of altered bone formation can be seen in astronauts, who experience zero-gravity on a regular a basis, which results in their modified bone shape and density (Tavassoli, 1986).

The formation of bones is promoted by two specific processes, intramembranous and endochondral ossification (Marolt et al., 2010). The former involves the

differentiation of condensed mesenchymal tissue into osteoblasts and subsequently form bone. On the other hand, endochondral ossification results in the formation of cartilaginous anlage, which consequently becomes calcified following the invasion of blood vessels, resulting in new bone formation (Bhumiratana and Vunjak-Novakovic, 2012). During intramembranous ossification, mesenchymal stem cells (MSCs) give rise to bone forming cells osteoblasts and osteocytes in the process known as osteogenesis (Wei et al., 2013). Spindle-shaped osteoblast precursors arise from MSCs and shift into large cuboidal osteoblasts during the osteogenesis process in bone (Davies, 1996, Clarke, 2008). During this process, osteoblasts secrete osteoid (Tenenbaum and Heersche, 1982) which contains type-I collagen and non-collagenous proteins such as osteopontin (Pinero et al., 1995) toward the bone formation surface (Clarke, 2008). Osteoid acts as the basic matrix for mineralization and bone formation. Alkaline phosphatase (ALP), also produced by osteoblasts, helps extracellular matrix (ECM) calcification (Pinero et al., 1995, Takeyama et al., 2001, Clarke, 2008). The precise function of osteoblasts in bone apatite formation remains unknown, however a crystallization role has been proposed (Boonrungsiman et al., 2012).

Osteoclasts, developed from mononucleated precursor cells both in bone marrow and the circulatory system (Quinn et al., 1998), are stimulation responsible for bone resorption during the bone remodelling process (Orriss and Arnett, 2012). Their differentiation direction is comparable to macrophages and dendritic cells (Alvarez et al., 1992) with coming from receptor activator of nuclear factor kappa-B ligand (RANKL) and macrophage colony-stimulating factor (M-CSF) (Shirai et al., 1999, Vaananen et al., 2000, Heinemann et al., 2011). M-CSF and RANKL, expressed by MSCs and osteoblastic cells, are presented to osteoclasts and its progenitors by cell-cell contact (Heinemann et al., 2011). This has been proved essential in inducing expression of enzymes specific to bone resorption, such as tartrate-resistant acid phosphatase (TRAP) (Bune et al., 2001), cathepsin K (Xia et al., 1999, Nakayama et al., 2011), matrix metalloproteinase (Visse and Nagase, 2003) and vacuolar type H⁺-ATPase (V-ATPase) (Blair et al., 1989).

1.4.3 Bone defects

Bone is unique in that, unlike a majority of other connective tissues, it does not form scars upon reconstitution of an injury due to molecular and cellular processes involved in the repair being sequential (Arvidson et al., 2011). This repair process is carried out by a regulation mechanism controlled by specific factors, although the full extent to the molecular and cellular processes that contribute to these phases is still not fully understood. Large bone defect repairs occur primarily via endochondral ossification and include a cascade of events known to be haematoma, inflammation, angiogenesis, chondrogenesis, osteogenesis, and finally bone remodelling (Figure 1.1) (Phillips, 2005). Each of the phases mentioned involve various levels of cell migration and differentiation coupled with processes linked with calcification (Arvidson et al., 2011). When looking at the process in more detail a familiar pattern can be identified whereby the inflammatory response that occurs coordinated with the haematoma formation, contributes to the initiation of the bone healing cascade through the action of specific cytokines, and promotes endochondral bone formation and remodelling (Gerstenfeld et al., 2003a). Sequentially, osteogenic events such as mesenchymal and osteoprogenitor cell proliferation and differentiation occur, via the activity of biological factors including members of the transforming growth factors (TGF) family such as bone morphogenetic protein (BMPs) and insulin-like growth factors (IGF) (Tsiridis et al., 2007).

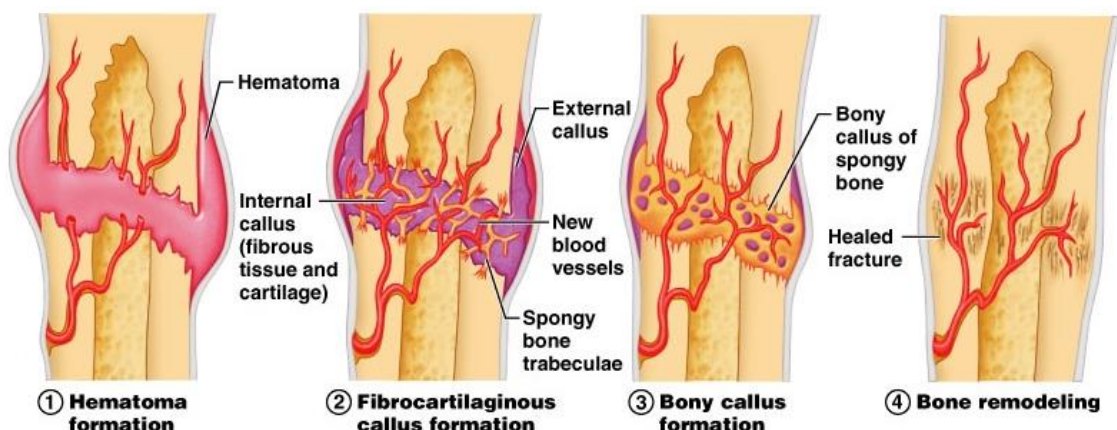


Figure 1.1 Stages involved in bone repair cascade. Copyrights of images owned by Benjamin Cummings (2004) Pearson Education. Inc

The cascade is concluded with the process of angiogenesis regulated by the angiopoietin pathway (Gerstenfeld et al., 2003b) and vascular endothelial growth factor (VEGF)-dependent pathway, where osteoblasts and osteoblast-like cells induce VEGF expression in relation to endochondral bone formation (Deckers et al., 2002). A full understanding of the cascade that takes place is not complete and links are still being made between several molecules and processes in the bone repair mechanism.

After fully healing, bone shape and mechanical properties are restored (Barrere et al., 2008). The main physiological bottleneck rectifying such injuries is that there is a size limit to which bone can self-repair. This limit is defined as the critical size defect, and states that defects of this size and larger will not naturally heal during the lifetime of an animal (Schmitz and Hollinger, 1986, Trounce et al., 2000). This creates an opportunity for tissue engineering and it is currently wide open. The full level to which the osteogenesis process can be optimized is still not fully understood. There are many strategies widely being studied but one major limitation of the tissue produced in these studies is that it does not exhibit the same load bearing qualities especially when concerning large bone defects.

The most common methods of treatment for bone defects favoured by surgeons are autografts, involving the transplantation of bone from another part of the patient, originating usually from the pelvis, to the defective site (Kucera et al., 2012). One of the setbacks is that its supply is limited and associated with inherent pain from isolation for the grafts. Synthetic options are required to treat the one million plus patients who require treatment for bone defects every year. Interventions are used to satisfy this insufficient availability of bone, through the mixing of bone graft extender material with the autograft, generally in the form of calcium phosphate. These granules form a putty-like substance when mixed with the host's blood, which is pressed into the defect. The benefits of this are that the blood improves the handling on the material, with the added advantage of providing natural growth factors to aid bone repair (Jones, 2013). With demographics showing that a majority of bone related injuries and diseases associated with the elderly, and form of cell therapy replacement will need to aid the healing process due to the reducing regeneration potential with age.

1.5 Biomaterials and filling the gap

1.5.1 Biomaterial properties

The product profile of a potential implantable bone regeneration scaffold is that it should be able to act as a three-dimensional (3D) structure to aid bone repair. The structure should be temporary in nature while being able to enable natural human regeneration, by bringing together bone marrow stem cells and blood vessels to regenerate new bone and vascularise the newly formed tissue respectively.

During the last few decades, attention has been put upon the use of bioactive materials and their fixation to connective tissues, by bonds formed with strengths up to six-fold of those seen commonly within a collagen structure. This quality can be attributed to the *in vivo* growth of a dense layer of hydroxyl-carbonate apatite layer which binds to the collagen fibrils (Hench, 1998). Metals and non-degradable ceramics have been used predominantly for connective tissue repair, due to the qualities they possess such as high tensile strength (Barrere et al., 2008).

One useful tool of certain biomaterials is their ability to induce an osteogenic response. This osteoinductive characteristic has been studied in animal models such as goats (Kruyt et al., 2004, Habibovic et al., 2006) and has shown that bone production can occur in areas not akin to bone formation. This property can be helpful in regenerating areas in which the bone defects tend to be large by nature. Prior examples of osteoinductivity extend back to 1969, where poly-hydroxyethylmethyl-methacrylate (poly-HEMA) sponges were reported to induce bone formation in soft tissues (Winter and Simpson, 1969). Calcium phosphate is a common example, where dissolution-precipitation processes incur surface transformations, which promote bone bonding (Habibovic et al., 2006). It is the calcium phosphate that promotes the ionic exchange that affects the surrounding milieu and has been identified as a key promoter amongst others of osteoinduction. The full nature of osteoinductive influence is not clearly understood, however some factors thought to play a role in the process include porosity of the biomaterial along with the surface physio-chemistry (Habibovic et

al., 2006). These porous structures exist either when initially formed (Winter and Simpson, 1969, Fujibayashi et al., 2004, Habibovic et al., 2006) or due to the degradation of the structure (Gosain et al., 2002). This attribute of porosity was illustrated in earlier studies with titanium implants inducing greater osseointegration where the implant had a rough nature (Wall et al., 2009). The surface roughness exhibited by the titanium implant, while reducing cellular proliferation increased the induction into an osteogenic phenotype, which was evident from the early mineralization of the matrix. When considering titanium macroporous structures, 3D structures show osteoconductive tendencies when compared to regular fibrous meshes, which did not induce a bone formation response (Fujibayashi et al., 2004) implying only specific pore geometries promote bone formation (Magan and Ripamonti, 1996).

A variety of different bioactive materials undergo degradation by nature in that they exhibit physical, chemical structure and appearance variations. The degree of degradation is dependent on the nature of the biomaterials. There are a range of factors which initiate material degradation and vary from material to material. It is essential to understand how the fluid and cells used influence the rate of biomaterial degradation. Controlling the rate of degradation and allowing it to synchronize effectively with the rate of tissue growth to ensure full regeneration of tissue is achieved, is a great challenge that is still faced in the biomaterial field. Efforts are being focused on trying to improve degradation kinetics, with techniques such as multiphase calcium phosphate mixing, using different ratios of soluble and highly soluble materials to adjust the kinetics of the bioactive material to that of the bone formation kinetics (Arinzeh et al., 2005).

1.5.2 Commercial bioactive glasses

The current biomaterial market is improving vastly, with a plethora of bioactive substances being tested; however, discrepancies lie between what engineers deem key factors for a commercially successful scaffold, and the qualities surgeons require. Bioactive glasses are a class of biomaterial which have shown to induce specific biological responses. Deciding which composition to use when generating a bioactive glass can be a tedious task; however, there are essential

qualities which all types must hold. Bio-functionality and biocompatibility cover these properties, with the bio-functionality aspects including properties such as tensile strength, mechanical properties, Young's Modulus, surface chemistry and degradation to name a few (Barrere et al., 2008). Biocompatibility, on the other hand, looks at the ability for the material to perform with an appropriate host response (D.F. Williams, 1999). Historically, bioactive glasses have been defined as a material which when implanted into a host, leads to the formation of an apatite-like layer that is responsible for the materials bond with hard and soft tissues. There are many commercially available glass-based products for bone defect regeneration including BioGlass, Biogran® (BIOMET 3i, Palm Beach Gardens, FL) and BonAlive® (S53P4) (BonAlive Biomaterials, Turku, Finland) all derived from the same silicate structure. Since the development of BioGlass in 1969, it has been used to treat over a million patients with bone defects. Considering the age of the product, it has gained limited commercial success. To date, the most marketable iteration of it has come in the form of NovaMin® (GlaxoSmithKline, UK), the active ingredient in Sensodyne®, responsible for the mineralization of the tiny pores in dentine, reducing overall tooth sensitivity. Further modified versions of BioGlass have also been used to treat deafness, where a patient received treatment for the degradation of two bones within the eardrum (Rust et al., 1996, Stanley et al., 1997). Another product BonAlive when used with autologous bone allowed the integration of titanium roots into the porous maxilla, with significantly improved bone repair and a thicker trabeculae when compared to autograft alone (Turunen et al., 2004). Furthermore, trials with S53P4, the key ingredient of BonAlive, showed improved bone quantity and quality when compared to synthetic hydroxyapatite (HA) (Peltola et al., 2006). While fusion rates are comparably higher from autografts than the commercially available substitutes, the results from most studies and trials indicate promising results. An associated issue with S53P4 is the lack of full resorption, which could be related to the silicate content, with observed glass granules remaining even after 11 years (Heikkila et al., 2011, Perna et al., 2011). More clinical data is readily available for BonAlive than for BioGlass, with greater clinical results associated with BonAlive, however illustrate less than ideal degradation rates.

The first particulate based therapy to enter the market was PerioGlas®, now sold by NovaBone (NovaBone Products LLC, Alachua, FL), used in periodontal disease. With a particle size of 90-710 µm, it is used to regenerate bone around the damaged root of a tooth, and to provide support for damaged bones in the jaw for anchoring titanium implants. Studies carried out *in vivo* and in clinical trials indicated that PerioGlas generated significantly higher amounts of bone compared to controls (Schepers and Ducheyne, 1997, Froum et al., 1998). The successes of the periodontal treatments using these particulates lead to the development of NovaBone, a treatment for orthopaedic bone grafting on non-load-bearing sites. It showed great advantages over autografts in treating adolescent idiopathic scoliosis, with fewer infections and mechanical failures, and the added benefit that a donor site is not required (Jones, 2013).

1.5.3 Phosphate glasses and metallic oxides

The initial use of phosphate glasses were for their applications as achromatic optical elements based on their low dispersion and relatively high refractive indices (Kreidl and Weyl, 1941), however they have been conceptualized to a range of purposes from securing nuclear waste to semiconductors (Marasinghe et al., 1997, Brow, 2000).

The unique properties of a biomaterial candidate relevant to the purpose of tissue engineering research are its ability to degrade and its chemical components. The degradation of phosphate glasses can be controlled, and this becomes important when used in different solubilising media types. These materials when manufactured properly can remain stable *in situ* for periods ranging from as little as a couple of hours to 1 year or longer. This is simply done by the modification of the phosphate glasses ternary structure ($P_2O_5 - Na_2O - CaO$), through the addition of suitable metal oxides which form quaternary structures, therefore reducing the solubility level of these glasses. These components of the ternary structure have a vital role to play in the interactions between the phosphate glass and the osteogenic environment *in vitro* and *in vivo*. The key elements within the glass (e.g. P, Na, and Ca) are common inorganic minerals found within the bone and therefore their interactions in a physiological similar bone based environment

need to be understood (Anselme, 2000). The vast majority of glasses tend to comprise of a high quantity of pure P_2O_5 by composition, however its hygroscopic nature negates its potential use as a biomaterial (Hudgens et al., 1998). The initial studies carried out on phosphate glasses looked at methods to stabilize the structure, making them more suitable as candidates for biological applications. This was done through the addition of stabilizing oxides such as Na_2O and CaO (Burnie et al., 1981), generating the aforementioned ternary structure which allowed the first iteration of phosphate glasses flexibility in their degradation rates. This is illustrated in the opposite effects noticed with the calcium and sodium ions, with the former having a stabilizing effect on the phosphate glass dissolution rate, while the sodium ions have a depolymerising effect, consequently increasing the glass solubility in aqueous solutions (Pickup et al., 2007, Vitale-Brovarone et al., 2011). While the first generation of these ternary glasses showed potential in their flexibility and ability to be tailored, their rates of dissolution were relatively high which caused abnormally high fluctuations in pH therefore reducing their biocompatibility. More recent studies have looked to improve this issue of degradation closely by the addition of metallic oxides relevant to the purpose of eliciting an improved cellular response. The metal oxides studied to date include Fe_2O_3 , CuO , Al_2O_3 , TiO_2 , MgO , ZnO , Ag_2O , Ga_2O_3 and SrO (Lakhkar et al., 2015b). The metallic oxides not only serve a purpose in their stability role, but also their ions released induce biological responses such as antimicrobial effects and cell proliferation/differentiation qualities (Knowles, 2003, Abou Neel et al., 2009b).

1.5.3.1 Titanium dioxide

Titanium dioxide's toxicity to human tissue can be potentially chronic and this is dependent on factors such as concentration and the physical and chemical properties of the compound. Systematic *in vitro* and *in vivo* methods are required to validate the toxicity when the compound is used in biomaterials (Chellappa et al., 2015). Studies such as those using Titanium dioxide in nanoparticle form, have identified that Titanium dioxide is not cytotoxic at specific concentrations (Jin et al., 2008). Phosphate glasses doped with titanium dioxide have been studied thoroughly, in terms of their structural and mechanical properties (Brow

et al., 1997, Brow, 2000, Abou Neel et al., 2008). TiO_2 acts as a nucleating agent, and while it is miscible at the high temperatures during glass formation, it induces phase separation during the cooling period post melt (Monem et al., 2008). The introduction of TiO_2 improves the stability of the phosphate glass due to the high field strength observed with its oxide. This stability induces an overall reduction in the dissolution and hence ion release is kept to a minimum. The subsequent effect is that the biocompatibility of the phosphate glass is improved (Zhang and Santos, 2001, Abou Neel et al., 2008, Monem et al., 2008). The rapid degradation of an unstable structure could lead to extreme fluctuations in pH and ionic concentrations. This stability becomes very important when culturing cells, as a stable substrate is required for cell attachment and proliferation. Due to the nature of the oxide being small in structure and having such high ionic charge, upon its entry into the vitreous structure, a stabilizing effect is witnessed because of the cross linking between the phosphate chains and rings (Navarro et al., 2003). This observation has been studied with various TiO_2 concentrations, and results indicate that increased TiO_2 concentrations induce an observed reduction in solubility. The way in which TiO_2 improves this is through the formation of ionic cross links with phosphate chains and the generation of Ti-O-P covalent bonds that reinforce the phosphate glass, consequently minimizing the water diffusion at the glass/solution interface and hence limiting the dissolution rate. The reduced degradation associated by this, also limits the pH decrease observed caused by acidic degradation products (Vitale-Brovarone et al., 2011). Results from X-ray diffraction analysis of crystallized TiO_2 doped phosphate glass indicated that the main phases in a range of TiO_2 glasses studied were TiP_2O_7 and $\text{NaCa}(\text{PO}_3)_3$ (Abou Neel et al., 2008).

Some studies have accomplished to understand the limits to which TiO_2 can be incorporated into the phosphate glass. Abou Neel et al determined that the upper limit to which the ternary phosphate glasses nature remains amorphous was at a TiO_2 content of 15%. This was validated by this upper limit value capable of supporting cellular growth when used to grow an osteoblast-like cell line (MG63) (Abou Neel et al., 2008). However, physical properties were altered such as density and the temperature required to fabricate the material, factors which when

generating clinically relevant quantities of tissue engineered bone are key variables when trying to understand bioprocessing parameters.

Studies have been carried out to establish the effect of phosphate based glass doped with titanium upon a range of various cell types including fibroblasts (Guedes et al., 2012) and osteosarcoma cell lines (Abou Neel et al., 2007). The use of titanium dioxide in phosphate glasses has been studied within both *in vivo* and *in vitro* studies. TiO₂ doped phosphate glasses showed that increased biocompatibility was achieved by the addition of 5 mol% TiO₂ *in vitro*, however during early cell culture (D1-D3) lower levels of alkaline phosphatase (ALP), a by-product of osteoblast activity, were witnessed. These patterns were not concurrent with genetic expression on D14, where ALP and collagen type I alpha subunit I (COL1A1) showed significant increases, when compared to the commercially available control. There were also significant differences in composition of TiO₂ used, with 5 mol% showing higher levels of osteogenic gene expression than 3 mol% (Abou Neel et al., 2007).

Titanium dioxide has shown to enhance cell proliferation and gene expression of MG63 with 3 and 5 mol% illustrating the greatest effects. It was suggested that the improved cell properties were down to the reduced level of degradation of the compositions, henceforth maintaining conditions favourable to osteoblast formation due to the improved structural support. It was also put forward that the ideal TiO₂ content was 5 mol% in that it induced the higher cellular response. The content of TiO₂ also plays a significant role in the osseo-integration of these particles upon implantation, indicated by 1 and 3 mol% showing limited hard tissue formation in comparison to the 5 mol% (Abou Neel et al., 2007).

1.5.3.1.1 Material characterization

As previously mentioned, altering the glass composition and chemistry can control the degradation rates over several magnitudes (Abou Neel et al., 2008). A common trend observed with many of the glasses studied is the uniform linearity between weight loss and ion release of phosphate glasses, as a function of immersion time within a suitable solubilising agent (Ahmed et al., 2008, Khor

et al., 2011). Different species of phosphate glass ions in different amounts, from cyclic phosphates to orthophosphates (Ahmed et al., 2005a). This glass degradation process occurs with solubilising media in three distinct stages. The initial stage of slow degradation sees H₂O molecules diffuse into the structure of the glass covering the entire surface in the process. This occurs due to the saturation of the surface by H⁺ and OH⁻ ions released through acid/base reactions (Bunker et al., 1984, Gao et al., 2004) The second stage involves the uniform degradation of the phosphate glass, by the hydrated layer separating from the underlying partially hydrated section, causing dissolution, and leaching of ions into the surrounding medium. The concluding stage is a hydrolysis reaction, which causes the polymeric phosphate chains to disintegrate, rather than individual P-O bonds, due to hydrolytic attack (Bunker et al., 1984). The key factors responsible for the degradation include internal factors such as composition of phosphate glass and thermal preparation, and external factors such as pH, temperature of solution and surface area to volume ratio.

Establishing the effect that the release of phosphate ions, as well as the glasses additional components, has upon contact with physiological fluid is paramount; hence a considerable amount of work has been carried out in this area. The use of ion exchange chromatography and high-performance liquid chromatography (HPLC) are approaches used in identifying the distinct levels of varying phosphate ions released. Ion exchange chromatography is more common than most due to the process simplicity for smaller molecular weight phosphates (Baluyot and Hartford, 1996).

The addition of TiO₂ reduces the overall phosphate ion release due to its metal ion valency and atomic radius, hence creating a slower rate of degradation of these doped phosphate glasses (Abou Neel et al., 2008, Gayathri Devi et al., 2010). Raman spectrometry carried out by Navarro et al. on phosphate glasses (44.5P₂O₅.44.5CaO.11Na₂O where Na₂O is replaced with TiO₂) containing 0, 3 and 5 mol% of TiO₂, showed that an increase in TiO₂ content increased levels of TiO₅ and TiO₆ units, where an increase in these units was witnessed in the higher TiO₂ composition glasses. Furthermore, increasing the TiO₂ content increased the chemical durability and elastic modulus of the glasses (Navarro et al., 2003).

Thorough characterization studies have been previously carried out on the phosphate glasses doped with TiO_2 at 3, 5 and 7 mol% by Lakhkar et al. Thermal analysis validated initial density measurements using Archimedes' principle, showing as glass compositions increased in Ti content from 3 to 7 mol% an increase in the glass transition temperature from 489°C to 529°C is witnessed. The increased densification owes to the formation of TiO_5 and TiO_6 units formed creating P-O-Ti bonds (Abou Neel et al., 2009a). Degradation studies followed a similar trend, where Ti3 had a percentage cumulative weight loss per unit surface area of 0.0092% μm^{-2} after 80 hours in comparison to Ti7, whose degradation was approximately four times lower at 0.0024% μm^{-2} . When looking at pH measurements, all the different composition increased the levels of acidity when immersed in deionized water over a 21-day period, with the greatest release of phosphate ions observed between day 0 to day 1. The composition that generated the highest acidic environment was Ti3 with Ti7 generating an overall less acidic environment over the same period. The reason behind the reduction in pH is attributed to the released phosphate ions forming phosphoric acid under aqueous conditions. This release of phosphate ions was concurrent with the release of its cationic neighbours (Ca^{2+} and Na^+), again with the same trend witnessed with the other characterization studies. X-ray diffraction (XRD), nuclear magnetic resonance (NMR) and Ti K-edge X-ray near edge absorption data suggested there were no structural differences between the three compositions with coherent spectra across the three different concentrations (Lakhkar et al., 2012b). Regarding the other ions present in the structure of ternary phosphate glass (Ca^{2+} and Na^+) the release of these ions is at a rate inversely proportional to the CaO content of the glass. This is witnessed in glasses containing 45 to 55 mol% P_2O_5 , where this activity occurs due to CaO serving to densify the glass structure. This trend is also witnessed with phosphate glass when increasing amounts of high covalent metallic dopants are added to the structure (Ahmed et al., 2004b, Ahmed et al., 2004a, Ahmed et al., 2005b, Abou Neel et al., 2008).

1.5.3.1.2 Biocompatibility of TiO_2 doped phosphate glasses

Biocompatibility research of phosphate glass doped with Ti has been carried out through approaches including *in vitro* analysis of the material after immersion into

physiological similar solutions such as Tris-HCL, Tris buffer or simulated biological fluid (SBF) (Kasuga et al., 1999). The latter is very common in understanding how the material behaves when in direct interaction with physiologically relevant solutions containing ions such as Na^+ , K^+ , Mg^{2+} , Ca^{2+} and HCO_3^- to name a few, at concentrations approximately equal to human plasma. These studies provide an easy alternative to cellular based techniques to evaluate bioactivity through apatite formation upon the material surface in contact with the defined solution. Studies have revealed that phosphate glasses doped with TiO_2 formed apatite on the surface as opposed to phosphate glass doped with MgO (Kasuga et al., 1999). Other studies have contradicted such findings suggesting that no apatite formation was observed with TiO_2 -doped phosphate glass when immersed in SBF for 14 days at 37°C (Abou Neel et al., 2007, ElBatal et al., 2009, Gayathri Devi et al., 2010, Lucacel et al., 2010). While there isn't a clear understanding of the effect that the immersion of TiO_2 -doped phosphate glass in SBF has upon apatite formation, it should be made clear that apatite formation on the surface of such materials is not a pre-requisite for the material to be considered biocompatible (Kokubo and Takadama, 2006, Lee et al., 2006). Hence, *in vitro* analysis in SBF immersion alone can't provide a conclusive understanding of the bioactivity of phosphate glass. Further studies in the form of cell culture can provide better insight into the level to which TiO_2 phosphate glass can support the growth and maintenance of tissue.

Early studies using titanium phosphate glasses used MC3T3-E1 murine pre-osteoblast cells, identifying growth and differentiation characteristics at the cell-material interface over a 37-day period. Protein and genetic analysis indicated that normal proliferation and differentiation rates were supported (del Valle et al., 2003). Further studies indicated that glasses containing higher quantities of TiO_2 promoted better cell adhesion, growth, and proliferation (Dias et al., 2005, Brauer et al., 2006). Brauer et al. also considered the effect of porosity on MC3T3-E1 cells proliferation and adhesion using an MTT assay. The investigation showed that cell culture was initially inhibited by the porous surface, with proliferation rates and extensive cellular growth towards latter periods of culture (Brauer et al., 2006).

There have been minimal studies carried out using *in vivo* techniques when compared to the aforementioned *in vitro* studies. The existing studies focus on using rat and rabbit models by filling in defective areas with glass particulates of a specific size range and understanding how well the material can interact with the hosts tissue via light and polarized microscopy. Monem et al. implanted phosphate glass containing TiO₂ into rabbit femurs, where it was concluded that glasses containing TiO₂ concentrations above 0.5 mol% were associated with reduced bioactivity, with the stated concentration promoting improved bone cell growth (Monem et al., 2008). Other studies using different animal models showed that the required concentration for an effective bioactive response were magnitudes higher than those established by Monem et al. In calvarium defects of male rats it was found that a TiO₂ content of 5 mol% significantly increased the amount of bone tissue formation (Abou Neel et al., 2007). The combination of both *in vitro* and *in vivo* studies accentuates the link between the material composition and its biocompatibility. These promising results have provided an incentive for researchers to conduct research to gain a better understanding of the opportunities available using TiO₂ containing phosphate glasses.

1.6 Microcarriers for bone tissue engineering

When growing cells on conventional tissue culture plastic, contact-inhibition gradually decelerates the proliferation rate, hence requiring constant passaging of the cells into new and bigger flasks. Dynamic culture avoids such issues by allowing to culture large quantities of cells owing to the increased surface area to volume ratios, consequently maintaining high cell densities (Majd et al., 2011). When 3D scaffolds are used in static conditions, nutrient gradients are common, leading to inconsistent cell growth and differentiation (Volkmer et al., 2008). Recently, the tissue engineering approach to address bone defects has been 'bottom-up', where focus has looked at the development of smaller entities forming the building blocks of the required structures that mimic the morphology and composition of natural tissues, consequently binding these structures to treat macroscopic defects. Many methods have been tested including using cell saturated microgels (Du et al., 2008), cell aggregates (Kelm et al., 2006) and cell

based microsphere clusters (Martin et al., 2011), the latter being the method of application in the present research.

Microcarriers are an ideal entity for stem cell therapies as they have very high surface area to volume ratios, and hence already show advantages over the growth of stem cells in static T-flask culture. Furthermore, unlike scaffolds, microcarriers possess the ability to be motile and can be adjusted if necessary (Park et al., 2013). Studies have indicated that the optimization of cellular yield revolves around parameters such as cell seeding density, microcarrier density and microcarrier type (Fok and Zandstra, 2005, Abranches et al., 2007). Several types of microcarriers exist, with varying affinity and suitability to cell type. This is due to the ease at which cells can grow in/around the structure and is determined by factors such as surface topography, porosity, chemical composition, and diameter of carrier. Carriers can either come in porous or non-porous form, where the latter enables a monolayer surface to be grown to ensure homogenous mass transfer while the more common, porous, allows cell growth into the carrier, hence increasing the surface for growth (Park et al., 2013).

In order to recover the cells from the structure, enzymes such as trypsin or collagenase are used in a similar fashion to their use in T-Flask culture. Studies carried out provide a good basis for further expansion on the use of microcarriers as an adherent surface, with some studies producing positive results. Such studies include one carried out by Eibes et al., who used microcarriers coated with 2% fetal bovine serum (FBS) to increase the cell seeding efficiency producing a strategy to maximize cell proliferation. The experiment generated a maximum cell density of 4.2×10^5 cell/ml, which was an 8-fold increase in the total cell number. Furthermore, the potency of the cells was maintained after the culture, allowing differentiation of the MSCs into adipogenic or osteogenic lineages, while also maintaining their ability to clone further. This indicates that a microcarrier based culture system can provide the correct arrangement and condition to generate substantial amounts of cells (Eibes et al., 2010).

A diverse range of commercial microcarriers exist for bone tissue engineering. The extensive list includes microcarriers based on collagen (Cellagen™ by MP

Biomedicals) (Overstreet et al., 2003) ; polystyrene (HyQSphere™ by Solohill) (Ontiveros and McCabe, 2003, Zayzafoon et al., 2004) and dextran (Cytodex™ 1 (Howard et al., 1983, Sautier et al., 1992, Tang et al., 1994) and Cytodex™ 3 (Fok and Zandstra, 2005). Microcarriers have also been developed for specific applications using materials such as ceramics (Qiu et al., 1999, Hong et al., 2009), polycaprolactone (PCL) (Hong et al., 2009) and poly (lactic-co-glycolic acid) (PLAGA) (Botchwey et al., 2001). Studies with microcarriers have not only aided the development of culture systems but have also provided insight into the *in vitro* behaviour of the cells used (Malda and Frondoza, 2006). The use of microcarriers has helped to study the phenomena of bone loss within microgravity conditions such as space-flight. A rotating wall bioreactor was used to culture osteoblasts on gelatin-coated microcarriers (Solohill), allowing to generate a model depicting how microgravity resulted in the reduced expression of key bone formation regulators (Ontiveros and McCabe, 2003). Furthermore, evidence shows that progenitor cells and blasts of the osteogenic lineage proliferate on different types of microcarriers, having been used in both *in vivo* and *in vitro* studies (Howard et al., 1983, Sautier et al., 1992, Barrias et al., 2005)

The use of glass microspheres in bone tissue engineering for *in vitro* cell proliferation and bone tissue engineering provides unique benefits over commercially available platforms including microcarriers. When compared to tissue culture plastic, the magnitude of surface area for expansion in a given volume increases considerably, nonetheless this is an advantage common to all types of microcarriers. Many of the microcarriers available require cells to be harvested before implantation with a suitable scaffold material, however the biocompatible nature of phosphate glass eradicates these cell processing steps creating a more streamlined and resource efficient process.

1.7 Scale-up of microcarrier cultures for bone tissue engineering

A key aspect of bone tissue engineering is the use of scaling up and bioreactors. These vessels can be used to efficiently control oxygen and nutrient supply to

cells and generate specific environments to provide a desired lineage of stem cell differentiation (Chao et al., 2007). These controls can be used to manipulate the development of the bone and the characteristics associated with cartilage and bone regions, by stimulating and hence enhancing the load bearing aspect of the bones through the use biophysical stimulation (Marolt et al., 2010).

Critical quality parameters need to be considered when determining the bioreactor choice for cell culture. Uniform properties and high purity are essential for therapeutic medicines, and hence the importance surrounding bioprocess control is highly necessary if a full understanding is to be gained from stem cell culturing. Developments in differentiation and expansion of adult stem cells have gathered some pace, from the initial culturing of haematopoietic stem and progenitor cells (HSPC) in bioreactors. While such cell types grow extensively in stirred or suspended cultures, others such as mesenchymal stem cells thrive in perfusion reactors with the aid of 3D scaffolds (King and Miller, 2007). Limited work has been carried out on the scalability of biomaterials, and how well they can be incorporated into industrially relevant platforms, therefore parallel efforts need to be made to translate the plethora of biomaterials developed into commercially viable applications.

The most common methods for the expansion of MSCs in laboratories are tissue culture flasks which are easy to operate and provide good oxygen transfer with the external environment, however, due to limitations in surface area, large numbers of flasks are needed to generate cell yield at clinically relevant scales. This increases the overall manual handling, flask to flask variability and the chances of contamination. While current bioreactor culture techniques share common advantages such as the promotion of homogenous environments and controllability of crucial process parameters (e.g., temperature, dissolved oxygen, pH) when compared to static cultures, many contrasts still exist between the culture types (Table 1.1). The choice regarding culture system is complex as many challenges currently exist, including compromises needed due to hydrodynamic shear experienced at high mixing rates. Bioreactor properties are specific to each type, and hence it is important to carefully analyse each potential

candidate carefully, selecting the best one for the large-scale expansion and differentiation of MSCs for bone tissue engineering.

Table 1.1 Bioreactor comparison

Bioreactor type	Advantages	Disadvantages
Stirred suspension	<ul style="list-style-type: none"> • Homogenous conditions and can be used with microcarriers • Easily monitored and controlled 	<ul style="list-style-type: none"> • Prone to subject cells to hydrodynamic stress due to agitation • Cell agglomeration
Roller bottles	<ul style="list-style-type: none"> • Simple operation protocol • Low cost 	<ul style="list-style-type: none"> • Monitoring and control complex • Technology suited for anchorage cell cultures • Tend to produce concentration gradients
Wave	<ul style="list-style-type: none"> • Disposable technology hence minimized need for cleaning. More suitable for GMP and easier validation. 	<ul style="list-style-type: none"> • Relative difficulty in monitoring and sampling
Hollow-fibre	<ul style="list-style-type: none"> • Subject cells to low levels of shear 	<ul style="list-style-type: none"> • Monitoring and control not simple • Difficult to scale up technology • Concentration gradients formed, heterogeneous environment
Rotating Wall	<ul style="list-style-type: none"> • Efficient gas transfer • Subject cells to low levels of shear 	<ul style="list-style-type: none"> • Complex system which is not easily scaled
Parallel Plate	<ul style="list-style-type: none"> • Continuous removal of toxic metabolites. • High productivities 	<ul style="list-style-type: none"> • Effect of removal of secreted factors not fully understood as well as hydrodynamic effects of vessel
Fixed & Fluidized Bed	<ul style="list-style-type: none"> • Compatible with 3D scaffolding • Cellular interaction mimic <i>in vivo</i> structure 	<ul style="list-style-type: none"> • Scaling-up difficulties • Concentration gradients (Fixed bed) • Shear stress prone (Fluidized bed)

Modified from RODRIGUES, C.A.V., FERNANDES, T.G., DIOGO, M.M., DA SILVA, C.L. and CABRAL, J.M.S., 2011. Stem cell cultivation in bioreactors. *Biotechnology Advances*

The most commonly used platforms are stirred and shaken bioreactors. Continuous stirred-tank reactors are commonly used in bioprocessing, with the tissue engineering iteration developed from those used for fermentation of yeast (Martin and Vermette, 2005). A considerable proportion of work focusing on the use of MSCs in spinner flasks and stirred tank reactors utilises microcarriers with

the Mobius® 3L Bioreactor one of the first bioreactors reported to succeed in the expansion of hMSCs on microcarriers. A yield of 6×10^8 cells was obtained in a 2.4L working volume whilst retaining their basic cell characteristics and differentiation potential (Jing et al., 2013). Phenotypic properties have also been maintained in other studies carried out using the Biostat® B 1L and 5L after post-harvest analysis from microcarriers (Goh et al., 2013, Rafiq et al., 2013). Bone marrow derived MSCs (BM-MSCs) have also been successfully expanded in other stirred vessels, including the 1.3L Bioflo® reactor generating cell yields of approximately 1.4×10^5 cells/ml (Dos Santos et al., 2014). The added benefit of operating these vessels with different feeding strategies (batch, fed-batch, perfusion), adds flexibility in the supply of nutrients and reduces the level of undesired waste products (Rodrigues et al., 2011).

Establishing the correct impeller/stirrer speeds is critical when optimizing microcarrier based processes in stirred vessels, to determine the fluid dynamic conditions. Furthermore, the correct conditions are also needed to help promote efficient attachment of cells across the entire population of microcarriers. While agitation will ensure homogeneity of cell growth, the sensitivity of cell growth to hydrodynamic shear forces can result in cell lysis and altered cellular phenotypes (Cherry and Papoutsakis, 1988, Chen et al., 2013). However, with careful control and its associated benefits such as the affordable cost of equipment and the ease of process translation to a larger scale, allows spinner flasks to carry significant appeal in hMSC expansion.

The alternatives to spinner flasks are culture vessels agitated by an orbital motion. An estimated 90% of all mammalian cell culture experiments in biotechnology are carried out via this platform, with current trends looking at disposable versions of these shaken vessels for animal cell culture (Büchs, 2001). Studies have validated the efficacy of these systems up to scales of 1000L, showing efficient mixing and oxygen transfer (Zhang et al., 2009, Tissot et al., 2010). An additional advantage with shaken flasks when compared to other stirred bioreactor systems is the reduced formation of damaging bubble bursts due to air sparging (Olmos et al., 2015). The operating parameters that impact the bioprocessing factors (such as oxygen transfer, cell growth and cell viability)

include the flask's shape and size, the orbital agitation speed and diameter, and properties of liquid and particles within the flask (Büchs, 2001, Weheliye et al., 2013). The phenomenon of particle suspension is due to a combination of turbulent eddies, forces acting upon the particles (drag, buoyancy, gravity) along with particle interaction with the vessel and other particles. While stirred bioreactors have been studied thoroughly to understand the required agitation to suspend microcarriers, work is still being carried out on understanding the fluid dynamics within a shaken flask required to suspend particles. Studies have shown that the critical conditions that impact the suspension of microcarriers in a shaken vessel are the particle to liquid density ratios, geometrical ratios, the flask filling ratio and, to lesser extent, the particle to flask diameter ratio (Olmos et al., 2015).

Limited work has been carried out on understanding the expansion efficiency of microcarriers in an orbitally shaken system, and hence there is a great need to establish whether the simplest of vessel forms, could potentially provide the answer to culturing large quantities of shear sensitive mammalian cells.

1.7.1 Scaling orbitally shaken platforms

Immense importance has been placed on understanding the operating ranges required for effective cell culture using microcarriers, hence aiding translation to larger scales. Currently less than 2% of relevant publications have focused on the use of shaken bioreactors (flasks or microwells) limitations exist when trying to scale up shaken platforms to larger volumes and even to alternative reactor types such as stirred vessels (Büchs, 2001). Recently, progress has been made in understanding how fluid dynamics in orbitally shaken vessels are responsible for the suspension of microparticles, allowing the development of models establishing the minimal shaken speeds required to provide microcarrier suspension. The emergence of large shaken bioreactors at pilot and industrial scale has prompted greater clarification of mixing patterns and the awareness of spatial gradients. Previous work looked at using dimensionless analysis to establish macro-parameters such as power consumption and the volumetric mass transfer coefficient k_{La} , which provide an overall assessment of the bioreactor

rather than looking at flow dynamics at varying operating conditions (Zhang et al., 2005, Zhang et al., 2008).

The relationship between flow velocity in a cylindrical vessel, the orbital diameter of the shaker and the inner diameter of the well, allows for scaling between the various reactor sizes using a dimensionless scalable parameter, Froude number (Eq.1.1). The Froude number is the ratio between the characteristic flow velocity and the wave propagation velocity, where g is the gravitational acceleration, and V and l are the flow characteristic velocity and length scale respectively (Buchs et al., 2000).

In more recent studies, a further derivation of the fundamental equation has been developed which focuses on the ratios between inertial and gravitational forces to which Eq.1.2 is suggested. This equation is widely used in work carried out by Weheliye et al. and Ducci and Weheliye and for consistency will provide the basis of the work carried out in the project

$$Fr = \frac{v}{\sqrt{gl}} \quad (1.1)$$

$$Fr = \left(\frac{2do(\pi N)^2}{g} \right) \quad (1.2)$$

The Froude component provides a scaling parameter which provides better control over the process by determining an optimum window of operation. Ensuring effective mixing is essential, as the presence of spatial gradients in culture parameters produces heterogeneous cultures. To achieve such conditions, it was important to understand what types of mixing systems emerge within a well. According to Weheliye et al, during agitation, counter rotating toroidal vortices form (Figure 1.2). These vortices are present only in the upper part of the fluid in the well, which can be stated as Zone A. In the area below these vortices, Zone B, there is a relatively stagnant region of mixing due to lack of exposure to these vortices. Upon an increase in agitation speed, the vortices begin to extend to the bottom of the vessel with their intensity increasing in

magnitude, hence incorporating both zones within the mixing system. This distribution of different zones within the vessel were validated from previous experiments carried out at low shaker frequencies, producing what was stated as a convection zone (Zone A) and a diffusion zone (Zone B) (Tissot et al., 2010).

At higher agitation rates, a shift is seen towards a phenomenon known as out-of-phase flow, where the movement of the fluid is not in sync with that of the shaking platform. Such conditions are witnessed for vessels demonstrating $Fr > 0.4$, indicating most of the fluid is spread across the vessel wall (Weheliye et al., 2013).

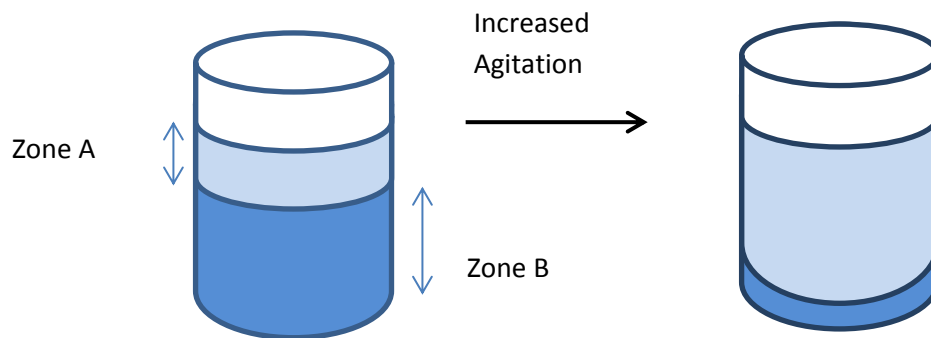


Figure 1.2 Mixing zones in a cylindrical vessel. The image highlights the change in height of mixing zone (Zone A) when fluid in a cylindrical vessel is subjected to increased agitation

Using the Froude number, studies then focused on the mixing and fluid dynamic in shaken bioreactors providing a detailed understanding of the single-phase flow created at different operating conditions including a range of orbital shaking speeds, internal diameters, orbital diameters, and filling volumes. A scaling law was derived to estimate the agitation rate at which this flow transition occurs, which is dependent upon the Froude number (Fr), the non-dimensional fluid height (h/d_i) and the non-dimensional orbital diameter (d_o/d_i). From these ratios two associated regimes are created whereby if $h/d_i \leq \sqrt{d_o/d_i}$ the Froude number can be obtained from Eq. 1.3, indicating that the active toroidal vortices reach the base of the cylindrical vessel before phase transition occurs, while if $h/d_i \geq \sqrt{d_o/d_i}$,

transition occurs without the toroidal vortex extending to the reactor base, hence Eq. 1.5 can be applied where h is the fluid height within the vessel, ao is the constant of proportionality ($ao = 1.4$ for fluid with water like characteristics) which is directly related to the fluid type and takes into consideration extra inertial forces, and d_i and d_o are the vessel inner diameter and the orbital diameter of the shaker, respectively. If Eq. 1.3 is satisfied, the transitional speed can be derived by using the critical wave amplitude from Eq. 1.4 (Weheliye et al., 2013).

$$Fr = \frac{1}{ao} \frac{h}{d_i} \left(\frac{d_o}{d_i} \right)^{0.5} \quad (1.3)$$

$$\left(\frac{d_o}{d_i} \right)^{0.5} = \left(\frac{\Delta h}{h_c} \right) \quad (1.4)$$

$$Fr_{di} = \frac{1}{ao} \quad (1.5)$$

The flow transition is dependent on the increase in size of the toroidal vortex with increasing agitation, N (i.e. Fr) and occurs when this vortex extends across the length of the cylindrical bioreactor. It was concluded that this phase transition is associated with more complete mixing of the fluid within the cylindrical vessel and is signalled upon reach Froude critical (Fr_c), corresponding to a critical agitation speed. Having established what Froude number is required to achieve complete mixing of the well, it can be assumed that particles of a specific size and density would be mixed in a similar manner within the cylindrical vessel, hence it is logical to assume that a homogenous suspension of microcarriers can be developed, controlled by specific orbital speeds.

1.7.2 Bioprocess forces

Static culture is a mode of material transport with many limitations due to the heterogeneous environment generated therefore supporting lower cell densities and cell numbers. To overcome mass transport issues associated with static culture, dynamic culture conditions are used (Panoskaltsis et al., 2005).

Hydrodynamic forces are ever present in bioprocesses, and influence cells particularly in stirred bioreactors. The diameter of a cell becomes an important factor when understanding these forces, because if the cell size is of similar magnitude to that of the turbulent Kolmogorov eddy size, damage will be induced, and this can be attributed to microcarriers as well as cell aggregates (Papoutsakis, 1991). When comparing either single cells, aggregates or cell supports, these known eddy sizes decrease with increased agitation, and hence at these agitation levels affect the large structures more. Furthermore, shear stress is also caused by the geometry, position and speed of the impeller used and further instruments such as probes, spargers and baffles also disturb the flow patterns exhibited (Gilbertson et al., 2006).

While this shear force can be monitored and controlled, there is a high possibility that exposure varies between different regions of a 3D structure (Yeatts et al., 2012). This effect is also true for nutrient and oxygen transport; however, unlike shear stress whose effects are known to effect osteoblastic differentiation, the role of oxygen is still not fully understood. Whilst commonly known that declining nutrient and oxygen level promote cell death some studies have shown that oxygen levels of 2% promoted cell proliferation and differentiation when compared to the exact same cell type in 20% oxygen (Grayson et al., 2007).

Enhancing biophysical signals in a developmental manner can improve the overall osteogenic process. Using perfusion systems (Sikavitsas et al., 2003, Grayson et al., 2008, Frohlich et al., 2010), and cyclic loading (Sittichokechaiwut et al., 2009) has been shown to improve osteogenesis by increasing mass transport and fluid shear to generate a homogenous bone construct. Mechanical stimulation has also shown to be influential on bone differentiation and the mineralization of the cells, due to fluid shear stresses (Bilodeau and Mantovani,

2006). It is stated that *in vivo* mechanical stresses instigate the remodelling of the bone, and hence this can be the basis for the hypothesis of fluid shear being responsible (Sikavitsas et al., 2001). It is the communication between terminally differentiated osteoblasts, known as osteocytes, and their link to osteo-progenitor cells that allow them to respond to shear stress. They tend to respond to shear stresses in the range of 8 to 30 dyn/cm² (Rubin et al., 2006). Just as the stated cells respond to shear *in vivo*, we can extrapolate that *in vitro* shear conditions should also affect bone cells. This can be seen from multiple studies which examined cells such as osteoblasts and MSCs alike and showed direct response to shear stresses (Grellier et al., 2009).

Studies have been carried out to indicate whether agitation can have an advantageous effect on proliferation and differentiation upon cells seeded on a 3D construct. This was done by the comparison of two methods for culture, spinner flask and static culture, whereby a stir bar and stir plate are used while scaffolds are suspended in culture. Spinner flasks are often used for culture of bone tissue as they promote the expression of alkaline phosphate and osteocalcin, osteoblastic markers which are present in lower values when in static culture and rotating-wall bioreactor. With static cultures, a gradient is established whereby nutrients are not sufficiently introduced into the centre of the scaffold. This is also evident in spinner flasks as studies have shown that osteoblastic lineage induced cells predominantly exist on the surface of the scaffolds (Sikavitsas et al., 2002). This is evidence that osteogenic differentiation occurs when exposed to shear, as the surface of the scaffold construct is exposed to a considerable amount of hydrodynamic stress (Wang et al., 2009). Results from such experiments also suggested that increasing agitation had an effect on osteoblastic differentiation due to higher expression of ALP (Yeatts and Fisher, 2011).

It is difficult to understand what parameters regarding shear stress have a direct effect on the proliferation of MSCs as shear frequency and magnitude are found to vary in many studies. Where some shear rates of high magnitude induce cell proliferation, the danger of cell death is possible, however limiting the levels could

potentially reduce levels of cell growth (Brindley et al., 2011). With all the efforts regarding the identification of the role of shear stress on the whole process of differentiation and proliferation of stem cells down a specific lineage, efforts were made to identify which stages of development showed the greatest response to shear forces. Hydrodynamic shear has also shown to be selective in proliferation, with MSCs showing decline in numbers where osteoblast proliferation flourished at a specific shear stress. This notion is known as osteogenic selection. This evidence shows that specific magnitudes of shear can be used to selectively promote the required lineage. Shear stress has a major effect on the transition through the osteogenic lineage effecting cellular/gene expression which can regulate the differentiation away from matrix production, to calcification and mineralization (Grellier et al., 2009). A study carried out by Kreke et al., aimed to identify which stages of osteoblastic differentiation are affected by the level and duration of shear stress. The first stages of differentiation are identified by proliferative effects (Lian and Stein, 1992), however surprisingly unlike prior studies carried out with rat bone mesenchymal stem cells (Nauman et al., 2001, Kreke and Goldstein, 2004) and neonatal calvarial osteoblasts (Klein-Nulend et al., 1996, Hillsley and Frangos, 1997) which showed the expected result, this study did not show proliferative signs (Kreke et al., 2005). Further studies show increase in proliferative levels such as the study carried out by Li et al., where bMSCs increased in cell number when stimulated by oscillatory flow (Li et al., 2004). From the contrast in results, shear-induced cell proliferation is dependent on multiple factors such as type of species used, mode of shear stress, magnitude of shear applied, as well as the stage of development of the cell.

After the early proliferative effects cease to exist, the latter stages of osteoblastic differentiation involve the expression of non-collagenous matrix proteins osteopontin, osteocalcin and bone sialoprotein (OPN, OCN, and BSP) (Lian and Stein, 1992). Expression of these late osteoblastic differentiation markers increased with prolonged exposure to shear stress, OPN and BSP in particular. Durations of 5, 30 and 120 minutes were used as periods of shear administration. While 30 and 120 minutes showed increased level of gene expression for the stated genes, 5 minutes did not seem a long enough period to enhance the levels of gene expression. The study carried out by Li et al., concurred with this data in

longer durations used generated higher levels of OPN and OCN genes when oscillatory flow was used (Li et al., 2004).

Shear stress can aid and control the osteogenic events that occur with MSCs by the activation of several regulating proteins known as metalloproteases (MMP's) and their respective inhibitors, tissue inhibitors of metalloproteases (TIMP). Main activity that occurs is associated with MMP2, MMP9, MMP13 and TIMP2, which all showed increased levels after mechanical stimulation in MSCs (Charoonpatrapong-Panyayong et al., 2007). The MMP13 is known to be highly involved in osteogenic differentiation of MSCs (Kasper et al., 2007). The exact extent of the effect MMPs have on osteogenesis is not fully understood, however hypothesis exist to suggest that mechanisms such as cryptic binding domains by cleavage of ECM components, release of matrix-bound bioactive molecules and alterations in matrix architecture and assembly aid cytoskeleton modifications (Mott and Werb, 2004).

Studies carried out *in vitro* suggest that the most sensitive cells to mechanical forces, such as shear stress, are the mature osteocytes which have a higher expression of prostaglandin E2 when mechanically stimulated, hence it was hypothesized that *in vivo*, a similar outcome is possible (Klein-Nulend et al., 1995). This could allow strategic shear manipulation to aid differentiation and proliferation when the more differentiated state is reached. However, other studies show that osteoblasts are affected by interstitial fluid flow as it promotes the release of nitric oxide (NO), an osteoblast mitogen. These studies used rat calvarial cells to identify whether fluid flow was the cause of this NO expression. Stationary culture produced negligible levels of NO; hence generating evidence to show fluid flow had an effect on proliferation and differentiation (Johnson et al., 1996). Although the level to which shear is needed was not identified, the magnitude was like other studies carried out using osteoblasts, with the varying results being down to the different organisms used. Further analysis indicates that there are two mechanisms related to mechano-sensation, based on nitric oxide levels. The first involves a response mechanism to steady shear, while the other involves calcium signalling and G-protein activation, which are sensitive to

transients in mechanical stress (Kreke et al., 2005). This potentially explains why certain cell types respond differently to different flow types (Jiang et al., 2002).

The correlation between the forces subjected upon stem cells and their resultant differentiation patterns, provides backing to the hypothesis that under controlled dynamic conditions and stimulation periods, cells can be proliferated and differentiated within one closed system.

Chapter 2 . Preliminary studies using human osteosarcoma cell line MG63 to determine efficacy of Ti-PGMs as a culture platform under static and dynamic conditions

2.1. Introduction

Human osteoblasts can be cultured on biomaterial substrates such as 45S5 BioGlass® and sol-gel derived 58S, produce collagenous ECM and ultimately bone nodules without the use of supplements or growth factors (Effah Kaufmann et al., 2000, Gough et al., 2004). When cultured on silicate-based glass materials, they can also upregulate the production of insulin growth factor II (IGF-II), resulting in a >3-fold increase in osteoblast proliferation (Xynos et al., 2001). Previous work has also demonstrated that human MG63 osteoblast-like cells can be cultured on phosphate glass discs (Abou Neel et al., 2008, Abou Neel and Knowles, 2008). The phosphate glass composition (50P₂O₅.30CaO.20Na₂O) makes it possible to dope ions into the glass by replacing Na₂O with, for example, TiO₂. Upon testing several concentrations of TiO₂ (0, 1, 3 and 5 mol%), 3 and 5 mol% were found to optimally support cell functions such as adhesion and proliferation, due to increased stability and reduced degradation. When compared to the control glass, the compositions containing TiO₂ at a concentration higher than 3 mol%, induced greater biological activity. However, concentrations beyond 5 mol% have not been studied in detail and so the full extent to which TiO₂ concentration exerts a dose-dependent response has not been determined. In addition to adhesion and proliferation, phosphate glasses containing 3 and 5 mol% quantities of TiO₂ upregulated the genes COL1A1, ALP, SPARC and CBFA1 (RUNX2), which are all associated with osteoblastic function (Abou Neel et al., 2007).

The efficacy of titanium phosphate glass microspheres (Ti-PGMs) to provide a platform for growth of MG63 cells is understood at a static level (Guedes et al., 2012). However, as suggested before, the application of this material should not be limited to static cell culture if it is to be used in tissue engineering at a commercially and clinically relevant scale.

The aim of this chapter was to undertake a preliminary study of whether Ti-PGMs can be used as a substrate for cell culture under dynamic culture conditions. The experiments were carried out using an MG63 cell line because these cells are a well-established tool for biocompatibility studies and their robustness enables bioprocess boundaries to be established (Abou Neel et al., 2009b, Guedes et al., 2012, Kiani et al., 2012, Lakhkar et al., 2012b). This inherent robustness and ability to rapidly proliferate on a majority of cell culture surfaces prevents a complete understanding from being established of the biomaterials ability to support clinically relevant cell types. Despite these limitations, human osteosarcoma cell lines allow to better understand osteoblast function because they initially represent clonal populations derived from the osteoblast lineage. However, in order that these cell lines produce data of physiological relevance, it is important that relevant cell lines are chosen for further investigation (Clover and Gowen, 1994)

Based on previous observations of the positive effect of fluid flow shear stress under laminar flow conditions (Kapur et al., 2003), it was hypothesized that dynamic agitation conditions would stimulate MG63 cell proliferation due to the associated fluid flow shear stress. As these cells are osteoblastic, it was expected that their tolerance to shear stress would be greater than that of immature mesenchymal stem cells, and the dynamic conditions induced further osteoblastic maturation. Furthermore, this chapter sought to examine whether the dose-dependent improvement in cell responses to TiO₂ would continue beyond 5 mol% and so an additional concentration of 7 mol% was tested. No higher concentrations were assessed due to significant increases in both density and stability reported with glasses containing TiO₂ above 10 mol%, limiting further their ability to be suspended (Abou Neel et al., 2008).

2.2 Materials & Methods

2.2.1 Formulation of glass

The phosphate glass compositions were manufactured according to techniques described in Abou Neel et al. (Abou Neel and Knowles, 2008), where stoichiometric quantities of the following precursor were mixed in a Seward Stomacher®400 Circulator (Wolf Laboratories, York, UK) at 200 rpm for 1 minute (unmodified purities of >99%, obtained from VWR-BDH, Poole, UK): phosphorus pentoxide, (P_2O_5), calcium carbonate ($CaCO_3$), sodium dihydrogen orthophosphate (NaH_2PO_4) and titanium dioxide (TiO_2). The precursor mix was consequently poured into a Pt/10% Rh type 71040 crucible (Johnson Matthey, Royston, UK). The process initiates with the removal of CO_2 and H_2O by preheating the composition at $700^\circ C$ and then melting the resulting mixture at a composition specific temperature listed below (Table 2.1). After melting at the conditions indicated, the glass is left to quench by pouring onto a steel plate at room temperature and allowing to cool overnight.

Table 2.1 Glass Compositions

Glass Composition	Composition Breakdown (mol.%)				Processing Temperature
	Calcium oxide	Sodium oxide	Phosphorous Pentoxide	Titanium Dioxide	Melting Temperature ($^\circ C$)/Time(h)
P50Ca30Na20 Ti0 (0 mol%)	30	20	50	0	1100/1
P50Ca30Na15 Ti5 (5 mol%)	30	15	50	5	1300/3
P50Ca30Na13 Ti7 (7 mol%)	30	13	50	7	1350/5.5

Modified from ABOU NEEL, E. A., CHRZANOWSKI, W. & KNOWLES, J. C. 2008. Effect of increasing titanium dioxide content on bulk and surface properties of phosphate-based glasses.

The quantities used in each of these compositions were calculated as follows with Ti5 as the basis of the example.

1) Sodium dihydrogen orthophosphate (NaH₂PO₄)

	2NaH ₂ PO ₄	→	Na ₂ O	+	P ₂ O ₅	+	2H ₂ O
Mol. wt. (g/mol)	240		62		142		36
Relative mol. wt. (g/mol)	1		0.26		0.59		0.15

Amount of NaH₂PO₄ required to produce 15 mol% Na₂O

$$= \frac{[(\text{Mol. fraction of Na}_2\text{O}) \times (\text{Mol. wt. of Na}_2\text{O})]}{(\text{Relative mol. wt. of Na}_2\text{O})}$$

$$= \frac{(0.15 \times 62)}{0.26}$$

$$= \mathbf{35.77g}$$

2) Phosphorus pentoxide (P₂O₅)

Amount of P₂O₅ produced in the reaction above

$$= (\text{amount of NaH}_2\text{PO}_4 \text{ required}) \times (\text{relative mol. wt. of P}_2\text{O}_5)$$

$$= 35.77 \times 0.59 = 21.10g$$

Amount of P₂O₅ required to produce 50 mol% P₂O₅

$$= 0.50 \times 142 = 71.00 g$$

Additional amount of P₂O₅

$$= 71.00 - 21.10$$

$$= \mathbf{49.9 g}$$

3) Calcium carbonate (CaCO₃)

	CaCO ₃	→	CaO	+	CO ₂
Mol. wt. (g/mol)	100		56		44
Relative mol. wt. (g/mol)	1		0.56		0.44

Amount of CaCO₃ needed in order to obtain 30 mol% CaO

$$= (0.3 \times 56)/0.56$$

$$= 30.00 \text{ g}$$

4) Titanium (IV) dioxide (TiO₂)

Mol. wt. of TiO₂ = 47.90 + (2 × 16)

$$= 79.9$$

Amount of TiO₂ to be added in order to obtain 5 mol% TiO₂

$$= 0.05 \times 79.9$$

$$= \mathbf{3.995 \text{ g}}$$

2.2.2 Preparation of Ti-PGMs

After a solid structure is formed, the quenched glass is then fragmented into microparticles with the use of manual methods using a mortar and pestle, and ball milling using a Retsch MM301 milling machine (Haan, Germany) operating at a frequency between 10-15 Hz. To separate the required fraction of microspheres for use during tissue culture, the particles were sieved (Endecotts Ltd, UK) down to 63µm-106µm using a sieve shaker (Fritsch GmbH, Germany). Studies have indicated that this range of microsphere as the optimal particle size for preparation due to fractions smaller than this range indicating ineffective particle spheroidization after fragmentation, while larger fractions having a

shorter residence time during the spheroidization step, generating irregular structure unsuitable for cell attachment and culture (Lakhkar et al., 2012b).

The glass microspheres generated after the sieving stage do not automatically possess a spherical structure required for ideal tissue adherence, therefore simplistic spheroidization apparatus were used to generate the required three-dimensional spherical structure. The spheroidization set up used was obtained from Lakhkar et al. and includes the following components: (1) blow torch, (2) feed and (3) collectors. The blow torch assembly is comprised of a Rothenberger Superfire 2 gas torch (Rothenberger Werkzeuge GmbH, Kelkheim, Germany), fitted to a 453g MAP-PLUS gas canister (Today's Tools, UK), a substitute for the standard MAPP gas (methylacetylene-propadiene propane) which generates a high flame temperature of 2925°C in the presence of oxygen. The feed consists of an aluminium trough (200 x 20 x 30 mm) with the outlet edge located ~10mm above the torch at an angle to the horizontal. A DC motor (15800 rpm, 4.5-15V, 35.8 mm diameter; RS Components, Corby, UK) is attached to the other end of the trough and is connected to a programmable power supply (RS Components, Corby, UK). A metal screw attached to the axle of the motor provides an offset, generating the vibrations required to propagate the microspheres through the trough, before entering the flame. The process occurs at its optimum when a programmable power supply of 4-6W is applied in a constant manner. The collecting section is comprised of 4 glass trays (275 x 150 x 60 mm) in an arrangement which sees the longer edges of each tray in contact with each other. The first tray is placed directly under the flame as to collect the particles that do not fall into the flame. Each consequent tray is placed in the axis of the flame as to collect any beads that enter its path. As the microparticles pass through the flame they undergo a spheroidization due to the surface tension forces and fall in to the 4 trays placed below (Lakhkar et al., 2012b).

After spheroidization, the microparticles in each tray are analysed using light microscopy to establish the proportion of spherical microparticles. Particles deposited in the first tray were discarded due to the mixture of non-spherical and

spherical particles exhibited. In the remaining trays, the proportion of non-spherical glass was minimal and therefore collected and stored for use in studies.

2.2.3 Preparation of MG63 cells

An MG63 cell line was used to assess the biological response to titanium doped biomaterials. These cells were obtained from in-house stocks (P3-P9) from the Biochemical Engineering Department, University College London which were stored in cryovials in liquid nitrogen. These cells were resuscitated by rapid thawing in a water bath at 37°C. Cells were first cultured in a 75cm² T-Flask at a seeding density of 1x10⁴ cells/cm² using Dulbecco's Modified Eagle Medium (DMEM) (1g/l glucose), supplemented with Fetal Bovine Serum (FBS) (10%) and antibiotic-antimycotic solution (1%) (all reagents acquired from Gibco®, Life Technologies Ltd., Paisley, UK unless specified otherwise) at 37°C and 5% CO₂. Cell passages were carried out when ~90% confluency was reached, established by visual observation through phase contrast microscopy. At this point, all existing media was removed, and the surface of the cells was washed with Phosphate Buffer Saline (PBS) (Sigma-Aldrich, UK) to remove any residual media; the cells were then incubated with 4ml 0.25% trypsin-ethylenediaminetetraacetic acid (Trypsin-EDTA) solution for 5 minutes at 37°C. Upon the conclusion of this step, the trypsin was inhibited by adding 8ml of fresh DMEM media; the resultant cell suspension was then transferred to an appropriate falcon tube and centrifuged at 300g for 3 minutes. The supernatant was carefully removed and discarded ensuring that the cell pellet formed wasn't disturbed. Based on the number of flasks harvested, an appropriate volume of fresh media was used to re-suspend the cell pellet prior to cell counting. Cell number quantification was carried out using a Neubauer haemocytometer and viability determined using Trypan blue dye exclusion method (Strober, 2001).

2.2.4 Cell culture on Ti-PGMs under static conditions in ultra-low attachment 96-well microplates

The static culture of MG63 cells was carried out in ultra-low attachment 96-well microplates (Corning® Costar®, Sigma-Aldrich, UK) to ensure that undesired cell

attachment didn't occur. A pre-calculated quantity of microspheres for each titanium concentration was inserted into wells of a 96-well microplate. The amount calculated was enough to cover the surface area of the well (5mg/well (± 0.1 mg)) in a monolayer. The calculation took into consideration the average cross-sectional area of the Ti-PGMs and the density of each material studied (0, 5 and 7 mol%). The beads were then UV sterilized for 1 hr and 40 minutes using a high intensity Blak-Ray B-100SP lamp (UVP, Cambridge, UK). The beads were then removed and equilibrated with 135 μ L of pre-warmed media to avoid direct contact of the cells with the dry surface of the microspheres. MG63 cells were trypsinized from the flasks to be used and cells were counted to ensure a sufficient amount was present for studies and controls. A cell density of 1×10^6 cells/ml was generated by either diluting or concentrating the cell solution accordingly, after which the MG63 cells were seeded on the microspheres (1.5×10^4 cells in 150 μ L of medium per well), upon which the plates were then incubated at 37°C in an atmosphere of 5% CO₂. A fed-batch system was applied, with spent medium replaced every 48 hours. Positive controls of 2D monolayer cultures of MG63s in Nunclon™ flat bottomed tissue culture 96-well microplates (Thermo Fisher Scientific, UK) were used to establish the relative cell attachment and growth on the microspheres. Static cultures were run with slow agitation (50rpm) for 5 minutes, prior to incubation, to ensure that there was even distribution of beads and cells in each well. Cells were cultured for 13 days with readings taken on days 1, 3, 5, 7, 9 and 13. with spent medium fully replaced every 48 hours. Media was extracted by tilting the microwell plate at an angle and aspirating media from the empty region of the well.

2.2.5 Cell culture on Ti-PGMs under dynamic conditions in ultra-low attachment 96-well microplates

Dynamic studies were carried out using ultra-low attachment plates placed on a KS260 control orbital shaker (IKA, Germany) with an orbital diameter of 10mm. Each well contained 5mg (± 0.1 mg) of beads and were seeded with 1.5×10^4 MG63 cells, comparable to the setup in the static studies. Plates were incubated at 37°C and 5% CO₂ for 24 hours overnight, to allow cells to adhere to the microspheres

before agitation. After 24 hours, the plates were transferred and secured to the orbital shaker. The plates were agitated for up to 13 days with readings taken on day 1, 3, 5, 7, 9 and 13 with spent medium fully replaced every 48 hours.

The agitation speeds used were selected based on relevant dimensionless numbers such as the Froude number (Fr). For this study, the Fr_c range calculated was 0.66 and 0.70, which took into consideration any changes in volume of media due to evaporation. These calculations were based on the directly and inversely proportional relationships between the non-dimensional fluid height h (min or max) and the non-dimensional wave amplitude (Eq.1.3).

$$\frac{h}{di} = a_o \left(\frac{h}{\Delta h} \right)_c Fr_c \quad (2.1)$$

Using the constant of proportionality α_o , a Froude number was generated (Eq. 2.1.) which was then used to calculate N , agitation speed from Equation 1.2 (Weheliye et al., 2013). A critical agitation rate was calculated to be 340-350rpm (Appendix A.1), with the range accommodating any evaporation affecting fluid height. Agitation speeds higher than the critical values would correspond to the single processing vortex flow pattern, explained in Chapter 1, and would correspond to higher turbulence levels. It can be therefore postulated that this flow pattern would correspond to a better microsphere suspension, albeit with more damage caused to the growing cells. Whilst a multitude of commercially available microcarriers are available with densities like water (1030kg/m^3 (Cytodex-1) – 1242 kg/m^3 (Sephadex G10)) (Olmos et al., 2015), the Ti-PGMs are characterised by density of 2.6-2.7 times the density of water. This property could potentially cause attached cells to be subjected to extremely high levels of shear at speeds of 340rpm, at which point the toroidal vortices would reach a relatively stagnant layer of microspheres, due to their densities limiting their ability to be suspended. To understand whether the benefits of agitated conditions could be exploited when used with this material, two different speeds were studied, 150 and 300 rpm, based upon the hypothesis that at a lower agitation speed than that

calculated at N_c , partial vessel mixing could result in increased vessel homogeneity, improved metabolism, and overall increased proliferation.

Upon cell seeding, agitation was administered for 5 minutes to ensure a homogenous distribution of cells and microspheres were present in each well. To allow for cells to adhere effectively the plates were left in static conditions for 24 hours, after which each agitation speed to be studied was applied. Limitations arose when carrying out the dynamic studies due to only one orbital shaker available with the same orbital diameter. This required carrying out each speed with different batches of MG63 cells, therefore calibration curves were required for each individual run carried. Furthermore, for each run a static control was always present to further increase the reliability of the study. By including a static control when carrying out the 150rpm and 300rpm study, three static runs were available to illustrate the comparability of each run and to also provide the basis to carry out statistics analysis on the three conditions; static, 150rpm and 300rpm.

2.2.6 Cell proliferation assay

The cell proliferation on each type of the microspheres in both static and dynamic conditions was measured using the Cell Counting Kit-8 (CCK-8) cell proliferation assay (Dojindo EU, Germany). Each CCK-8 test required 10 μ L of CCK assay for 100 μ L of media (10% v.v⁻¹) which would contain the Ti-PGMs and MG63 cells. After incubation with the assay, the resulting solution was aspirated into Nunclon™ flat bottomed tissue culture 96-well microplates leaving behind the microspheres and cells due to their interference with the spectrophotometer laser. All time points were assayed in triplicate with a mean and standard deviation calculated. At different points up to day 13, optical densities were measured at a wavelength of 450-490nm in a Safire2 plate reader (Tecan, UK). Cells cultured in the tissue culture grade plates were used as a positive control due to their ability to enhance cell proliferation. The absorbance reading provided would correlate to the number of cells; therefore, a calibration curve would be plotted prior to any cell viability calculations to establish the correlation of absorbance to cell number. The standard calibration curve allowed correlation between cell population in multiples of 1×10^3 (1×10^3 , 5×10^3 , 1×10^4 , 1.5×10^4 ,

2×10^4 , 3×10^4 , 4×10^4 , 5×10^4 and 6×10^4) and absorbance. To produce an accurate calibration curve, cells would be seeded in a tissue culture grade 96-well microplate in the aforementioned quantities, allowing them to fully attach (approx. 3 hours), before carrying out the CCK-8 protocol. The period used was to ensure that cell proliferation was kept to a minimum and the seeding densities were accurate representations of the absorbance provided. The attachment of cells was qualitatively estimated using a phase contrast microscope.

2.2.7 Metabolite analysis

Offline glucose and lactate analysis was carried out using a YSI bioanalyser (YSI Life Sciences, Yellow Springs, Ohio, USA) at days 1, 3, 5, 7, 9, and 13. Samples of various volumes depending on the overall volume of media present were taken and kept in 1ml Eppendorf tubes. This was to ensure that 100 μ L of media was available for the cell proliferation assay procedure (mentioned above), and to compensate for any evaporation of media that occurred during incubation. Each aliquot was kept in ice to ensure that the media did not reach a temperature below 4°C, preventing further metabolic activity or degradation. All samples were assayed in triplicate for consistency with a mean and standard deviation calculated.

2.2.8 Phase contrast microscopy imaging

Imaging of the well was carried out using an EVOS™ XL Cell Imaging System with images taken on the same days as the cell proliferation assay and metabolite readings. The samples were imaged prior to the addition of the assay, due to the colorimetric nature of the CCK-8 reducing agent. The lid of each of the plates to be imaged would be changed to a sterile version to reduce interference of any condensation present on the lid. Images were taken at 2x and 20x magnification to aid understanding of the complete well distribution and microsphere-cell cluster structure respectively. Properties of the image such as the level of lighting and focus were maintained at the same level for ease of comparison. Effort was made to ensure that the images used would represent the wells clearly and that no bias existed in selecting wells.

2.2.9 Confocal laser scanning microscopy imaging

Cell staining procedures were carried out to label the actin filaments of the cytoskeleton and the cell nucleus. Cells were first washed *in situ* in PBS, fixed with 4% paraformaldehyde (PFA) for 10 minutes at room temperature, once again washed twice with PBS, and consequently permeabilized with 0.5% Triton X-100 in PBS for 5 min at room temperature. The resulting cultures having had the Triton X removed, were then stained with Acti-Stain™ 488 phalloidin (2.5 vol% phalloidin methanolic stock solution in PBS) (Invitrogen, UK) for 20 minutes at room temperature in a dark chamber to reduce photobleaching and evaporation. Counter-staining with propidium iodide (PI) was carried out by staining the cells with a 1 µg/ml PI solution for 10 minutes also in dark conditions. Phalloidin and PI labelling were visualized under a Radiance 2100 confocal microscope (BioRad, Loughborough, UK).

2.2.10 Statistical analysis

All statistical analysis was carried out using IBM SPSS Statistics version 22. First and foremost, the data sets were analysed using a normality test (Shapiro-Wilks test) revealing that specific data sets did not have a normal distribution. The normally distributed data would then be examined for equal variance using the Levene's Statistics Test, at which point a one-way ANOVA would be carried out if the assumption of equal variance had not been violated. If the assumption of equal variance had been rejected, a Robust Tests of Equality of Means would be carried out using the powerful Brown-Forsythe test. Depending on the Levene's test and Brown-Forsythe test, a suitable post-hoc analysis was carried out to establish the significance; tests used were the Tukey Honest Significant Difference (HSD) and Games-Howell test depending on whether the data showed equal variance or unequal variance respectively. If the Shapiro-Wilks test indicated that the data wasn't normally distributed ($p \leq 0.05$) non-parametric tests were used, specifically the Kruskal-Wallis H test and Mann-Whitney U test depending on the number of variables. Consequently, multiple pairwise comparisons were made with corrections using the Bonferroni correction method. The level of significance assumed for statistical tests was 0.05, with the Bonferroni correction implemented by multiplying the calculated p-value

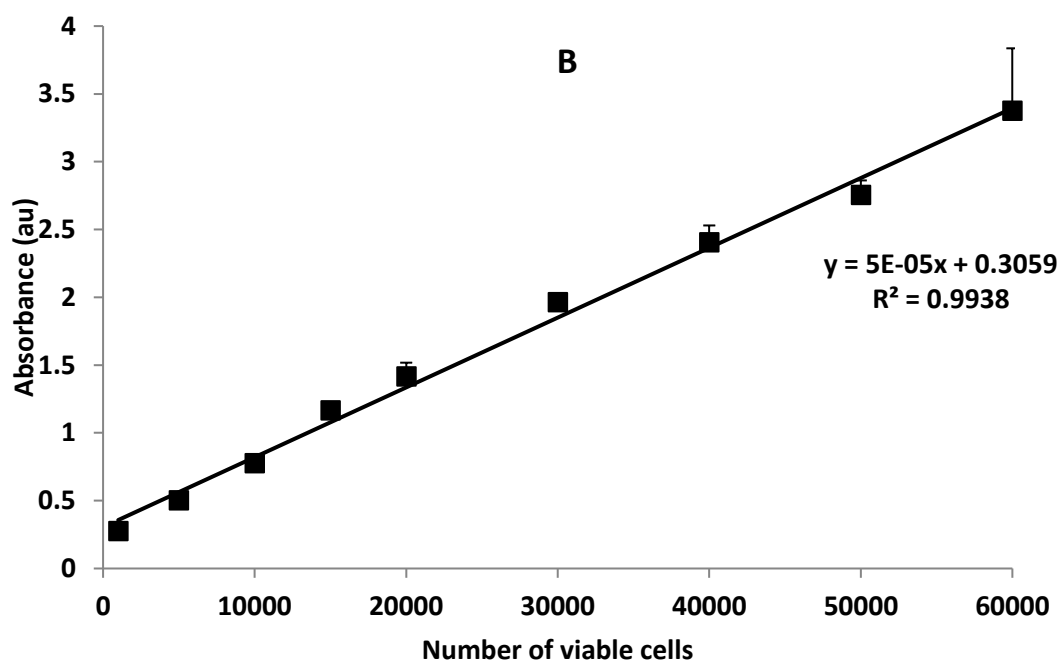
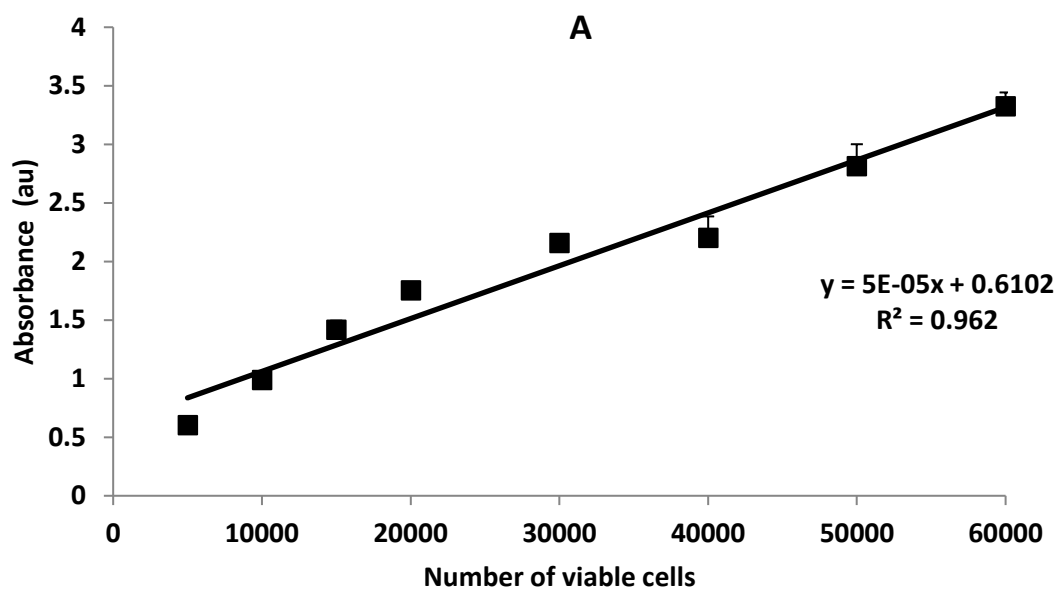
significance by the number of pairwise comparisons. The relevant statistical significance is illustrated on the graphical representations of the data which was produced in bar chart form. The repeats indicated with each figure identify the number of technical repeats rather than biological repeats, unless otherwise stated.

2.3 Results

2.3.1 Cell proliferation of MG63 cells cultured on Ti-PGMs under static and dynamic conditions

In the first experiment, cell proliferation was assessed on two different Ti-PGMs compositions (5 and 7 mol %) and compared to control tissue culture plastic (TCP) 96-well microplates. Prior to calculating the viable cell number an appropriate standard calibration curve was produced as shown in Figure 2.1 for each experiment run to account for batch variation.

Using the standard curve equations produced in Figure 2.1, allowed the data obtained from the CCK-8 proliferation assay over the 13-day period to be converted to a viable cell count from their respective absorbance values. Figure 2.2 shows the results of the CCK-8 cell proliferation assay carried out over the 13 days on the three different materials (Ti5, Ti7 and TCP) under the three different conditions; 0, 150 and 300rpm. Phosphate glass with 0 mol% TiO₂ doping has not been included due to the excessive degradation of the material within 24 hours of *in vitro* studies. The remaining compositions of phosphate glass promoted significant cellular growth from day 1 onwards. Glasses containing 5 mol% of TiO₂ cultured with MG63 cells showed increases in viable cell numbers between day 1 and day 9 under static and 150 rpm conditions while with 300rpm these increases were delayed until day 13. Viable cell number declined under static conditions on Ti5 after day 9 with a 25% decrease in cell number on day 13, whereas dynamic conditions resulted in significantly higher cell numbers when compared to static conditions (*p<0.05). Viable cell number under 300rpm agitation was significantly less on day 9 when compared to 150rpm (*p<0.05). Cell proliferation on Ti7 was similar to Ti5 over the course of the experiment. Significant differences were not documented between the different conditions when cells were cultured on Ti7. In comparison, cells cultured on TCP showed that under all agitation conditions, cells thrive early on with significant increases in cell numbers after only one day, however cell cultured in 300rpm conditions showed lower increases in cell numbers within the first 72 hours (*p<0.05).



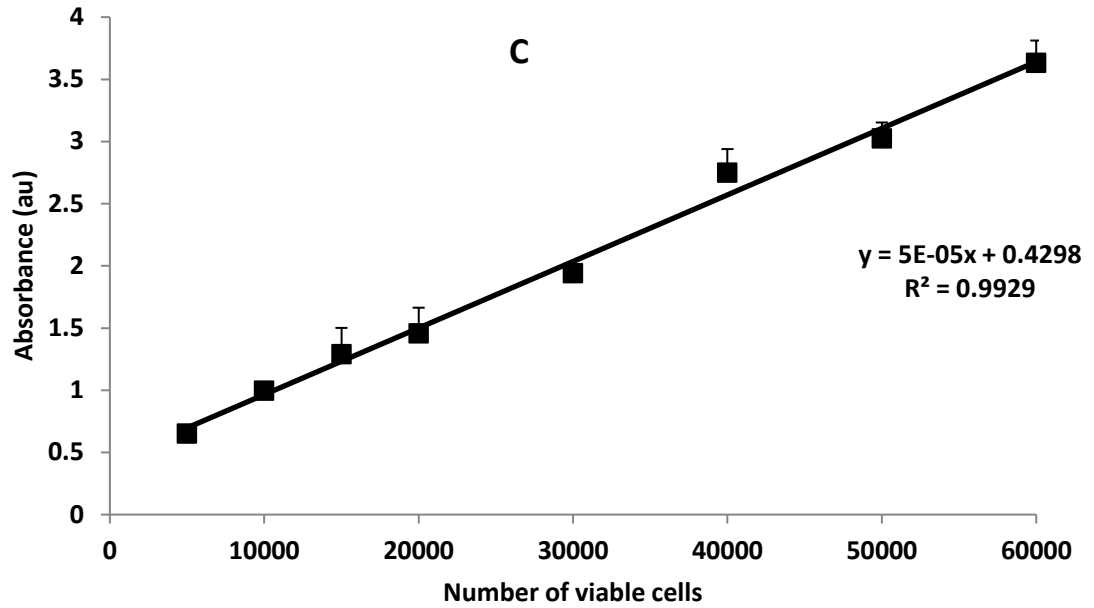


Figure 2.1 Standard curve of MG63 cell growth on tissue culture grade 96-well microplates. Line graph plotted as Absorbance (nm) versus Number of viable cells after using a CCK-8 proliferation assay upon complete attachment of the cells for the experiments involving the following conditions: (A) Static (B) 150rpm and (C) 300rpm. Absorbance based on a wavelength of 450nm. Values represent mean \pm SD (n=6)

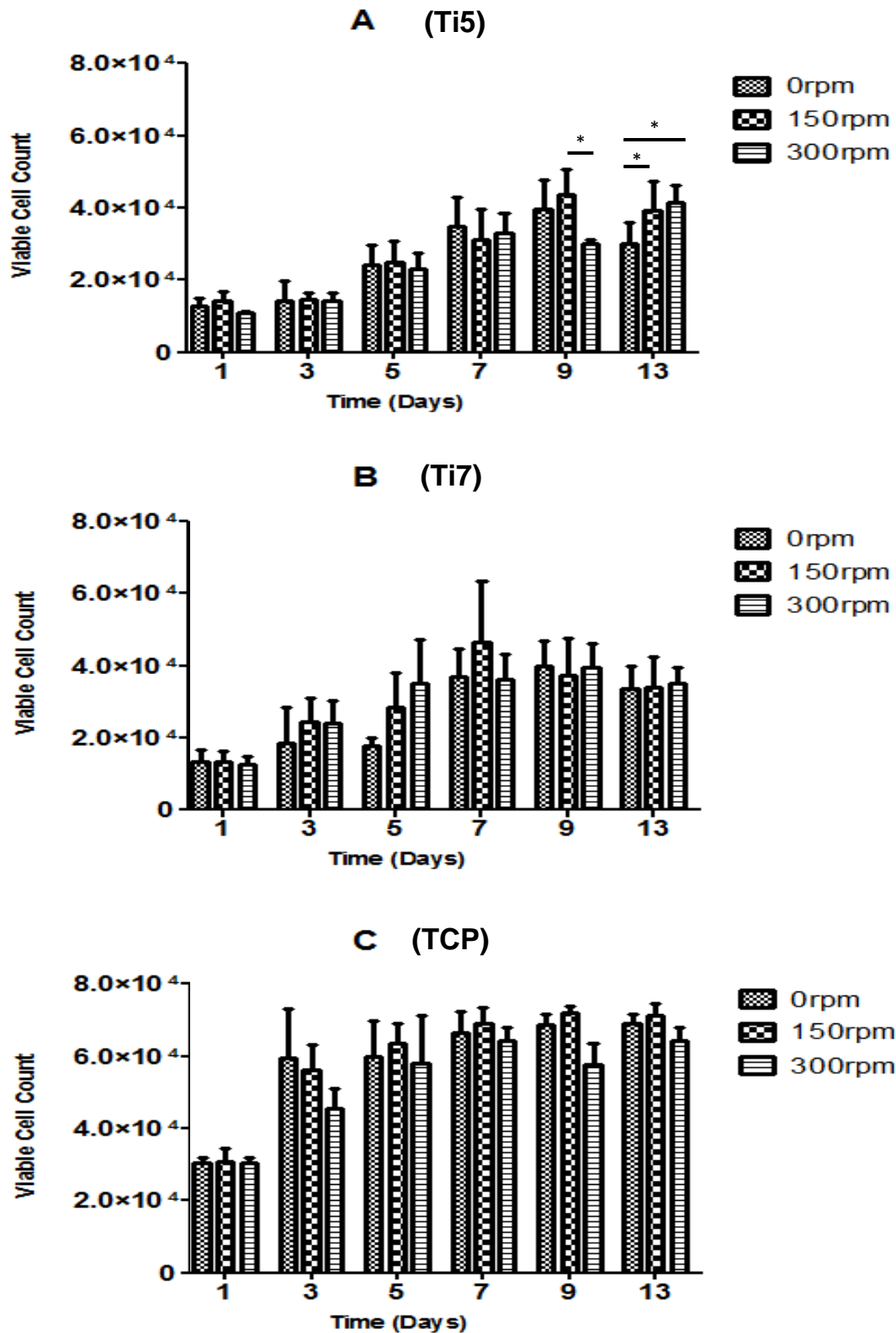


Figure 2.2 MG63 proliferation on (A) Ti5 (B) Ti7 microspheres in ultra-low attachment culture plates and (C) TCP (control). Bar charts comparing CCK-8 assay readings were at days 0, 1, 3, 5, 7, 9 and 13 under static and dynamic conditions. Values represent mean \pm SD (n=3). * indicates $p < 0.05$.

The overall best condition for supporting and proliferating MG63 cells on phosphate glass microspheres and on TCP is at 150rpm agitation (Table 2.2). The cell yields achieved under this speed are at least 5% higher than the other respective conditions for each material. While the two different phosphate glass materials produced similar values of fold increase in cell number, the cell yields achieved by TCP are significantly higher with a 42% difference to the next highest candidate within the agitation speed (*p<0.05).

Table 2.2 Fold increase values indicating the maximum cells yield achieved over the course of the experiment under the different conditions and materials used. Values within brackets indicate the time point maximum yield was achieved.

Material	Condition (Day)		
	0rpm	150rpm	300rpm
Ti5	2.64 (9)	2.92 (9)	2.77 (13)
Ti7	2.65 (9)	3.10 (7)	2.63 (9)
TCP	4.59 (13)	4.80 (9)	4.29 (13)

When assessing the same data based on material composition, there were limited differences between Ti5 and Ti7 with no significant differences at all three speeds studied (Figure 2.3). When compared to the TCP surface, there is a stark difference with cell proliferation on Ti-PGM. The cell numbers cultured on TCP were significantly higher across each day assessed when compared to the phosphate glass compositions on both static and 150rpm (*p<0.05) with 300rpm showing the same trend (*p<0.05) except on day 5 where there were no significant differences between Ti7 and TCP.

The maximum cell yield achieved under static conditions was expectedly highest with TCP across all the materials studied where 150rpm provided the highest overall cell yield at a 4.79-fold increase in cell numbers at day 9. When analysing the maximum yields produced by the two different phosphate glasses Ti7 produced its highest cell yield on day 7 with a 3.10-fold increase in cell number while Ti5 achieved a 2.9-fold increase on day 9 both occurring under 150rpm conditions.

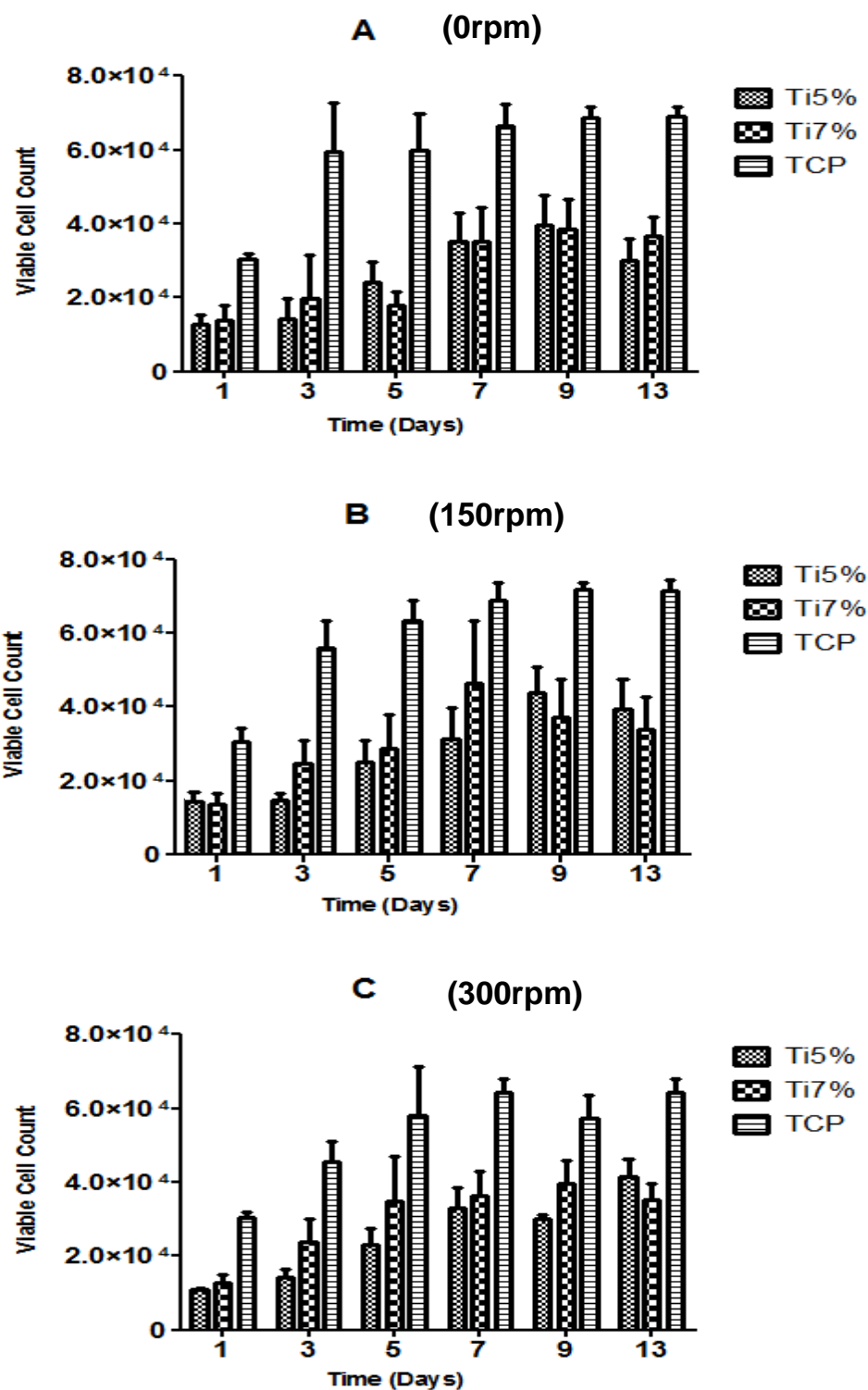


Figure 2.3 MG63 proliferation under (A) 0rpm (B) 150rpm and (C) 300rpm conditions at days 0,1, 3, 5, 7, 9 and 13 cultured on the two TiO₂ compositions and TCP represented via a bar chart. Error bars represents \pm SD (n=3). For representation purposes the significance between TCP and the phosphate glasses have not been indicated on the graph, however have been discussed further in the results.

As these experiments were undertaken in batches, the consistency across experiments was determined (Figure 2.4). Static cultures using Ti-PGMs were used as controls during each of the separately run 150rpm and 300rpm studies, therefore by showing that there are no significant differences amongst the three static cell proliferation profiles, it is possible to make comparisons across the different experiments.

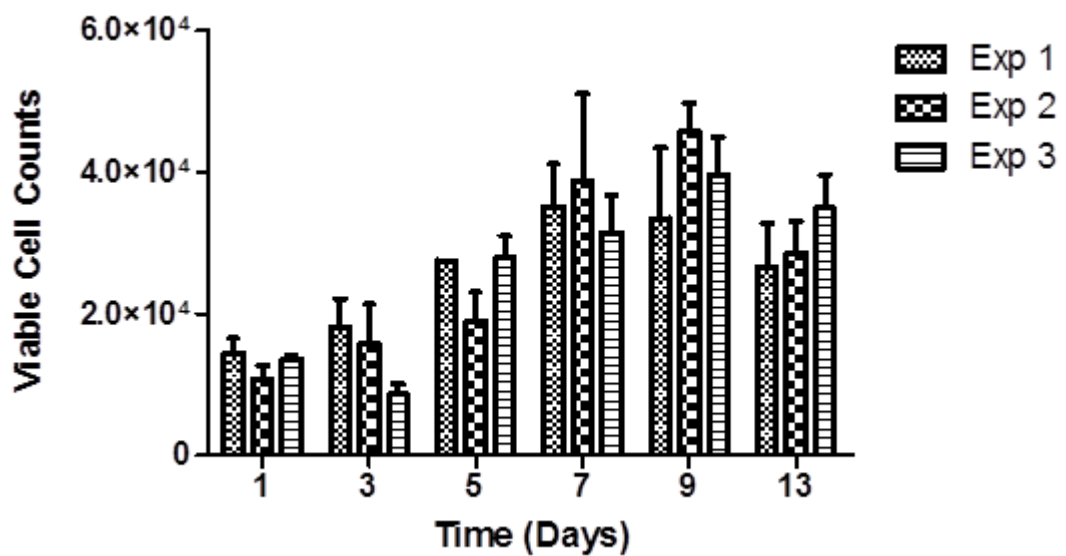


Figure 2.4 Comparison of different MG63 proliferation profiles under static conditions over 13 days on Ti5. Bar charts Exp 1, 2 and 3 denote three different static runs which were used as controls carried out in parallel with the dynamic studies (150rpm, 300rpm). Exp 1- Static only Exp 2- Static control for 150rpm study and Exp-3 Static control for 300rpm study. Values represent mean ± SD (n=3).

2.3.2 Impact of agitation rates on MG63 cell metabolism

Next, the metabolic activity of cells in culture was profiled (Figure 2.5). The profiles show the different level of glucose consumption and consequent lactate production under each condition investigated. The glucose profile for MG63 cells grown on Ti5 shows that more glucose was consumed by the cells in 96-well plates agitated under 150rpm conditions compared to static conditions at day 7 (*p<0.05). This trend continued through day 9 (*p<0.05) and by day 13 both dynamic conditions led to significantly higher levels of glucose consumption

compared to static conditions (** $p < 0.05$). The profiles for lactate production followed a similar trend in that cells cultured at 150rpm produced significantly higher amounts of lactate through the course of 13 days compared to static conditions ($p < 0.05$). By day 13 the MG63 cells agitated at 150rpm produced more lactate than both static (** $p < 0.001$) and 300rpm ($p < 0.05$), with both dynamic conditions producing higher amounts of lactate than the MG63 cells in static culture. Surprisingly, cells cultured on phosphate glass doped with 7 mol% of TiO₂ showed different trends in glucose consumption. The differences seen between conditions for cells cultured on Ti7 occurred earlier than with Ti5, where static and 150rpm conditions led to greater glucose consumption compared to the 300rpm condition up to day 5 ($p < 0.05$). By day 13 cells cultured under static conditions did not have as high glucose consumption compared to the dynamic conditions ($p < 0.05$). There were no significant differences in metabolite concentration between the different agitation speeds when cells were cultured on the TCP control. The lactate profile of cells cultured on TCP also showed minimal differences during the first nine days of culture. However, on day 5 the level of lactate production began to decrease and at day 13 an extremely significant difference could be seen between 300rpm and the other two conditions ($p < 0.05$).

When comparing this data across materials at a given agitation rate, Ti5 resulted in significantly lower levels of glucose consumption when compared to Ti7 and TCP surfaces between days 3 to 5 (** $p < 0.01$), in both static and 150rpm conditions. Under static conditions TCP reached minimal glucose levels towards day 13 of culture, whereas Ti7 showed reduced consumption of glucose when compared to day 9 with glucose concentration changing from 0.052 g/l to 0.13 g/l. Overall glucose consumption was higher under 150rpm agitation when compared to the other conditions across all the different culture surfaces. The change in level of glucose consumptions across 0 and 150 rpm, were mimicked by the opposing change in lactate concentrations. This trend however was not visible at 300rpm for TCP and Ti7, as lactate levels decreased at a point where glucose levels reached their limit.

Glucose

Lactate

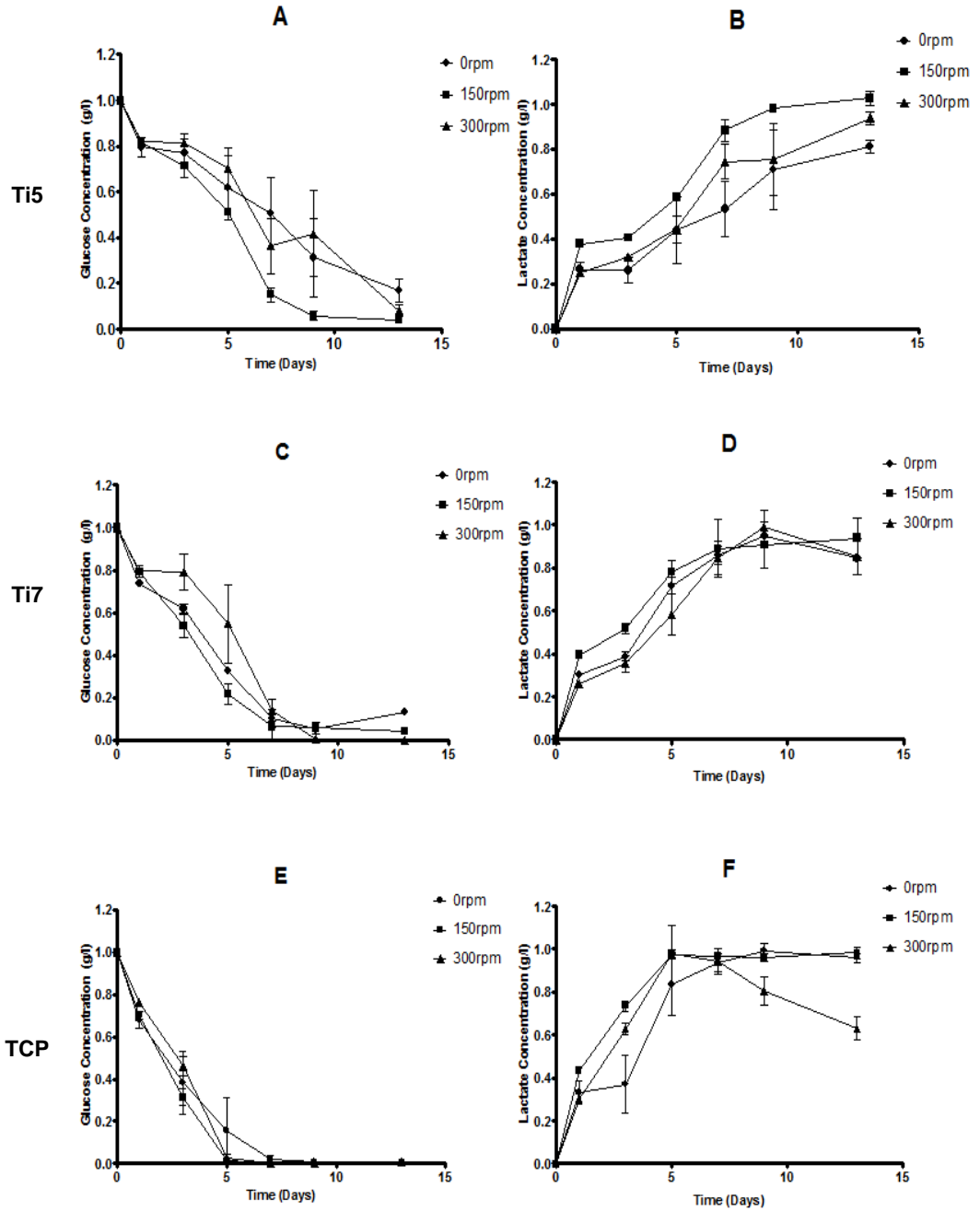


Figure 2.5 MG63 metabolic profiles for glucose consumption and lactate production based on agitation rate. Line graph represent glucose consumption (A, C, E) and lactate production (B, D, E) when cultured on Ti5 (A & B), Ti7 (C&D), and TCP (E & F) at days 0, 1, 3, 5, 7, 9 and 13 under ●- 0rpm ■- 150rpm and ▲-300rpm condition. Values represent mean ± SD (n=3).

Glucose

Lactate

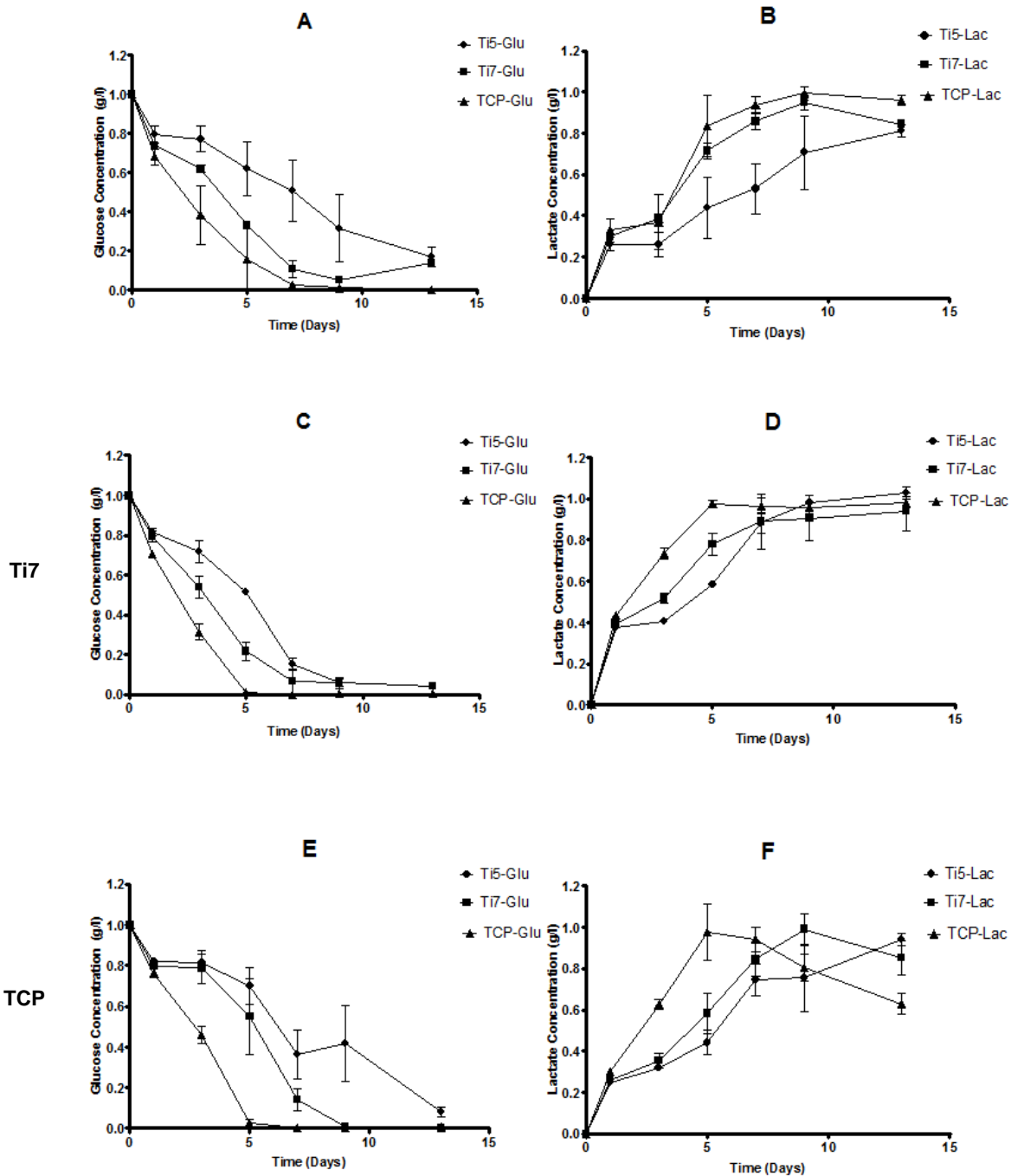


Figure 2.6 MG63 metabolic profiles for glucose consumption and lactate production based on culture material. Line graph represents glucose consumption (A, C, E) and lactate production (B, D, E) under 0rpm (A & B), 150rpm (C&D), and 300rpm (E & F) conditions at days 0, 1, 3, 5, 7, 9 and 13 when cells are culture on ●- Ti5 ■- Ti7 and ▲TCP. Values represent mean \pm SD (n=3).

2.3.3 Macroscopic evaluation of MG63 cell-Ti-PGMs clustering

Cells were imaged over the course of the experiment. Figure 2.7 shows cell distribution throughout the well, including presence of spaces between adjacent microspheres in the monolayer. As the ultra-low attachment plates were maintained in static conditions for the first 24 hours to allow settling of cells, there is no distinguishable difference between the day 1 images for any of the conditions, with the images showing cells scattered evenly amongst the microspheres on both Ti5 and Ti7 materials. By day 13, cells have formed networks bridging between microspheres, consequently bringing them together and forming densely packed clusters. The darker areas seen in each of the images show densely populated clusters of microspheres and cellular material. The opaque nature of the images indicates a multi-layered structure consisting of at least two layers of microspheres. There is no system or regularity in which these structures are formed, and their formations in even static conditions indicate that fluid flow created by orbital agitation isn't a prerequisite for allowing cells to bridge and form networks between the materials.

Macroscopic images were taken to show the extent of clustering of cell-microcarrier material across the whole well (Figure 2.8). As stated above there were no differences at day 1, but at day 3 it can be observed there are clear differences in the impact orbital agitation has upon the formation of microsphere clusters. The darker areas visible inside each of the wells corresponds to the denser structures that were noted in Figure 2.7. Under static conditions there are a large amount of small microunits already formed. When you compare these structures to the clusters formed under 150rpm and 300rpm, the sizes of these units are on average smaller in size and larger in quantity. When comparing the two orbitally agitated plates, while there doesn't seem to be a difference in cluster size between the two speeds, the numbers of clusters formed seem to be higher in 150rpm, based upon the visible empty areas within the well. As can be seen from Figure 2.8, by day 9 the clusters formed in static and 150rpm have developed into macrostructures and incorporate a vast quantity of microcarriers initially seeded in the well. The structure in the static plate is less uniform than that visible in 150rpm with large parts of the structure seeming to be in the initial stages of integration into the main structure.

The microunits formed in 300rpm are comparably smaller than those produced under static and 150rpm conditions. Furthermore, the quantity of clusters formed and number of microcarriers remaining suggests that increasing the rate of agitation is limiting the ability of the clusters incorporating the microspheres adjacent, illustrated by a large proportion of microspheres remaining unused by day 13.

However, the image in Figure 2.8 for day 13 under 300rpm conditions shows a large quantity of microspheres remaining, while the cell proliferation assay (Figure 2.2 (A)) indicates that 300rpm has the highest viable cell count. There are two potential reasons for this lack of agreement between the cell proliferation assay on Figure 2.2 (A) and the phase contrast images of Figure 2.8: firstly, the aggregates may contain an apoptotic core, where only cells that form the periphery of the clusters represent the cell numbers in Figure 2.2 (A), or that the CCK-8 assay was unable to effectively penetrate through the thick collagenous matrix produced by the MG63 cells evident from Figure 2.7. It is important that multiple analytical techniques are used to generate a conclusive picture of what occurs within each of the wells.

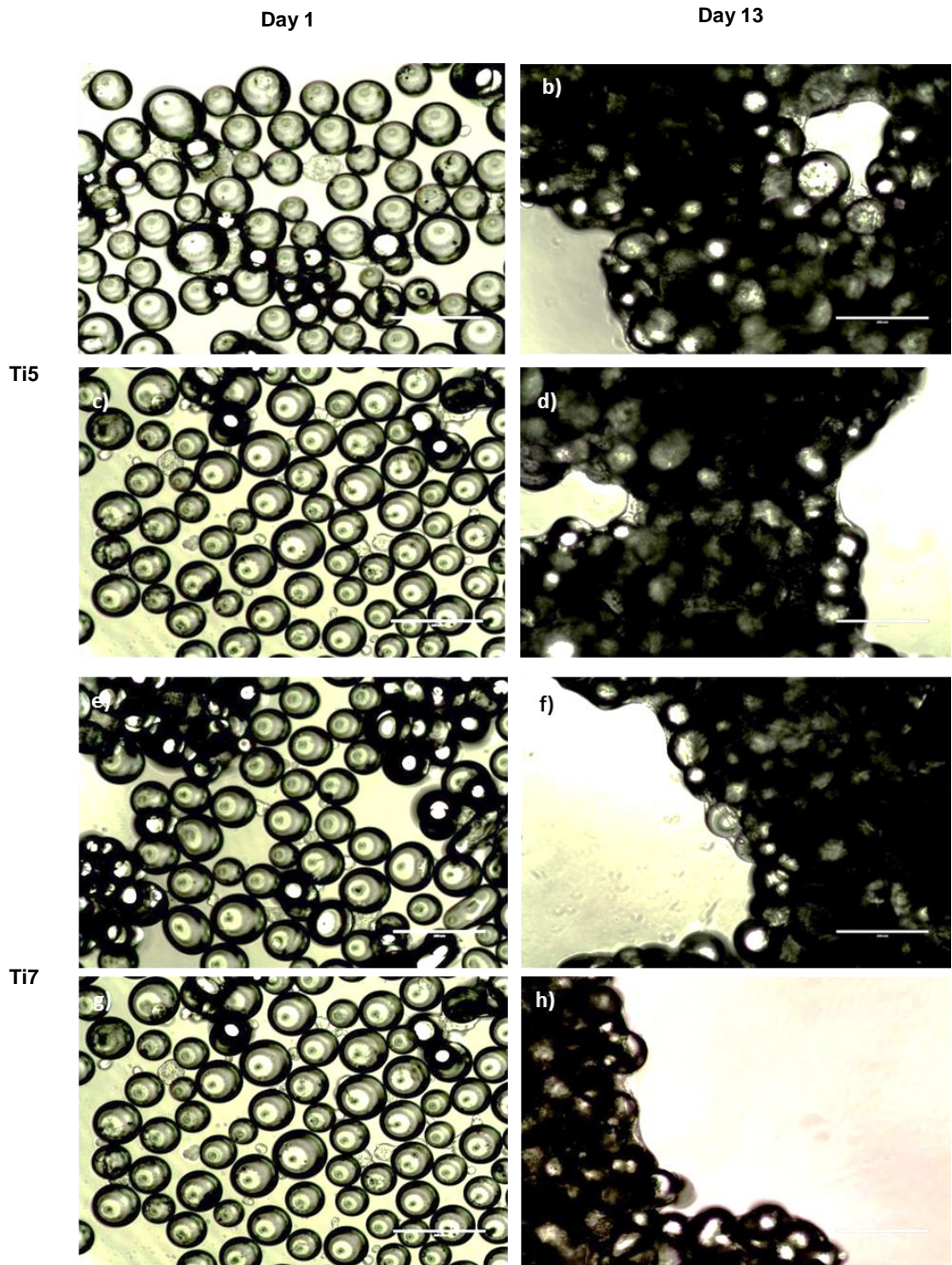


Figure 2.7 Formation of networks between MG63 cells and Ti-PGMs under different agitation rates. Phase contrast images illustrating MG63 cultured on Ti-PGMs over a 13-day period. Images of phosphate glasses doped with 5 mol% (a-d) and 7 mol% (e-h) were taken on day 1 (a, c, e, and g) and day 13 (b, d, f, and h) cultured under static (a, b, e, and f) and 150rpm (c, d, g, and h) conditions. Images were taken under 20x magnifications where scale bars represent 200 μ m

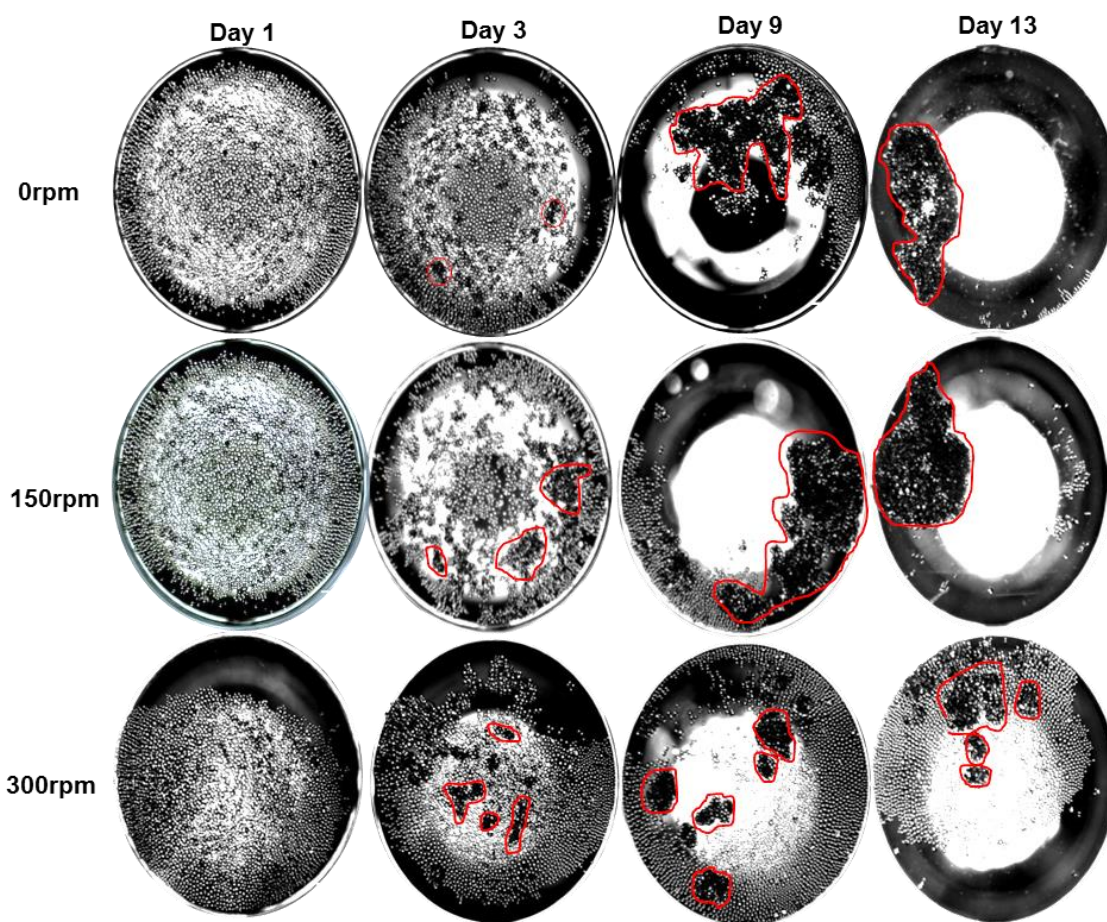


Figure 2.8 Formation of Ti-PGM-cell clusters under different agitation rates. Phase contrast microscopy images of individual wells illustrating MG63 cells cultured on Ti5 over a 13-day period using the same well from day 3 onwards. Red markings highlight areas of clustering. Images were taken under 2x magnification.

2.3.4 Matrix deposition by MG63 cells on Ti-PGMs

To further characterise the nature of MG63 cell interactions with TiO₂ microspheres, imaging was undertaken using confocal laser scanning microscopy. Representative images in Figure 2.9 show cells attached to Ti5 microspheres at day 13 post culture. The cells actin filaments are clearly stained with phalloidin, illustrating good alignment along the curved surface evenly covering the entire microsphere (Figure 2.9b). Processes developed from the edges of the cells, aided the bridging between multiple microspheres forming clusters of cell-microsphere aggregates. The spaces between microspheres are densely populated with MG63 cells (Figure 2.9a).

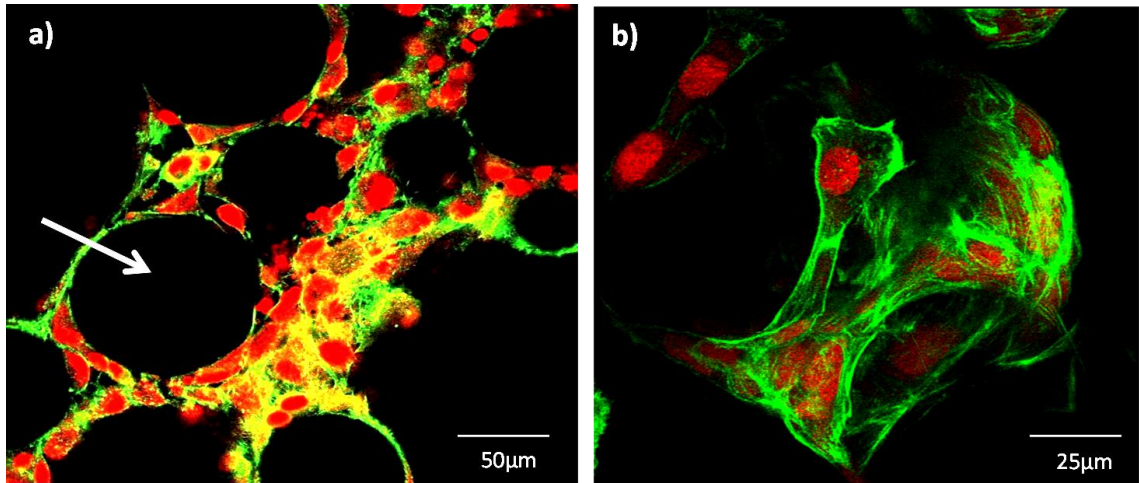


Figure 2.9 MG63 cells attached to Ti5 glass microspheres on day 13 under 150rpm conditions using confocal laser scanning microscopy. Phalloidin stain was used to identify the actin filaments of the cytoskeleton (green) while the propidium iodide (PI) stain was used for the nuclear staining (red). Image a) provides a sliced cross-section through a cluster of microspheres cultured with MG63 cells, while image b) illustrates a 3D rendered image of an individual microsphere. Scale bar is a) 50µm and b) 25 µm respectively.

2.4 Discussion

The present study examined the interaction between Ti-PGMs and MG63 osteosarcoma cells under two types of conditions: (1) static and (2) dynamic culture on ultra-low attachment cell culture plates. The dynamic culture speeds studied were predetermined using the scalable mixing dimensionless Froude number, which provided the critical agitation speed, 340rpm. The aim was to understand whether Ti-PGMs could be used in a dynamic bioprocess environment to support the growth of osteoblastic cells that will underpin the creation of tissue engineered bone. Within this study, we wanted to know whether increasing the quantity of TiO₂ within the microsphere would promote further proliferation of MG63 cells based on improved structural stability and surface properties. The results obtained from the study provide a preliminary insight into the biocompatibility of the Ti-PGMs and provide a basis for the subsequent results chapters.

Firstly, the microspheres produced were cultured with MG63 cells under static and dynamic conditions. From the three microsphere materials produced (Ti0, Ti5 and Ti7), the composition with no TiO₂ doping, Ti0, was deemed unsuitable for applications relating to cell culture due to rapid degradation within 24 hours resulting in an inability to provide the structural integrity required to support cell attachment and growth. These effects are in agreement with the previous observations made by Abou Neel et al. who showed that both 0 or 1 mol% TiO₂ underwent rapid degradation and limited MG63 cell growth (Abou Neel and Knowles, 2008). The remainder of the microsphere types were assessed for their suitability as culture substrates for MG63 cells using the quantitative cell proliferation assay CCK-8. A positive control of MG63 cells on TCP was used. The quantity of Ti-PGMs used was calculated based on their cross-sectional area rather than total surface area. While this increases the surface area available for cell growth compared to the surface of a 96-well microplate well, the spherical surface of the Ti-PGMs limits the efficiency of cell attachment. To establish a better understanding of how cells grow on the material when compared to TCP, disc forms of the biomaterial could be created of the same surface area as the well.

The formation of formazan dye in the assay is directly proportional to the number of living cells. This assay provides advantages compared to other commonly used assays such as the MTT assay, which relies primarily on metabolic activity as opposed to the number of living cells. The results indicate that Ti5 and Ti7 provided support for cell attachment and growth, albeit to a lesser degree than the chemically enhanced TCP, which provides an optimal substrate for attachment and proliferation (Figure 2.3). These findings are consistent with those found previously in the lab, using fibroblast cells, where TCP exceeded the cell growth on the Ti-PGMs by approximately 50% (Guedes et al., 2012). This is an expected outcome since the surface of TCP is optimized for cell attachment being hydrophilic and its flat surface providing improved conditions for cell proliferation. While the MG63 cells showed decreased proliferative capacity on Ti-PGMs compared to TCP, the substrate's ability to induce an osteogenic response has not been matched by commercially available substrates, therefore the trade-off to culture fewer cells with enhanced osteogenic properties could be deemed more than acceptable. The ultra-low attachment plates used are coated with a covalently bound hydrogel layer that inhibits the attachment of cells to the surface, allowing the true affinity of the microspheres to be understood. Both Ti5 and Ti7 compositions showed significant increases in cell number over the 13-day culture period. There were no significant differences between the Ti5 and Ti7 microspheres in terms of overall cell proliferation, except for the days upon which maximum cellular yield was achieved, with Ti7 yielding higher cell numbers when subjected to 150rpm conditions on day 7 as opposed to day 9 at which Ti5 reached its maximum yield. The limited differences in cell proliferation indicate the suitability of both materials as potential candidates for MG63 cell attachment and growth and further quality markers of cell identity and function would need to be assessed to determine optimal substrate.

Confocal laser microscopy images illustrated the ability of the cells to wrap around and cover the curved surface of the microspheres (Figure 2.9b). It has been established in previous work carried out by Abou Neel et al., that phosphate glasses doped with 5 mol% TiO_2 showed partial release of PO_4^{3-} ions after 13 days when in a solubilising solution, however the local environment created by the release of these ions from Ti5 microspheres, the more soluble of the two Ti-

PGMs studied, provided no detrimental effect upon cell viability after 13 days illustrated by the densely packed areas in the confocal images (Figure 2.9a) (Abou Neel and Knowles, 2008).

Studying the effect dynamic culture conditions have upon cell proliferation provides crucial insight into the applicability of the material as a substrate for use in dynamic bioreactors, and the effect the mechanical processes have upon cell proliferation. The use of the Froude scaling law (Weheliye et al., 2013) provided a foundation for identifying which orbital agitation speeds should be studied to understand the impact mixing patterns have upon cell proliferation. This was done because applying a model that defines critical orbital agitation speed (at which the contents of a cylindrical vessel are thoroughly mixed and the microspheres contained within are theoretically in suspension), should lead to effective cell expansion due to reduced nutrient and oxygen gradients. The effect the dynamic culture conditions had upon cell numbers were evident from Table 2.1, which indicated that the highest cell yields could be achieved by 150rpm agitation, with values of 2.9 and 3.1-fold increases when cells are cultured on Ti-PGMs compared to values for 0 and 300rpm ranging from 2.64 to 2.77-fold increase.

The data obtained from the YSI Bioanalyser in Figures 2.5 and 2.6 provide an insight to the consumption of the feed substrates and their conversion to waste products within the whole well. The glucose and lactate concentrations were monitored to indirectly evaluate cell viability. Glucose acts as a primary source for mammalian cells to produce ATP through oxidative phosphorylation or via anaerobic glycolysis (Schop et al., 2009). The values produced by the YSI Bioanalyser provide an overall average of the metabolite concentration in the well, therefore to fully grasp how well each condition and material can support cell metabolism, it is important to normalize these values to viable cell number. As media changes were made every 48 hours, which were carried out after each cell proliferation assay time point, calculating the respective glucose consumptions for the current time point was possible and subsequently these values were normalized to viable cell number. The ratio of lactate production to glucose consumption per cell ($Y_{\text{Lac/Glc}}$) indicates the metabolic pathway the cells prefer to use as a mode of energy production (Ljunggren and Haggstrom, 1994,

Schop et al., 2009). Schop et al. stated that a $Y_{\text{Lac}/\text{Glc}}$ value of 2 indicates that the cells inefficiently convert glucose using the glycolytic pathway as opposed to oxidative phosphorylation to produce energy. The ratio indicates that the 2 moles of lactate, the maximum yield possible, are created per mol of glucose. A lower ratio indicates that glucose consumption generates fewer units of lactate in a more energy efficient process (Schop et al., 2009). Cells cultured under 300rpm ($Y_{\text{Lac}/\text{Glc}}= 1.33$) showed higher conversion ratios than both 0rpm ($Y_{\text{Lac}/\text{Glc}}= 0.96$) and 150rpm ($Y_{\text{Lac}/\text{Glc}}= 0.97$), values that are found to be consistent with studies carried out by Schop et al., who analysed metabolic activity of MSCs on microcarriers (Schop et al., 2008). The values show that 300rpm produced the least favourable conditions amongst those studied, correlating with the lower cell yields. It is concluded that the cells are not finding the higher agitated conditions ideal as they are unable to efficiently metabolise glucose. Shear stress from fluid flow can contribute to metabolic quiescence in some cell lines via the action of transcription factors (Doddaballapur et al., 2015), a potential explanation to why higher $Y_{\text{Lac}/\text{Glc}}$ ratio are produced with 300rpm. It has been well documented that there are significantly lower oxygen transfer rates in 96-well microplates inducing potential anaerobic conditions, however this factor would not influence the results as each condition carried the same volume of media with limited variations in both ultra-low attachment and surface treated TCP (Running and Bansal, 2016). A potential explanation lies in the size of the construct formed at 150rpm potentially limiting the dynamic benefit of oxygen and nutrient transport. It is hard to conclude whether the unfavourable shift in metabolic pathway is attributed to the shear stress caused by fluid flow, or potentially down to limited oxygen and nutrient transfer into the core of the structure.

The differences witnessed between the conditions studied do not corroborate with the initial hypothesis that complete mixing of the fluid within the cylindrical vessel would induce greater cell proliferation caused by the complete suspension of microspheres allowing effective seeding and expansion of the MG63 cells. The agitation rate correlating to Fr_c , 300rpm, on average produced the lowest yield increase across all three different materials studied, which would bring into question the ease of implementing the model developed by Weheliye et al. (Weheliye et al., 2013) to identify the ideal speed needed for effective cell seeding

and expansion. The model has a limitation in that it fails to incorporate the density of any particulates higher in density than the fluid within the vessel. The densities of the materials used in the study are 2.65 and 2.71 g/cm³ for Ti5 and Ti7 respectively, which are magnitudes higher than commercially available microcarriers with many of them lying in a similar range to the density of water (1 g/cm³). The high densities of the Ti-PGMs limited their movement to the base of the cylindrical wells of the microplate; therefore, the mixing that occurred at 150rpm would be above the microspheres in the two toroidal vortices, while at 300rpm the vortices are closer to the surface. From the results, it can't be deduced that N_c provides optimal agitation for culturing MG63 cells on the microspheres in question; however, there is foundation to assume that agitation rates below N_c could provide better fluid mixing systems for culturing cells on dense microspheres.

The MG63 cells are very robust in nature and have a tendency to show high proliferation rates (Mohseny et al., 2011). Therefore, while the cells have given an early indication to the ability of the material to support cell growth under both static and dynamic conditions on both types of phosphate glass studied, the cells' ability to withstand comparatively higher shear and their documented growth kinetics can't be directly translated to clinically relevant cell types. Their lack of reliability necessitates further studies to be carried out with more immature cells such as MSCs, to establish the full extent that fluid dynamics impacts on cell proliferation and differentiation when cells are cultured on these doped phosphate microspheres. The next chapter looks to use the preliminary data obtained in this chapter, more specifically the impact of cluster formation and cell growth and translate the experimental environment to cell types more clinically relevant such as MSCs.

Chapter 3 . Critical functional responses of human bone marrow derived mesenchymal stem cells and Ti-PGMs

3.1 Introduction

Reconstructive medicine often involves designing a biocompatible scaffold, where its clinical use elicits limited side-effects or immunological responses (O'Brien, 2011) which when coupled with stem cells produces a high capacity to repair damaged tissue. The multi-lineage differentiation potential and high expansion capacity of MSCs, along with their prominent immunomodulatory role, makes these cells an ideal candidate for bone tissue engineering. Furthermore, as these cells can be sourced in large quantities from patients themselves, the limitation of obtaining osteoprogenitors from a compromised source, is overcome by MSC therapy.

The work in this chapter explores the interactions between hBM-MSCs and Ti-PGMs under static and dynamic conditions. BM-MSCs have greater osteogenic differentiation potential when compared to MSCs originating from other sources such as adipose-derived MSCs (Im et al., 2005). The different compositions of Ti-PGMs produced were compared to commercially available Corning Low Concentration Synthemax II Microcarriers (Corning® Costar®, Sigma-Aldrich, UK) assessing both cell proliferation and differentiation. The chapter develops on the work carried out on MG63 osteosarcoma cells in Chapter 2 by considering the effect dissolution ions of Ti-PGMs have upon osteogenic differentiation. Having demonstrated that controlled agitation at speeds lower than N_c induced better cellular responses the aim of this chapter was to determine the effects of dynamic culture on growth and differentiation of hBM-MSCs. While osteogenic differentiation of MSCs cultured in the presence of dexamethasone, β -glycerophosphate and L-ascorbic acid-2-phosphate is well known (Pittenger et al., 1999), some studies have demonstrated that mechanical stress, particularly in

the form of fluid flow, can stimulate multiple intracellular signalling pathways associated with osteogenic differentiation (Reich et al., 1990, Bancroft et al., 2002, Kreke and Goldstein, 2004, Li et al., 2004, Kreke et al., 2005). In addition, hMSCs are highly responsive to their immediate environment such as topographical features which the cells respond to by reorganising cytoskeleton and cell adhesion apparatus (McBeath et al., 2004, Engler et al., 2006). The sensitivity of MSCs under culture *in vitro* highlights the need for stringent process controls that are required to limit variability in the cell differentiation process. This sensitivity of MSCs when compared to progenitor cells, more specifically osteoblasts, would indicate that higher agitation speeds would impact cell behaviour of MSCs more than mature cell types. Evidence exists to show that MSC with a flatter morphology tend to mature towards an osteoblastic fate compared to round cells which promote adipogenesis, therefore it is important that MSCs bind effectively to the surface of the microspheres (Lavenus et al., 2010). It has also been observed in other studies that MSCs which had higher numbers of focal adhesions were associated with a greater commitment to an osteogenic lineage (Lavenus et al., 2011). Tailoring a process to take advantage of the mechano-sensitivity of hMSCs allows control of its fate *in vitro* to optimize osteogenic differentiation. The effect of fluid flow has a limiting effect on cell proliferation when used excessively (Kreke and Goldstein, 2004) and therefore a careful balance is needed to ensure that cell growth occurs to its highest efficiency with cues that can be used to promote a specific phenotype. Taking the above into consideration, the pre-determined speeds calculated for the studies in the Chapter 2 were deemed potentially excessive and therefore a lower range of speeds were used for this study. The rationale behind changing the orbital speed range for this study was down to the immaturity of the hBM-MSCs when compared to the osteoblastic cell line previously used, coupled with improved cluster formation at speeds lower than that at Nc.

3.2 Materials & Methods

3.2.1 Preparation of human bone marrow derived mesenchymal stem cells

Human bone marrow MSCs (Lonza, Belgium) were sourced from in-house stocks (P3-P6) at the Biochemical Engineering Department, University College London which were stored in cryovials in liquid nitrogen expanded from an individual P0 vial. These cells were restored by rapid thawing within a water bath at 37°C. The hBM-MSCs were cultured using the same protocol as described previously in section 2.2.3, however a different seeding density (2×10^3 - 4×10^3 cells/cm²) was used to ensure the cell line grew in optimal conditions. Cell passages were carried out when cells reached 80-90% confluency, confirmed by visual observations through phase contrast microscopy.

3.2.2 Cell characterization

3.2.2.1 Multilineage differentiation

Mesenchymal stem cell functionality was determined using an identification assay. The human mesenchymal stem cell functional kit (R&D Systems, Bio-Techne Ltd, UK) was used to differentiate the cells into different mesenchymal lineages. Media preparation for osteogenic and adipogenic differentiation started with the combination of aMEM basal media with 10% FBS and 1% Penicillin-Streptomycin-Glutamine. Chondrogenic media consisted of DMEM/F-12 basal media supplemented with 1% Insulin-Transferrin-Selenium (ITS) supplement and 1% Penicillin-Streptomycin-Glutamine, which was consequently stored in dark conditions for prolonged stability. Each differentiation procedure was carried out in Nunclon™ flat bottomed tissue culture 24-well microplates (Thermo Fisher Scientific, UK) according to the supplier's protocol.

Adipogenic and osteogenic differentiation started with harvested hBM-MSCs seeded at a density of 2.1×10^4 cells/cm² in adipogenic basal media and 4.2×10^3 cells/cm² seeded in osteogenic basal media cultured up until 100% and 50-70% confluency respectively, at which point the basal media was replaced with the respective differentiation media. The media was changed every 3-4 days for a period of up to 21 days, and consequently fixed for detection of adipogenic

marker FABP4 and osteogenic marker osteocalcin using immunocytochemistry techniques. The osteogenic and adipogenic differentiation of both samples were also assessed by Alizarin Red S (Sigma, UK) and Oil Red O staining (Sigma, UK), respectively. Alizarin Red staining was carried out by leaving the solution with the cells incubated at room temperature for 10 minutes and rinsed with dH₂O thrice to avoid any non-specific staining, with cells imaged using a Nikon microscope. Oil Red O solution was used to stain the cells by incubating 500µl of the solution with cells at room temperature for 10 minutes. Cells were gently rinsed with dH₂O twice and incubated for 1 hour with 2% isopropanol to visualize lipid droplets

The procedure for assessing the hBM-MSCs chondrogenic differentiation capacity differed from the supplier's protocol. The harvested cells were resuspended in basal chondrogenic media at a concentration 1.6×10^7 cells/ml. This concentrated suspension of cells was used to then form a micromass culture by seeding a 5 µL droplet of cell solution in the centre of the microwell. The resultant pellet was maintained in high humidity conditions for 2 hours without any supplemented media, after which chondrogenic media is added. The media was changed every 2-3 days for up to 14 days, after which immunocytochemistry and Alcian Blue staining were carried out. All fluorescent images were counterstained with Hoechst 33342.

3.2.2.2 Flow cytometry of hBM-MSCs

Human BM-MSCs of the highest passage used during the research (P6) were examined for expression of mesenchymal markers (CD73, CD90 and CD105), together with a lack of expression of monocyte and macrophage markers (CD11b), a haematopoietic progenitor and endothelial cell marker (CD34) and leukocyte marker (CD45) by flow cytometry. Dual staining was carried out with the following conjugated antibodies: Mouse-anti human CD73 (IgG₁, APC), CD90 (IgG₁, FITC), CD105 (IgG₁, PerCP™5.5), CD11b (IgG₁, PE), CD34 (IgG₁, PE) and CD45 (IgG₁, FITC) (All from BDBiosciences, UK). The combinations of two stains used per sample were of antibodies with different fluorochromes to prevent signal overlap. Three tubes of cells (5×10^5) were stained with 100µL of the

combined conjugated antibody solution using the manufactures specified concentrations for 30 minutes at 4°C. Tube 1 was stained with CD45 and CD73, Tube 2 with CD11b and CD106, and Tube 3 with CD34 and CD90. The cells were consequently washed in PBS with 2% FBS for 5 minutes at 1200rpm under room temperature conditions. Cell were analysed in a BD Accuri™ C6 Flow Cytometer using isotype controls for each of the fluorochromes to compensate for non-specific background signal caused by the conjugated antibody.

3.2.3 Interaction of hBM-MSCs on Ti-PGMs cultured under static and dynamic conditions

3.2.3.1 Cell culture on Ti-PGMs and Corning Synthemax II-SC microcarriers under static condition in ultra-low attachment 96-well microplates

The cultured hBM-MSCs were harvested and trypsinized by the same method described in section 2.2.3. Static culture of the hBM-MSCs was carried out in the similar manner as described previously in section 2.2.4, where the sterilization protocol and the amount of Ti-PGMs used per well were the same. The control microcarriers (Corning Synthemax II-SC) were added in quantities of 3.5mg to each well providing the equivalent cross-sectional area as the Ti-PGMs. These microcarriers were weighed and sterilized in the same manner as the Ti-PGMs, after which all microspheres were equilibrated with 135µL of pre-warmed media and seeded with 5×10^3 cells/well. As per the method in section 2.2.4, static cultures were initially mixed under slow agitation to ensure even cellular and microsphere distribution. Cell culture was carried out for 13 days with reading taken on days 1, 3, 5, 7, 9 and 13 with media changes occurring every 48 hours.

3.2.3.2 Cell culture on Ti-PGMs and Corning Synthemax II-SC microcarriers under dynamic conditions in ultra-low attachment 96-well microplates

The dynamic studies were carried out in parallel to the static cultures in ultra-low attachments plates using the method described in section 2.2.5. The differences between the two protocols lie in the changes in orbital agitation speeds the cells were subjected to and the seeding density in each well. The orbital agitation

speeds used for this study were, 0, 70, 100 and 150rpm, with the rationale behind these choices explained further in the discussion. The seeding density was in accordance with the static studies; therefore, a cell seeding density of 5×10^3 cells/well was used. Agitation was used for a brief period to ensure a homogenous distribution of cells and microspheres. To allow for effective cell attachment, the dynamic plates were left in static conditions for 24 hours after which they were kept at the selected speeds. Furthermore, for each dynamic experiment run, a static control plate was used using the method described in section 2.2.5.

3.2.3.3 Cell proliferation assay

Cell proliferation on both the Ti-PGMs and the Synthemax II-SC under static and dynamic conditions were quantified using the CCK-8 assay, as per the method provided in section 2.2.6. Standard calibration curves were produced for each condition studied to correlate absorbance to absolute cell values.

3.2.3.4 Phase contrast microscopy imaging

Phase contract imaging of the ultra-low attachment plate was carried out using the same method described in section 2.2.8.

3.2.3.5 Confocal laser scanning microscopy

Samples were prepared for confocal microscopy by fixing them *in situ* with 20% PFA for 20 minutes at room temperature. The fixed samples were then washed and preserved in PBS until immunostaining was carried out. Cell staining was carried out to label the extracellular matrix proteins fibronectin (Mouse monoclonal, ab6328, Abcam, Cambridge, UK) and type-1 collagen (Rabbit polyclonal, ab34710, Abcam, Cambridge, UK), and bone specific extracellular matrix proteins osteopontin (Mouse monoclonal, ab69498, Abcam, Cambridge, UK) and osteocalcin (Rabbit polyclonal, ab10911, Millipore, UK). Both fibronectin and type-1 collagen were used in a 1:200 dilution while, osteopontin and osteocalcin were used in 1:100 dilutions, both diluted in PBS. The fixed samples

were incubated overnight in the primary antibody staining solution and kept at 4°C. Counterstaining was carried out with each antibody's respective secondary antibody accompanied with their suitable fluorochromes. During the counterstaining process, the samples were kept in the dark at room temperature for 1 hour, consequently washed and kept in PBS until imaged. Confocal light microscopy was carried out using a Zeiss LSM 700 microscope, ensuring that the capture properties of each image are the same for accurate comparison.

3.2.4 The effect of conditioned-media on cell/microsphere interaction

3.2.4.1 Cell culture using conditioned-media

This part of the study focuses on understanding the effect different media types have upon the proliferation and differentiation of hBM-MSCs. The media types studied can be categorised into 3 main groups of media type: 1) TiO₂-Conditioned media 2) osteogenic differentiation media 3) DMEM (control). The production of TiO₂-conditioned media involved DMEM being mixed with powders of 5 mol% Ti-PGMs. These particulates had diameters within the range of 0-62µm and were used as powders which could be dissolved within low-glucose DMEM. Different concentrations of TiO₂-conditioned media were formed by addition of pre-defined quantities of powders to a 125ml Corning Erlenmeyer flask (VWR, UK) containing 50ml of media. The flasks were kept in an incubator on a KS260 control orbital shaker (IKA, Germany) and left to agitate for 72 hours. After this period, the media was then filtered using a Millex-GP Syringe filter with a 22µm (Millipore, UK) to reduce and undesired residuals remaining in solution. The osteogenic differentiation media was made using a hMSC Osteogenic BulletKit (Lonza, UK) following the suppliers protocol. The basal media was supplemented with dexamethasone, L-glutamine, ascorbate, penicillin/streptomycin, mesenchymal cell growth supplement and β-glycerophosphate. All media types were stored at 4°C in suitable media bottles for use in cell culture. Cells were cultured in Nunclon™ flat bottomed tissue culture 96-well microplates (Thermo Fisher Scientific, UK) using a seeding density of 3x10³ cells/well. Cell proliferation was determined on days 1, 3, 5 and 7 with media changes carried out every 48 hours.

3.2.4.2 Cell proliferation assay

Cell proliferations of the hBM-MSCs were quantified using the CCK-8 assay, using the method provided in section 2.2.6.

3.2.4.3 Immunofluorescence imaging

Immunocytochemistry was established using immunofluorescent techniques described in section 3.2.3.5. Samples were fixed on day 7 and were fixed using PFA and were stained for Type-I collagen, osteocalcin and osteopontin. Samples were stored at 4°C to minimize degradation and allow for images to be acquired post-staining.

3.2.5 Statistical analysis

All statistical analysis was carried out using IBM SPSS Statistics version 22. Analysis was carried out using the techniques described in 2.2.10.

3.3 Results

3.3.1 Characterization of human bone marrow mesenchymal stem cells

The cells were analysed in terms of their ability to undergo tri-lineage differentiation along adipogenic, osteogenic and chondrogenic lineages. Additionally, the hBM-MSCs were characterized by their ability to adhere to plastic surfaces and by the expression of hBM-MSC's surface markers through flow cytometry.

The capacity for hBM-MSCs to differentiate along multiple lineages in response to specific induction media is shown in Figure 3.1. Adipogenic differentiation of P6 hBM-MSCs was induced by culturing them with adipogenic media for 21 days, after which the formation of lipid droplets, a key indication of adipogenic differentiation, was observed (Figure 3.1a). Osteogenic differentiation was evaluated by the calcium deposition observed via Alizarin Red S staining using light microscopy, which is an orange red colouring as seen in Figure 3.1c. Chondrogenic differentiation was observed by immunofluorescent staining of the micromass formed in Figure 3.1e using Aggrecan. Differentiation was also observed by performing immunofluorescent labelling of protein markers specific to osteoblasts (osteocalcin) and adipocytes (FABP4). It is evident from Figure 3.1 that after 21 days of selective differentiation each of the surface markers selected were positively expressed by the hBM-MSCs. Results from the flow cytometry experiments are displayed in Figure 3.2. The data confirms that the P6 hBM-MSC population tested was CD73⁺ CD90⁺ CD105⁺ CD34⁻ CD45⁻ CD11b⁻. Gates respective to each of the surface markers were set using isotype controls.

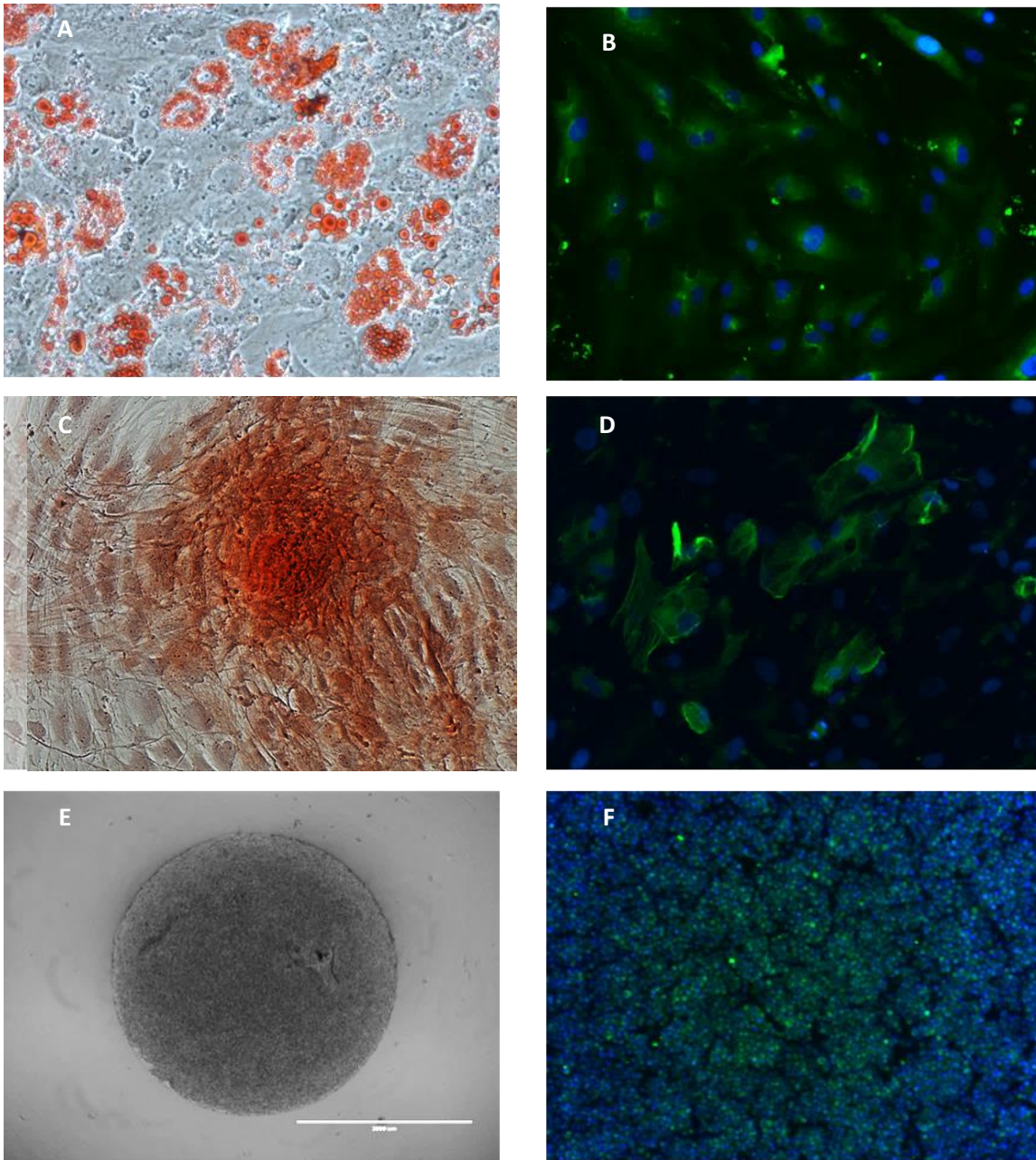


Figure 3.1 Tri-lineage differentiation of hBM-MSC. Light microscopy (A, C, E) and immunofluorescent (B, D, F) images indicating the differentiation potential of the cells to differentiate towards adipogenic (A, B), osteogenic (C, D) and chondrogenic (E, F) lineages. hBM-MSCs cultured in adipogenic media were positively stained with Oil Red O after 21 days (A) and were positive for FABP4 (B; green signal). After 21 days in osteogenic culture media, hBM-MSCs were positively stained with Alizarin Red S (C) and were positive for osteocalcin expression (D; green signal). Chondrogenic differentiation in a cell pellet was characterised using Alcian Blue stain (e) and Aggrecan (F; green channel) after 21 days. Immunofluorescent images were counter-stained with Hoechst 33342 (blue). Images were captured at 4x (Fig 3.1 - E) and 10x magnification (Fig 3.1 – A, B, C, D and F)

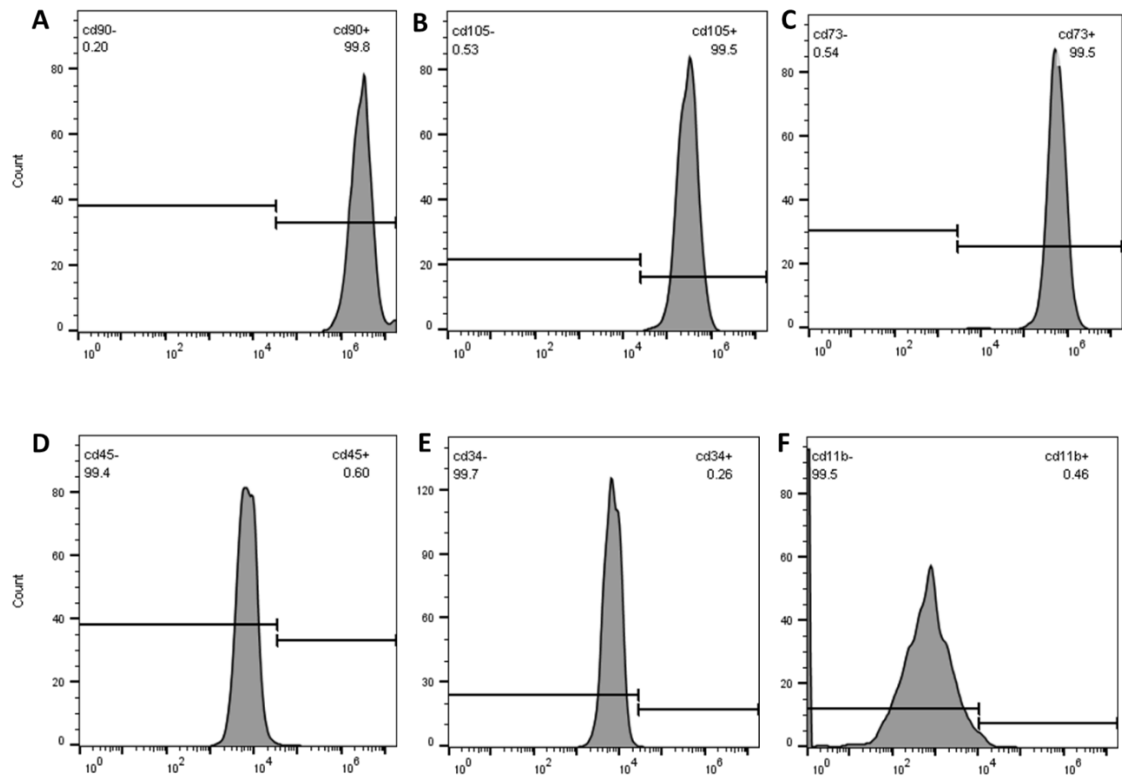


Figure 3.2 Phenotypic analysis of hBM-MSCs and expression of pluripotency markers. A single cell suspension of hBM-MSCs was examined for the expression of mesenchymal markers (A) CD90, (B) CD105, (C) CD73) and hematopoietic markers (D) CD45, (E) CD34 and (F) CD11b. Matching isotype controls were used to ensure observed staining is due to specific antibody binding.

3.3.2 Interaction of hBM-MSCs on Ti-PGMs cultured under static and dynamic conditions

3.3.2.1 Cell proliferation of hBM-MSCs on Ti-PGMs under orbital agitation

Cell proliferation levels of hBM-MSCs cultured on the different Ti-PGMs and Synthemax microcarriers were determined by referencing against a standard curve that was generated (Figure 3.3). The high R-squared values highlights the linearity between the absorbance and the viable cell count numbers indicating a strong positive relationship and validates the use of the assay with the cell type used. As mentioned in the previous chapter, three separate standard curves were produced due to each condition being run as batches.

Growth profiles of hBM-MSCs cultured on the three different culture materials (Ti5, Ti7, and Synthemax) under static and agitated conditions are shown in Figure 3.4. Limited differences are observed from seeding on day 0 to proliferation of hBM-MSCs on day 5 between the 4 conditions studied on each material. However, after day 5 significant differences can be observed between the different conditions, with cells cultured under 70 rpm conditions showing significantly higher viable cell counts on all three surfaces ($*p < 0.01$). For hBM-MSCs cultured on Ti5 microspheres under 70 rpm conditions, significantly higher cell numbers can be observed on day 7 when compared to 0rpm ($*p < 0.05$) and 150rpm ($***p < 0.001$), where 0rpm viable cell counts were also significantly higher than 150rpm ($*p < 0.05$). The difference noted between 70rpm and 150rpm remains constant from day 7 until day 13 with significant differences on both day 9 ($**p < 0.01$) and on day 13 ($***p < 0.001$). Furthermore, on day 13, 150rpm conditions showed significantly lower cell count values compared to 100rpm ($*p < 0.05$). The trends noticed on Figure 3.4A are also mimicked by cells cultured on Ti7 (Fig 3.4B) microspheres, with clear differences illustrated from day 7 onwards. The same result is produced on day 13 with 70 rpm again providing the best conditions for culture with significantly higher viable cell counts than those on all the other conditions studied. In addition, static cultures on Ti7 produced significantly higher viable cell counts when compared to 150rpm ($**p < 0.01$). The differences in viable cell counts on Synthemax are only clear on day 13 with large error bars contributing to the inability to draw statistically valid conclusions. This was partly down to processing issues including Synthemax lost during media changes and during the viability assay procedure. With Synthemax highly influenced by pipetting action, extraction of media from the well was challenging without interacting with the microcarriers. While measures were in place to minimize undesired removal of Synthemax, these processes had inherent losses which led to large error bars, especially when larger viable cell numbers existed. Nevertheless, day 13 viable cell count values show that both static and 70rpm conditions provided more favourable conditions for cell culture when compared to both 100rpm and 150rpm.

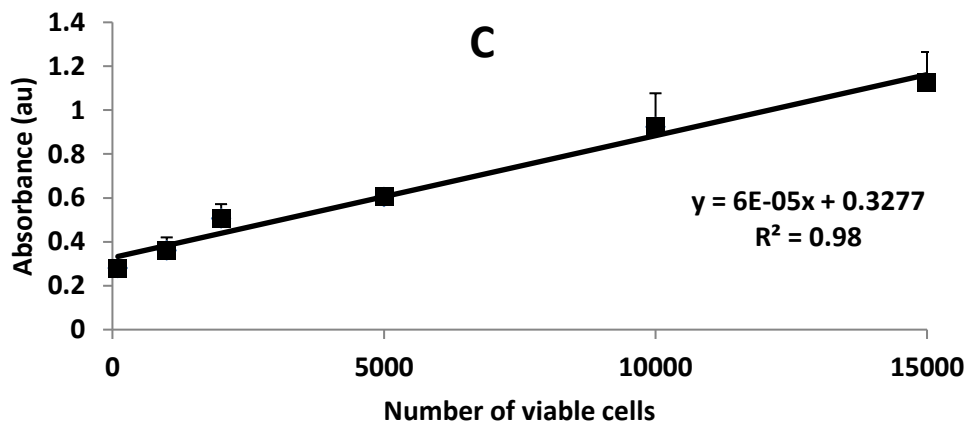
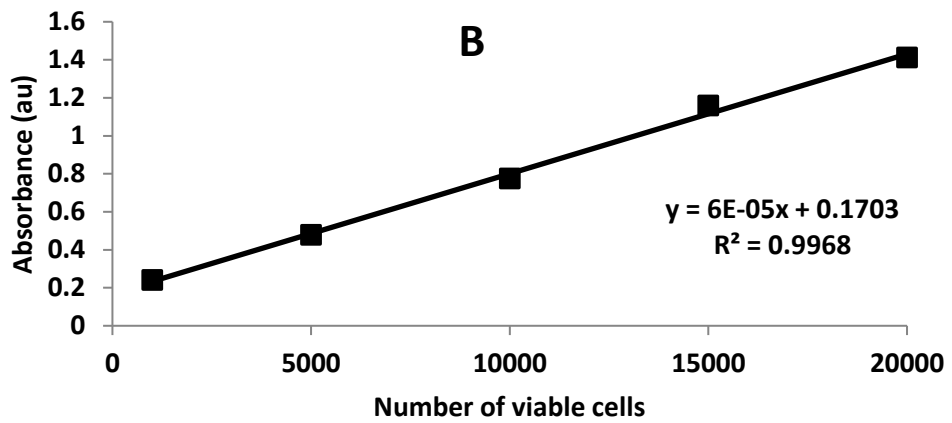
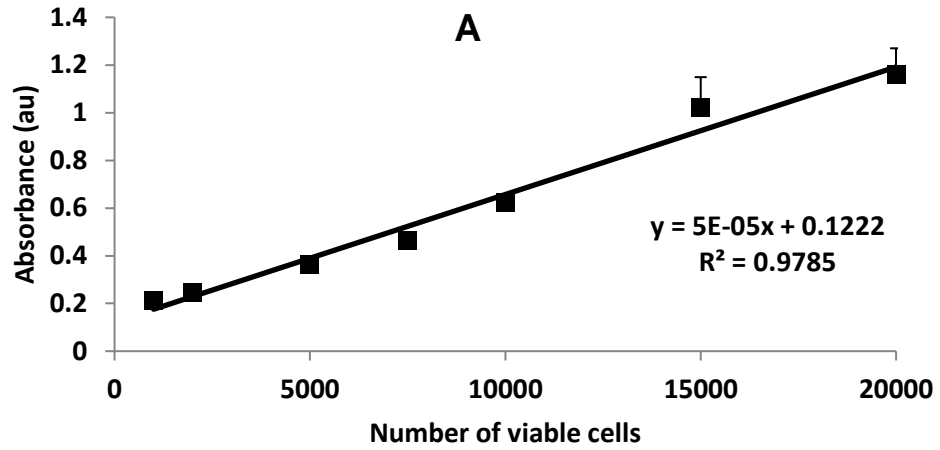


Figure 3.3 Standard curve of hBM-MSC's cell growth plotted as absorbance (nm) versus number of viable cells using a CCK-8 proliferation assay. Readings were taken after complete attachment of cells for (A) 70rpm (B) 100rpm and (C) 150rpm. Absorbance based on a wavelength of 450nm. Error bars represents + SD (n=3)

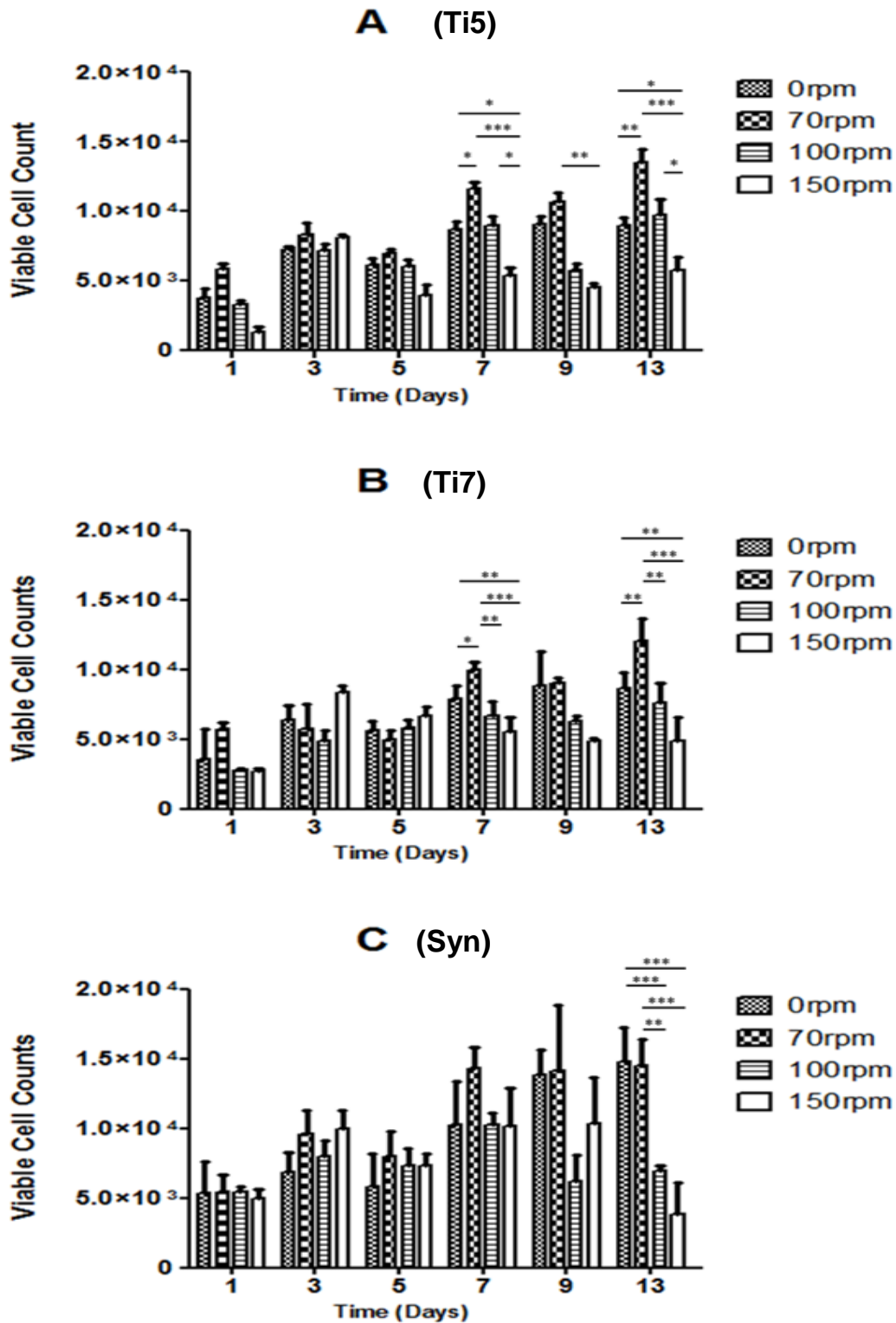
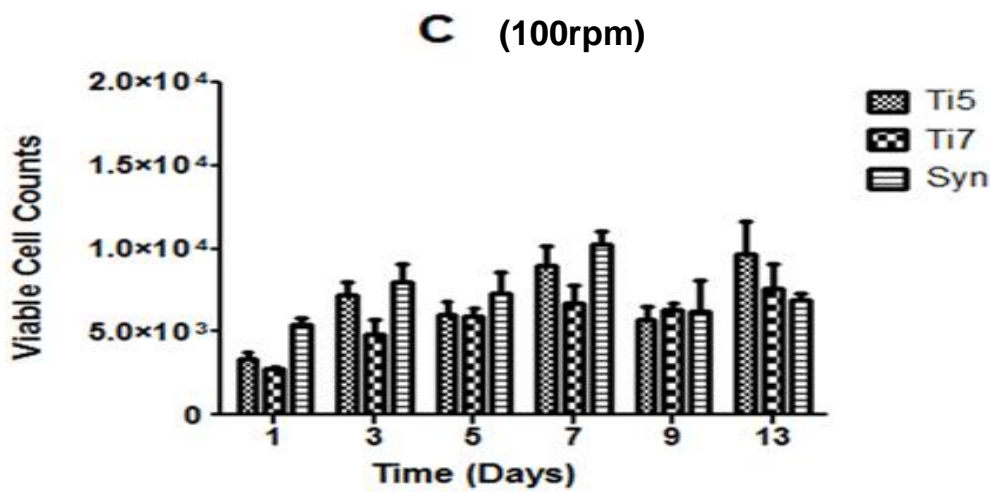
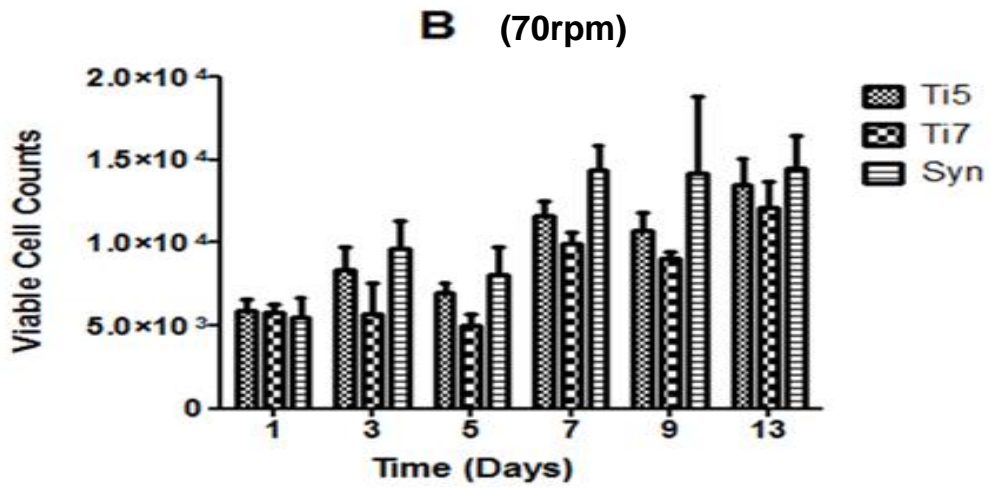
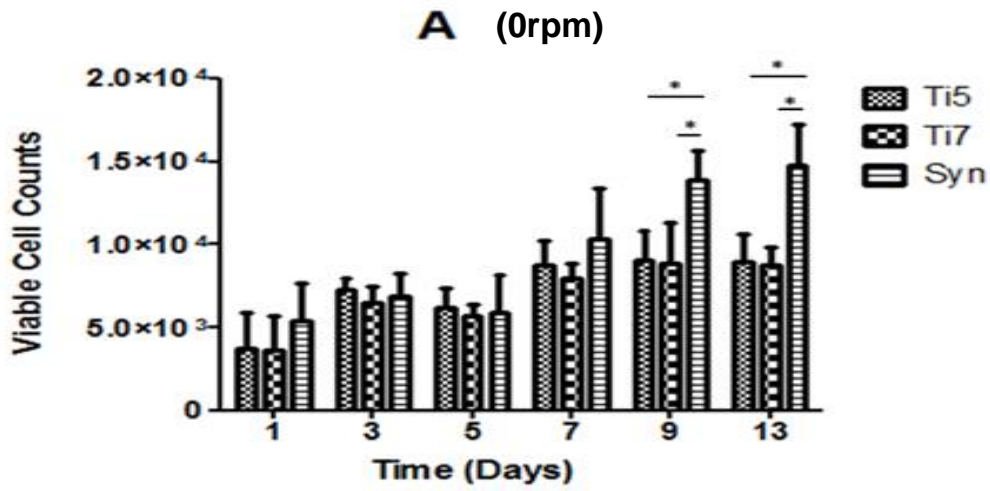


Figure 3.4 Proliferation of hBM-MSC cultured on (A) Ti5, (B) Ti7 microspheres and (C) Synthemax in ultra-low attachment well microplates under static and dynamic conditions. Readings were taken on days 0, 1, 3, 5, 7, 9 and 13. Error bars represents + SD (n=3). Significance values denoted by *= $p < 0.05$, **= $p < 0.01$ and ***= $p < 0.001$.

When comparing the effect of culture substrate on cell proliferation (Fig 3.5), it was observed that across the different conditions studied there was no substantial difference between Synthemax microcarriers and the Ti-PGMs. Under static conditions Synthemax did perform significantly better than both the Ti-PGMs after day 9 (* $p < 0.05$) showing that the material response to Synthemax is superior to Ti-PGMs. The remaining three dynamic conditions indicated no distinct difference in ability to support hBM-MSC proliferation suggesting that under stimulation similar yields can be achieved on Ti-PGMs as Synthemax. High agitation rates, regardless of substrate type are detrimental to cell growth. The cells cultured on Synthemax under 150rpm conditions however did show significantly higher cell numbers on day 7 (* $p < 0.05$), however the larger error bars indicating potential sampling error. A progressive shift can be seen from static culture through to 150rpm, illustrated by Figure 3.5A and B showing that a majority of cell proliferation occurs towards the latter days with lower viable cell counts between day 1 and 5, while cell agitation under 100rpm conditions (Fig 3.5C) the step rise in cell number isn't as pronounced with a flatter growth curve. The change is even more visible under 150rpm agitation where the largest average increase in cell number occurs on day 3. Cell yield values in Table 3.1 further corroborate this idea that as agitation intensifies there is a shift to when maximum cell yields are achieved and provide an insight to the impact each agitation had upon the levels of cell yields achieved by the different culture materials. It is evident from Table 3.1 that 70rpm generates the best cellular yield across the Ti-PGMs, with fold increase of 2.70 and 2.42 for Ti5 and Ti7 respectively. On the other hand, cell growth performance on Synthemax was optimal under static conditions. These yields were achieved between days 9 and 13 with the largest percentage increase in viable cell numbers occurring between days 5 and 7 for each material's respective optimal condition.



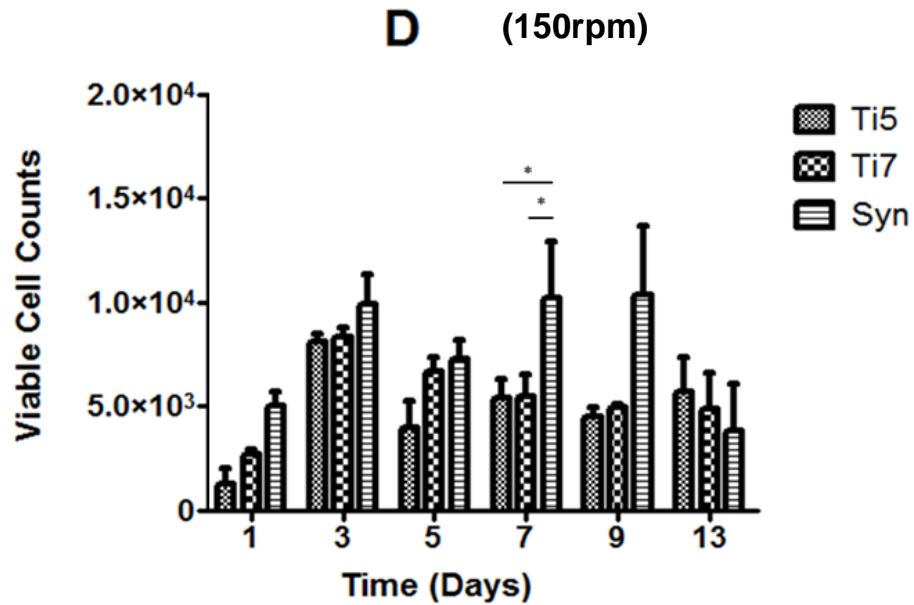


Figure 3.5 Proliferation of hBM-MSC cultured under (A) 0rpm, (B) 70rpm, (C) 100rpm and (D) 150rpm conditions. Readings taken on days 0, 1, 3, 5, 7, 9 and 13 of cells cultured on the two TiO₂ compositions and Synthemax in ultra-low attachment well microplates. Error bars represents + SD (n=3). * = p<0.05

Table 3.1. Fold increase values of cultured hBM-MSCs indicating the maximum cells yield achieved over the course of the experiment under the different conditions and materials used. The time point (in days) at which the maximum yield was achieved is indicated within the parentheses.

Material	Condition (Day)			
	0rpm	70rpm	100rpm	150rpm
Ti5	1.8(9)	2.7 (13)	1.9 (13)	1.6 (3)
Ti7	1.8 (9)	2.4 (13)	1.5 (13)	1.6 (3)
Synthemax	3.0 (13)	2.9 (13)	2.0 (7)	2.0 (9)

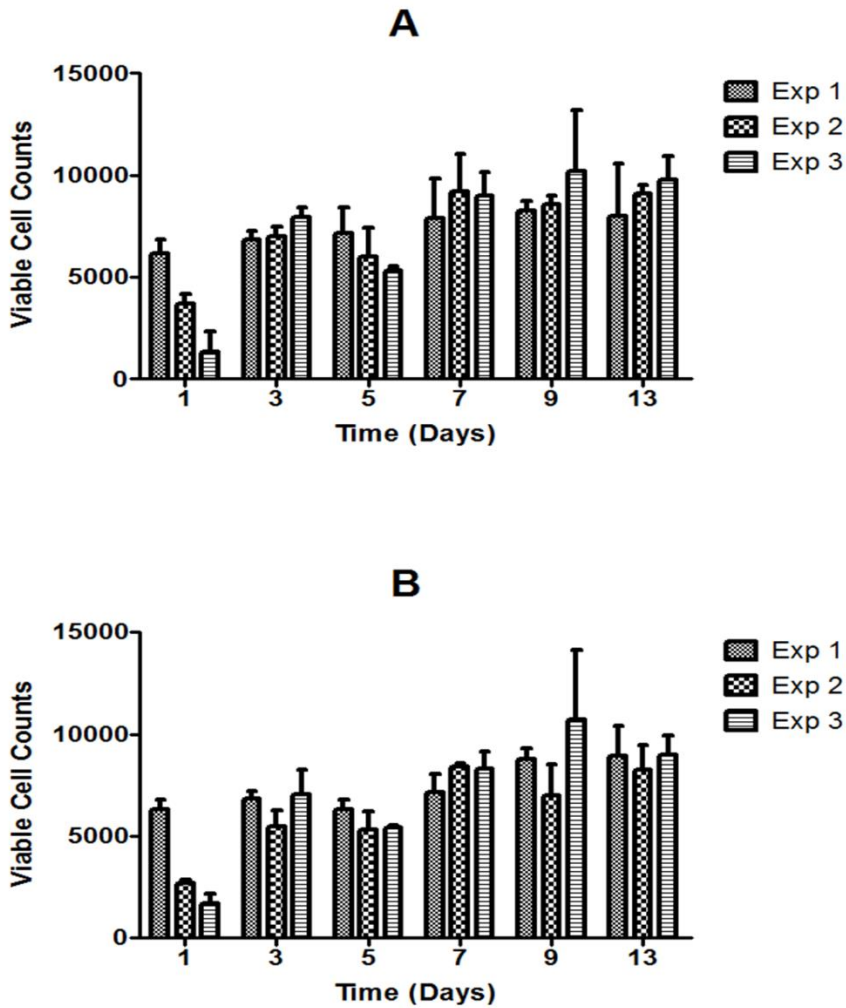


Figure 3.6 Comparison of static controls used when studying hBM-MSC proliferation on Ti5 over 13 days where Exp 1, 2 and 3 denote three different static runs which were used as controls carried out in parallel with the dynamic studies (70rpm, 100rpm and 150rpm). Exp 1- Static control for 70rpm, Exp 2- Static control for 100rpm study and Exp-3 Static control for 150rpm study. Error bars represents + SD (n=3).

As was seen in Chapter 2, a static control plate using Ti-PGMs was present in all three dynamic conditions studied, to determine comparability and batch consistency across the independent experiments. The only difference visible between the runs would be the attachment seen on day 1 between the different runs (Figure 3.6). This potentially owes to the variability in seeding efficiency during the first 4 hours.

3.3.2.2 Macroscopic evaluation of hBM-MSC – Ti-PGM clustering

The effects of agitation were captured visually using phase contrast microscopy (Figure 3.7). The interaction between Ti-PGMs and hBM-MSCs was captured over time under specific agitation speeds. As Figure 3.8 suggests, the Ti-PGMs on day 1 formed an even monolayer when all plates were kept under static conditions. On day 3 clusters begin to form in all conditions, with size and number of clusters varying from condition to condition. The clustering observed on day 3 under static and 70rpm conditions showed fewer clusters that were more densely packed while at 100 and 150rpm conditions the clusters were spread around the well. When the culture period extends to day 7, few differences in cluster number and size were observed, with large macrounits visible under all conditions. The remaining number of Ti-PGMs not incorporated into these structures also remained similar. However, detailed information about the behaviour within the core of the structures could not be fully concluded. The only observable difference on day 7 was that within the unused Ti-PGMs smaller clusters still seemed to be forming under static and 70rpm conditions, while for the 100 and 150rpm conditions the remaining Ti-PGMs seemed to remain in the periphery of the well. Clear differences are highlighted on day 13 between 150rpm and the other culture speeds. The fastest agitation speed of the group showed considerably lower levels of cluster formation compared to the three other speeds, with a large quantity of Ti-PGMs remaining within the well. The structure that had formed on day 7 seems to break down during the days leading up to day 13 into two distinguishable macrostructures. As for the other three speeds, there are minimal observable differences between them, with all three conditions illustrating clusters which have incorporated a majority of the available Ti-PGM's to form one large Ti-PGM-cell structure.

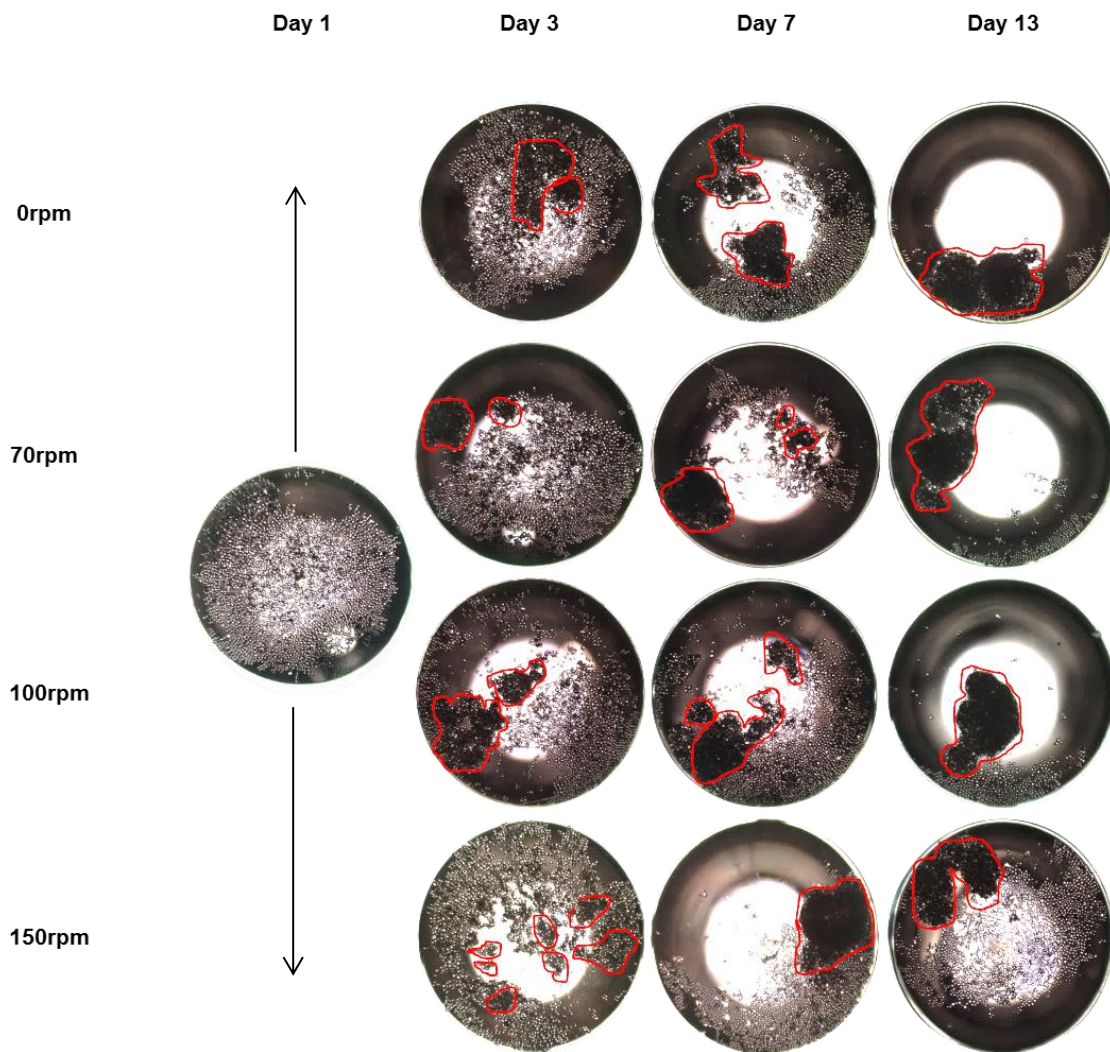


Figure 3.7 Formation of Ti-PGM-cell clusters under different agitation rates. Phase contrast images of an individual ultra-low attachment microwell illustrating hBM-MSCs cultured on Ti5 over a 13-day period using the same well from day 3 onwards. Red markings highlight areas of clustering. Images were taken under 2x magnification.

In comparison, Figure 3.8 shows the development of Synthemax clusters over the course of 13 days. In contrast to hBM-MSC cultured on day 1 on Ti-PGMs, Synthemax microcarriers seem to have improved attachment with clusters forming relatively early. Based on the darker areas indicating more densely packed clustering, it can be observed that on day 3 static conditions allowed improved cluster development compared to the dynamic conditions. As the culture progresses to day 7 the clustering under each condition progresses slowly, with minimal differences noted between days 3 and 7. However on day

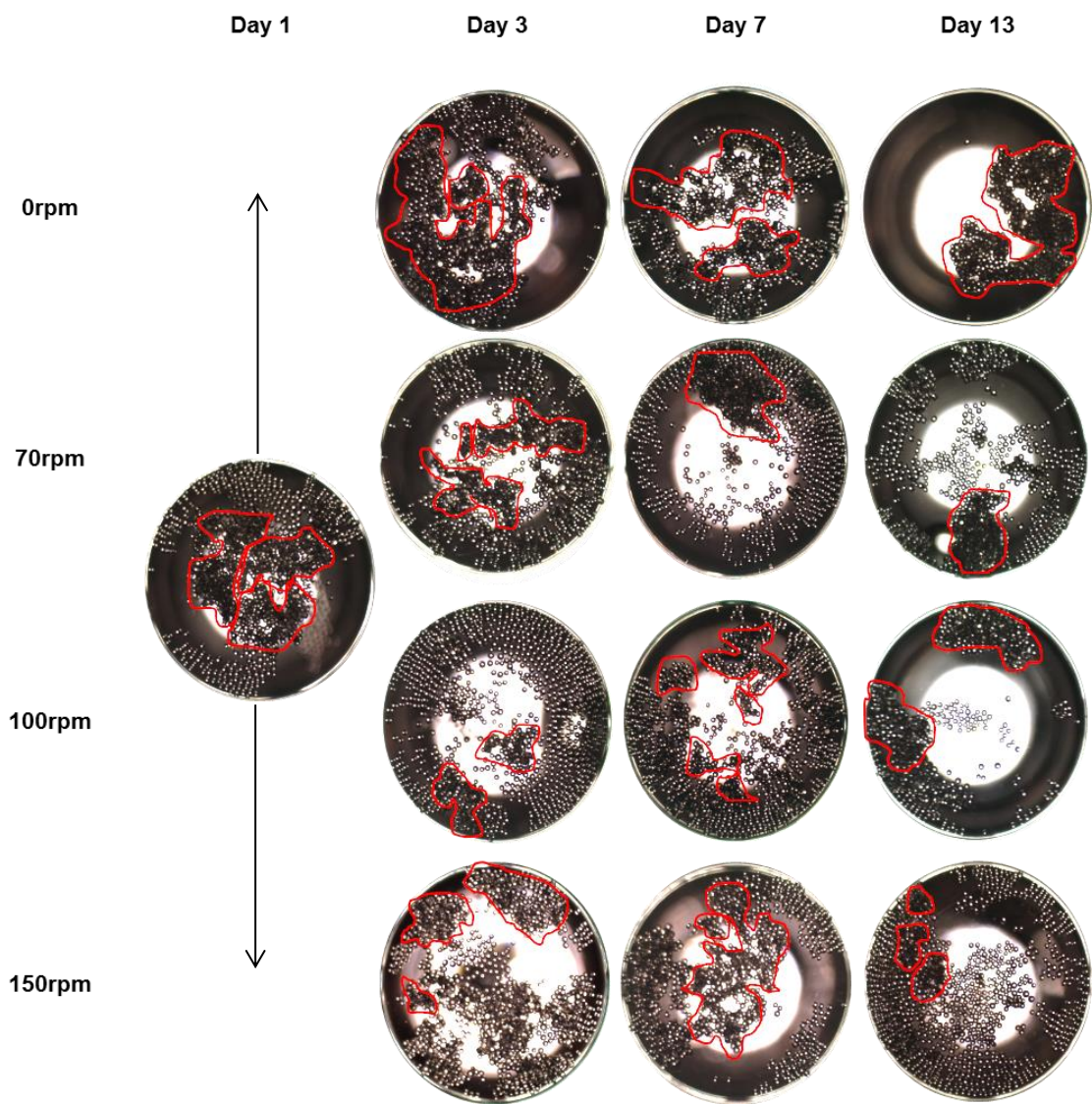


Figure 3.8 Formation of Synthemax-cell clusters under different agitation rates. Phase contrast images of an individual ultra-low attachment microwell illustrating hBM-MSCs cultured on Synthemax over a 13-day period using the same well from day 3 onwards. Red markings highlight areas of clustering. Images were taken under 2x magnification.

13, as was noted with the Ti-PGM's, 150rpm conditions were notably less effective at maintaining the clusters formed towards this latter time point. The three other agitation speeds produced clusters which maintained their structures from day 7 through to day 13, and static conditions showed visibly favourable conditions in aiding the ability of bringing together the remaining microcarriers. The interesting thing to note here is the correlation between these images and

the cell proliferation assays. While the phase contrast images of 0rpm and 150rpm corroborate well with the cell proliferation graphs, 70rpm and 100rpm agree to a lesser degree with the images of 70rpm not conclusively validating the agitation speeds ability to yield high viable cell numbers. One potential explanation for this discrepancy is the inability to visualize all the Sythemax microcarriers or clusters formed in the well. This is due to density of the microcarriers and the liquid surface tension of the microwell. Both of these factors coupled together meant cell clusters became buoyant preventing them from being imaged clearly, as they would be out of focus.

3.3.2.3 Matrix deposition by hBM-MSCs on Ti-PGMs

Analysis of matrix deposition by hBM-MSCs cultured on Ti5 and Ti7 microspheres under static and dynamic conditions in ultra-low attachment plates was undertaken at 7 and 13 days (Figures 3.9 and 3.10). Fibronectin expression surrounding the cells cultured on the Ti-PGMs was visibly higher around both materials when cultured for 13 days under 70rpm conditions (Figure 3.9). The cells cultured on Ti5 under static conditions for 13 days generated extremely mature ECM compared to Ti7 under the same conditions. While cells cultured on Ti5 showed more fibronectin expression on day 7 compared to Ti7, its expression on day 13 except for cells cultured under static conditions, showed no clear differences between Ti5 and Ti7. There was limited expression of fibronectin under 150rpm conditions on both day 7 and 13. Compared to fibronectin, type-I collagen expression under the different conditions was distinctly lower. When comparing their immunofluorescent profiles (Figures 3.9 and 3.10) a trend is evident in their respective protein expressions, whereby the cells cultured on day 13 expressed more type-I collagen than on day 7, and furthermore 150rpm overall showed lower expression than the other conditions. There were no observable differences in type-I collagen expression between the two types of Ti-PGMs studied. Cells cultured under the higher agitation rates showed stretched, fibrous structures while the expression of ECM under static conditions seemed more rigid and mature. It should be noted that Synthemax microcarriers' images have not been used due to the following reasons; firstly, processing caused degradation of the Synthemax-cell clusters through pipetting action required for the multiple

washing and staining steps, the remaining microcarriers were kept for staining however their tendencies to float in solution hindered proper focussing of Synthemax.

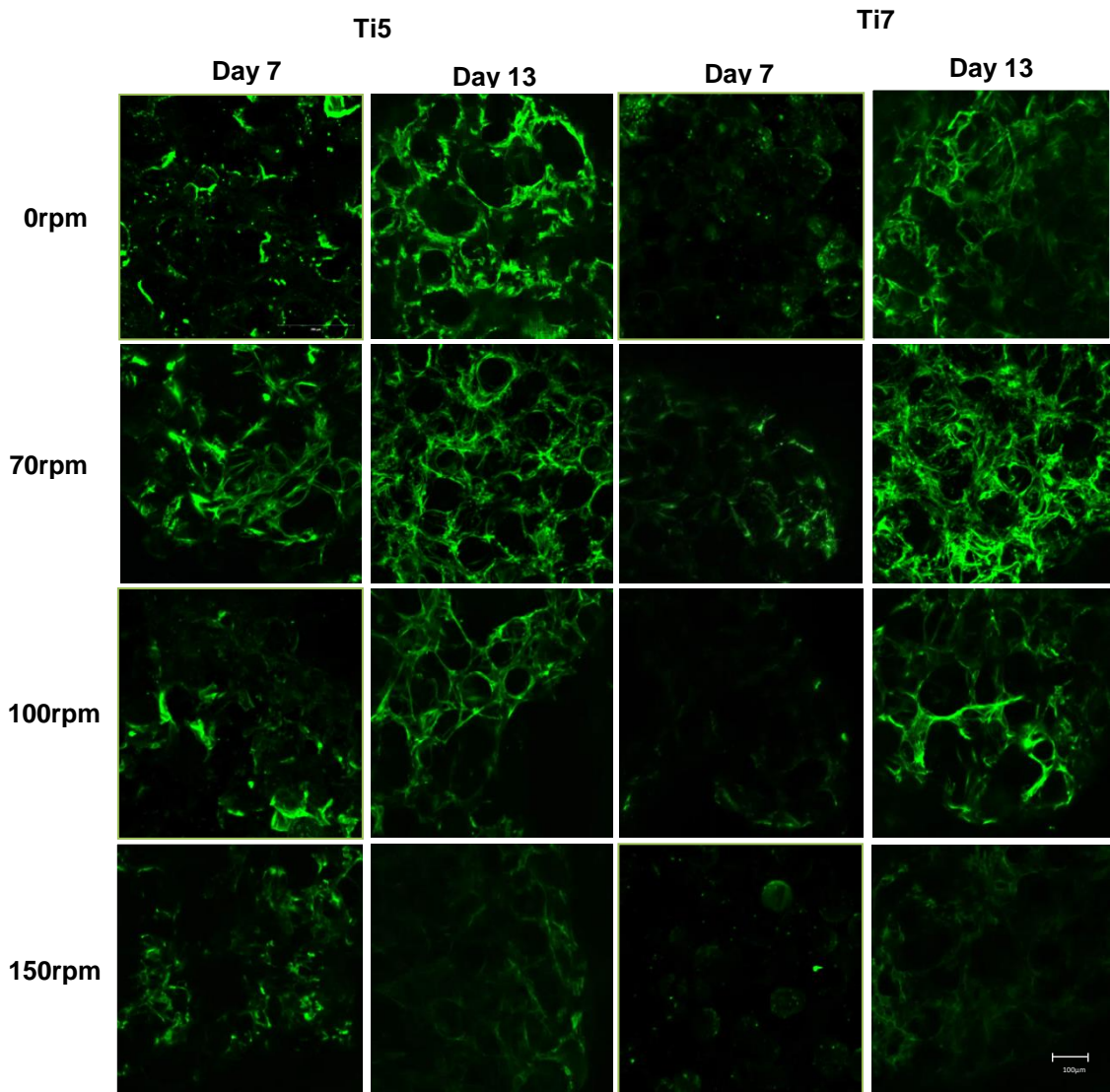


Figure 3.9 Fibronectin expression by hBM-MSCs cultured on Ti-PGMs in ultra-low attachment 96-well microplates at a range of agitation rates on days 7 and 13 post culture using confocal laser scanning microscopy. Images were acquired and converted into Z-stack images which were rendered to produce a maximum intensity projection of cross-sections up to 150µm. Images taken at 10x magnification where scale bar is 100µm.

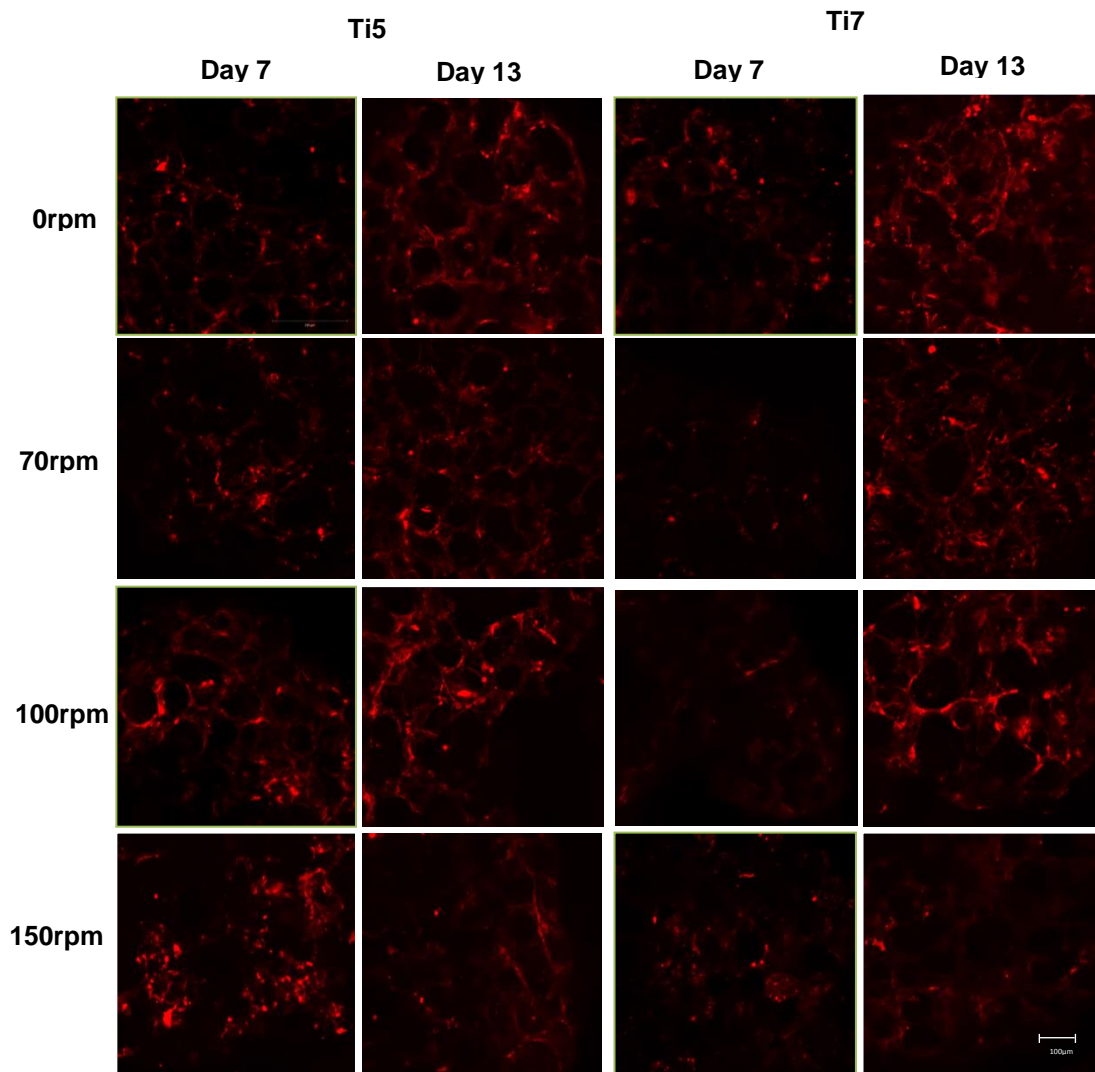


Figure 3.10 Type-I collagen expression by hBM-MSCs cultured on Ti-PGMs in ultra-low attachment 96-well microplates at a range of agitation rates on days 7 and 13 post culture using confocal laser scanning microscopy. Images were acquired and converted into Z-stack images which were rendered to produce a maximum intensity projection of cross-sections up to 150µm. Images taken at 10x magnification where scale bar is 100µm.

3.3.3 The effect of an altered biophysical environment on cell/microsphere interaction

3.3.3.1 Cell proliferation of hBM-MSC cells cultured in conditioned media

Cell proliferation was examined to determine if hBM-MSCs had improved growth profiles when cultured in conditioned media. The absorbance values generated from the CCK-8 assay identified the different levels of proliferation when hBM-MSC cultured in various types of conditioned media (TiO₂-conditioned, Osteogenic differentiation and DMEM) over a 7 day period when grown on TCP is represented in Figure 3.11. It was observed that for all the different culture media tested, cell number increased over time, from day 1 to 7 ($***p < 0.001$). From day 1 to day 3 cell number increased across all media types ($***p < 0.001$), however there were significant increases in cell proliferation in both 2mg/ml TiO₂-conditioned media ($*p < 0.05$) and osteogenic differentiation media ($***p > 0.001$) when compared to the DMEM control. TiO₂-conditioned media at a concentration of 2g/l showed significantly higher cell viability than media containing a 20mg/ml concentration. By day 5 greater numbers of cells were found in 2mg/ml TiO₂-conditioned media than 20mg/ml TiO₂-conditioned media, osteogenic differentiation media ($**p < 0.01$) and DMEM ($***p < 0.001$). By the end of culture on day 7 both 2g/l and 10g/l TiO₂-conditioned media resulted in increased cell number, compared with the DMEM control ($***p < 0.001$). Compared to the hBM-MSC population in DMEM, 2mg/ml and 10mg/ml TiO₂-conditioned media were 49.4% and 27.1% higher respectively.

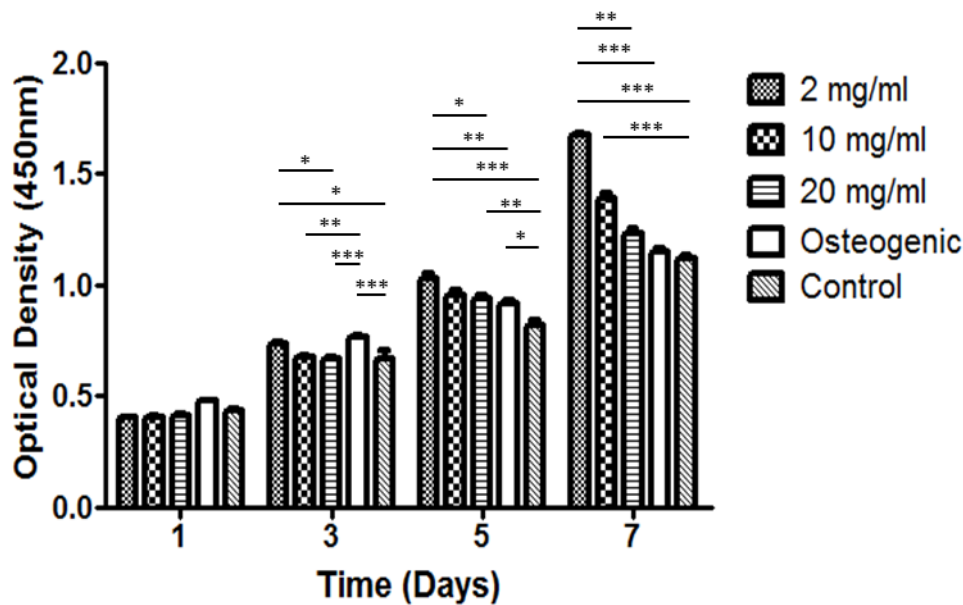


Figure 3.11 Optical densities readings of hBM-MSCs proliferated in different conditioned medias. hBM-MSCs were cultured in conditioned media in Nunclon™ flat bottomed tissue culture 96-well microplates (Thermo Fisher Scientific, UK) and CCK-8 assay readings were taken at time points 1, 3, 5 and 7. Ti-conditioned media, commercially available osteogenic media (Lonza, UK) and commercially available DMEM (Gibco®, Life Technologies Ltd., Paisley, UK) were the studied conditioned media types. Error bars represent +SD and n=3 biological repeats. *= $p < 0.05$, **= $p < 0.01$ and ***= $p < 0.001$. Note that the differences shown in the bar chart, while not visibly clear to be statistically significant are determined using specific models based on prerequisites of normality and variance. Box-and-whisker plots in Figure A.4 of the Appendix provide a more accurate representation of the differences observed between the different media types.

3.3.3.2 Extracellular matrix protein immunofluorescent expression

The expression of type-I collagen from hBM-MSC cells which have been cultured for 7 days in various types of media (TiO₂-conditioned media, osteogenic differentiation media and DMEM) on Nunclon tissue culture 96-well microplates is shown in Figures 3.12. Images taken of the cells cultured in the TiO₂-conditioned media showed similar type-I collagen expression to standard DMEM after 7 days of culture. Osteogenic differentiation media on the other hand showed higher levels of type-I collagen expression when compared to the control and other media types.

The expression of extracellular structural protein osteopontin and osteoblast secreting protein osteocalcin are illustrated in Figures 3.13 and 3.14 respectively. Osteopontin expression was negligible on day 7 of culture across most of the conditions studied. One of the only conditions to show upregulation of osteopontin expression compared to the DMEM control was that of the hBM-MSCs cultured under osteogenic differentiation media. Limited expression was observed with the late differentiation marker osteocalcin across all media types.

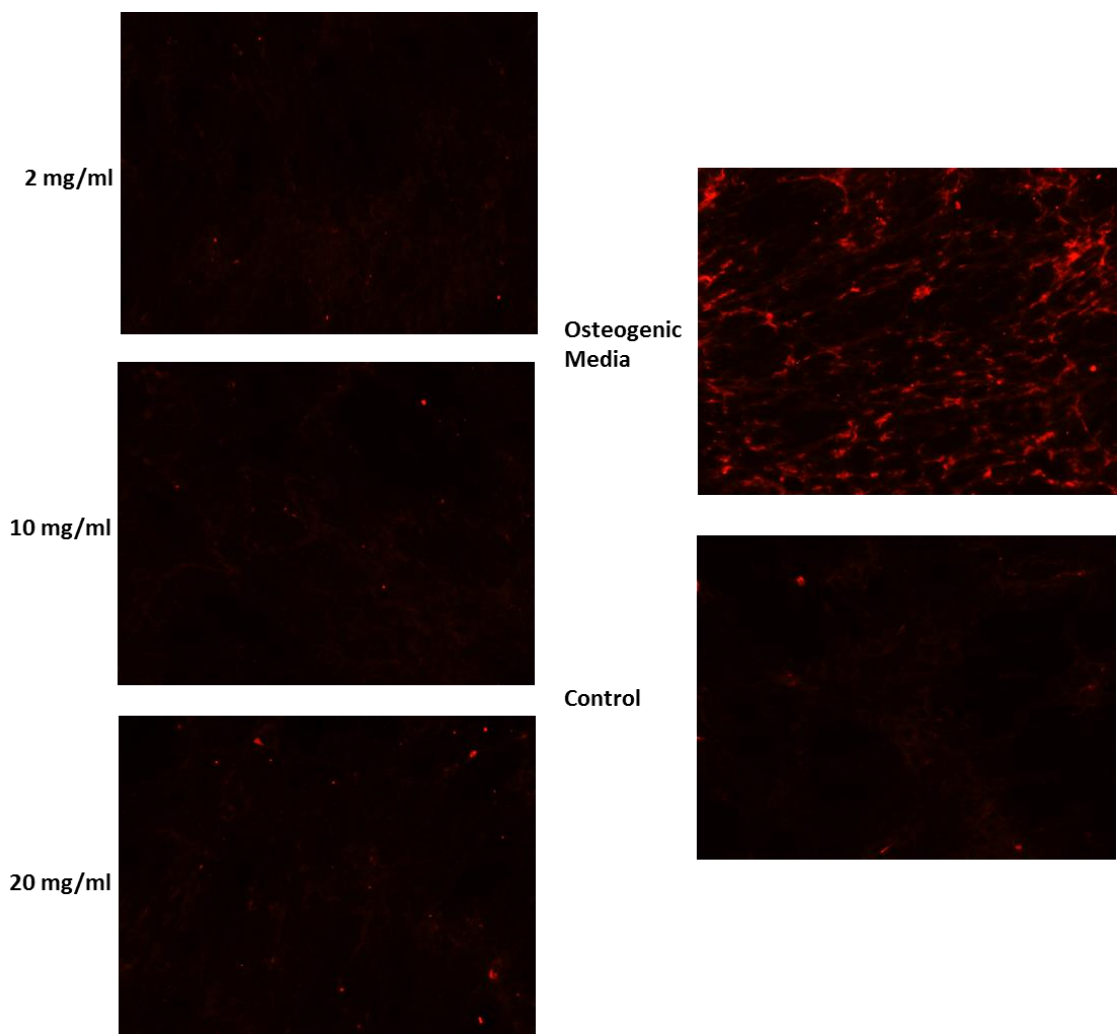


Figure 3.12 Type-1 collagen expression by hBM-MSCs cultured in Nunclon™ flat bottomed tissue culture 96-well microplates (Thermo Fisher Scientific, UK) after 7 days of culture in Ti-conditioned media, commercially available osteogenic differentiation media (Lonza, UK) and DMEM (Gibco®, Life Technologies Ltd., Paisley, UK). Images take at 20x magnification

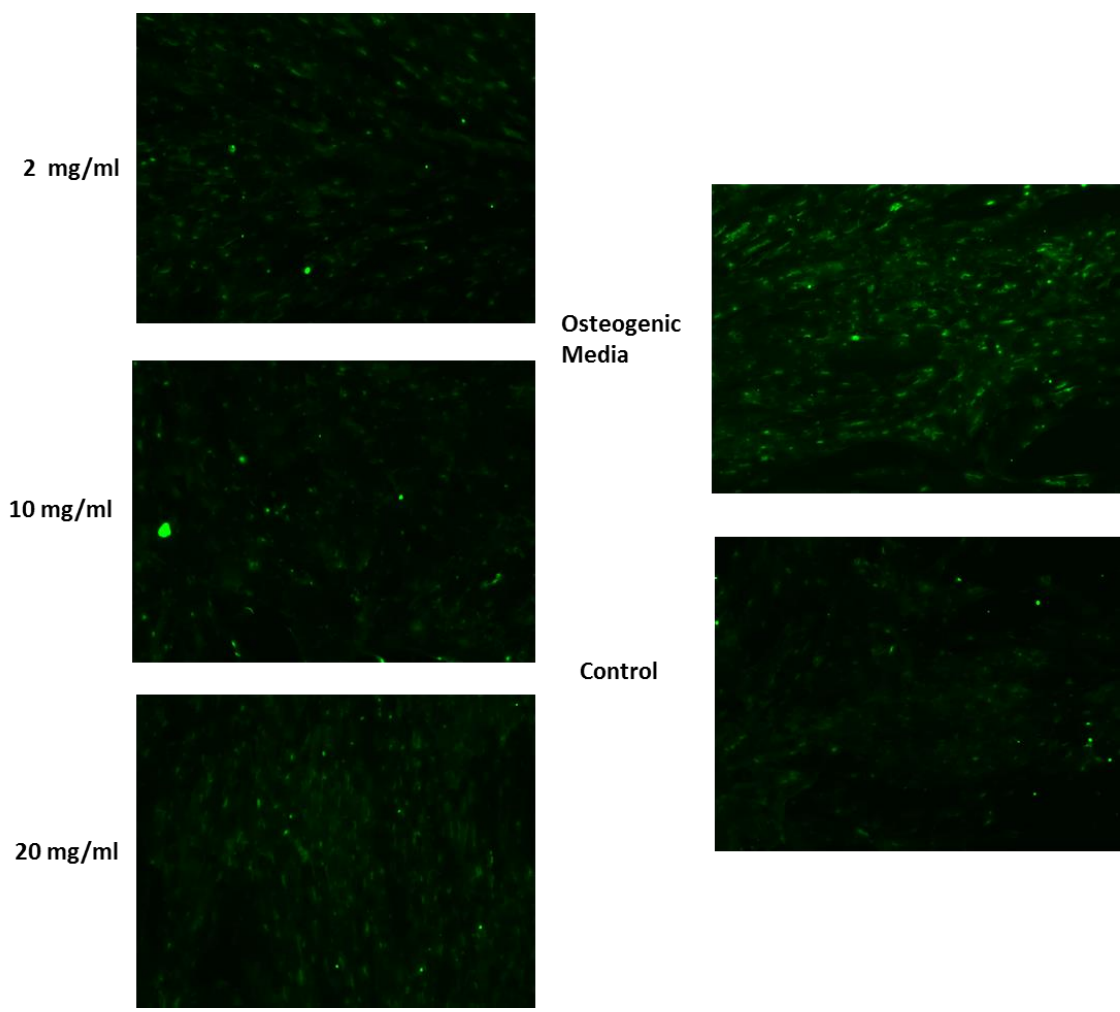


Figure 3.13 Osteopontin expression by hBM-MSCs cultured in Nunclon™ flat bottomed tissue culture 96-well microplates (Thermo Fisher Scientific, UK) after 7 days of culture in Ti-conditioned media, commercially available osteogenic differentiation media (Lonza, UK) and DMEM (Gibco®, Life Technologies Ltd., Paisley, UK). Images take at 20x magnification

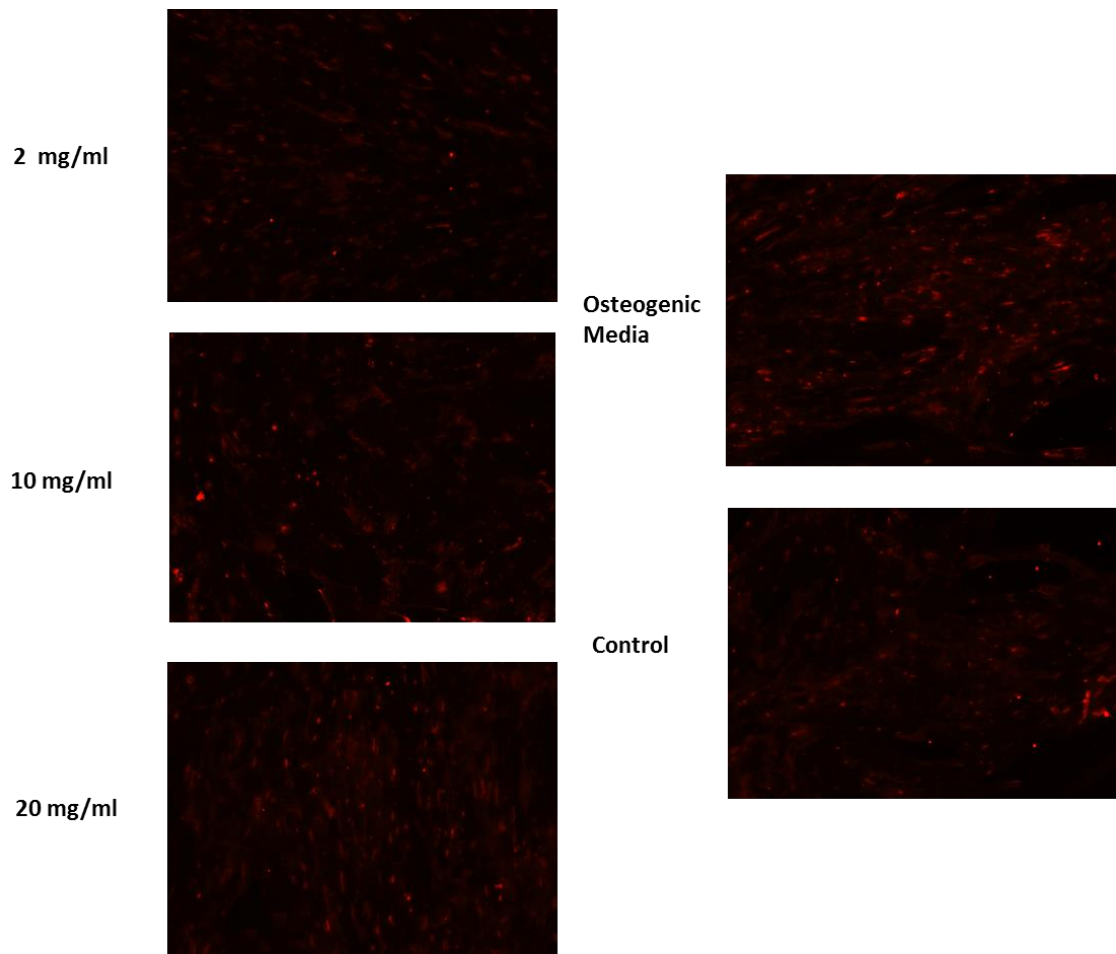


Figure 3.14 Osteocalcin expression by hBM-MSCs cultured in Nunclon™ flat bottomed tissue culture 96-well microplates (Thermo Fisher Scientific, UK) after 7 days of culture in Ti-conditioned media, commercially available osteogenic differentiation media (Lonza, UK) and DMEM (Gibco®, Life Technologies Ltd., Paisley, UK). Images take at 20x magnification

3.4 Discussion

The main objective of this chapter was to determine whether Ti-PGMs can support hBM-MSCs responses that are critical for cell expansion and osteogenic differentiation. Having found in Chapter 2 that Ti-PGMs can support osteoblastic MG63 cell proliferation, we sought to follow up that study with an analysis of MSCs, which are a more clinically relevant cell type for tissue engineering. While the agitation speeds chosen in Chapter 2 were directly based on Froude mixing patterns (Weheliye et al., 2013), the speeds chosen for the hBM-MSC cell line were established using the results obtained from the previous chapter as a reference point but also following the rationale that the optimal agitation rate determined for MG63 cells could be excessive for MSCs in light of previous studies carried out on MSCs in shaken vessels (Oh et al., 2009, Deutsch and Guldberg, 2010, Siddiquee and Sha, 2013). While limited research has been carried out on shaken culture of MSCs, especially on microspheres, an estimate of the required agitation rate used in this chapter could only be gauged from previous studies by identifying the vessel dimensions, volume of liquid used, and the orbital diameter of the shaken platforms used in these studies. By using these parameters to identify the mixing patterns created in each respective study, suitable speeds could be determined to carry out the experiments in this chapter. Most of the agitation rates used in these studies corresponded to a Froude number that was a magnitude lower than that associated with the speeds calculated from Fr_c in Chapter 2. Consequently, new agitation speeds were determined based around these Froude values to study the impact of dynamic culture conditions on hBM-MSC proliferation. These were 75rpm, 100rpm and 150rpm.

First and foremost, it was necessary to ensure that the hBM-MSCs maintained the required functional characteristics of MSCs such as multi-potency and ability to differentiate along adipogenic, chondrogenic and osteogenic lineages. According to the International Society for Cellular Therapy (ISCT) the minimal criteria required to define human MSCs is their ability to adhere to plastic surfaces, under standard culture conditions, the ability to express key surface markers (CD73, CD90 and CD105) and be void of expression of other specific

markers (including CD34, CD45, CD11b) and finally differentiate to osteoblasts, adipocytes and chondroblasts *in vitro* (Dominici et al., 2006). The hBM-MSCs used in this research were cultured to an upper passage limit of P6; therefore, it was important to ensure that the cells maintained their differential capacity. As cells become subjected to increased numbers of passages, the probability that their genes involved in cell cycle, DNA replication and DNA repair are significantly down-regulated increases (Wagner et al., 2010, Oliveira et al., 2014). Therefore, as aforementioned the cells used were not used past their sixth passage. Having carried out the differentiation of the hBM-MSCs it was clear to see that the cell line used had its intrinsic property to differentiate into adipocytes, chondrocytes and more importantly osteoblasts (Fig 3.1). Furthermore, the highest passages of cells used also retained their pluripotency, confirmed through flow cytometry.

It was important to consider how best to determine the quantity of Synthemax microcarriers used for this study. As the Synthemax microcarriers are larger in dimension (125-212 μm) compared to the Ti-PGMs there was no practical way to generate a monolayer and ensure that equivalent surface areas for cell attachment was available. It was decided that using a quantity of microcarriers and Ti-PGMS that had the same cross-sectional areas was a compromise between the Ti-PGMs having a larger total surface area and the Synthemax occupying a large volume of the well. In future, it is recommended that a more suitable microcarrier is chosen with dimensions similar to the Ti-PGMs studied. Comparing the performance of Ti-PGMs and Synthemax in terms of cell proliferation, a clear trend wasn't evident and each material performed differently under different conditions. Under static conditions Synthemax performed significantly better than the Ti-PGMs (Fig 3.5). However, under dynamic conditions there were no clear differences on average between the culture-substrates studied. The observed differences seen under static conditions may arise from the density differences between Synthemax and the Ti-PGMs. As the density of Synthemax (1.026 g/cm³) is lower than that of Ti-PGMs (2.65-2.67 g/cm³), the higher agitation may have a greater impact on Synthemax mobility compared to Ti-PGMs which could become detrimental to cell attachment and growth. As the highest agitation rate studied with the hBM-MSCs was half the N_c , the turbulent mixing zone wouldn't have reached the base of the vessel, where

the hBM-MSCs attached to the Ti-PGMs remained throughout culture. This effectively harboured the hBM-MSCs cultured on Ti-PGMs away from a high shear zone. However, this stagnation of the Ti-PGMs can become detrimental, because if the heavy Ti-PGMs resist the flow of fluid, surface shear on the Ti-PGMs will increase. The effects of static/low agitation culture conditions would be favourable for Synthemax culture as cells would be able to proliferate on the protein coated surface undisturbed. The suppliers recommended protocol for culture of MSC's on Synthemax microcarriers suggests agitation speeds of 30-40rpm; however, this is when used with a spinner flask. It can be expected that the performance of the microcarriers reduce as shaken agitation speed increases from static conditions to agitation higher than 50rpm. Fold expansion was determined (Table 3.1) and revealed that Ti-PGMs performed better under low agitation rates, with maximum cell numbers on both Ti-PGMs being achieved at 70rpm conditions.

However, when agitation was increased past this point the effects of fluid flow became limiting with lower cells yield achieved. The difference in concentration of TiO₂ within the Ti-PGMs had limited effect on proliferation under each condition. The Ti-PGMs matched Synthemax proliferation under agitated conditions, providing clear evidence to suggest that the Ti-PGMs can efficiently support hBM-MSC proliferation under dynamic conditions. Mild agitation had a positive effect on hBM-MSC proliferation when cultured on Ti-PGMs; however, this was not the case for Synthemax which could achieve better cell growth from the outset. The use of agitation to enhance proliferation of BM-MSCs has been well documented. Conflicting reports have been made in studies examining the impact of fluid flow on cell proliferation. In the studies which have reported improved MSC proliferation, the cells were exposed to oscillatory fluid flow of 1Hz and a shear stress of 10 dyn/cm² for 2 hours, with proliferation assessed after 24 hours (Li et al., 2004). The effects of oscillatory fluid flow also increased mRNA levels of both osteopontin and osteocalcin. Studies have shown that human alveolar bone marrow-derived mesenchymal stem cells subjected to long periods of high agitation had reduced cell proliferation compared to when cultured for shorter periods, however the speeds only created laminar shear stresses, suggesting that light agitation is required to improve proliferation (Lim et al.,

2014). However, other studies exist reporting a lack of cell growth when shear stresses of 1.6-2.7 dyn/cm² were applied, considerably lower than those applied in the study carried out by Lim et al (Kreke and Goldstein, 2004, Kreke et al., 2005). The loss of cell viability upon administration of fluid flow has been hypothesized to be down to the loss of a non-osteogenic subset of MSCs unable to adapt or lacking the inherent qualities to respond with the appropriate mechanotransduction tools (Kreke et al., 2005).

Cell-microsphere clustering can be used as an indicator that cells are interacting and forming bridges across to adjacent microspheres, resulting in the formation of complex 3D structures. Therefore, cultures were imaged to determine whether clusters formed and to what extent. The phase contrast microscopy images support the cell proliferation assay findings, where the cell cultured in 150rpm conditions on both Ti-PGMs and Synthemax exhibited limited clustering by day 13 when compared to the other conditions studied. While clusters were formed under static, 70 and 100rpm conditions when hBM-MSCs were cultured on Ti-PGMs, substantial clustering was only observed in wells containing Synthemax under static conditions. The change in fluid dynamics upon increasing agitation could affect the clustering formed on both materials. Moreover, as Synthemax has a lower density and is buoyant, there is a greater distribution of microcarriers throughout the whole culture volume, reducing the collision events that can lead to bridging and clustering. This differs from the clusters formed with Ti-PGMs which remain at the bottom of the well. As described by Weheliye et al., upon agitating a cylindrical vessel in an orbital manner, two distinct zones form, an upper zone where toroidal vortices enable effective mixing, and a stagnant region towards the base of the well (Weheliye et al., 2013). Therefore, the impact of increasing agitation would have a larger effect on particulates in suspension, in this case Synthemax, rather than microspheres at the base of the vessel, such as Ti-PGMs.

ECM proteins type-I collagen and fibronectin are important for cell responses including induction of osteogenic differentiation and have been shown to regulate MSC behaviour when coupled with the ECM rich reservoir of endogenous and

exogenous growth factors (Bi et al., 2005, Schwab et al., 2013). Osteogenic differentiation is highly dependent on the external microenvironment, and the presence of key ECM proteins can influence the process (Salasznyk et al., 2004). A plethora of research has been published on ECM-mediated osteogenic differentiation of MSCs cultured on biomaterials (Bierbaum et al., 2012, Penolazzi et al., 2012, Polo-Corrales et al., 2014, Noh et al., 2016), including bioactive glasses (Harvestine et al., 2016). Studies have shown that the presence of type-I collagen and fibronectin during culture induces osteogenic differentiation (Moursi et al., 1997, Salasznyk et al., 2004, Cool and Nurcombe, 2005, Donzelli et al., 2007, Schneider et al., 2010), therefore the relative decrease in type-I collagen and fibronectin expression at 150rpm compared to the other agitation rates studied indicates that high agitation can negatively influence osteogenic differentiation. The influence of fibronectin is predominantly via its capacity to promote cellular adhesion and it has been shown to promote MSC attachment (Hidalgo-Bastida and Cartmell, 2010). However, type I collagen is more abundantly secreted by differentiating osteoblasts, therefore is more commonly used as a marker of early stage osteogenic differentiation (Salasznyk et al., 2004). However, the timing of type-I collagen upregulation is very specific as studies have shown that immature osteoprogenitor cells do not express type-I collagen, whereas it is upregulated by mature osteoprogenitor cells (Huang et al., 2007). This is evident on both Ti-PGMs with visibly increased type I collagen expression on day 13 under static 70 and 100rpm conditions.

The effect of increased TiO₂ concentration on ECM synthesis was negligible and this may result from improved stability, hence reduced rate of degradation associated with glasses doped with high quantities of TiO₂. While Abou Neel et al., showed that increasing TiO₂ content from 3 mol% to 5 mol% in phosphate glasses led to up-regulated type I collagen expression, it was concluded that concentrations beyond 5 mol% did not produce any significant changes in degradation and therefore would show no increase in TiO₂ dissolution (Abou Neel et al., 2007). There are, however, conflicting reports of the effect of agitation upon type-I collagen expression of hBM-MSCs. While some studies concluded subjecting the cells to agitation resulted in increased expression (Augst et al., 2008) some studies have shown that increased exposure to fluid flow and shear

have reduced type-I collagen expression (Grellier et al., 2009). Clearly the rate of agitation is an important factor and there may be a critical threshold after which fluid flow no longer positively stimulates, but instead negatively impacts on cell outputs.

The degradation of Ti-PGMs *in vitro* causes release of Ca^{2+} and inorganic phosphate ions which can affect surrounding cells. Calcium and phosphate ions exist in basal DMEM media at a concentration of 1.8mM and 0.09mM respectively, as the ion plays an essential role in maintaining growth and function of the cells. However, the concentration of Ca^{2+} present during the process of bone remodelling by the action of osteoclasts is significantly higher at 40mM, a local concentration increase that has proven important in regulating osteoblast proliferation and differentiation. Therefore cells responsible for bone formation should be able to withstand these conditions (Silver et al., 1988). The differentiation process of bone-forming cells is highly regulated by Ca^{2+} , influencing transcription factors via Ca^{2+} signal transducers (Parrington and Tunn, 2014). Liu et al., concluded that the ionic concentrations of Ca^{2+} and inorganic phosphate found in medium were optimal for MSC cell growth with deviations from these quantities resulting in no change or inducing cell apoptosis dependent on the ionic species altered (Liu et al., 2009). The hBM-MSCs cultured in 2mg/ml TiO_2 -conditioned media showed improved cell proliferation over 7 days of culture; however, this was not coupled with improved differentiation. However, cells cultured in higher concentrations of TiO_2 -conditioned media had reduced cell growth over the 7-day period. The short period of time used during to culture cells in conditioned media limits their ability to produce the key differentiation markers studied, with both OPN and OCN regularly expressed after only 14 days. Research carried out by McCullen et al., supported these findings, showing that human adipose-derived stem cells proliferated better when cultured in media containing slightly increased levels of calcium. However, when these levels increased further, proliferation was inhibited (McCullen et al., 2010). Other studies have reported that MSCs achieve accelerated growth in culture medium containing reduced calcium (Lin et al., 2005), while research also claims that higher concentrations promote osteogenic differentiation (Nakamura et al., 2010). The significant improvement in growth observed from cells cultured in 2mg/ml

TiO₂-conditioned media compared to DMEM suggests that the products of Ti-PGMs could promote further proliferation during early cell culture, however longer culture is required to establish if the dissolution ions could potentially enhance mineralization and osteogenic differentiation. Furthermore, identification of the actual concentrations of calcium and phosphate ions in solution should be quantified to identify the optimal conditions for proliferation and differentiation of hBM-MSCs.

The work in this chapter forms the basis of exploring larger scale culture vessels and the application of Ti-PGMs in the proceeding chapter. Having studied the effects of agitation speeds on proliferation and differentiation of hBM-MSCs at microwell scale, efforts were made to understand whether these cell characteristics can be mimicked at a larger more clinically relevant scale, more specifically a 125ml Erlenmeyer flask.

Chapter 4 . Scale-up of hBM-MSC culture in 125ml Erlenmeyer shake flasks using Ti-PGMs

4.1 Introduction

Having established that hBM-MSCs can be expanded on Ti-PGMs in microscale culture systems, the next goal was to determine whether hBM-MSC culture can be scaled up to produce clinically relevant quantities of engineered bone-like material.

To this end, Chapter 4 focuses on bringing together the knowledge gained regarding the use of Ti-PGMs for cell culture from previous chapters and applying it to clinical scale manufacturing of tissue engineered microunits of bone.

The process bottlenecks identified in previous chapters with cell culture on Ti-PGMs such as their inability to be suspended were addressed in this chapter. Having determined in the previous chapters that specific Ti compositions (Ti5/Ti7) did not induce significant differences in hBM-MSC growth characteristics nor show differences in ECM protein expression, only one Ti-PGM composition was carried forward in these scale-up studies. With Ti5 being advantageous in terms of reduced amounts of TiO₂, which therefore reduces raw material costs, and limited differences in degradation rate in Ti-PGMs containing in excess of 5 mol% TiO₂ (Abou Neel et al., 2007), it was considered acceptable to move forward with the Ti5 composition. The ability to support hBM-MSC function under scaled up dynamic conditions was compared to that of Synthemax at different agitation speeds. Cell characteristics including proliferation, protein and gene expression were assessed.

Previous work by Olmos and colleagues devised a model to determine the critical agitation speed necessary for suspension of microcarriers in orbitally shaken Erlenmeyer flasks (Olmos et al., 2015). The model corroborated with observations by Weheliye et al., where similar flow patterns were observed in

cylindrical vessels (Weheliye et al., 2013). The Olmos model differed slightly, by taking into consideration the dimensions of the particles (d_p) and the relative density of the material (ρ^*), highlighted in equation 4.1. Here, Fr_s indicates the suspended Froude number and the constant A depends on the geometry of the vessel used ($A=0.12$ for an Erlenmeyer flask).

$$Fr_s = \frac{2(\pi N_s)^2 d_i}{g} = A \cdot \left(\frac{d_o}{d}\right)^{-0.25} \cdot \left(\frac{h_l}{d}\right)^{0.49} \cdot (\rho^*) \cdot \left(\frac{d_p}{d}\right)^{-0.07} \quad (4.1)$$

The model however was only validated using a specific range of values for each of the parameters and the relative density of the Ti-PGMs is greater than the upper limit of the particles used to develop this model.

4.2 Materials & Methods

4.2.1 Preparation of human bone marrow derived mesenchymal stem cells

Human bone marrow derived MSCs sourced from in-house stocks were cultured as mentioned earlier in section 3.2.1. Cells were cultured using the same media and seeding density.

4.2.2 Cell culture on Ti-PGMs and Corning® Synthemax in a 125ml Erlenmeyer flask under static and dynamic conditions

Large scale culture of hBM-MSCs was carried out in Corning® 125ml Polycarbonate Erlenmeyer flasks (Corning, UK). A pre-calculated quantity of Ti-PGMs ($0.5\text{g} \pm 0.05\text{g}$) and low concentration Synthemax® II (Corning, UK) ($0.37\text{g} \pm 0.037\text{g}$) were added to separate dry culture dishes (Nunclon, UK), covered and sterilized for 90 minutes using a high intensity Blak-Ray B-100SP lamp (UVP, Cambridge, UK). Fresh DMEM containing FBS (10%) and antibody-antimycotic solution (1%) (Gibco®, Life Technologies Ltd., Paisley, UK) were added to each culture dish enabling transfer of the two different microspheres into their respective Erlenmeyer flask. The 2ml solution of media and microspheres were transferred from the culture dishes using a 1000 μl Gilson pipette into their respective 125ml Erlenmeyer flask. The culture dishes were rinsed with a further 2ml of media to ensure any residual microspheres had been transferred. Once all the material had been transferred to their respective flasks, an additional 35ml of media was added to bring the total volume within the flask to 39ml. After hBM-MSCs were harvested using the protocol described in section 2.2.3 a cell suspension of 1×10^6 cells/ml was created. From the resulting solution 1ml was transferred to each flask bringing the total volume to 40ml. The flasks were then incubated at 37°C in an atmosphere of 5% CO₂ for 24 hours under static condition. The reason the full working volume was not added to the flask was due to the poor seeding efficiency attributed to the increased fluid height. After 24 hours, an additional 40ml of fresh media was added to each of the flasks, which were then placed in their corresponding conditions.

The dynamic conditions calculated were determined by the mixing model developed to establish particle suspension speeds (N_s) in cylindrical vessels including Erlenmeyer flasks (Olmos et al., 2015). Using this model, a N_s speed of 320rpm ($Fr_s=0.58$) was calculated, however results from Chapter 3 indicated that using an agitation higher than (N_c assumed to be like N_s at the time of study) inhibited proliferation potentially through excessive shear forces and therefore it was assumed the same effect would be created at large scale with similar mixing dynamics created. Therefore, the upper agitation limit to be studied was determined as 160rpm. The other speed studied in this chapter were related to the conditions studied at microwell scale including 40rpm and 80rpm ($0.25N_s=0.5N_c$) to fully understand the effect of the scaling law on microsphere cell culture. While 40rpm agitation at large-scale did not directly correlate to a speed studied at microwell scale, it was studied to further understand the optimum agitation rate. As higher agitation rates at small-scale were detrimental to cell proliferation, it was assumed that the optimal speed may exist between static conditions and $0.5N_c$, and hence 40rpm ($0.25N_c$) was chosen. The preparation of the Erlenmeyer flasks for dynamic culture was the same as the static flasks, however after the first 24 hours the flasks were kept in their respective conditions. After this period, the flasks were transferred into an incubator and placed on a KS260 control orbital shaker (IKA, Germany) and kept at 37°C and 5% CO₂. Media changes were carried out on days 1, 4, 7, 10, 14, 17 and 21 where only 40ml of the total 80ml volume was removed,

4.2.3 Metabolite analysis

Offline glucose and lactate analysis was carried out using a Bioprofile FLEX Analyser (Nova Biomedical, UK) on days 1, 4, 7, 10, 14, 17 and 21. At each specified time points, 2ml samples were aspirated from each flask in triplicates ensuring no microspheres were removed in the process, with each sample kept on ice to minimise metabolic activity and sample degradation. Media changes occurred after sample isolation with fresh media compensating for the removed sample volume.

4.2.4 Confocal laser scanning microscopy

Immunofluorescent staining of the tissue engineered constructs formed in the 125ml Erlenmeyer flasks was carried out using the same protocol as that described in section 3.2.3.5. Taking into consideration the previous imaging issues when imaging cells cultured on Synthemax, optically enhanced Sensoplate™ 24-well glass bottom microplates (Grenier Bio-One Ltd, UK) were used to ensure image resolution was not lost and high-quality images could be obtained. Samples were isolated on day 21 using a sterilised FisherBrand™ Stainless Steel spooned spatula (Thermo Fisher Scientific, UK) and transferred to a microplate containing 1x PBS. Samples were fixed and stained to fluorescently label extracellular matrix proteins fibronectin (Mouse monoclonal, ab6328, Abcam, Cambridge, UK) and type-1 collagen (Rabbit polyclonal, ab34710, Abcam, Cambridge, UK) and bone specific extracellular matrix proteins osteopontin (OPN) (Mouse monoclonal, ab69498, Abcam, Cambridge, UK) and osteocalcin (OCN) (Rabbit polyclonal, ab10911, Millipore, UK) as described in 3.2.3.5.

4.2.5 Scanning electron microscopy

Clustered samples were fixed in Nunclon™ flat bottomed tissue culture 24-well microplates (Thermo Fisher Scientific, UK) using 3% glutaraldehyde (Sigma-Aldrich, UK) to fix the specimen, and were stored in solution at 4°C until required for SEM preparation. The glutaraldehyde fixative was replaced with a graded series of the following alcohols to dehydrate each sample: 70% EtOH for 10 minutes, 90% EtOH for 10 minutes and 100% EtOH for 10 minutes (3 times). The final 100% EtOH step was followed by adding hexamethyldisilazane (HMDS; TAAB Laboratories, UK) and leaving for 1–2 minutes to carry out critical point drying, after which the HMDS was removed and the samples extracted and dried on blotting paper. The samples were then spread on carbon adhesive discs fixed to aluminium SEM specimen stubs, with any loose residual material blown off using a compressed air duster spray. The adhered specimens were then sputter-coated with gold/palladium by a Polaron E5100 coating system (Polaron CVT, UK). The coated samples were observed using a scanning electron microscope

(JSM 5410LV, JEOL, Japan) under different magnifications, operating at a 10kV voltage.

4.2.6 Quantitative polymerase chain reaction (qPCR)

Various cell/microsphere clusters were isolated from each flask and transferred to Nunclon™ flat bottomed tissue culture 24-well microplates (Thermo Fisher Scientific, UK). The cells were harvested from their culture substrate using 0.5ml 0.25% trypsin-ethylenediaminetetraacetic acid (EDTA) solution for 5 min at 37°C. The trypsin was then inhibited by adding 1ml of fresh DMEM, with the resultant mix of cells, media and microspheres passed through a sterile Falcon® Cell Strainer (Corning, UK) with 40µm pores to separate the cells from the microspheres. The cell suspension was then transferred to a 2ml Eppendorf and centrifuged at 300g for 5 minutes.

The process of isolating RNA for cDNA synthesis started with the lysis of the cell pellet using RLT buffer (Qiagen, Germany). The resulting lysate was homogenized using a QIAshredder spin column, which was centrifuged at 10,000rpm for 2 minutes. The total RNA was isolated from the homogenized cells using the RNeasy MicroKit (Qiagen, Germany) according to the manufacturer's instructions, with 14µl of RNase-free water used to elute the isolated RNA. The RNA concentration was established using the NanoDrop 1000 (Thermo Fisher Scientific, UK). Genomic DNA elimination was carried out using the Quantitect Reverse Transcription Kit (Qiagen, Germany) to ensure no DNA was present in the RNA template solution. The RNA template was then annealed with the cDNA components of the kit, and the reverse transcription reaction was carried out for each RNA sample for 15 minutes at 42°C and then 3 minutes at 95°C to inactivate the reverse transcriptase enzyme.

The cDNA synthesised from each sample was amplified by the CFX connect Real-time PCR Detection System (Bio-Rad) using Quantitect SYBR RT-PCR Kit (Qiagen). The presence of nucleotides specific to the hBM-MSK cell line and their transcription rate were quantified by the amplified SYBR signal after 35-40 thermal cycles. The total process volume was 25µl containing 5µl of cDNA, 2.5µl

of Primer Assay and 12.5µl of Quantitect SYBR Mastermix. Using CFX Manager 3.0 software relative expression studies were carried out against the expression of rRNA encoding housekeeping gene β -actin (. The cDNA was targeted for sequences of COL1A1 (QT00037793, Qiagen), RUNX2 (QT00020517, Qiagen) and SPP1.

4.2.7 Statistical analysis

All statistical analysis was carried out using IBM SPSS Statistics version 22. Analysis was carried out using the techniques described in 2.2.10.

4.3 Results

4.3.1 Expansion of hBM-MSK in scaled up culture vessels

The first experiment assessed the effect of static and dynamic culture conditions in 125mL Erlenmeyer culture flasks. The agitation speeds chosen for this part of the research focuses on the same relationship between the dimensionless Froude number and rate of agitation that was studied in the previous chapters. The underlying difference between the speeds chosen for the current scale and those studied previously was the different models chosen to determine the Froude number for each vessel type. As the correlation between the Froude number and agitation speed remain the same across both model, the mixing patterns studied could be mapped effectively from microplates to shake flask. As illustrated in Figure 4.1, the relationship between the agitation speed studied and the N_c speed is similar at both scales.

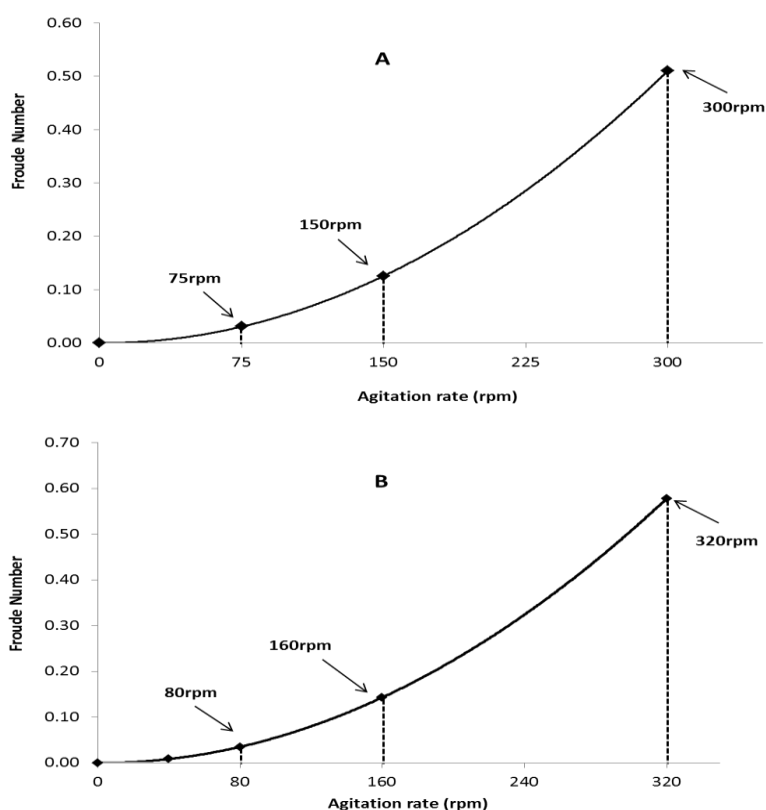


Figure 4.1 Correlation between Froude number and rate of agitation. An XY scatter plot was used to scale agitation rates from (A) 96-well microplates to (B) 125 ml Erlenmeyer shake flasks. The figure highlights the speeds chosen in relation to highest agitation rate used (300rpm) at microwell scale and how the mixing dynamics have been mimicked at shake flask scale where a N_s of 320rpm was calculated.

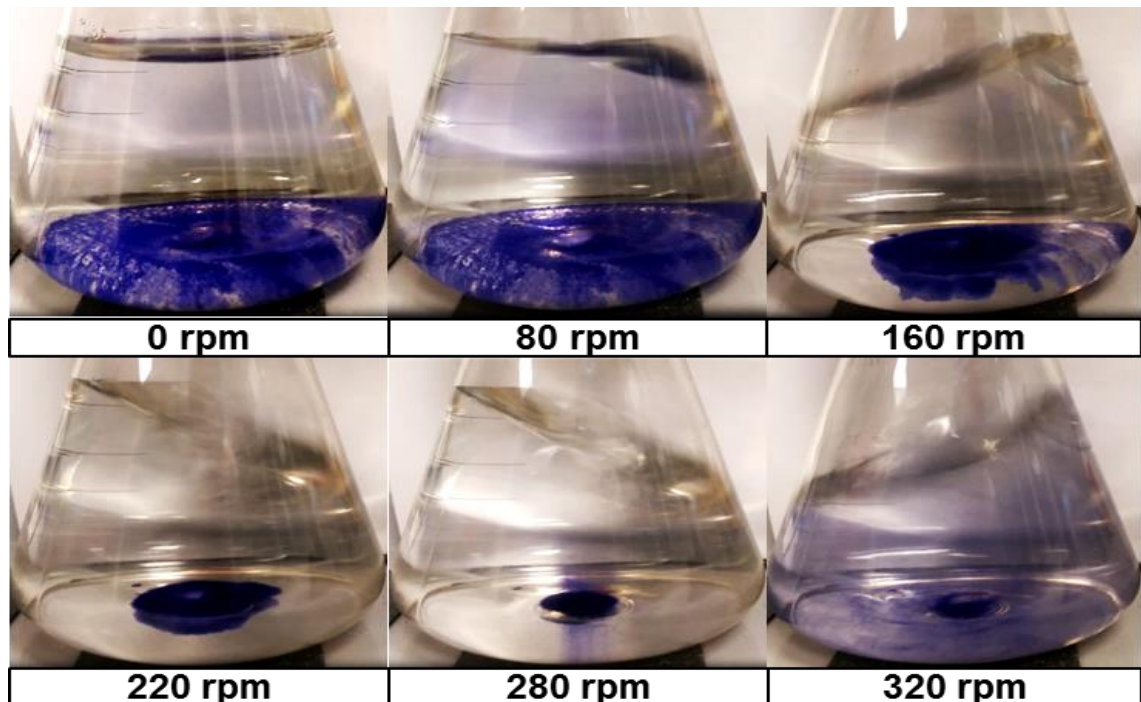


Figure 4.2 Progressive changes in Ti-PGMs monolayer with increasing agitation rate. Increased orbital agitation leads to the complete suspension of Ti-PGMs (additionally doped with a minimal amount of Co^{2+} to visualize microspheres) in a 125 mL Corning® Erlenmeyer flask containing distilled water. Operating conditions are $V_L=80$ mL, $d_o=1.0$ cm, and agitation rate: $N=0$ rpm, 80rpm, 160rpm, 220rpm, 280rpm and 320rpm. Complete suspension was observed for $N_s=320$ rpm

Visualizing the effect of increasing agitation on suspension of Ti-PGMs, provided an initial observation to understand how well the Froude number could aid dynamic cell culture on the microspheres. Using a clamp firmly fixed to the orbital plate shaker enabled the movement pattern of Ti-PGMs to be followed as agitation speed progressively increased. It can be seen from Figure 4.2 that as agitation increases from 0 to 160rpm the stagnant layer of microspheres slowly concentrates together in the centre of the flask. The microspheres concentrate further until suspension of the Ti-PGMs is achieved at approximately 320rpm as predicted by the model developed by Olmos et al. (Olmos et al., 2015)

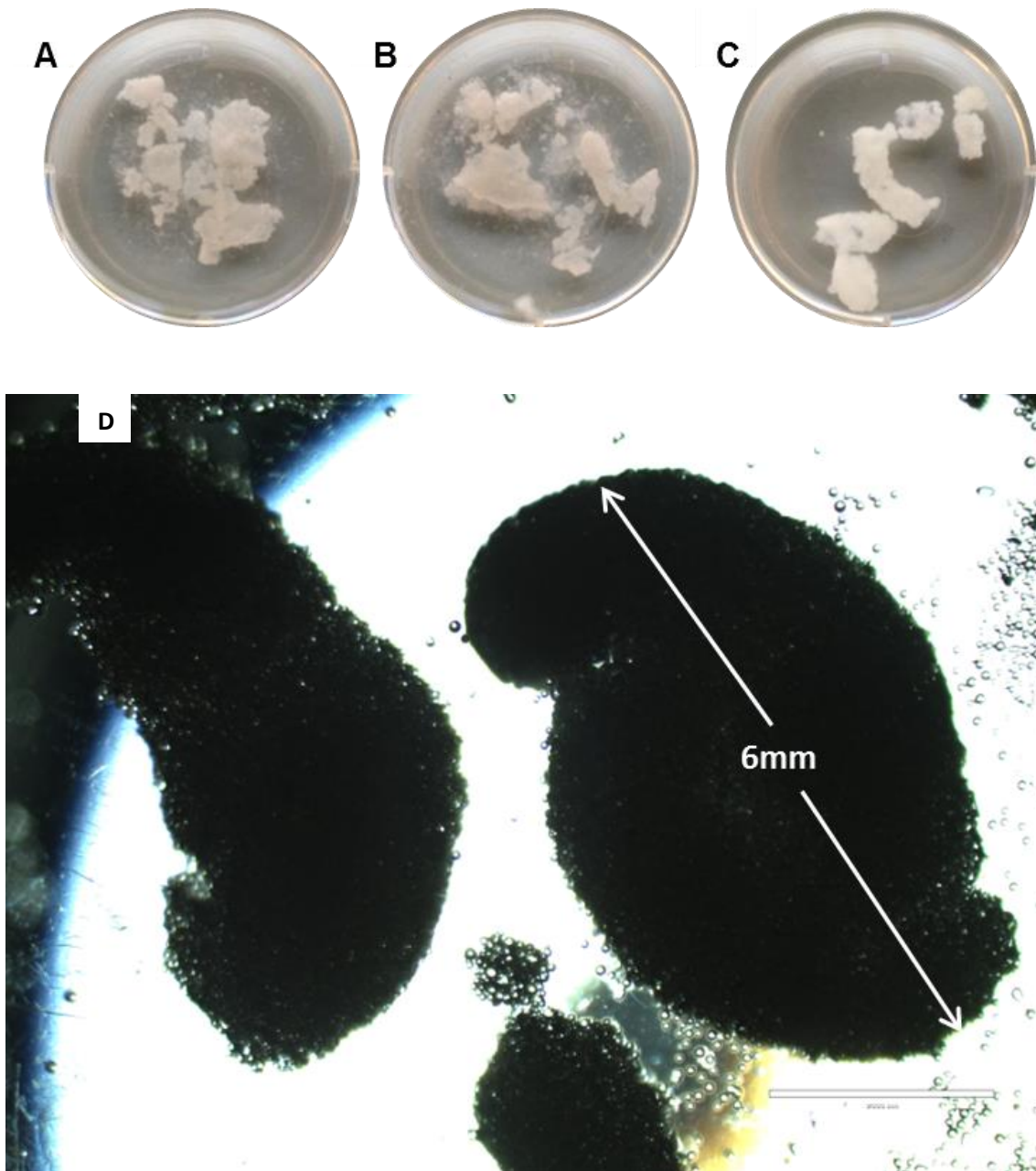


Figure 4.3 Cellular/microsphere structures formed in 125ml Erlenmeyer shake flask after 21 days of culture. Different clusters formed when hBM-MSCs are cultured on Ti-PGMs under (A) 0rpm (B) 40rpm and on Synthemax under (C) 0rpm conditions. (D) Size of the Ti-PGM/cell structures formed with the largest cluster measured at 6mm in length. Image was taken at 2x magnification. Scale bar is 2000µm.

4.3.2 Metabolite analysis

Metabolic profiling was undertaken to determine whether agitation speed affects the metabolic kinetics of the cells. The metabolic profiles in Figure 4.4 show the rates of glucose consumption and lactate production under each condition and material investigated. Cells cultured on Ti-PGMs consumed glucose at a greater rate when cultured at 160rpm for 21 days (Fig 4.4A), with significant increases observed between days 4 to 14 when compared to 0rpm (** $p < 0.01$) and 40rpm (* $p < 0.05$), while a significant increase was observed on day 10 compared to 80rpm (** $p < 0.01$). The lactate production profile of Ti-PGMs (Fig 4.4B) showed that the cells produced the same amount of lactate over the first 4 days of culture. Between days 4 and 17 variability in lactate production rate could be observed between the different conditions. However, the largest difference was seen between day 17 and 21 where cells cultured on 160rpm showed a significant decrease in lactate production compared to the other conditions. This reduction in lactate occurred in parallel to an increase in media glucose concentration. Limited differences were observed in the glucose consumption profile of Synthemax (Figure 4.4C). However, the lactate profile showed that under 160rpm conditions lactate production was significantly lower than the other conditions studied (* $p < 0.05$).

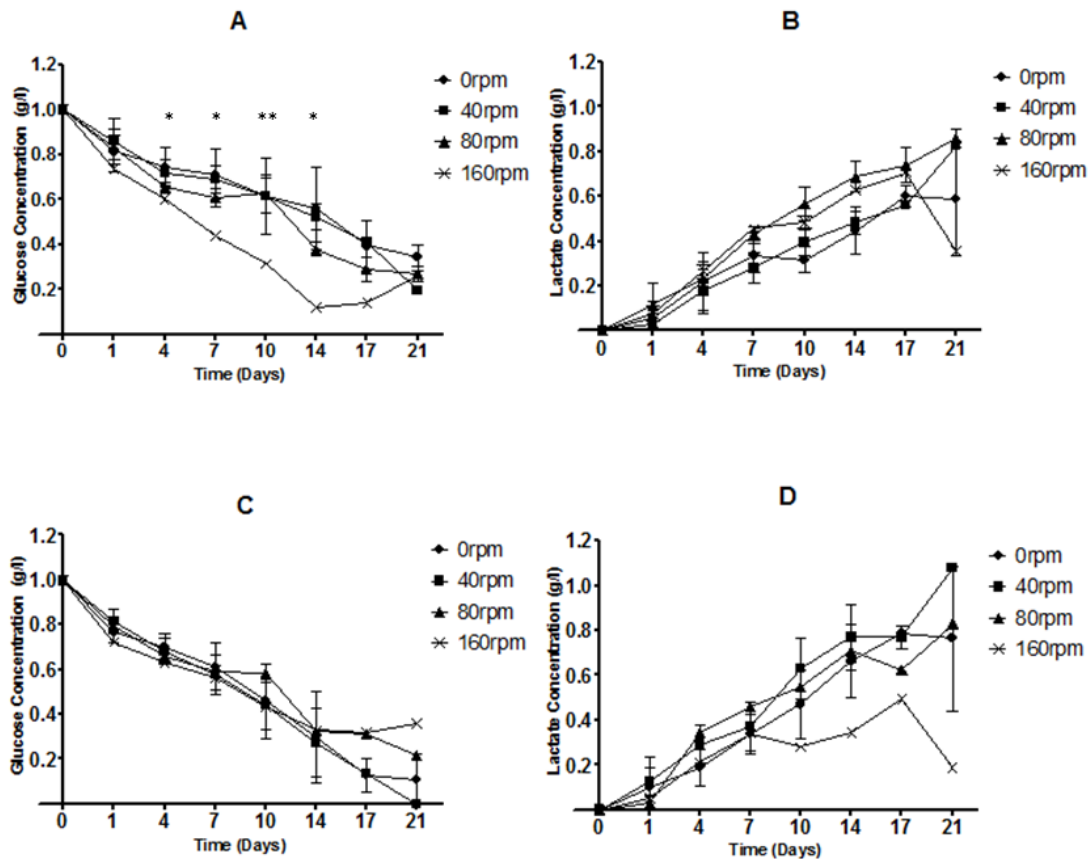


Figure 4.4 hBM-MSCs metabolic profiles when cultured on different substrates under different agitation rates. Line graphs show glucose consumption (A, C) and lactate production (B, D) when cultured on Ti-PGMs (A & B) and Synthemax (C&D) at days 0, 1, 4, 7, 10, 14, 17 and 21 under ● - 0rpm ■ - 40rpm ▲ - 80rpm and x – 160rpm condition. Values represent mean ± SD (n=3). Significance values denoted by *=p<0.05 indicate significant differences between 160rpm and both 0 and 40rpm while **=p<0.01 indicates significant differences between 160rpm and all other conditions.

When comparing the metabolic profiles of Synthemax to those produced by Ti-PGMs, there were significant differences in glucose consumption across most of the agitation speeds studied. When hBM-MSCs were cultured under 0rpm and 40rpm conditions (Fig 4.5A & B), reduced glucose consumption was observed by cells growing on Ti-PGMs compared to Synthemax over the 21 days (*p<0.05). These differences were significant at both speeds between day 14 to 21 (**p<0.01). Cells grown at 80rpm however showed no significant differences during the 21-day culture period, however the trend observed at lower agitation speeds was not seen at 160rpm, where Ti-PGMs promoted increased glucose

consumption when compared to Synthemax from day 10 onwards (** $p < 0.01$). As expected higher lactose production was associated to conditions that favoured higher glucose consumption illustrated through Figure 4.5 & 4.6.

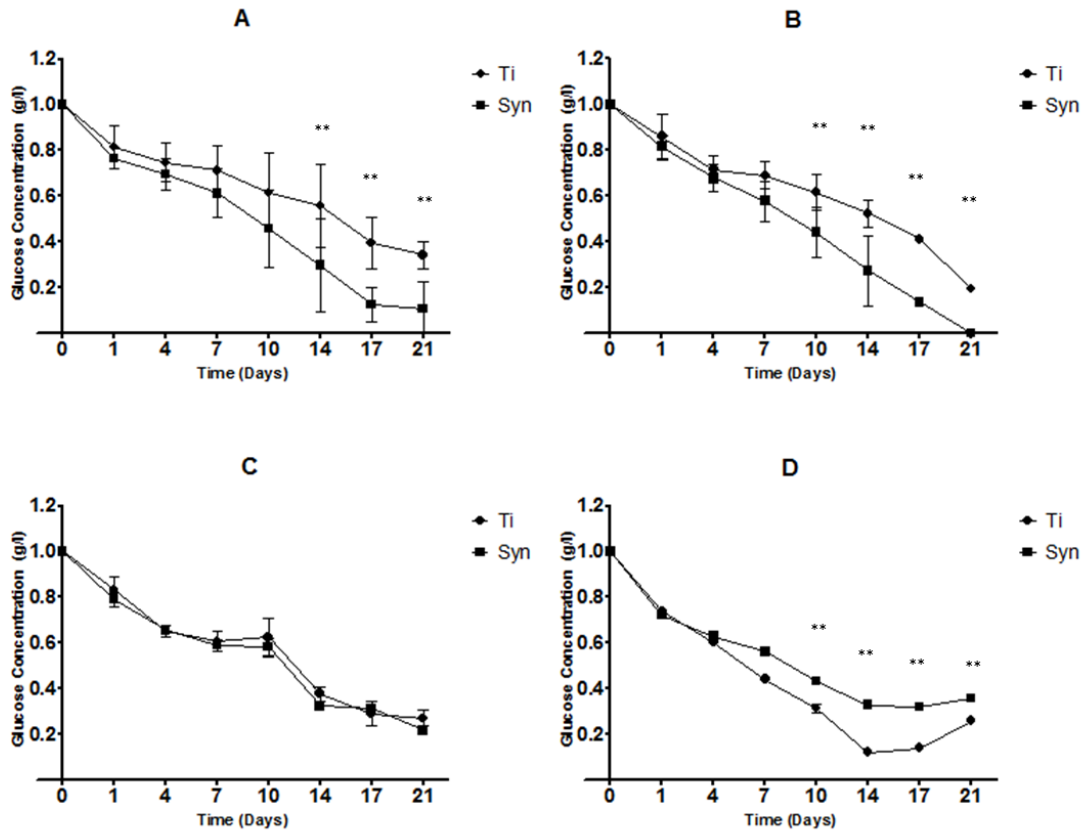


Figure 4.5 Glucose consumption of hBM-MSCs cultured on Ti-PGMs and Synthemax. Line graphs showing glucose levels at days 0, 1, 4, 7, 10, 14, 17 and 21 under (A) 0rpm, (B) 40rpm, (C) 80rpm, and (D) 160rpm condition. Values represent mean \pm SD (n=3). Significance values denoted by * = $p < 0.05$, ** = $p < 0.01$ and *** = $p < 0.001$.

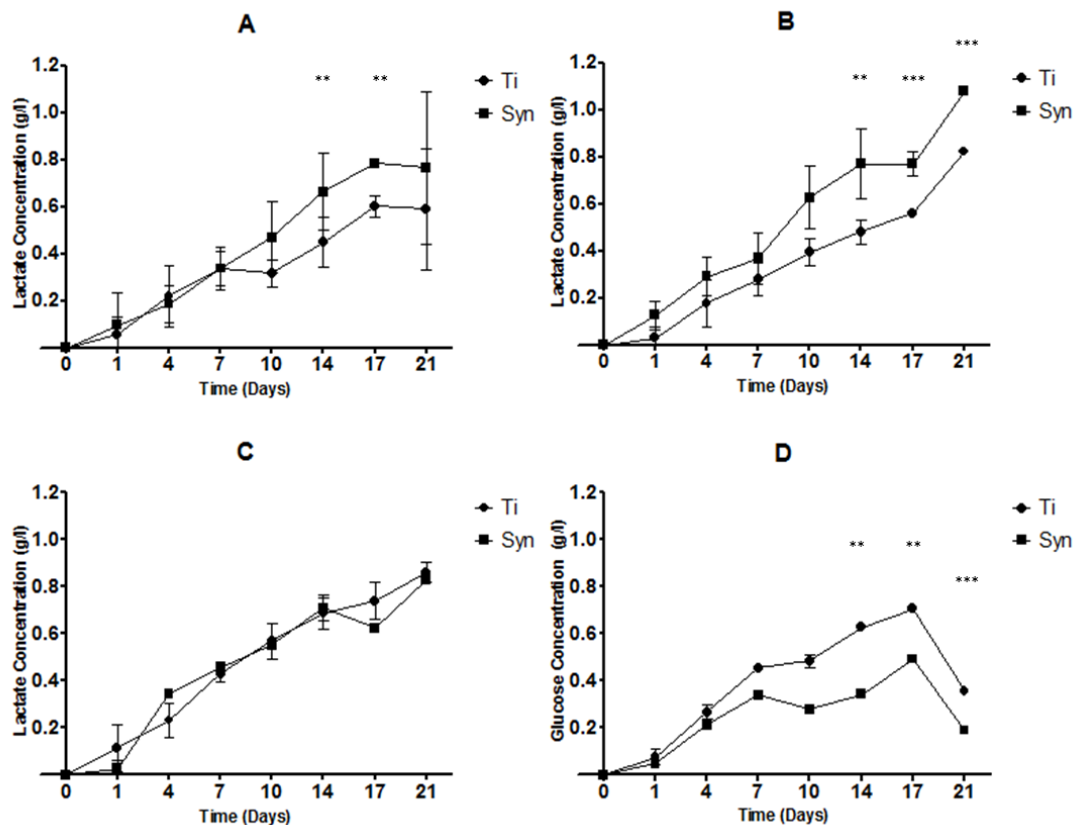


Figure 4.6 Lactate production of hBM-MSCs cultured on Ti-PGM sand Synthemax. Line graphs comparing lactate levels at days 0, 1, 4, 7, 10, 14, 17 and 21 under (A) 0rpm, (B) 40rpm, (C) 80rpm, and (D) 160rpm condition. Values represent mean \pm SD (n=3). Significance values denoted by * = p<0.05, ** =p <0.01 and *** = p< 0.001.

To understand the effect each condition had as the culture progressed, rates of glucose consumption and lactate production per hour were determined over the 21 days illustrated by Figure 4.7. Rates of both glucose consumption and lactate production increased over the first 4 days. Distinct differences can be seen between the glucose consumption rates of cells cultured on Ti-PGMs and Synthemax under 160rpm conditions, where on Ti-PGMs the higher speeds induced improved glucose uptake per hour until day 14 after which point the rates were by matched the remaining conditions. However, cells cultured on Synthemax showed lower glucose consumption rates after day 4 reducing to near zero levels by day 21. Lactate production rates were similar across all conditions studied when hBM-MSCs were cultured on Ti-PGMs however, Synthemax showed rates that fluctuated over time with 160rpm conditions showing lower production rates over the 21 days.

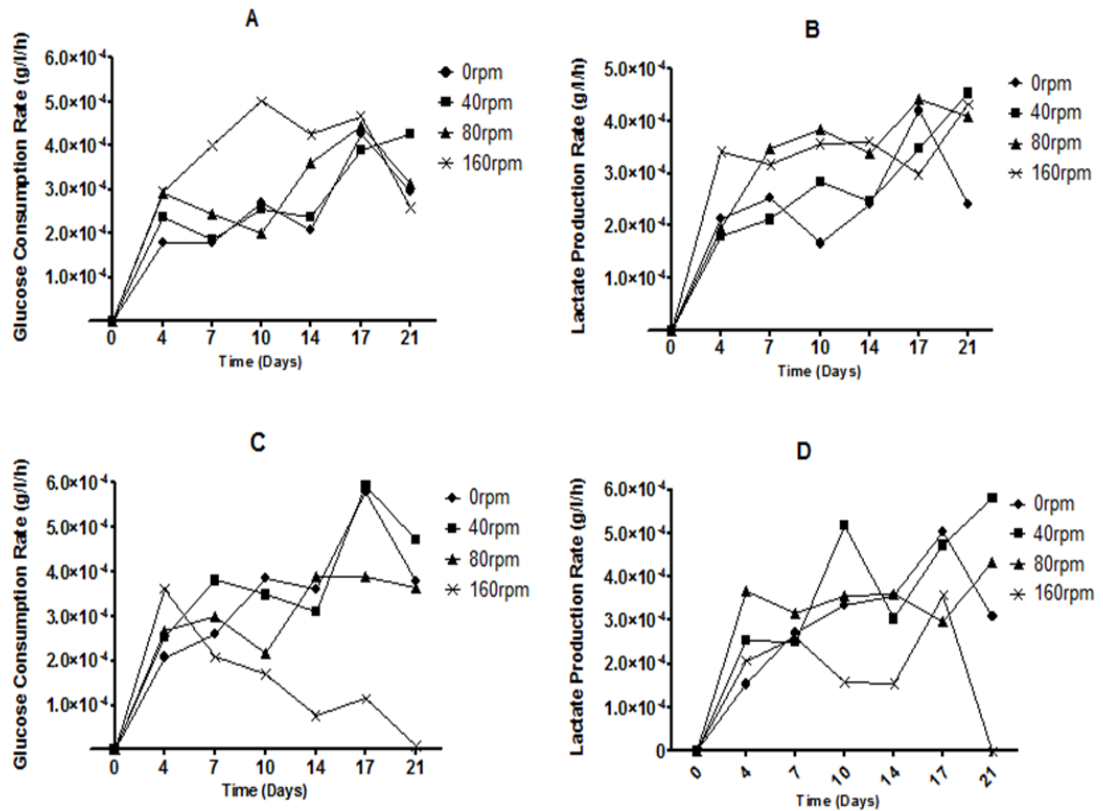


Figure 4.7 Glucose consumption and lactate production rates per hour of hBM-MSCs during culture. Line graphs compare the metabolic rates of hBM-MSCs cultured on Ti-PGMs (A & B) and Synthemax (C & D) at days 0, 1, 4, 7, 10, 14, 17 and 21 under 0rpm, 40rpm, 80rpm and 160rpm condition.

4.3.3 Cell interactions with Ti-PGMs and Synthemax cultured in 125ml Erlenmeyer flasks

Details of the interaction between hBM-MSCs and microspheres when cultured using both Ti-PGMs and Synthemax in Erlenmeyer shake flask cultures was assessed using SEM, which enabled high resolution images to be acquired. The images in both Figures 4.8 and 4.9 were taken 21 days post seeding. From both figures differences in cell interactions and tissue morphology can be observed. Initially, the stark differences in average size of the different types of culture substrate can be noticed with Synthemax occupying a larger volume as expected. Furthermore, the mode in which the hBM-MSCs use the substrates as a tool for growth and support differs with changes in agitation. While the cells grown on Synthemax tend to bind strongly to the surface of the carriers and wrap around

the particle when subjected to high agitation, the hBM-MSCs grown on the Ti-PGMs use the material as support tool to grow and network with other cells to form ECM. The networking ability of the cells grown on Synthemax under high agitation is limited when compared to the cells grown on the substrate under static conditions.

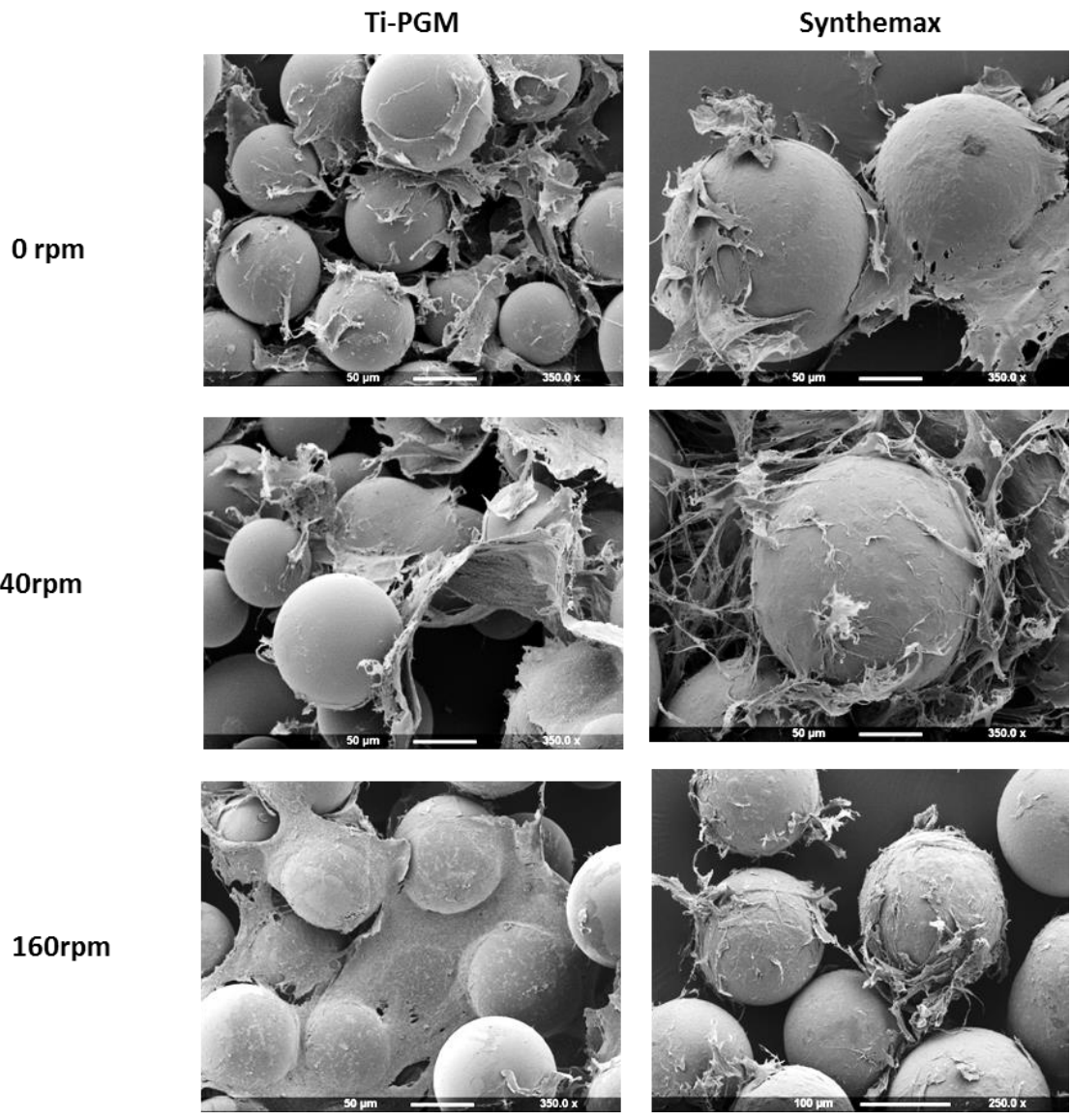


Figure 4.8 hBM-MSCs cultured on both Ti-PGMs (left column) and Synthemax (right column) after 21 days of culture under 0rpm, 40rpm and 160rpm conditions in 125ml Erlenmeyer shake flasks. Scanning electron microscopy images showing differences in microsphere size and morphology of cells cultured under different conditions. Images were taken at various magnifications

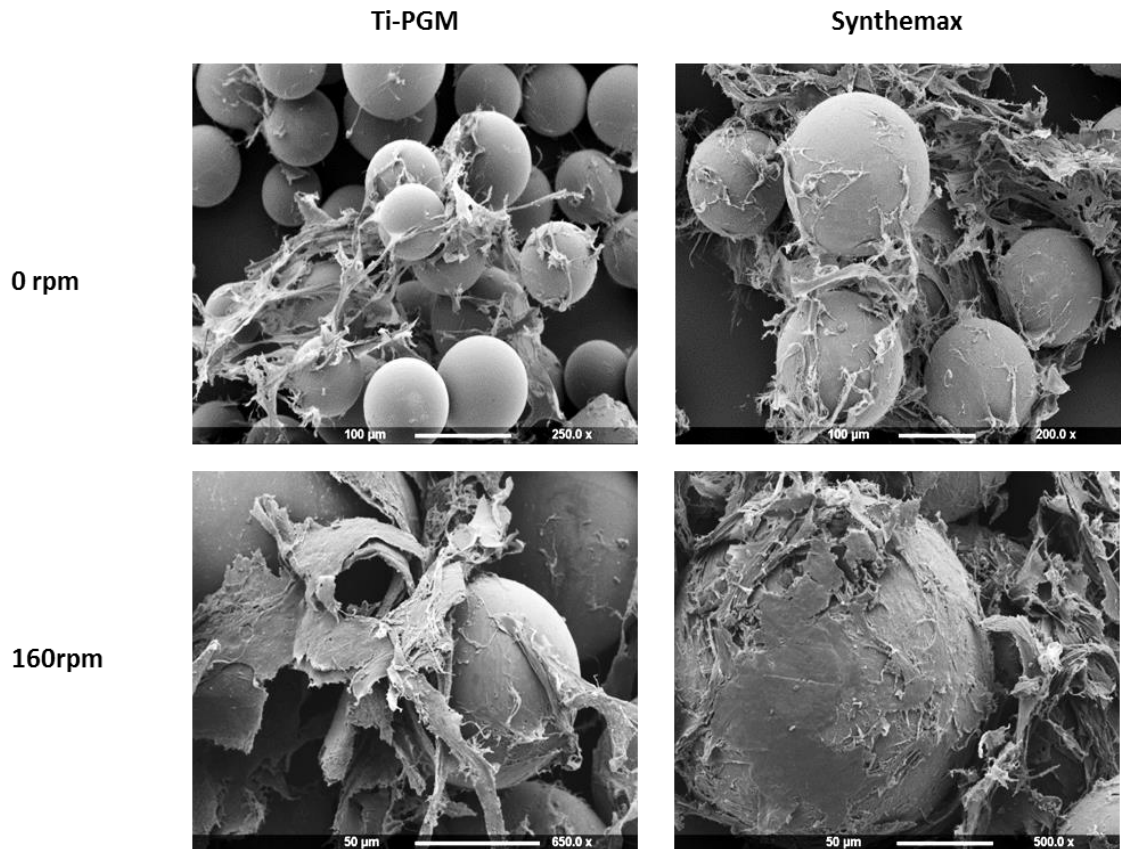


Figure 4.9 hBM-MSCs cultured on both Ti-PGMs (left column) and Synthemax (right column) after 21 days of culture under 0rpm and 160rpm conditions in 125ml Erlenmeyer shake flasks. Scanning electron microscopy images showing differences in thickness of tissue formed under static and high agitation conditions. Images were taken at various magnification and scale bars indicates 50μm and 100μm.

4.3.4 Matrix deposition by hBM-MSCs on Ti-PGMs cultured at large scale

Next, we assessed ECM production and deposition on the microcarriers. After labelling cell-microsphere structures with antibodies against type-I collagen and fibronectin, we then performed confocal microscopy to visualise the deposits. The images in Figure 4.10 and 4.11 show the cells attached to Ti-PGMs and Synthemax on days 14 and 21, illustrating fibronectin and type-I collagen production. For cells cultured on Ti-PGMs under static conditions, fibronectin and type-I collagen expression was lower than when cultured under both 40rpm and 80rpm on day 14. However, when cultured at 160rpm, expression of both ECM markers was lower than both the other dynamic speeds. By day 21, fibronectin expression was the same under all conditions studied, and relatively higher than

the expression observed on day 14. However, type-I collagen expression by hBM-MSCs cultured under static conditions was considerably lower than those cultured under dynamic conditions.

When comparing the expression of ECM markers by cells cultured on Synthemax versus Ti-PGMs, higher expression was observed on Synthemax under static and 40rpm culture conditions compared to the higher agitation speeds. The expression of both fibronectin and type-I collagen was lower for cells cultured under 80rpm and 160rpm on both day 14 and 21. The images illustrate that densely packed ECM fibres are generated under static and 40rpm conditions when cells were cultured on Synthemax, while the cells cultured on Ti-PGMs were less dense and more branched in nature. The morphology of cells cultured on Ti-PGMs remained the same when cultured under all conditions, as illustrated by the fibronectin staining. This was not apparent for cells cultured on Synthemax, which showed a looser, stretched out structure when under high agitation conditions. The cell morphology and ECM structure are further highlighted in Figures 4.12 & 4.13 which provide a detailed image of the cells cultured on Ti-PGMs and Synthemax respectively under static conditions. The Hoechst staining suggests that cells tend to proliferate to a greater extent on the Synthemax surface under static conditions compared to Ti-PGM.

When looking at the homogeneity of ECM protein expression across the whole structure (Figure 4.14), there is an even distribution across both clustered structures A and B. The quantity of ECM present in both clusters cannot be assumed to be the same due to the difference in microsphere quantity within the cluster, hence different volumes in both clusters, coupled with the images limited to 150µm in cluster depth. The characteristics of the cells surrounding the constructs show no distinguishable differences in density or distribution of ECM produced.

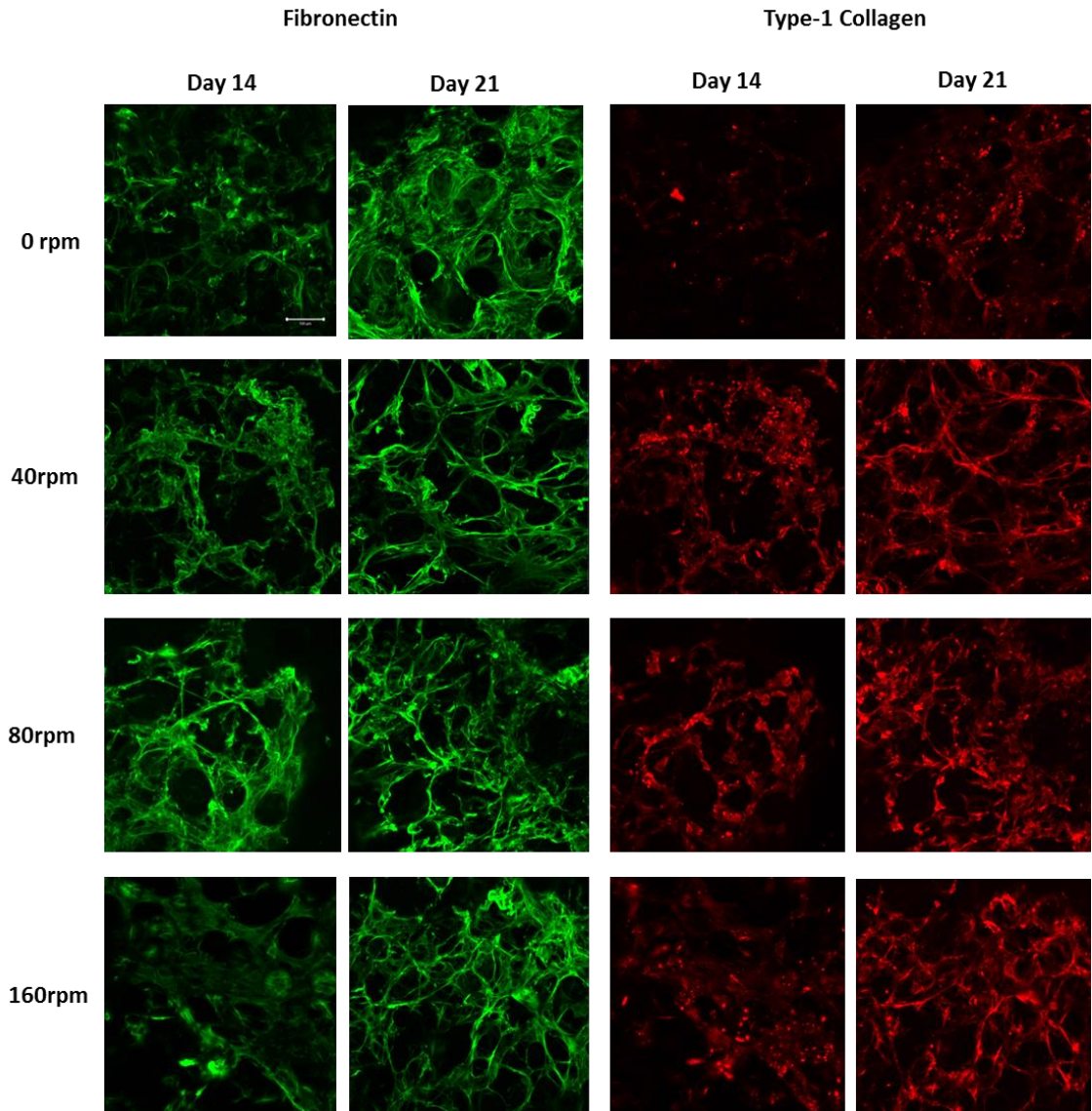


Figure 4.10 Fibronectin and type-1 collagen expression by hBM-MSCs cultured on Ti-PGMs at days 14 and 21 of culture. Confocal laser scanning microscopy Z-stack images were rendered to produce maximum intensity projection of cross-sections up to 150µm. Staining pattern highlights fibronectin (green) and type-1 collagen (red) expressed in the extracellular matrix. Images taken at 10x magnification where scale bar is 100µm.

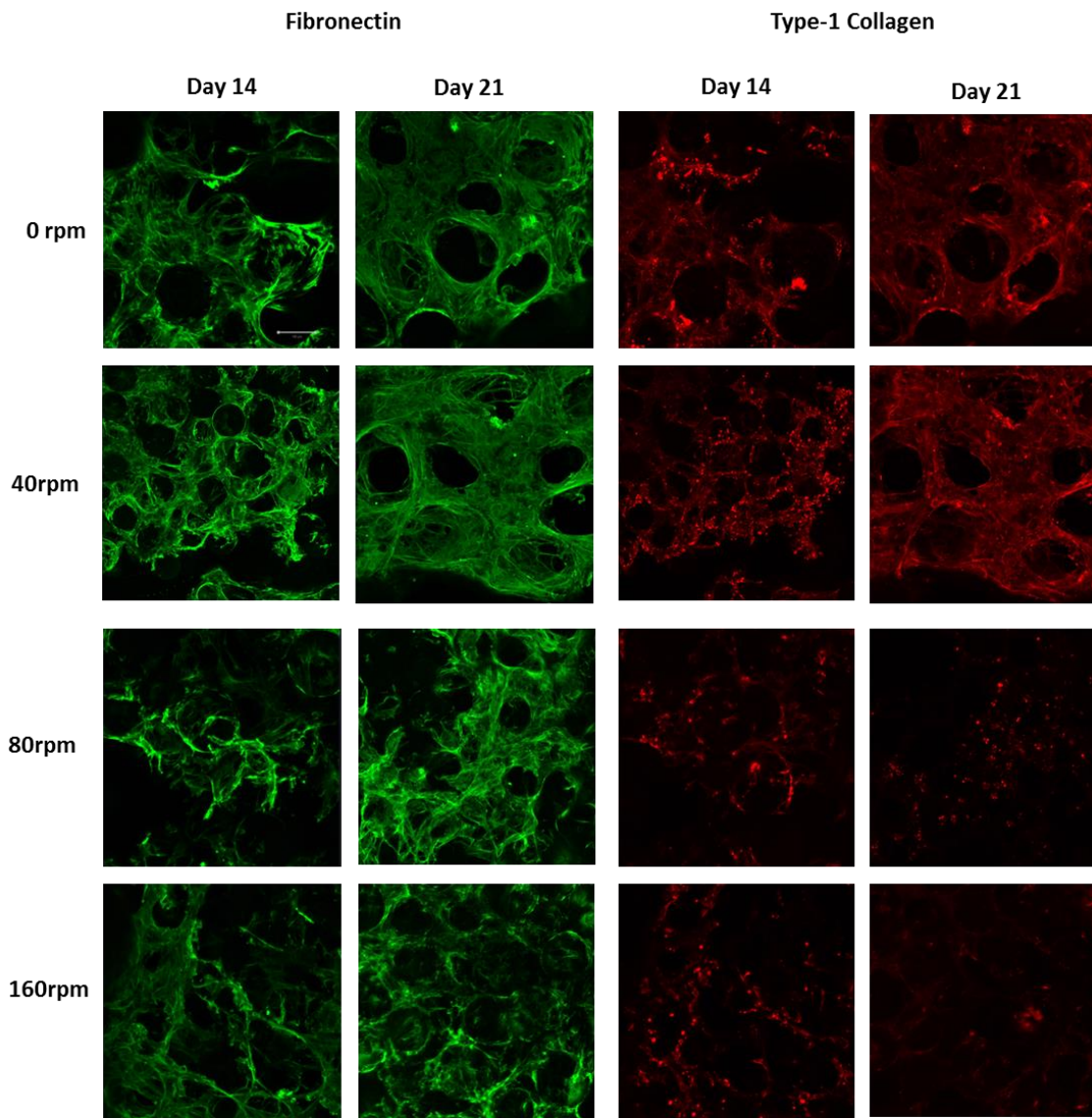


Figure 4.11 Fibronectin and type-1 collagen expression by hBM-MSCs cultured on Synthemax at days 14 and 21 of culture. Confocal laser scanning microscopy images of were acquired and converted into Z-stack images which were rendered to produce a maximum intensity projection of cross-sections up to 150 μ m. Staining pattern highlights fibronectin (green) and type-1 collagen (red) expressed in the extracellular matrix. Images taken at 10x magnification where scale bar is 100 μ m.

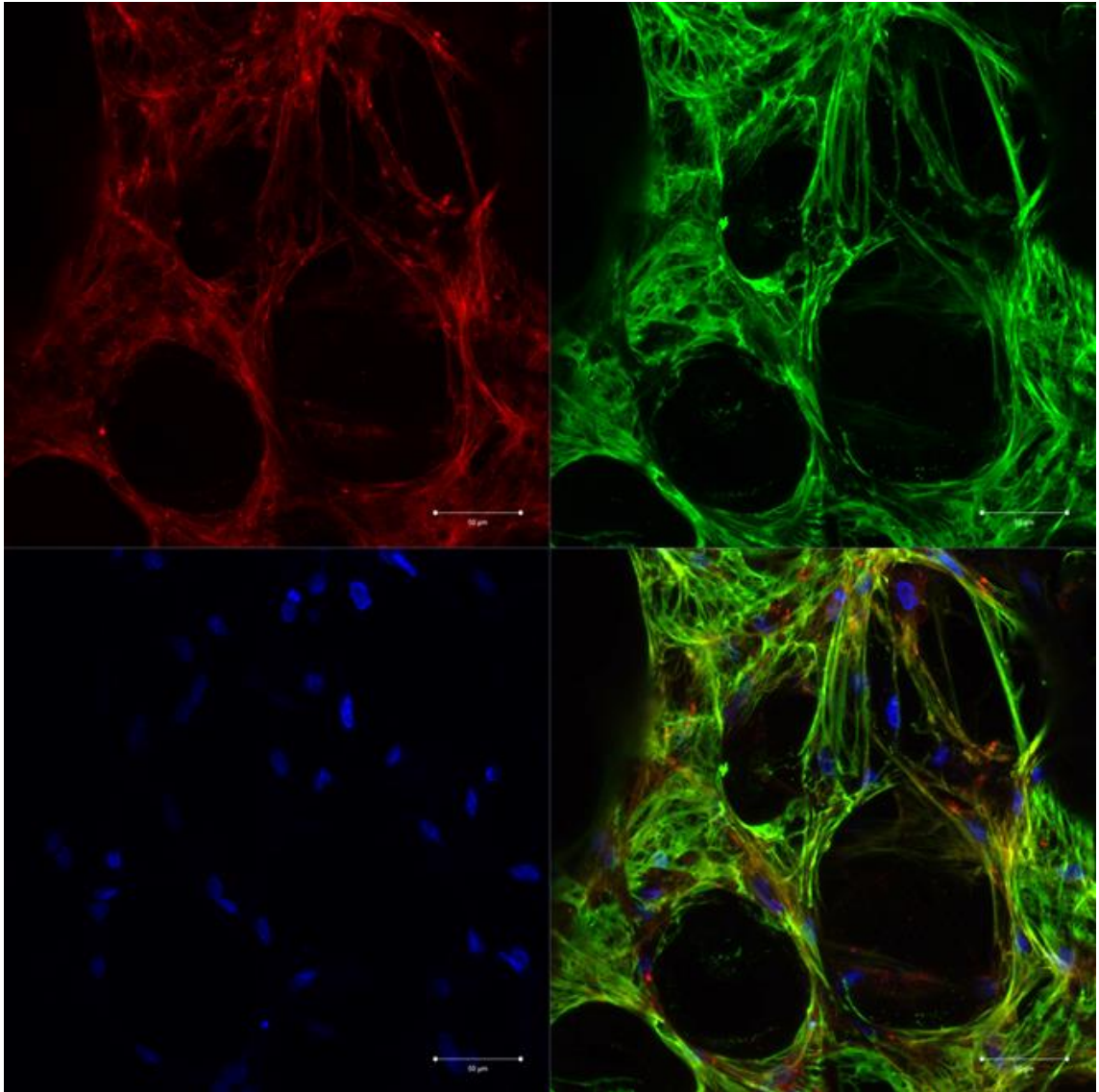


Figure 4.12 hBM-MSCs cultured on Ti-PGMs at day 21 of static culture in a 125ml Erlenmeyer flask. Confocal laser scanning microscopy images were acquired and converted into Z-stack images which were rendered to produce a maximum intensity projection of cross-sections up to 150 μ m. Staining pattern highlights fibronectin (green) and type-1 collagen (red) expressed in the extracellular matrix. Nuclear staining was carried out using Hoechst 33342 (blue). Images taken at 20x magnification where scale bar is 100 μ m.

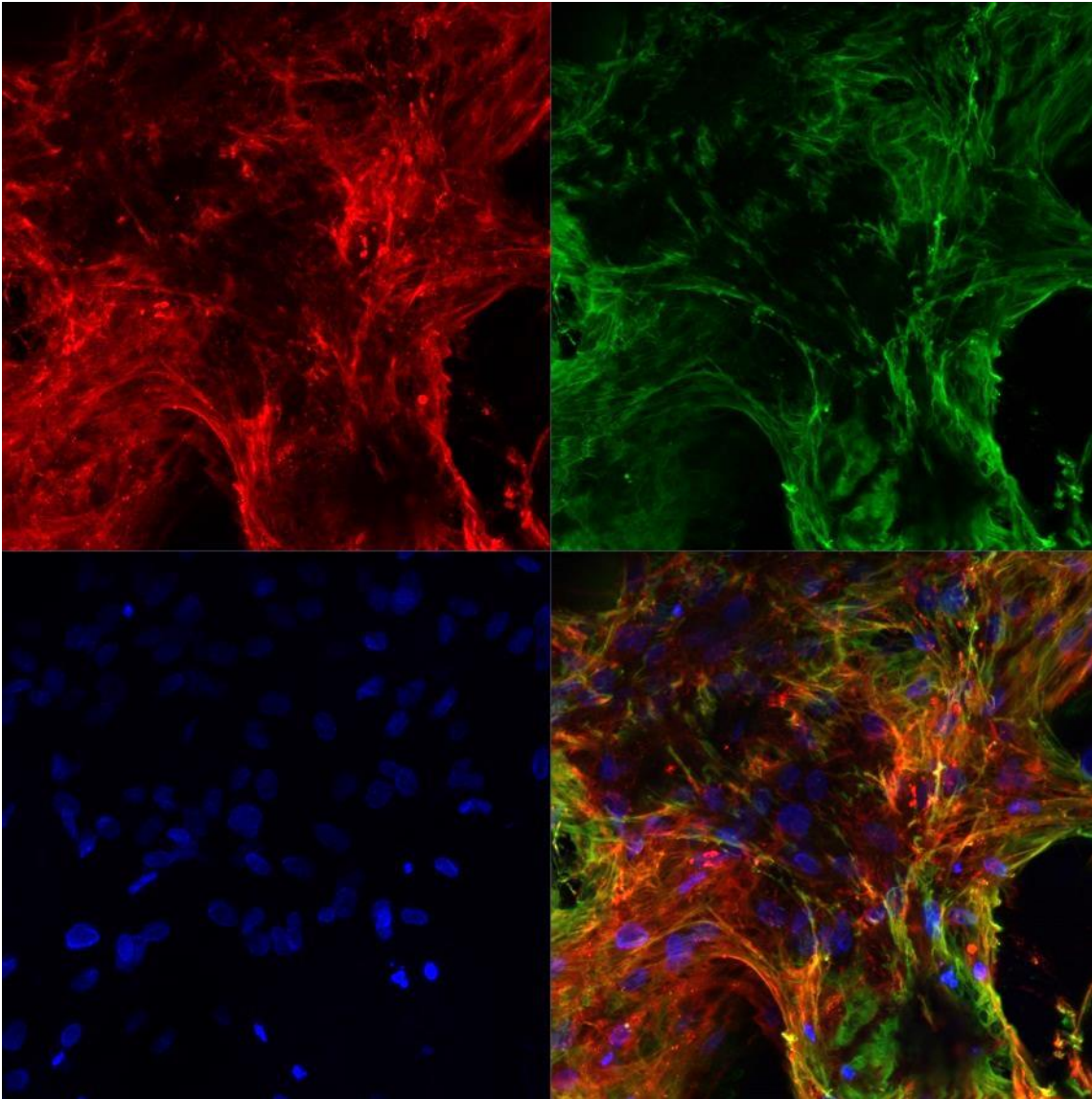


Figure 4.13 hBM-MSCs cultured on Corning® Synthemax at day 21 of culture when cultured under static conditions. Confocal laser scanning microscopy images were acquired and converted into Z-stack images which were rendered to produce a maximum intensity projection of cross-sections up to 150 μ m. Staining pattern highlights fibronectin (green) and type-1 collagen (red) expressed in the extracellular matrix. Nuclear staining was carried out using Hoechst 33342. Images taken at 20x magnification.

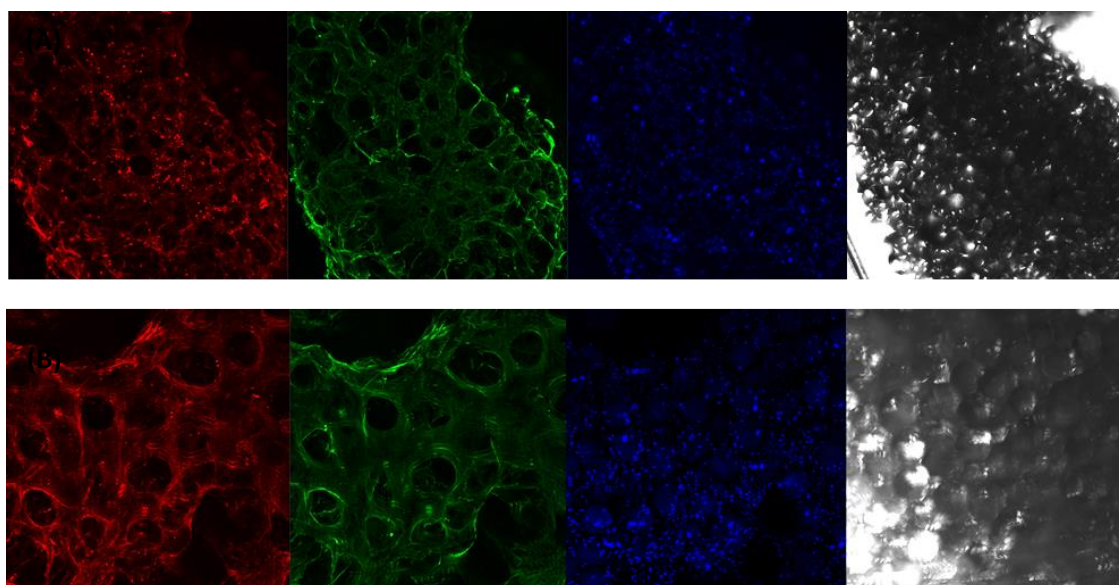


Figure 4.14 hBM-MSCs cultured on (A) TI-PGMS and (B) Corning® Synthemax at day 21 of static culture. Confocal laser scanning microscopy Z-stack images were rendered to produce a maximum intensity projection of cross-sections up to 150µm. Staining pattern highlights fibronectin (green) and type-1 collagen (red) expressed in the extracellular matrix. Bright field images (far-right) show the distribution of microcarriers in the cluster. Nuclear staining was carried out using Hoechst 33342. Images were taken at 5x magnification.

Next, key markers of differentiation were studied. Cells were cultured on microspheres and immunolabelling with antibodies against osteopontin and osteocalcin was undertaken (Figure 4.15 & 4.16). hBM-MSCs cultured on Ti-PGMs were found to deposit osteopontin after 14 days. The staining intensity was decreased at 21 days for all agitation speeds studied, indicating that the marker reached peak expression and then declined. On the other hand, osteocalcin was upregulated from 14 days to 21 days, under agitation culture.

Expression of osteopontin and osteocalcin from hBM-MSCs were compared between static and dynamic conditions. Both expression markers when hBM-MSCs were cultured on Ti-PGMs under dynamic conditions, were higher than that achieved under static conditions except for 80rpm conditions which showed lower levels of expression of osteopontin on day 14 and 21 of culture. In contrast, hBM-MSCs cultured on Synthemax showed lower expression of osteocalcin at day 21 across all conditions when compared to Ti-PGM, however showed similar osteopontin expression on both days with marginally higher expression achieved

on day 21 under 160rpm compared to Ti-PGM. Both markers showed marginally higher expression on day 21 of Synthemax culture at 160rpm when compared to the other speeds studied.

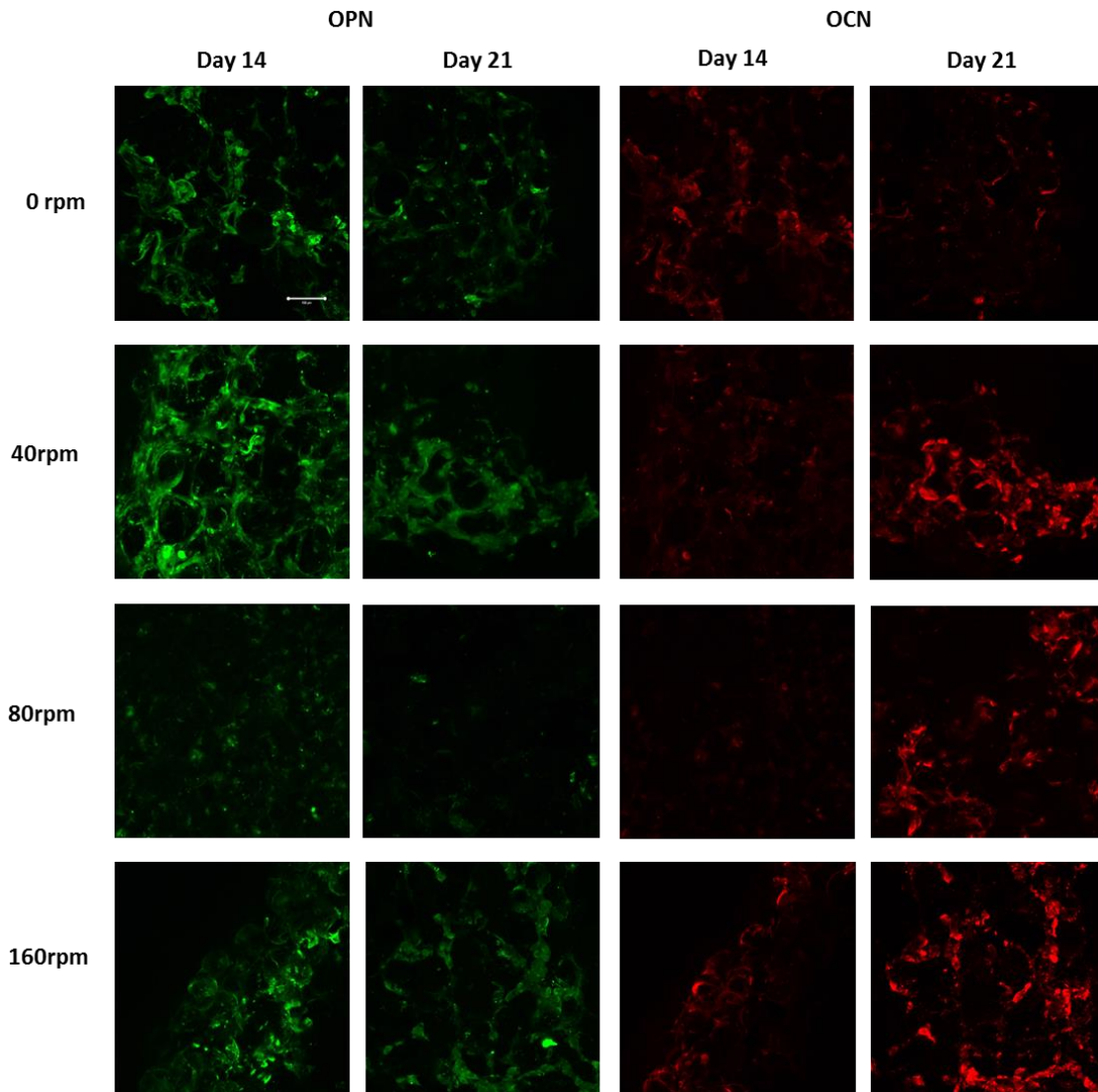


Figure 4.15 hBM-MSCs cultured to Ti-PGMs at day 21 of static culture. Confocal laser scanning microscopy Z-stack images were rendered to produce maximum intensity projection of cross-sections up to 150 μ m. Staining pattern highlights osteopontin (green) and osteocalcin (red) found in the extracellular matrix. Images taken at 10x magnification where scale bar is 100 μ m.

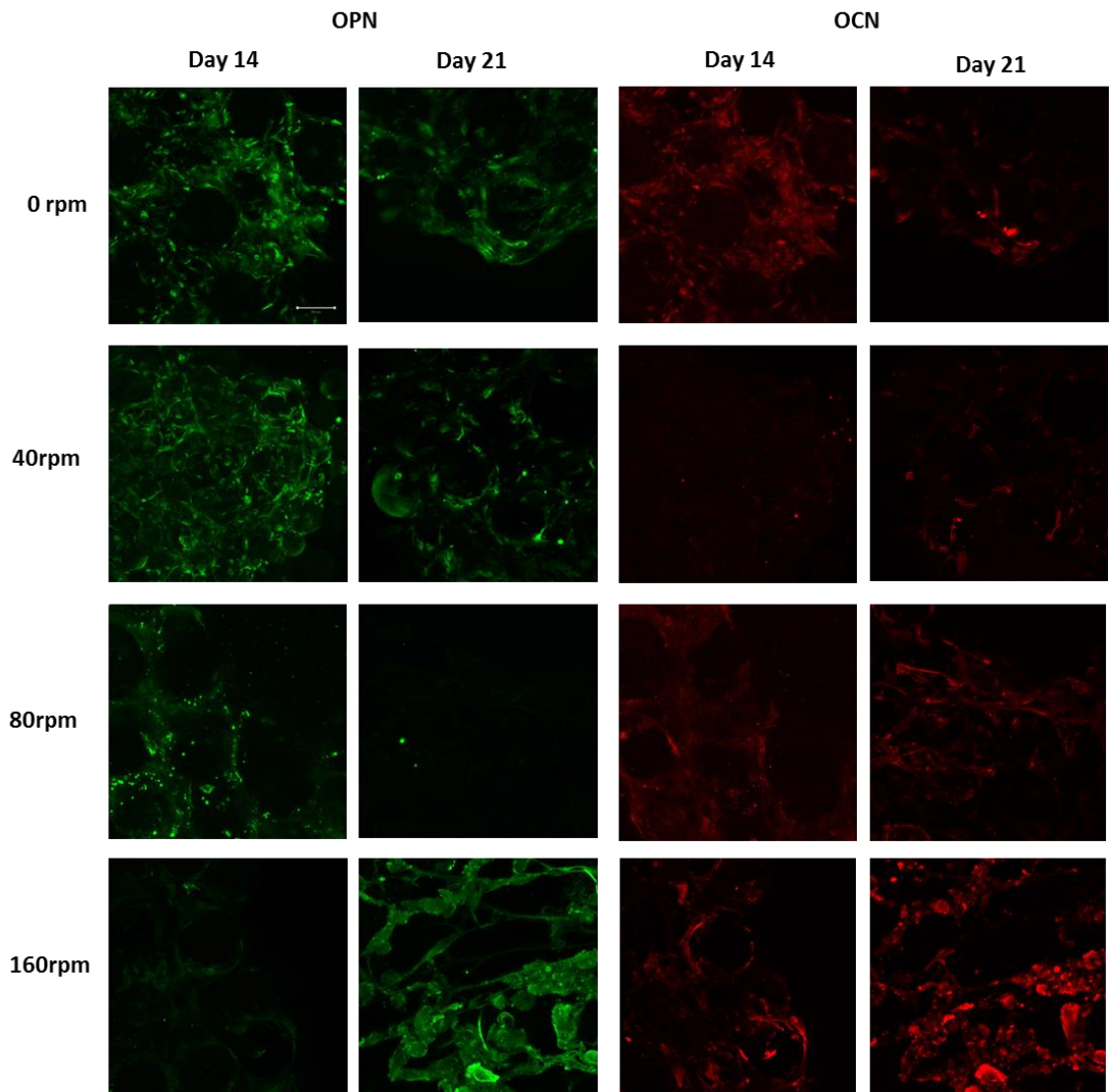


Figure 4.16 hBM-MSCs cultured on Synthemax at day 21 of static culture. Confocal laser scanning microscopy Z-stack images were rendered to produce maximum intensity projection of cross-sections up to 150 μ m. Staining pattern highlights osteopontin (green) and osteocalcin (red) found in the extracellular matrix. Images taken at 10x magnification where scale bar is 100 μ m.

4.3.5 hBM-MSC osteogenic gene expression

Gene expression was assessed to understand the effect the different culture substrates and agitation conditions had on osteogenic differentiation. Cells isolated on day 21 from each condition were processed to quantify levels of osteogenic specific genes (COL1A1, RUNX2 and SPP1) expressed by the cells. The level of gene expression for each sample was normalized against expression of the housekeeping gene β -actin, and that product was then normalized relative to Synthemax cultured under static conditions. For COL1A1, significant differences in expression between the different speeds studied for both substrates were only observed under 40rpm conditions where up-regulation of COL1A1 was observed on Ti-PGMs compared to Synthemax (** $p < 0.01$).

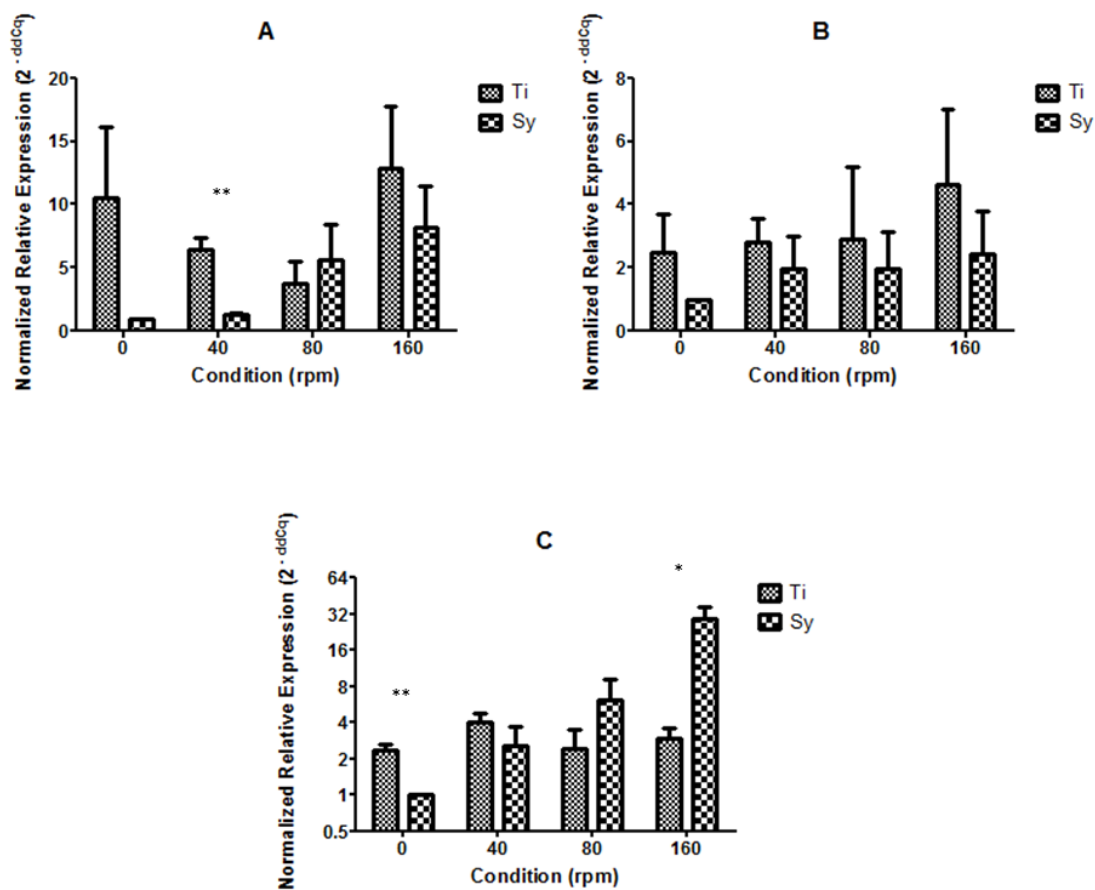


Figure 4.17 Relative quantification of gene expression of (A) COL1A1 (B) RUNX2 and (C) SPP1 in hBM-MSCs seeded on Ti-PGMs and Synthemax after 21 days in culture. Significance values denoted by * = $p < 0.05$, ** = $p < 0.01$ and *** = $p < 0.001$ indicate highly significant gene expression compared to Synthemax. Error bars represent the mean value considered for three replicate specimens (\pm SD).

There was no significant difference in RUNX2 expression (Fig 4.17(B)) between the different conditions or substrates studied over the 21-day period, even though there was a non-significant tendency in favour of Ti at each time point. On the contrary, there were significant differences observed in SPP1 expression between the different materials studied. When hBM-MSCs were cultured under static conditions, Ti-PGMs showed up-regulated SPP1 expression compared to Synthemax (** $p < 0.01$). However, under 160rpm conditions the inverse was observed where Synthemax supported higher SPP1 expression (* $p < 0.05$). The difference observed at 160rpm resulted from the relative increase in SPP1 expression by hBM-MSCs cultured on Synthemax compared to the other three speeds studied with significant upregulation in comparison to 0, 40 (** $p < 0.001$) and 80rpm (** $p < 0.01$).

4.4 Discussion

The focus of this chapter was effectively scale up hBM-MSC culture to improve overall production of bone-like material. The interactions between hBM-MSCs and Ti-PGMs or Synthemax in a 125ml Erlenmeyer flask (reflecting scale up for production of clinical quantities of autologous material), were investigated to understand cell behaviour when scaling up a two-phase culture system with orbital mixing. This chapter consolidates work carried out at small scale using both MG63 and hBM-MSCs to understand the impact of fluid flow and explored further the application of Ti-PGMs in guiding osteogenic differentiation of immature hBM-MSCs. The research carried out will aid future efforts in understanding mixing regimes and help develop strategies to develop tissue engineered bone using bioactive glass for clinical bone defects.

Research has been undertaken to understand how expansion of stem cells can be improved using microcarriers in shaken flask culture systems by determining the agitation speeds necessary to suspend the culture material therefore improving homogenous cell expansion. Initial work carried out by Weheliye et al., (2013) focused on looking at the mixing patterns achieved in microwells/cylindrical vessels (Weheliye et al., 2013). Subsequent work by Olmos et al., (2015) focused on creating a model to determine the critical agitation speed of microcarriers in various Erlenmeyer flasks using parameters that were closely associated to the initial model developed by Weheliye et al (Olmos et al., 2015). While the first iteration focused on understanding the in-phase to out-of-phase transition of the contents in a cylindrical vessel, the second iteration developed by Olmos et al., incorporated factors contributed by a second phase, the microspheres. When determining the N_c using Weheliye's model where relative density of the Ti-PGMs is not considered and is applicable only to cylindrical vessels, an agitation speed of 160rpm was calculated. The images illustrating the progressive suspension of Ti-PGMs when agitated in a 125ml Erlenmeyer flask (Figure 4.2) show that at 160rpm the Ti-PGMs begin to be pulled to the centre of the flask base, indicating the transition from in-phase flow to out-of-phase flow. However, the microspheres glide across the base of the flask, remaining relatively static. This phenomenon was observed also by Pieralisi et al., (2016), who

showed, using GE Cytodex 3 microcarriers, these microcarriers being pushed from the periphery towards the centre of the reactor base at the point of flow transition (Pieralisi et al., 2016). However, the microcarriers were subsequently suspended into the bulk flow. The density dependent model calculated that the N_s speed required to suspend the Ti-PGMs was 320rpm, which correlates with the images in Figure 4.2. The density of the Ti-PGMs, while exceeding the limits of the model developed by Olmos et al., correlates well with the expected mixing patterns. Based on these two models, between the N_c speed calculated using Weheliye's model (160rpm) and the N_s determined using Olmos' model (320rpm), a mixing system change occurs between the two speeds which needs to be studied further.

As aforementioned, small scale studies carried out in Chapter 3 showed that hBM-MSCs cultured at $0.5N_c$ induced lower levels of cell proliferation and therefore it was used as the upper limit agitation in this study. Metabolite analysis from extracted media samples was undertaken to make an inference of relative growth occurring under each condition studied. The specific rate of both glucose consumption and lactate production could not be determined due to the inability to quantify viable cell number at each time point. The high density of Ti-PGMs coupled with the different cluster sizes formed by Synthemax and Ti-PGM, generated variability in the sampling process. Cell growth was therefore inferred using the metabolite data to determine non-specific rates of glucose consumption and lactate production. The accumulation of Ti-PGMs to the centre of the flask induced by 160rpm agitation promoted better cell metabolism and growth possibly due to the proximity of the microspheres. This allowed the cells to proliferate better, helped by the ability to easily bridge between microspheres, which formed a scaffold-like structure, utilising the available surface area more effectively. The high agitation conditions were however detrimental to hBM-MSCs cultured on Synthemax, whose metabolic rates were reduced. This varying effect induced by a high agitation rate is further corroborated by the $Y_{Lac/Glc}$ ratio with Ti-PGMs under 160rpm conditions. The ratio of 0.896 was the lowest ratio amongst all conditions studied using Ti-PGM, while Synthemax generated a ratio of 1.209, the highest for its material. The optimal regime for Synthemax culture was under static conditions with a ratio of 0.886 with progressively higher ratios as agitation

increased (40rpm=1.006, 80rpm=1.104). Metabolite ratios of Ti-PGMs followed the same trend until 160rpm with an increase in ratio value as agitation increased (0rpm=0.985, 40rpm=0.995, 80rpm=1.14).

The growth patterns witnessed at a larger scale differed depending on the culture substrate examined. The patterns were mimicked closely when considering Synthemax due to the similarities of its N_s and N_c , and due to the limited impact, the density of the microcarriers had on their ability to be suspended. However, Ti-PGMs exhibited different effects at the two scales studied. This fundamentally owes to the difference in the models developed by Weheliye et al., and Olmos et al. The small-scale studies carried out in this research focused on the transition of in-phase mixing to out-of-phase mixing with the assumption that when N_c was administered the microspheres would achieve suspension ($N_{Cr} \sim N_s$). At the time of the small-scale studies no model existed for the mixing of two-phase systems, therefore N_s could not be determined. The transition model was limited to cylindrical vessels and could not be applied confidently to Erlenmeyer flasks. Therefore, the speeds studied at the different scales were determined using the transition model rather than the suspension model. Nevertheless, considering the magnitude of the N_s relative to N_c (Table 4.1), mixing dynamics of dense microspheres at different scales are better compared by N_c values calculated using the transition model rather than the suspension model due to the high agitations required. The values provided in Table 4.1 should be considered as estimates for two reasons. Firstly, the model developed by Weheliye et al., was used here to determine the N_c in Erlenmeyer flasks where transition from in-phase to out-of-phase occurs, even though the model has only been validated with cylindrical vessels. Additionally, the relative error stated with the suspension model in regards to cylindrical vessel is 10.2% (Olmos et al., 2015).

Table 4.1 Critical (N_c) and suspension (N_s) agitation speeds based on models developed by Weheliye et al., (Weheliye) and Olmos et al., (Olmos).

Scale	96-well microplate		Erlenmeyer flask (125ml)	
Model	Weheliye	Olmos	Weheliye	Olmos
Parameter	N_c	N_s	N_c	N_s
Orbital Speed (rpm)	340	787	160	320

Inducing osteogenic differentiation through fluid flow has been studied extensively using parallel plate flow technology, and orbital cultures have shown to provide the same effects in a less homogenous manner (Kreke et al., 2005, Huang et al., 2010). Models have been developed by different research groups aiming to understand the effects of fluid flow on mammalian cell cultures. However, no clear agreement has been reached in the literature available (Thomas et al., 2011, Lim et al., 2014, Nienow et al., 2014, Velasco et al., 2016). Many of these studies have examined the effects of shear in a global nature within a vessel, where cell properties such as product titre were related to flow patterns and shear stress. These techniques provide limited understanding of local shear stresses which becomes crucial when considering microcarrier culture where vector and magnitude of shear stresses impact stem cell fate (Sargent et al., 2010). Although research has been carried out on understanding the effect of orbital mixing on two-phase culture systems, no work has been carried out to understand the effects these different mixing regimes have on cell growth and phenotypic behaviour when attached to microspheres. The effect of fluid flow on hBM-MSCs ability to be differentiated to an osteogenic phenotype when cultured on Ti-PGMs can be better understood by examining the expression of osteogenic markers OPN (SPP1) and OCN. OPN is a phosphoprotein that is associated with mineralization of ECM synthesized by bone forming cells (Butler, 1989) and OCN is a calcium binding protein (Aubin et al., 1995). Expression of OPN was observed in day 14 of hBM-MSCs culture on both Ti-PGMs and Synthemax, however was down-regulated on day 21. This was expected due to OPN being an early marker of osteogenic differentiation (Zohar et al., 1998, Köllmer et al., 2013, Granéli et

al., 2014). When hBM-MSCs were cultured on Ti-PGMs, osteogenic differentiation was induced after 21 days under dynamic conditions, highlighted by a marked increase in type-I collagen and OCN expression compared to static culture. hBM-MSCs cultured on Synthemax in the presence of fluid flow however, did not show increased type-1 collagen or fibronectin expression when agitation speed increases, potentially due to the levels of shear becoming detrimental to cell maturation. However, increased expression of OPN and OCN was observed when hBM-MSCs were cultured on Synthemax for 21 days at 160rpm compared to the other conditions potentially indicating that high agitation levels can be osteoinductive. This effect was also confirmed by qPCR data showing a progressive increase in OPN expression as cells were exposed to higher agitation for 21 days. The increase in OPN expression in response to fluid flow has been well documented (You et al., 2001, Kreke et al., 2005, Sharp et al., 2009, Yourek et al., 2010) with evidence to show that OPN is more shear-responsive than other osteogenic markers such as bone morphogenetic protein 2 (BMP-2). As hBM-MSC proliferation was limited on Synthemax at 160rpm, the total number of cells possessing osteogenic properties would be low in number, however high in percentage. Orbital mixing at 160rpm influences the mixing dynamics of Synthemax greater than Ti-PGMs due to their density differences, hence this would explain the significant difference in OPN expression. Increased levels of OPN and OCN expression by BM-MSCs when low magnitudes of shear stress were applied have been documented in research carried out in studies showing that fluid flow could be used as a tool for isolating osteogenically sub-populations through mechanotransduction (Kreke et al., 2005).

While the upregulation of OPN on Synthemax can be attributed to the effects of fluid flow as opposed to the osteoinductive properties of the polystyrene material, it can't be concluded that the effect of flow is the sole factor in inducing osteogenic differentiation on Ti-PGMs. The ability of the materials to induce an osteogenic response can be better understood by examining phenotypic properties under low flow conditions where cell numbers are relatively similar. When looking at the osteogenic differentiation of hBM-MSCs cultured under lower agitation speeds, Ti-PGMs have overall significantly greater osteoinductive properties than Synthemax with higher gene expression of both COL1A1 and OPN documented.

This increased expression of OPN under static culture was previously observed when hMSCs were cultured on Ti5 compared to silica glass microspheres (Lakhkar et al., 2015a). The reason behind the enhanced osteogenic response was due to the release of various phosphate species from the glass structure; however, the exact mechanism still needs to be studied to understand the pathways involved in improved osteogenic differentiation. The confocal images on day 21 under static conditions indicate that Synthemax expresses larger amounts of COL1A1 compared to Ti-PGM, however due to its weak staining this could be down to auto-fluorescence or ineffective washing steps of the dense ECM. A clear positive control was not used when conducting the PCR experiments therefore it would be necessary to compare genetic expression of cells cultured in osteogenic media cultured on Synthemax.

The attachment of the cells is an area that hasn't been fully addressed thus far in this research and based upon the SEM images, shows a potential avenue for development. The differing levels of cell adhesion after 21 days of culture on Ti-PGMs and Synthemax indicates that surface modifications are required to optimize the performance of Ti-PGMs as a platform for cell attachment and rapid proliferation. It is unknown whether processing steps when fixing and imaging the samples disturbed cells and cell-secreted ECM from the microspheres. However, the Synthemax underwent the same process and cells remained adhered to the microcarrier surface. The use of protein coatings as a biofunctionalization tool, mainly biomimetic ECM, has been studied on different material surfaces (Chrzanowski et al., 2012, Shin et al., 2012, Truong et al., 2012, Pérez et al., 2013, Kang et al.). However, limited work exists on phosphate glasses. Fusion protein fibronectin-osteocalcin (FN-OCN) has been identified as potential dual-purpose protein by enhancing cell attachment (FN) and inducing osteogenic differentiation through OCN simultaneously, which is reported to have a high affinity for hydroxyapatite (HA) (Lee et al., 2013). The formation of a biologically active HA layer has classically been deemed as a requirement of biomaterials when present in a physiological environment, due to its compositional similarity to apatite found in bone and its bone-bonding qualities (Kokubo et al., 2004). However, the use of such fusion proteins or biofunctionalization coatings that depend on a HA coating will be redundant due to the lack of HA formation on Ti-

doped phosphate glasses when in physiological fluid (Abou Neel et al., 2007). The presence of adhesion proteins in FBS also provides additional factors to promote adhesion which need to be taken into consideration (Hayman et al., 1985). While developments of various coatings could improve the attachment of MSCs to the Ti-PGMs surface, further work is needed to understand the affinity of the surface to these coatings.

In summary, scale up of hBM-MSCs was examined using Ti-PGMs under static and dynamic conditions. The microspheres have shown their ability to support limited cell proliferation but provide strong guidance for differentiation when used at large scale. The effect of fluid flow to enhance osteogenic differentiation was also observed. However, better understanding of spatial shear stress is needed inside a shaken vessel. While the sizes of macrostructures produced in this part of the study are magnitudes smaller than those needed to treat a majority of critical size defects, the motivation to continue scaling up now exist having confirmed that scale up can be achieved. The constructs created in this study are of suitable sizes to treat critical size maxillo/craniofacial defects in animal models such as mouse and rats (Poser et al., 2014). In order to create quantities of materials suitable to treat the upper limit of human maxillo/craniofacial defects further scale up is required. Other modes of increasing the size of the overall construct should be explored, such as running multiple 125ml cultures in parallel, consequently bringing the structures formed into a larger vessel, similar to a seed train or using larger vessel sizes within the constraints of the Olmos model (maximum limit of 1L Erlenmeyer flask). However, further tissue characterization would be needed, and additional risk is introduced by creating an open system. The Froude number was used to effectively scale microwell processes (Chapter 3) to cultures in Erlenmeyer flasks, providing a greater understanding of the use of biomaterials in clinically relevant culture processes. Furthermore, the model developed by Olmos et al., has been used outside ranges permitted, validating its use for biomaterials with high densities. It is important to further understand whether the constructs produced in this study can be used individually or combined with additional macrounits to meet clinical needs.

Chapter 5 . Qualitative analysis of in vitro osteoclast resorption of Ti-PGMs and effect of modified surfaces on hBM-MSc behaviour

5.1 Introduction

A majority of the work carried out with Titanium-doped phosphate glass has focused on its ability to aid cell proliferation by recognising its biodegradability and slow release of ions (Abou Neel et al., 2008). However, no demonstration of its reactivity to other bone remodelling cells such as osteoclasts has been performed. The scope of this chapter is to examine the activity of bone resorbing cells cultured on Titanium-doped phosphate glass.

Where osteoblasts form bone, osteoclasts resorb it. Osteoclasts are formed through the fusion of hematopoietic precursors resulting in multi-nucleated cells (Teitelbaum and Ross, 2003). Their adhesion to bone tissue is controlled by the interaction of integrins such as vitronectin receptor $\alpha V\beta 3$ (VNR) along with bone tissue ECM, which stimulates adhesion and migration (Duong and Rodan, 2001). However, there is no evidence to indicate the molecular components of Titanium-doped phosphate glass induce osteoclast attachment. The osteoclastogenesis process is fully elucidated, with formation of sealing zones and a ruffled membrane (Vaananen et al., 2000) both indicative markers of osteoclast resorption activity. Lysosomal enzymes are released from the ruffled membrane into the resorption site during the resorption process, while the sealing zone is essential for attachment and to initiate bone resorption (Xia et al., 1999, Nakayama et al., 2011). Within this resorptive environment, osteoclasts function by the acidification and release of bone degrading enzymes such as cathepsin K, tartrate resistant acid phosphatase (TRAP) and matrix metalloproteinase 9 (Blair et al., 1986, Teitelbaum et al., 1997, Boyle et al., 2003, Teitelbaum, 2007). The migratory action of osteoclasts during the resorption process is induced by cellular processes called filopodia and lamellipodia (Mattila and Lappalainen,

2008). The migration of these cells coupled with the resorption action forms resorption trails. *In vitro* differentiation of monocytes to osteoclasts occurs on synthetic surfaces like TCP and glasses. However, the formation of sealing zones is not documented (Saltel et al., 2004) implying that osteoclast activity and cell morphology is inhibited by different substrates. As the bone matrix represents the natural environment of osteoclasts, Titanium-doped phosphate glasses may limit osteoclastogenesis, with poor formation of inorganic hydroxyapatite (Abou Neel et al., 2007) and organic components such as type-I collagen only formed when culturing bone forming cells.

With no current agreement for quantitatively comparing different osteoclastic resorption models and low efficacy in mimicking osteoclast action *in vitro*, it is very difficult to understand the true resorption of biomaterials by osteoclasts. Common cell lines such as RAW 264.7 are widely used to understand osteoclastogenesis *in vitro*, however primary cells are a better tool to understand the whole osteoclastogenic process. Osteoclasts of various species have been used including mouse (Benghuzzi et al., 1999, Leeuwenburgh et al., 2001), rat (Zheng et al., 1998, Monchau et al., 2002) and human (Schilling et al., 2004), on biomaterials such as calcium phosphate, hydroxyapatite, tricalcium phosphate and aluminium calcium phosphorous oxide, which could be resorbed by osteoclasts. However, coated silica glass showed resistance to resorption (Taylor et al., 2002). There is currently no existing literature published identifying the resorption of TiO₂ doped phosphate glass by osteoclasts.

This chapter assessed the process of osteoclastogenesis specifically on Titanium-doped phosphate glass discs (Ti-PGD), examining monocyte cell differentiation when cultured on the biomaterial and the resorption activity of osteoclasts formed. Undifferentiated cells were used rather than pre-differentiated cells, as the mechanism of osteoclastogenesis *in vivo* commences with monocytes forming into osteoclasts on the surface of the resorbed material. The choice to use discs was made after initially culturing the cells on Ti-PGMs, however having stained the cells it was clear the curvature limited the efficiency of image capture. In addition to assessing the differentiation potential and resorbability of the material, the effect of RANKL concentration was assessed as

it is known to stimulate osteoclastogenesis and improve resorption. Finally, as it was hypothesized that osteoclast resorption would affect the surface of the Ti-PGMs/Ti-PGDs by increasing surface roughness through the production of pits and migration trails, the consequent bone remodelling process on this surface was examined by culturing hBM-MSCs on acid etched Ti-PGDs to understand if cells could proliferate after the action of osteoclasts.

5.2 Materials and Method

5.2.1 Preparation of Ti-PGD

Phosphate glass containing 5 mol% TiO₂ was prepared using the same protocol described in section 2.2.1. However, the cooling steps were different as the melted crystal was then poured into 15mm (for use in 24-well microplates) rod-shaped moulds, which had been pre-heated at 420°C to promote homogenous cooling within the mould during the cooling process. The material was kept under 420°C for 2 hours before cooling at room temperature. The rods were consequently cut with a microtome diamond blade cutter (Leica SP1699, UK) where the 15mm diameter rods were cut into 2mm thick disks. The different cooling procedures used in manufacturing both the rods and microspheres, may potentially alter the material properties and surface chemistry, therefore further characterization is required. Furthermore, MAPP gas flaming of the rods was not carried out as the surface upon which the cells were seeded on would not be in direct contact with flame prior to the rod being sliced. Care was taken when producing the glass rods as the viscosity of the melted glass coupled with the rapid cooling makes pouring the molten solution into the mould very difficult. In the case where large quantities of material remained within the crucible a further reheating process was used to bring the material into its molten phase to minimize material wastage.

5.2.2 Isolation of mouse monocytes from mice and osteoclast differentiation

A standard protocol was used to carry out initial studies (Orriss and Arnett, 2012). Mice (7-11 weeks MF-1 Female) were sacrificed by cervical dislocation at day 0 and collected from UCL Biological Services. They were dissected using sterile surgical tools to isolate the mouse femur and tibia for monocyte extraction. Boneheads were removed by using dissection scissors after which a G-25 PrecisionGlide needle and 10ml disposable syringe (both from BD Biosciences Europe, UK) were used to flush the bone marrow with flushing buffer (1x PBS and 2% fetal bovine serum). The resulting suspension was pelleted in S1 media (Table 5.1), seeded into T-75 flasks and incubated overnight at 37°C/5% CO₂

post-centrifugation. Suspended mouse bone marrow derived monocytes were then collected and counted after 24 hours, while the attached cell populations were discarded. The isolated cells were resuspended in S2 media (Table 5.1) in preparation for cell seeding.

Table 5.1 Different media types used during the monocyte isolation and osteoclast differentiation processes

S1 Media

Media components	% of total volume
Minimal essential medium (MEM) (Gibco, UK)	~88
Fetal bovine serum (FBS) (Gibco, UK)	10
Antibiotic-antimycotic solution (Gibco, UK)	1
100ug/ml Wyeth M-CSF (416-ML, R&D Systems, UK)	0.0001

S2 Media

Media components	% of total volume
Minimal essential medium (MEM)	~88
Fetal bovine serum (FBS)	10
Antibiotic-antimycotic solution	1
100ug/ml Wyeth M-CSF	0.0001
20ug/ml RANKL (462-TEC, R&D Systems, UK)	0.00015

Upon seeding the required numbers of monocytes, S2 cultures were left for 7 days during which half S2 media was changed every 2 days. After day 7, acidified media was used to induce the resorption process. As the optimal conditions were achieved at pH 7, adjustments were made by the addition of small quantities of 12.5M hydrochloric acid (HCL) into 100ml of S2 media, until the right pH was reached, identified using a pH probe. Monocytes were incubated with acidified

S2 media for 48 hours after which qualitative analysis was carried out using different techniques.

5.2.3 Seeding density study for monocyte cell culture on Ti-PGD

Monocyte seeding density experiments were carried out to understand the levels of cells numbers needed to effectively form osteoclasts when monocytes were seeded on Ti-PGDs. Four different cell concentrations (2.5×10^5 , 5×10^5 , 1×10^6 and 2.5×10^6 cells/cm²) were studied on Ti-PGDs placed in ultra-low attachment 24-well microplates. The Ti-PGDs were sterilized using a high intensity UV lamp for 90 minutes before seeding, after which the cells were maintained in the media regimes and durations stated in section 5.2.2.

5.2.3.1 Tartrate-resistant acid phosphatase staining (TRAP)

Cells underwent a staining process for tartrate-resistant acid phosphatase (TRAP) to understand the osteoclastogenesis and resorption activity on Ti-PGDs. A Leukocyte Acid Phosphatase Kit (387-A, Sigma, UK) was used for staining according to the supplier's protocol. Initially samples were fixed with 4% PFA for 15 minutes and consequently washed twice with 1x PBS. The cells were then washed and probed for TRAP ((1:1:1:2:4:22.5) Fast Garnet GBC Base Solution: Sodium Nitrite Solution: Naphthol AS-BI Phosphate Solution: Tartrate Solution: Acetate Solution: Deionized H₂O)) for 1 hour in the dark at 37°C. Counter-staining was achieved using Haematoxylin solution Gill No.3 and after incubation for 2 minutes the cells were washed with deionized H₂O several times to remove residual staining solution. The TRAP positive cells were visualized under a light microscope at 20x magnification.

5.2.3.2 Immunofluorescent staining

To evaluate the morphology, differentiation and multi-nuclearity, PFA-fixed samples of monocytes grown on Ti-PGDs were stained for Cathepsin K (Rabbit polyclonal, AB19027, Abcam) F-actin (Alexa Fluor® 488 Phalloidin, A12379, ThermoFisher Scientific, UK) and nuclear acids (Hoechst 33342, ThermoFisher,

UK). Samples were incubated for 60 minutes with each primary antibody and subsequently for 15 minutes in the dark to complete nuclear staining. After washing with PBS cells were incubated in a secondary antibody solution (Goat Anti-Rabbit Alexa-Fluor® 594 A-11012, ThermoFisher),

5.2.3.3 Scanning electron microscopy imaging (SEM)

Osteoclast morphology and resorption activity was assessed using SEM with samples prepared using the same technique as described in section 4.2.5.

5.2.4 Effect of RANKL concentration on osteoclastogenesis

Having studied osteoclastogenesis on Ti-PGDs using culture protocols used for osteoclastogenesis on bone-like substances such as dentine, experiments were carried out to understand the effect of increased concentrations of RANKL (Biotechne, UK), a protein key in the differentiation of monocytes, osteoclast formation and resorption. The study involved using the protocol described in section 5.2.2 and a seeding density of 2.5×10^6 cells/cm² with 3 different concentrations of RANKL. S2 media and acidified S2 media were supplemented with 0, 3 and 30 ng/ml of RANKL to map the optimal RANKL concentration for osteoclastogenesis on Ti-PGDs.

5.2.4.1 Scanning electron microscopy imaging

Osteoclast morphology and resorption activity was assessed using SEM with samples prepared using the same technique as described in section 4.2.5.

5.2.5 hBM-MSCs culture on acid-etched Ti-PGDs

The effect of surface porosity on the ability of hBM-MSCs to proliferate was analysed by acid-etching the surface of the Ti-PGDs and assessing their ability to support cell growth. This method aimed to mimic the acidic environment produced during which active osteoclasts resorb the bone surface. By using an acidic solution which created the same pH allowed the Ti-PGDs to be subjected

to the same environment. The mechanism of resorption and development of resorption pits varies significantly between natural osteoclast activity and the method used here, however this study should provide an understanding of how well hBM-MSCs can repopulate highly etched surface. Phosphoric acid (85% H₃PO₄, Sigma-Aldrich, UK) was used to form a 30% H₃PO₄ solution (diluted in distilled H₂O) which was stored in a glass bottle at room temperature. Individual wells of ultra-low attachment 24-well microplates were filled with individual 15mm Ti-PGDs which were sterilized using a high-intensity UV lamp. The 30% H₃PO₄ was added in quantities of 500µL to wells containing Ti-PGDs and were kept incubated at 37°C in an atmosphere of 5% CO₂ for 15 minutes and 24 hours. The acid-etched Ti-PGDs were washed with DMEM (10% FBS, 1% AA) to ensure all acid had been removed from the wells. This was aided by the colour change of the media when in the presence of acid from a red to a yellow colour. Once the media maintained its red appearance, 2x10⁴ hBM-MSCs were seeded into each well and were incubated at 37°C in an atmosphere of 5% CO₂. Cells culture was carried out for 3 days after which samples were fixed for analysis.

5.2.5.1 Scanning electron microscopy imaging

Proliferation of hBM-MSCs was qualitatively assessed using SEM with samples prepared using the same technique as described in section 4.2.5.

5.2.6 hBM-MSC culture on acid-etched Ti-PGMs

The effect of porosity was further explored on Ti-PGMs to understand how cells proliferated on the microsphere versions of the discs. Ti-PGMs were acid-etched prior to hBM-MSC culture, by treatment for 15 minutes with 30% H₃PO₄ solution. After removing the solution and washing out the remaining acid with DMEM media, 5x10³ cells were seeded into the wells and were incubated at 37°C in an atmosphere of 5% CO₂. Untreated Ti-PGMs and Synthemax were chosen as suitable controls to understand the effect porosity had on cellular growth. Cell proliferation was determined on days 1, 4, and 7 using a CCK-8 kit with media changes carried out every 48 hours.

5.3 Results

5.3.1 Mouse bone marrow-derived monocyte culture and differentiation on Ti-PGDs

The tartrate-resistant acid phosphatase (TRAP) staining of the cells visualized by the dark bodies on the crystalline Ti-PGD surface showed that as cell seeding density increased, the proximity of adjacent monocytes increased, therefore encouraging fusion to form multi-nucleated cells. Minimal numbers of cells were visibly stained in cultures with the lowest seeding density with the frequency of stained cells increasing with increasing cell density. However, from the TRAP images (Fig 5.1) it is unclear whether the aggregates formed are functional osteoclasts or cells closely packed together. Further, giant osteoclasts cannot be identified after 9 days of culture on Ti-PGDs. Furthermore, the crystalline structure of the Ti-PGDs prevented accurate identification of multi-nucleated bodies, as light would refract while travelling through the material. No visible resorption trails can be identified on the surface with a lack of TRAP staining present around the larger bodies formed.

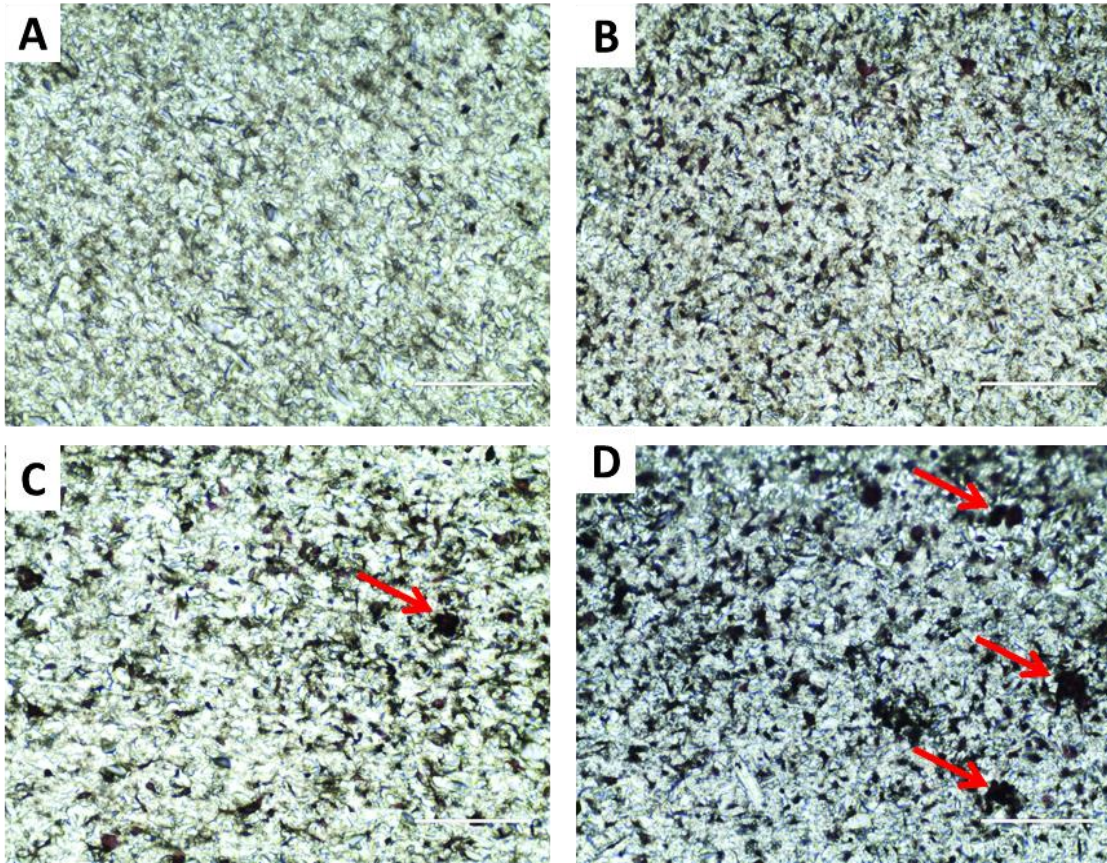


Figure 5.1 TRAP-staining showing monocyte distribution and osteoclast formation using different seeding densities. The different densities used were A- 2.5×10^5 cells/cm² B- 5×10^5 cells/cm² C- 1×10^6 cells/cm² and D- 2.5×10^6 cells/cm². The red arrows indicate areas of possible osteoclastogenesis. Images were taken at 20x magnification with the scale bars representing 200 μ m.

Next, confocal microscopy was used to visualize cathepsin K expression, one of the enzymes responsible in bone degradation. Cathepsin K enzyme expression was prominent in monocytes cultured on Ti-PGDs, with many areas populated with high numbers of cells showing higher expression than individual cells. The lack of resorption trails is further validated through the immunofluorescent imaging, with no faint cathepsin K staining visible around a multi-nucleated osteoclast. Faint cathepsin K staining is used as an indication that an active osteoclast is migrating across the material surface. Furthermore, no F-actin cytoskeleton ring was visible even at high cell densities, which highlights the lack of sealing zone formation at this stage of culture. Hoechst staining allowed visualising the cell nucleus; however, it was not evident from immunofluorescent

imaging whether multi-nucleated osteoclasts existed with clusters of cell visible without a distinguishable actin ring.

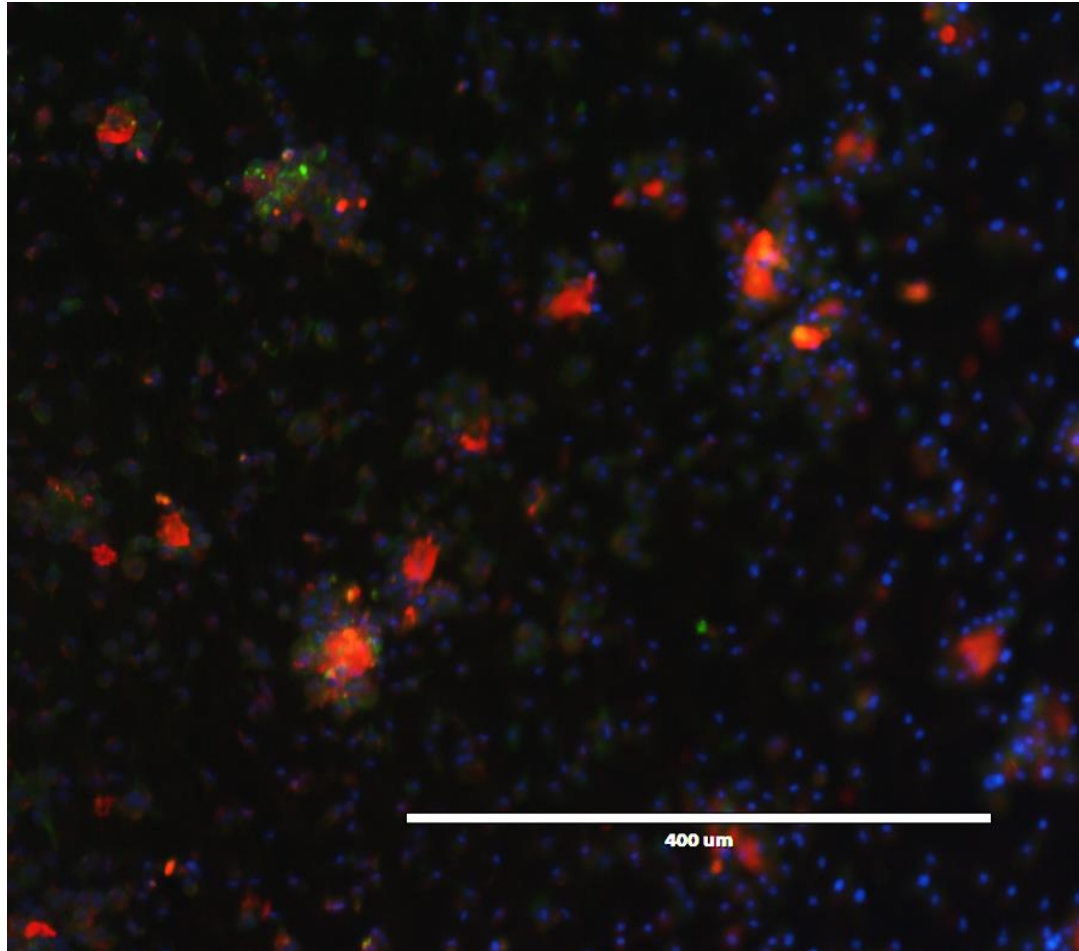


Figure 5.2 Cathepsin K expression from mouse monocytes cultured on Ti-PGDs. The immunofluorescent image illustrates expression of bone degrading enzyme cathepsin K (red) when 2.5×10^6 cells/cm² were seeded on Ti-PGDs. Staining of F-actin (green) and nuclear stain (blue) Hoechst 33342 were carried out to highlight actin ring formation and multi-nuclearity respectively. Scale bar indicates 400μm with images taken at 5x magnification.

Cathepsin K activity in Figure 5.2 indicates that enzymes involved in the resorption process are produced, however SEM was used to confirm that the materials could be degraded by the enzyme. When examining the SEM images (Figure 5.3) the ability of osteoclasts to resorb the Ti-PGDs is observed with clear pits formed under the active cell. Inactive monocytes showed no material

resorption indicating an earlier phase of osteoclastogenesis. The acidification action of the pre-osteoclasts allowed the material directly in contact with the cells to be resorbed; however, little migration occurs to allow further lateral axis resorption. From Figure 5.4 the resorption activity of pre-osteoclasts is validated with a potential resorption occurring in a perpendicular manner to the surface of the Ti-PGDs indicated by the deep cavity produced. Also illustrated by Figure 5.4A are the differences between activated osteoclast precursors and inactive precursors. While the cell in the cavity shows no visible attachment to the Ti-PGD surface (inactive), the cell adjacent to it on the right (denoted by the red arrow) shows cell processes used to bind to the surface (active).

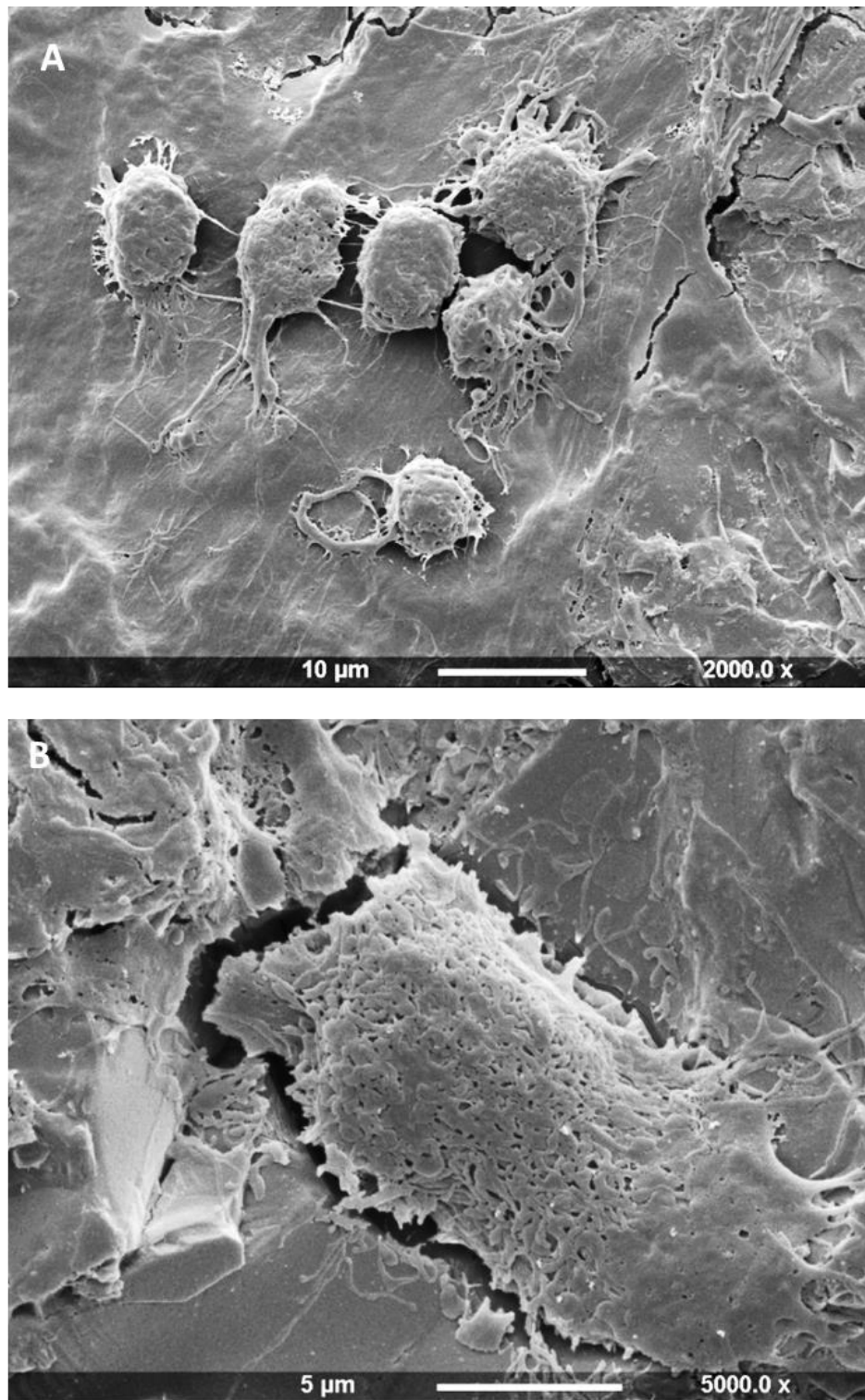


Figure 5.3 Monocyte culture and differentiation into pre-osteoclasts on the Ti-PGDs. SEM images of individual monocytes are illustrated in image A after 9 days of culture, while image B shows potential pre-osteoclasts and the lateral resorption. A hollow evacuated area can be seen under the cell with a similar shape to that of the cell. The degraded edge of the Ti-PGDs can be seen detached from the cell. Images were taken at various magnifications.

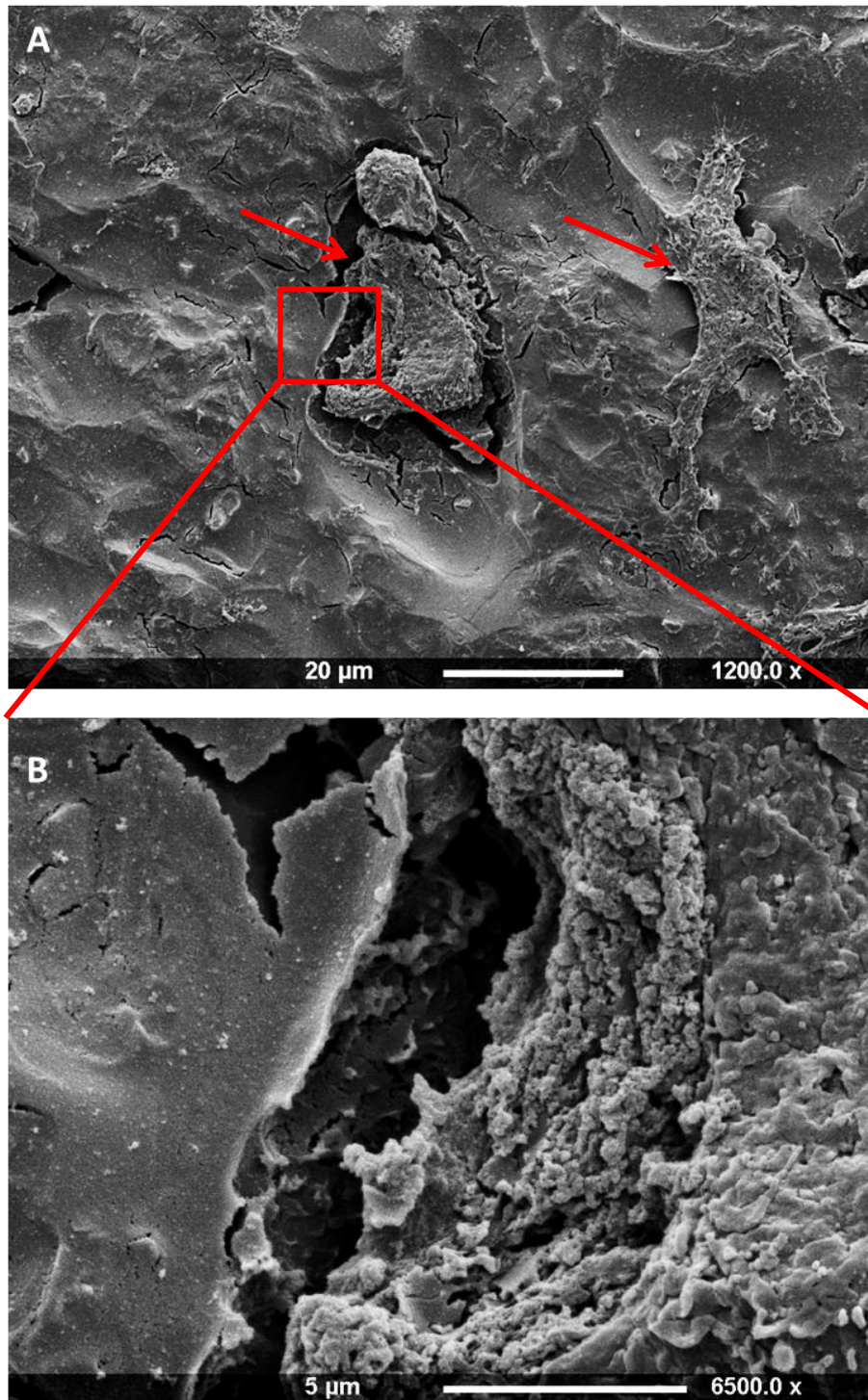


Figure 5.4 Pre-osteoclast resorption activity of the Ti-PGDs. The SEM images shows the differences between cellular material, the Ti-PGD surface and the resorption pit. The evacuated area can be seen under the cell with differing surface morphology to the Ti-PGD. Image B focuses on a section of image A to highlight the differences in textures of the modified surface. The arrows in image A indicate active (with cell processes) and inactive cells (without cell processes) adjacent to each other. Images were taken at various magnifications.

5.3.2 Effect of RANKL concentration on osteoclastogenesis

Next, the effect of different concentrations of RANKL was assessed, to determine whether there is a dose-effect on osteoclastogenesis. Assessing the morphology of the cells cultured under the three different conditions helps to evaluate the efficacy of the osteoclastogenesis process on the Ti-PGDs at different RANKL concentrations. As RANKL concentration increased, there was a tendency for the cells to locate closer to each other on the Ti-PGDs. Cells cultured under the highest RANKL concentration produced flatter, pancake-like inactive osteoclasts which had larger diameters than those visible under standard RANKL concentration (3ng/ml). As was visible in earlier experiments, cell processes (filopodia) were not visible at all concentrations studied, limiting cell migration.

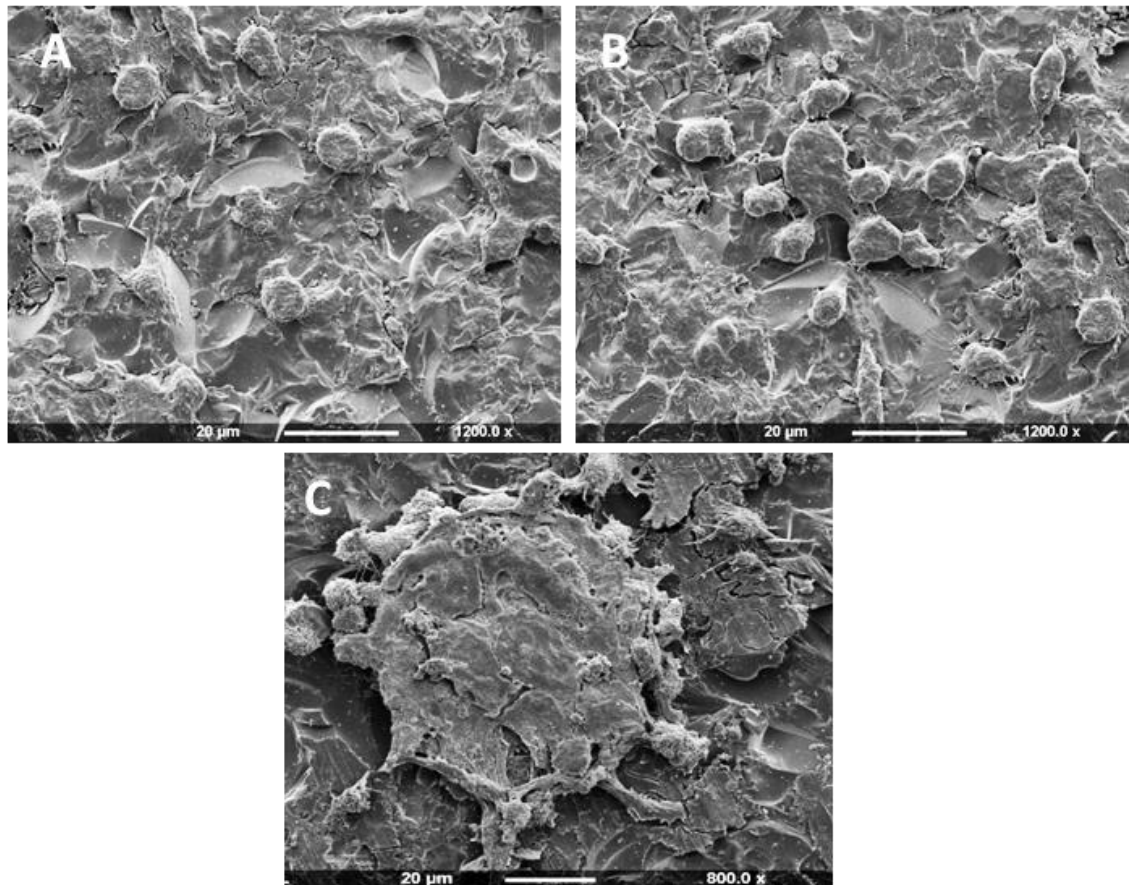


Figure 5.5 Mouse bone-marrow derived monocytes cultured on Ti-PGD for 9 days at different concentrations of RANKL. The different concentrations are highlighted by (A) 0 ng/ml (B) 3ng/ml and (C) 30ng/ml, with images taken at different magnifications. Scale bars represent 20μm intervals.

5.3.3 Evaluation of acid-etched Ti-PGDs to support hBM-MSC culture

To assess the effect of Ti-PGD surface modification on consequent bone formation, modified Ti-PGDs were produced using acid etching techniques and then examined the interaction of hBM-MSCs with the altered surface. From Figure 5.6 clear differences were seen between the surfaces of the Ti-PGDs acid-etched for different treatment times. When comparing the Ti-PGDs surface-treated for 15 minutes compared to the control group, a more contoured surface can be witnessed in both the light and scanning electron microscopy images. However, Ti-PGDs acid treated for 24 hours showed the most significant difference when compared the control group with the surface showing deep networking valleys across the surface of the structure. There was no distinct trend to the location of the valleys; however, this could be due to the heterogeneous distribution of ions in the glass disc during the melting and quenching process of the glass.

The application of Ti-PGDs were further assessed by seeding hBM-MSCs on the modified structures to understand whether effective cell interactions could occur on modified surfaces caused by acid treatment that is akin to the osteoclast-mediated acid degradation that occurs *in vivo*. From Figure 5.7, which illustrates the morphology of cells grown on Ti-PGDs that have been acid treated for 24 hours, it can be deduced that hBM-MSCs can interact well with the modified surface, highlighted by the thick layered sheet of cells above the valleys. Interestingly, images taken at higher resolution uncovered the formation of horizontal valleys through which cell processes were found to be passing, highlighting the ability of the hBM-MSCs to network through a degrading structure.

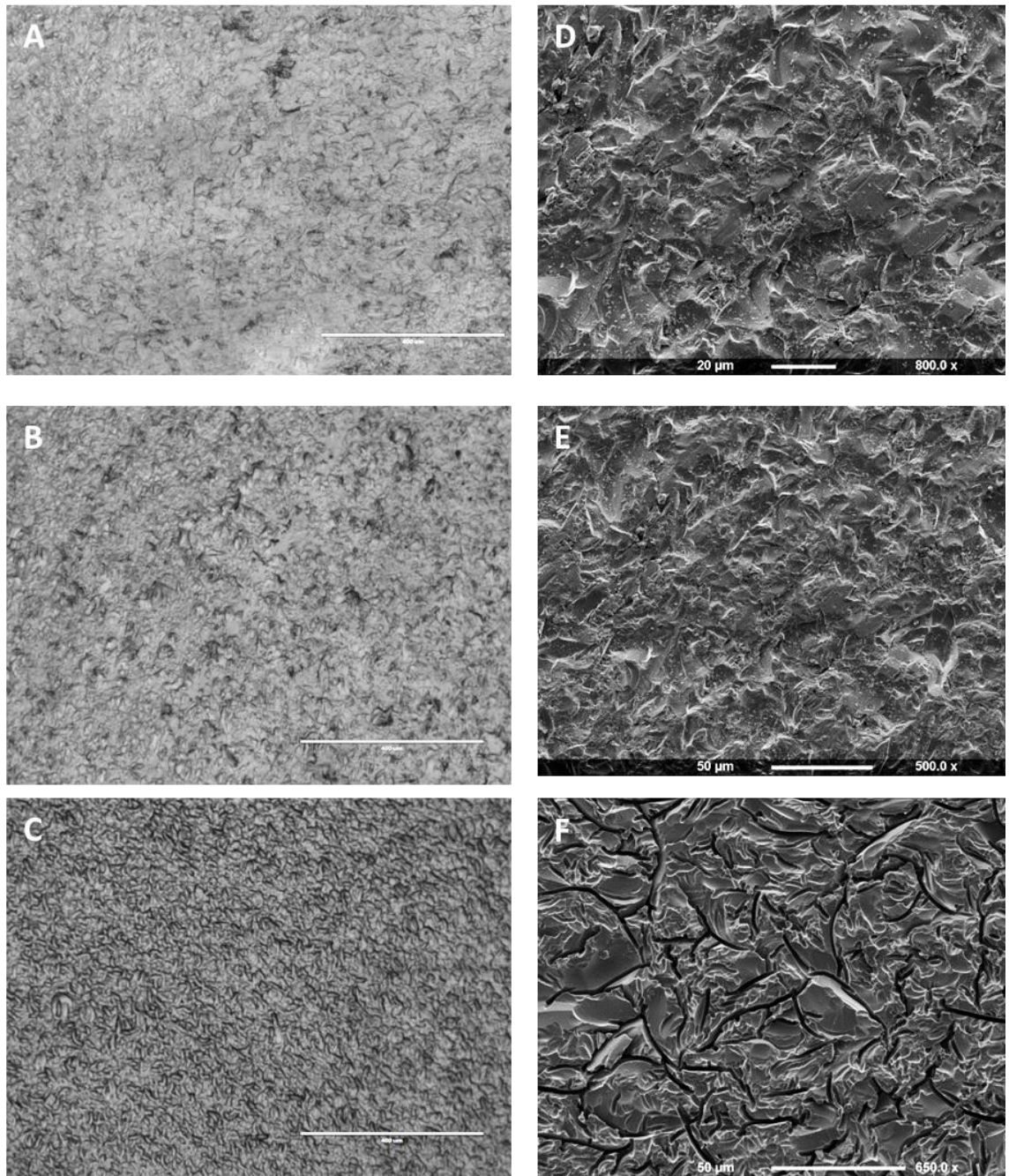


Figure 5.6 Effects of different incubation periods in 35% H_3PO_4 on the surface of Ti-PGDs. Images A-C were acquired using light microscopy technology while the images D-F were acquired using SEM. The different periods of time studied were: A/D- Untreated control, B/E- 15 minutes, and C/F- 24 hours. Scale bars for the light microscopy images indicate 400 μ m with images taken at 5x magnification. SEM images were taken at various magnification.

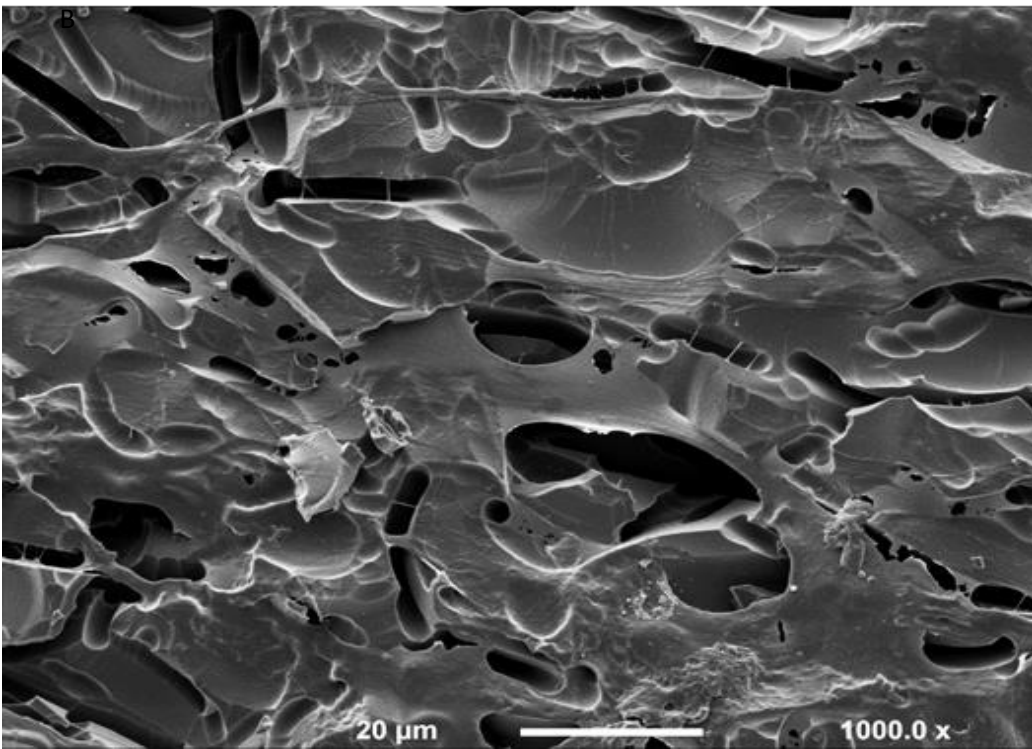
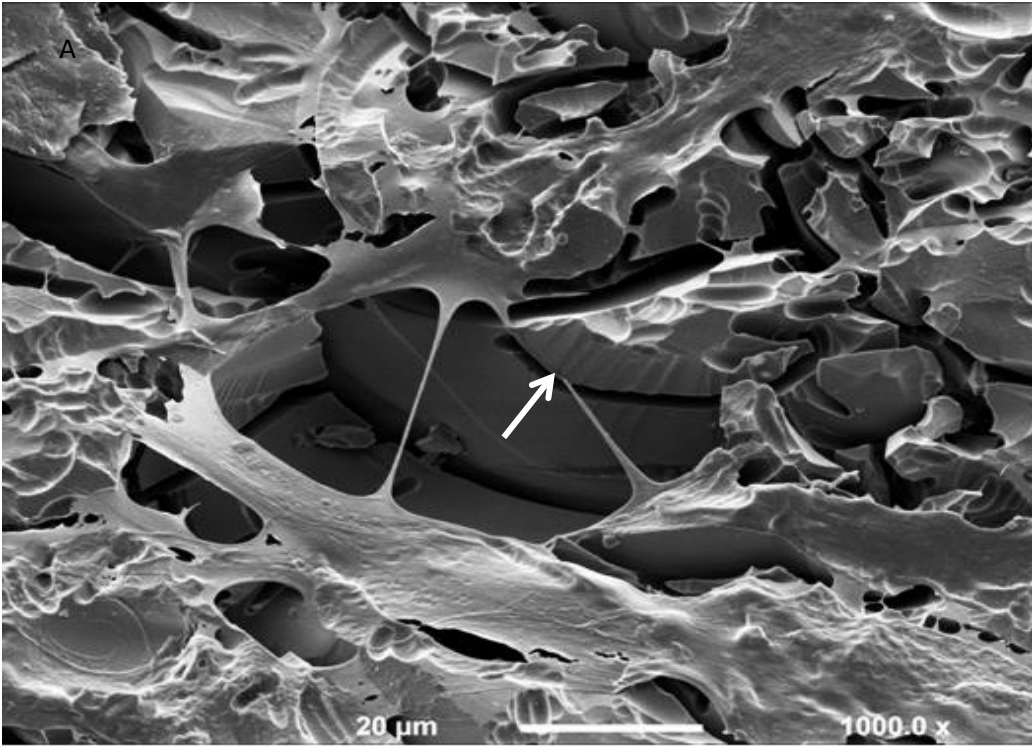


Figure 5.7 hBM-MSCs cultured on Ti-PGDs acid treated for 24 hours. The SEM images highlight the networks formed by hBM-MSCs within the channels created by the acid etching process of the Ti-PGDs, after 3 days of culture. The white arrow highlights a cell process passing through a horizontal valley. Images were taken at 1000x magnification with scale bars indicating 20μm.

5.3.4 Cell proliferation of hBM-MSCs on acid-etched Ti-PGMS

The CCK-8 proliferation assay values were used to understand the effect acid etching had on cell attachment and proliferation over the course of 7 days, presented in Figure 5.8. Examining the cell viability based on the absorbance values, it can be seen that Synthemax showed improved cell attachment and growth over the first 24 hours when compared to both the control Ti-PGM group and the acid etched Ti-PGMs. On day 4 of culture, Synthemax maintained their enhanced proliferative ability however cell cultures on untreated Ti5 microspheres showed increased viability from day 1 to 4. By day 7 hBM-MSCs cultured on acid etched Ti5 microspheres showed significantly lower cell absorbance values than untreated Ti5 microspheres (** $p < 0.001$).

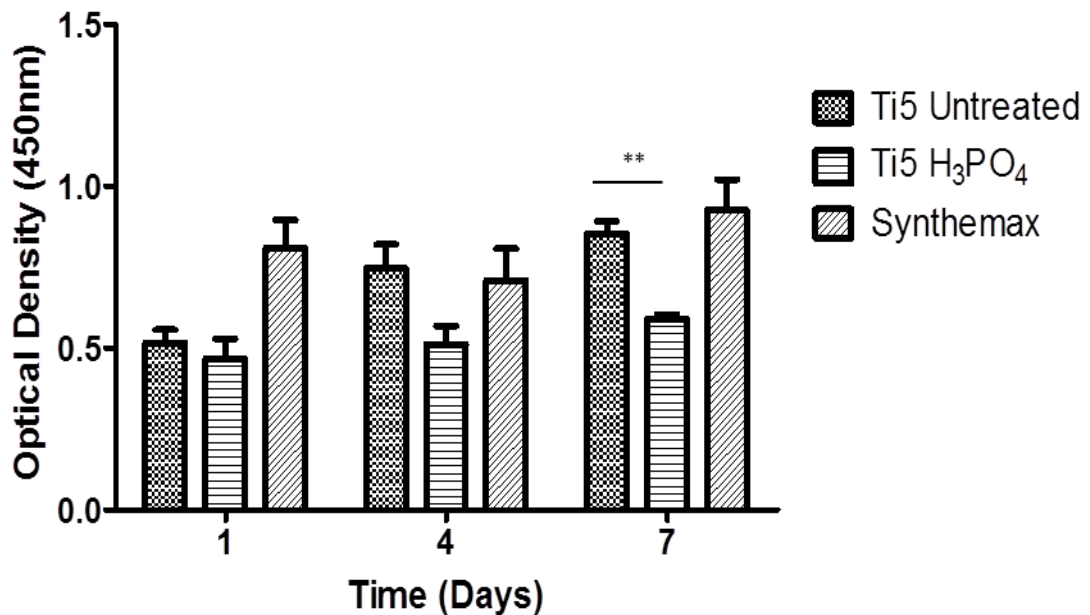


Figure 5.8 Proliferation of hBM-MSCs on untreated Ti5 and acid-etched Ti5 microspheres compared to Synthemax. CCK-8 assay readings were taken at time points day 1, 4 and 7 Error bars represent +SD (n=3). **= $p < 0.01$.

The differences in surface topography can be observed through the SEM images presented in Figure 5.9. Images A and B illustrate the porous layer created due to the effects of the H₃PO₄. The pores generated do not extend through the microsphere to form a network, however generates a rough surface for cell attachment. The pores are visibly heterogenous in character such as depth and

width, and are located in an irregular manner across the surface. Figure 5.9C and D examine the surface properties of Synthemax which shows a rough surface due to the protein surface coating administered to the polystyrene microcarriers, which aids surface attachment. The raw untreated microcarriers (Fig 5.9E) show a smoother surface with limited changes in surface topography when compared to the Synthemax surface (Fig 5.9C).

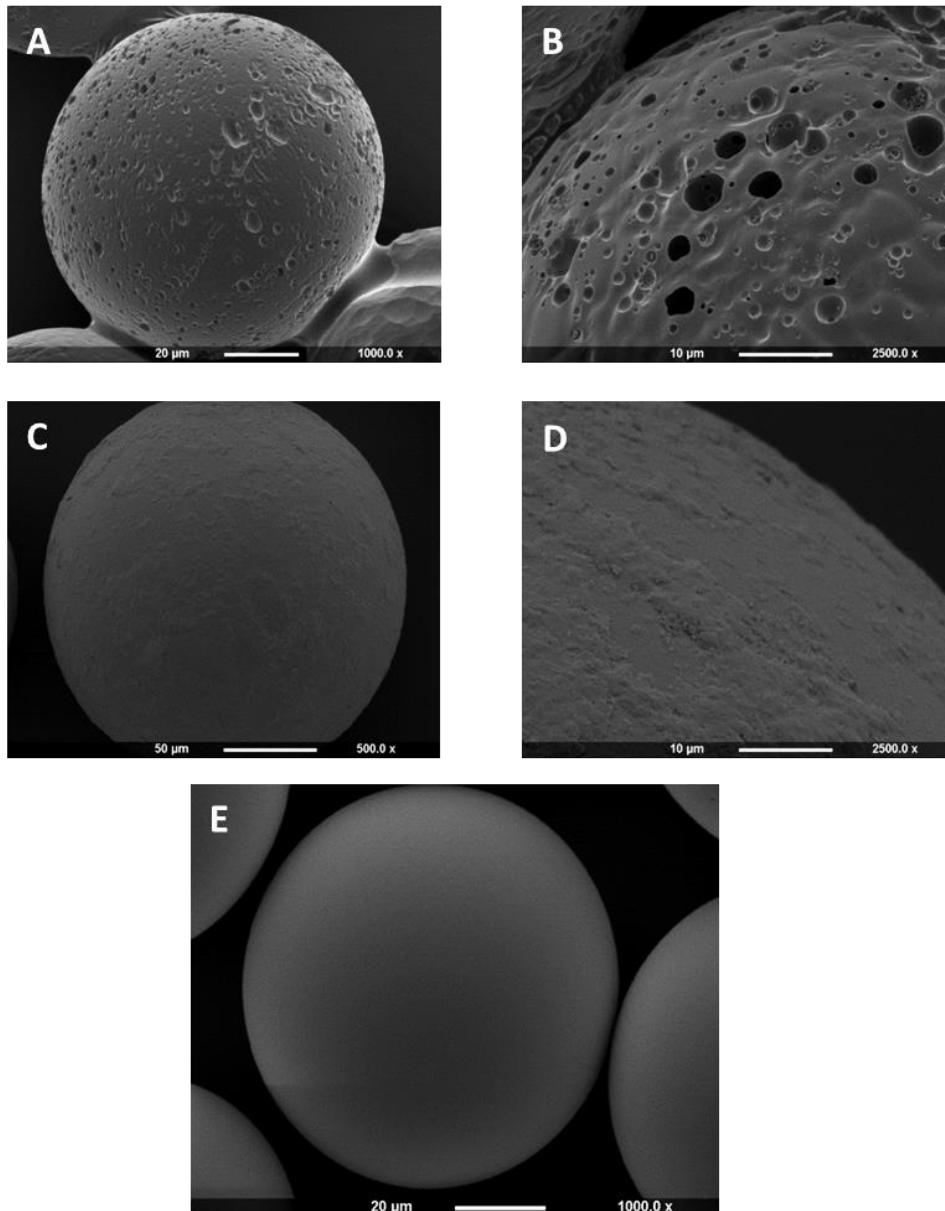


Fig 5.9 Scanning electron microscopy images showing the surface topography of Ti-PGMs incubated in H_3PO_4 . Samples were acid-treated for 15 minutes (A, B), Synthemax microcarriers (C, D) and untreated titanium phosphate microspheres (E). Images were taken at different magnifications.

5.4 Discussion

This chapter of the research aimed to determine whether titanium-doped phosphate glass is capable of being resorbed by osteoclasts. Initially, the capacity of the material to support osteoclastogenesis was assessed, followed by the resorptive capability of the developed osteoclasts. The initial experiments focused on understanding what seeding density of monocytes is required to initiate osteoclastogenesis. Various seeding densities have been suggested in the literature, from 5×10^4 cells/cm² (Wittrant et al., 2008) up to 2.5×10^6 cells/cm² (Orriss and Arnett, 2012). Having studied a range of different densities on the Ti-PGDs it was evident that higher densities were required to promote effective osteoclast formation, illustrated by TRAP staining. One reason for the low numbers of giant osteoclasts formed may be due to a lack of inorganic components in the material. The material's relative bio-inert nature when compared to physiological bone (due to a lack of bone specific proteins such as collagen and other proteins, factors paramount in the activity of osteoclast) limits the ability of osteoclast progenitors to bind effectively to the surface, fuse together, and consequently migrate and resorb the Ti-PGDs.

Vitronectin and osteopontin act as ligands, by binding to integrins found on the cell membrane such as vitronectin receptors $\alpha V\beta 3$ (VNR) (Chambers and Fuller, 2011), therefore osteoclasts have limited affinity to biomaterials without these present. The lack of these regulatory proteins for attachment, will concurrently lead to the absence of a resorption trail. Therefore, future work could assess potential approaches to functionalisation of the materials via coatings using a range of bioactive molecules.

While giant active osteoclasts are more effective at resorbing bone-like materials compared to smaller active osteoclasts due to the surface area they occupy, there is no conclusive evidence directly correlating material type with its ability to induce the formation of large osteoclasts. In fact, giant, inactive (non-resorbing) osteoclasts have been cultured on tissue culture plastic, a material incapable of being resorbed by active osteoclasts (Orriss and Arnett, 2012), hence cell size

shouldn't be solely used to assess the biomaterials ability to generate functional osteoclasts.

The use of cathepsin K enzyme secretion as a molecular marker of osteoclast activity is also under dispute, with authors of studies concluding that cathepsin K expression is independent of substrate, where no difference in expression is observed between monocyte cells cultured on plastic, bone particles or in suspension (Rieman et al., 2001). While surface properties have been shown to have no effect on cathepsin K expression, it was necessary to understand whether cells grown on Ti-PGDs could synthesis enzymes necessary for remodelling and resorption of the biomaterials. The immunofluorescent images indicated that cells were capable of secreting cathepsin K, and high cathepsin K expression was associated with areas of high cell clustering, suggesting that the osteoclastogenesis process was initiated. The lack of a positive control for this study owes to the Ti-PGDs thickness being magnitudes higher than the dentine discs obtained, therefore future work should look at having a suitable control that to compare resorption rates of the materials. Future studies should look to either create thinner Ti-PGDs or find a suitable resorbable substance to compare Ti-PGDs to. While cathepsin K expression presents uncertainty as a key marker of active osteoclasts, the role of F-actin is undisputed. F-actin ring formation occurs during the resorption process carried out by osteoclasts, and the actin rings create sealing zones between the cells and the bone-like material (Jurdic et al., 2006, Teitelbaum, 2007). The formation of this sealing zone is identified as the point at which resorption is initiated (Chambers and Fuller, 2011). The ability to identify actin ring formation is an indicator of an active osteoclast, confirmed by osteoclasts cultured on tissue culture plastic, which are unable to form actin rings or are limited to forming podosome dots (actin ring precursors) (Wilson et al., 2009, Kleinhans et al., 2015), and are therefore considered inactive. The osteoclasts formed on the surface of the Ti-PGDs showed no distinct actin ring formation even in areas showing the presence of high cathepsin K expression and pits. The lack of visible actin ring may be due to the culture period being too short to support the formation of the necessary structures specifically on the Ti-PGDs.

Interestingly, the osteoclasts which exhibited resorptive activity maintained no sealing zone commonly seen with resorbing osteoclasts. Instead they resided within the resorbed pit with no cellular processes, which suggests either the osteoclasts were resorbing in a downwards fashion into the material, or the environment surrounding the osteoclasts inhibited any further osteoclast function. From the SEM images, evidence is provided to illustrate that resorption of the biomaterial can be achieved, however the lack of resorption trails suggests the cells are unable to migrate on the material. This owes to the limitation of the material; as aforementioned, it doesn't provide support for monocyte cell attachment and its metallic dopant (Ti^{4+}) potentially inhibits osteoclastogenesis. Future work could assess the application of surface coatings e.g. collagen to the material as a means of enhancing monocyte attachment and osteoclastogenesis.

It is well documented that metallic oxides of different valences alter the activity of osteoclastogenesis. While doping specific biomaterials can enhance stability of the structure and promote osteoblastic formation, the effects of these ions on osteoclastogenesis and osteoclastic resorption are generally detrimental. When looking at bivalent cations such as Mg^{2+} , Sr^{2+} and Zn^{2+} evidence exists that these ions inhibit or at least slow down differentiation of precursor monocytes into mature osteoclasts (Hadley et al., 2010, Janning et al., 2010, Tat et al., 2011, Yamaguchi and Weitzmann, 2011, Roy and Bose, 2012, Bose et al., 2013, Ostrowski et al., 2015). Other research has concluded that elevated levels of extracellular inorganic phosphate (Pi) ions may be responsible for reduced osteoclast activity and potential osteoclast apoptosis, however understanding of the mechanism involved has not been fully elucidated (Yates et al., 1991, Hayashibara et al., 2007).

Stimulation of the osteoclast progenitor surface receptor RANK by RANKL is a significant cue for osteoclast maturation (Lacey et al., 1998). Therefore, to improve osteoclast activity it was deemed appropriate to increase RANKL concentration and determine whether enhanced resorption could be achieved. While there was no change in resorptive activity between the different RANKL concentrations studied (0, 3, 30 ng/ml), the structure and sizes of cells formed varied a great degree. Whether this is achieved during the initial stages of cell

culture by monocytes aggregating in suspension, or at the stage of attachment where RANKL induces cells to migrate to one another, evidence exists to show that osteoclastogenesis is affected by RANKL concentration.

While the challenge to develop a perfectly resorbable biomaterial still exists, there lies a question of whether bone-forming cells will repopulate and fill the resorption pits created. The idea envisaged is that the ideal material would trigger coordinated osteoblastic formation and osteoclastic resorption. The geometric structure of a biomaterial can be a cue for cell adhesion and consequently proliferation (Dalby et al., 2014). Improvements in biomaterial microarchitecture need to be achieved to enhance these tissue regeneration responses. It has been documented that pore size in tissue engineered substrates greatly influences mechanical properties (Jones et al., 2009). While small pores could restrict cell infiltration into a structure and revascularization, large pores can reduce structural stability (Jones et al., 2009). It has been documented that scaffolds with larger uniform pore sizes resulted in better functional bone regeneration (Guda et al., 2014). The level of porosity also plays an important role in tissue regeneration, as differing scaffold porosities influence both cell proliferation and osteogenic differentiation. Work carried out by Horst et al., showed that increased surface porosity accelerated cell proliferation *in vitro* (Horst et al., 2014). While other studies have shown that increased surface porosity suppresses early cell proliferation (Wall et al., 2009). However, there is no universally accepted pore size dimension known to induce osteogenic differentiation (Bohner et al., 2011).

Limited work to our knowledge, has been carried out on understanding the effect of porosity on MSC proliferation on micro-spherical phosphate glass particles. Therefore, understanding whether the effects observed in this study are representative to those witnessed in the broader tissue engineering community can't be confirmed. However, when comparing the pore sizes created through acid-etching of the Ti-PGMs compared to the sizes shown to promote better cell proliferation, the smaller sizes could be a potential reason for the lower cell proliferation after 7 days compared to the untreated surface. Cell type may also play a role in the effect of pore size and porosity on cell proliferation. With the average size of MSCs significantly larger than osteoblastic cells, care needs to

be taken in determining the architecture of the microspheres for culture and differentiation.

It can be concluded that Ti-PGMs subjected to a short period of acid-etching have reduced proliferative capacity when compared to control Ti-PGMs and Synthemax. Wall et al., showed that MSCs don't like to reside on acid-etched Ti-discs while Harle et al., showed that osteoblasts preferred to, indicating the two cell types that are born of the same precursor respond differently (Harle et al., 2006, Wall et al., 2009). This suggests further work is required to understand how well MSCs can repopulate a degrading structure. Additionally, the effect of porosity may have an impact on the fluidization of the microspheres during large scale cell culture. Extended periods of acid exposure will inevitably reduce the overall density of the microspheres, making them more buoyant and increasing the likelihood that they could be brought into suspension. However, a careful balance is necessary to ensure that the additional porosity doesn't inhibit cell attachment.

Overall, this chapter showed that some key responses associated with osteoclast formation are evident on phosphate glass microcarriers. However, the absence of critical parameter, F-actin ring formation, means that further work is needed to determine whether osteoclastogenesis can truly take place on these materials and hence promote resorption. Acid etching, to mimic the acid resorption that takes place *in vivo* did not yield positive results for MSC proliferation, even though a dense carpet of cells was identified at the surface.

Chapter 6 . Summary: General conclusion and future work

6.1 Research objectives and conclusions

The present research was undertaken with the hypothesis that that spheroidized phosphate glass microspheres can support critical cell responses that will ultimately enable scalable production of bone-like tissue microunits. The overall goal was to demonstrate the potential of Titanium-doped phosphate glass to support production of bone-like tissue in a manner that is transferable to scalable bioreactor-based cell culture. To achieve this goal, the following aims were defined:

- 1) Assess the biocompatibility of the material with the following differentiated and primary cell types:
 - a) Osteosarcoma cell line (MG63)
 - b) Human bone marrow-derived mesenchymal stem cells (hBM-MSCs)
- 2) Determine the effects of fluid flow forces induced by dynamic culture on cell/engineered tissue quality.
- 3) Establish whether scale-up of cell culture can be achieved to create increased quantities of engineered bone-like material.

The following section summarises the key findings identified in the studies carried out and identifies direction for future work to address the various challenges encountered throughout the research.

The first objective was to determine whether Ti-PGMs could support MG63 and hBM-MSCs culture. Initially, three different glass compositions were developed containing 0, 5 and 7 mol% quantities of TiO₂. However, during the study the 0 mol% composition degraded within 3 days when in solution. Therefore, only the

5 and 7 mol% compositions were taken forward and extensively studied with both cell types.

One major limitation of the study which should be considered when drawing conclusions from the results is the lack of material characterization carried out in this study. Prior characterization of this material has been carried out within the laboratory on the stoichiometric compositions studied ((Lakhkar et al., 2012a). However, as the experiments carried out in this study used a different batch of material from the aforementioned study and additionally multiple batches were used in this research it is important to clarify that the lack of control in regard to the characterization of the material could potentially play a role in the cell behaviour.

Initial cell culture studies using MG63 cells indicated that the material was biocompatible and able to support cell growth. No difference was observed between the two compositions studied in terms of cell growth, indicating that both were structurally suitable for cell growth and support. Over the 13 days of culture 2.64- and 2.65-fold increases were achieved by Ti5 and Ti7 respectively. However, this was lower than proliferation on commercially available tissue culture plastic, which increased viable cells by 4.59-fold. The studies served as a starting point into understanding whether bone forming cells could be cultured on the materials. In comparison with commercially available surface-treated polystyrene microcarriers, Synthemax, which are classified as an entity optimized for MSC attachment, Ti-PGMs exhibited similarity in their ability to support hBM-MSC proliferation across most of the conditions studied. The fold increase values supported the hypothesis that Ti-PGMs could effectively support hBM-MSC proliferation and essentially provided the foundation to explore how microscale cultures could be translated to 125ml shaken cultures. Light microscopy revealed that both cell types when cultured on Ti-PGMs could form networks between microspheres and consequently create clustered macrostructures.

Unlike the MG63 cells that were studied in Chapter Two, hBM-MSCs are influenced by their local environment more than MG63 by forces such as fluid flow, a characteristic that can be used to aid cell differentiation. The studies using

hBM-MSCs not only focused on the proliferation of immature stem cells but also on understanding the influence of Ti-PGM on their osteogenic differentiation. During cell culture, attachment protein fibronectin and early bone differentiation marker type-1 collagen were both up-regulated after 13 days of culture. Further studies examined whether soluble factors released from the substrates can induce an osteogenic response, using conditioned media from 5 mol% powders. The results indicated that the dissolution components of the material didn't have as prominent an effect as commercially available osteogenic media. However, they did support cell proliferation at low concentrations.

Having studied the responses of MG63 and hBM-MSCs on different compositions of Ti-PGM's at small scale, a choice was taken to narrow down the compositions to be studied at large scale to one Ti-PGM type. As earlier results showed limited differences activity of MG63 cells on the different Ti-PGMs, yet for hBM-MSCs Ti5 produced higher cell yields, large-scale studies were carried out using only Ti5.

The second objective of this research was to establish whether dynamic culture could improve cell activity on Ti-PGMs due to the associated action of mixing. The Froude number, a scalable dimensionless number dependent on vessel geometry, fluid height and orbital diameter (Weheliye et al., 2013) was used to determine the agitation rates chosen for studies of both MG63 and hBM-MSC responses. MG63 cell growth in microplates orbitally shaken at speeds calculated to achieve optimal mixing showed no enhanced response compared to static culture conditions. However, the cell-microsphere structures that formed varied greatly with high speeds creating small clusters, but static and intermediate agitation rates creating larger clusters. The high agitation rates also forced the cells to metabolise in an ineffective manner, generating more lactate per unit of glucose consumed compared to the other conditions. The effect of dynamic culture on hBM-MSCs is generally well understood, with evidence clearly showing that fluid flow can positively influence hBM-MSC differentiation (Reich et al., 1990, Bancroft et al., 2002, Kreke and Goldstein, 2004, Kreke et al., 2005).

Moderate agitation was stimulatory to and enhanced proliferation of hBM-MSCs on Ti-PGMs compared to static culture, whereas higher agitation speeds were detrimental to hBM-MSCs growth, when compared to static conditions and moderate agitation rates. Regarding cluster formation, similar observations were seen for MG63 cells, with higher agitation rates leading to small clusters. It is concluded that moderate agitation rates are beneficial when using Ti-PGMs due to the mixing patterns created. At high agitation rates cell growth is limited, therefore complete mixing within a reactor vessel shouldn't be used for cell culture using the conditions chosen (media and microcarrier type) unless carried out in a shear-controlled manner.

The final objective of this research was to explore the opportunity to use the knowledge gained from small scale to translate to large scale, using the different Froude models to predict the agitation speeds required. Having explored the use of different bioreactors (perfusion and magnetic-wheel bioreactor) and their compatibility in aiding the use of Ti-PGMs as a platform for large scale culture, shaken culture was chosen as it best mapped to the mixing mode used in small scale studies and therefore extrapolation of observations across the two scales should be more achievable.

The assessment of each of the reactor types considered will be discussed briefly towards the end of this section. Using a model developed by Olmos et al., (Olmos et al., 2015) to understand mixing systems at large scale under shaken culture taking into account parameters studied by Weheliye et al., (Weheliye et al., 2013), agitation speeds could be determined for large-scale culture which would map to the mixing systems used in small-scale studies. Large-scale culture of hBM-MSCs in 125ml Erlenmeyer flasks showed the same trends that were witnessed at small scale. Cell proliferation on Synthemax decreased when orbital agitation was increased, while culture on Ti5 was better under static and moderate agitation conditions. Interestingly, when extremely high agitation rates were used at large scale the Ti-PGMs would concentrate into the centre of the vessel, in an area which cells proliferated and secreted ECM, indicating that the effects of fluid flow shear were low in the centre of the vortex created. The major highlight of the research was the Ti-PGMs ability to match, and under higher agitation conditions

exceed Synthemax's ability to support cell proliferation. The large-scale use of Ti-PGMs validated previous studies carried out at small scale using the material of its ability to provide cues for osteogenic differentiation. With limited work existing on the use of shaken platforms and bioactive materials to support the formation of tissue engineered macrostructures at a clinically relevant scale, further work is required in the field to characterize the materials created at the studied scale and to understand whether the Olmos model used in this study can be validated for Ti-PGMs at larger vessel sizes.

Additionally, this research explored how well the substrate could be reabsorbed by cells responsible for bone remodelling *in vivo*. Using mouse bone marrow derived monocytes; the Ti-PGDs were assessed for their ability to support osteoclastogenesis. Overall, the formation of functional osteoclasts was not evident through visual analysis, attributable to the lack of attachment proteins available in Ti-PGDs. While limited attachment of what were deemed as pre-osteoclast cells was observed, many cells showed their resorptive capacity of Ti-PGDs. Further work is necessary to understand whether the substrate can be altered to improve osteoclast attachment and migration, therefore improving osteoclast migration and hence substrate resorption. The resorption activity was also mimicked through acid etching of Ti-PGMs and MSC proliferation was assessed. The acid-etching studies also provided an understanding of how well bone-forming cells could function on a porous structure, an eventuality from structural degradation.

6.2 Future Work

The mode of using Ti-PGMs to produce tissue engineered constructs of bone in order to treat critical size defects cannot be determined until further characterization of the tissues formed, as well as the feasibility of further scale up have been established. This research has provided an insight to the potential uses of Ti-PGMs within a dynamic environment; however, work in the future should look to determine specific operating ranges to exploit the impact of dynamic culture conditions and fluid flow shear stresses. By narrowing down specific agitation windows to optimize proliferative and differentiation conditions, a single closed vessel has the potential to eliminate other modes of cell expansion and reduce the costs of expensive differentiation media required to generate bone tissue *in vitro*.

One key area to focus on highlighted by limited resorption is the incorporation of active biological ingredients such as attachment proteins into the structure or through surface coatings. As discussed in Chapter 4, the use of protein coatings as a biofunctionalization tool has been studied extensively; however, the benefits of the applied coating would be limited to the outer surface of the material. Sol-gel synthesis presents a useful alternative to the melt-quench method used in this research to produce glass. Formation through the hydrolysis and dehydration of inorganic salts and metal hydroxides, permits sol-gel glasses to be processed at low temperatures therefore allowing proteins to be incorporated into the glass structures (Arcos and Vallet-Regí, 2010). The loading of osteogenic compounds within Ti-PGMs could allow it to act as a drug delivery system by the supplementation of osteo-regenerative agents to the injured site.

While the material showed promise as a biomaterial, its density creates a challenge for use in microsphere format in scaling up cell culture. There was some evidence from the acid-etching studies that it is possible to etch pores into the material and could be explored further as a means of reducing density and increasing buoyancy of the material. Successful transition of shaken culture from microscale to large-scale was achieved, through proven cell proliferation and improved osteogenic differentiation compared to commercially used

microcarriers, however the use of Ti-PGMs in different bioreactor types showed the limitations that need to be addressed, including its ability to be suspended to create a homogeneous cell culture environment. Techniques such as thermally induced phase separation (TIPS), used with other biomaterials such as PLGA, could aid the production of highly porous structures, increasing the overall buoyancy on the Ti-PGMs. However, *in vitro* characterization will need to be carried out to ensure any newly formulated microsphere can provide the same physical and structural properties of its predecessor (Parmar et al., 2015).

Besides single-use shaken bioreactors, other disposable bioreactors were considered, including PBS Biotech's novel MagDrive bioreactor which employs a low shear, pneumatic mixing system with high oxygen transfer rates. The PBS 0.1 MAG was used to determine how well Ti-PGMs could be cultured in a stirred vessel with a relatively low shear environment. Initial work studied three different agitation speeds (0, 25, and 50 rpm) using both Ti-PGMs and Synthemax. While both substrate types could be cultured and monitored through metabolite analysis, the process of extracting cell-microsphere material post-culture created problems, more so for the Ti-PGM's due to accessibility. The positioning of the vertical wheel prevented the extraction of the dense Ti-PGMs which were situated under the wheel, with any alternative intervention breaking the structures formed (Figure 6.2). However, the Synthemax microcarriers were used effectively with the PBS 0.1MAG bioreactor with both dynamic conditions improving cell proliferation with significantly higher ($*p<0.05$) rates of glucose consumption at day 10 compared to static culture in the same vessel.

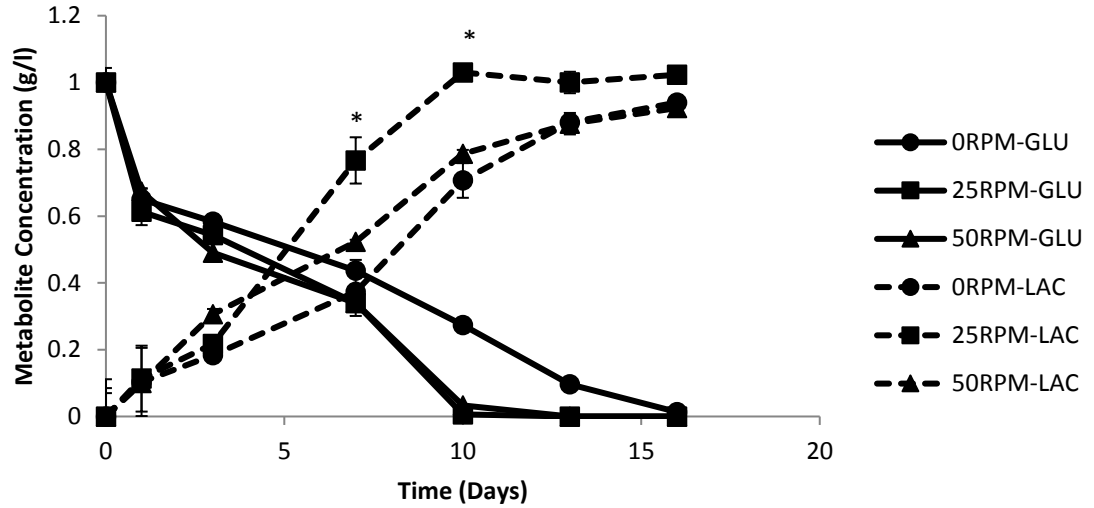


Figure 6.1 Glucose consumption and lactate production of hBM-MSCs cultured on Synthemax using a PBS 0.1MAG bioreactor. The magnetically driven air wheel bioreactor was run at 0, 25 and 50 rpm with samples of media taken on days 1, 4, 7, 10, 13 and 16. $*=p<0.05$. Error bars indicate \pm SD.

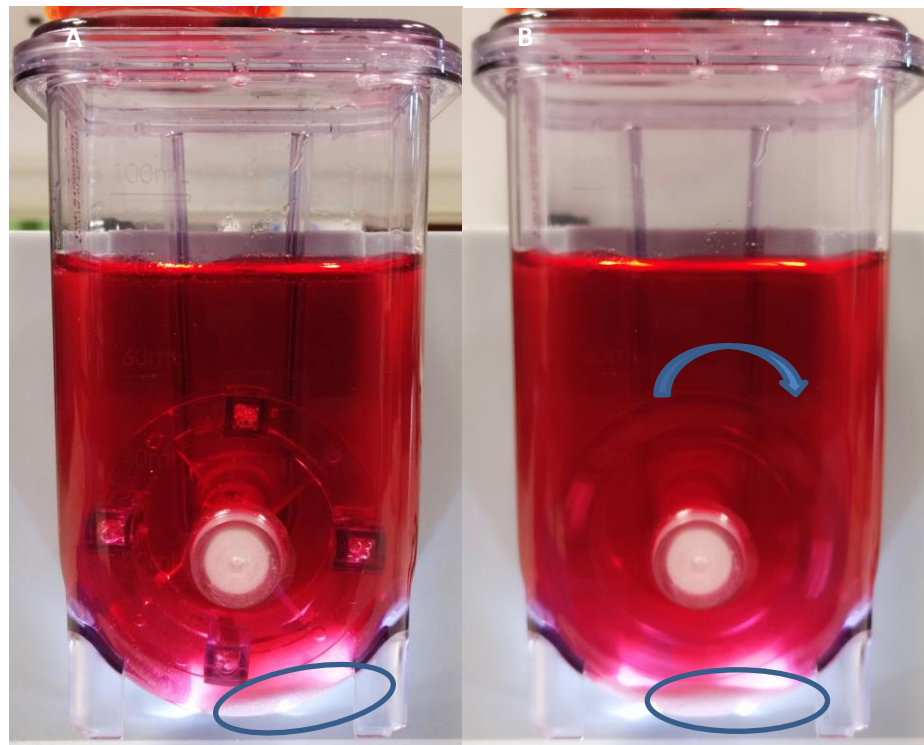


Figure 6.2 PBS 1.0 MAG Bioreactor containing Ti-PGMs under static (A) and 50rpm (B) conditions. The image illustrates the Ti-PGMs (1g) circled in blue remaining static at the base of the reactor when the highest speed was administered. Furthermore, the location of the magnetic drive prevents extraction of the material in an effective manner. The arrow indicates the direction of wheel rotation.

The use of perfusion bioreactors is a heavily researched area that offers interesting possibilities for the development for small-sized bone tissue that can be used to combat bone loss caused by injuries, congenital deformities or disease (Yeatts and Fisher, 2011). Basic perfusion bioreactor systems generally comprise a substrate material (either a scaffold or microparticles) placed along with cells inside a chamber. Cell culture medium flows through the chamber in a closed loop via tubes passing through a peristaltic pump that controls the medium perfusion rate. Perfusion bioreactor systems allow a laminar flow of medium and mass transport of nutrients and oxygen throughout the entire volume of the construct and are therefore able to overcome the diffusional limitations associated with other bioreactor types (e.g. rotating wall bioreactors). By varying the perfusion rate using the peristaltic pump, the fluid shear stresses exerted on the tissue can be optimised to provide the environment for optimal growth of small-sized bone tissue.

An in-house designed perfusion device (Fig 6.3) was used to understand the effectiveness of a perfusion bioreactor to be used with the Ti-PGMs. The idea was to create a homogenous expanded bed microsphere system to improve seeding and expansion of the hBM-MSCs, and consequently study the effects of different flow rates on cell proliferation and osteogenic differentiation. However, having calculated the Galileo fluidization parameter to determine the flowrate required to overcome the terminal falling velocity, the force required to maintain the Ti-PGMs in suspension exceeded the value of the pump that had been used (Richardson et al., 2002a, Richardson et al., 2002b). This limited studies to be carried out in packed bed mode, which had their inherent disadvantages such as concentrations gradients at low perfusion rates, and limited cell attachment at high flow rates. Although preliminary work on using perfusion bioreactors with Ti-PGMs has been carried out in the author's present laboratory, it is expected that the selection of an appropriately sized perfusion chamber and optimisation of the seeding and culturing protocol, together with on-going developments in microsphere surface functionalization and specialised stem cell medium production, will in the long term lead to the realisation of the main objective of the research, which is to develop viable bone tissue *in vitro* for use in bone replacement therapies.

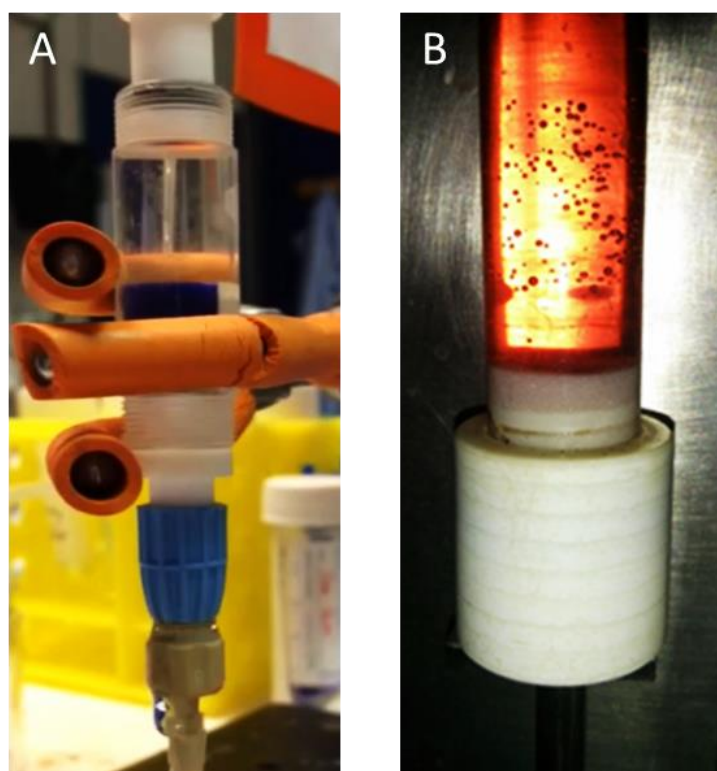


Figure 6.3 Different perfusion devices used to study the effects of fluidization of Ti-PGMs (A - doped with 5 mol% Co^{2+} and B – Ti5). The Faculty of Engineering and Design Group at the University of Bath tested the Ti-PGMs in their in-house developed perfusion device (A), while an in-house perfusion reactor (B) developed within the UCL Biochemical Engineering Regenerative Medicine lab was used to compare different perfusion reactor dimension on fluidization of the microspheres. The perfusion devices was connected to a Watson Marlow 205U (Wolf labs, UK) peristaltic pump where various flow rates were administered from 0 to 20 ml/min. Under maximum flowrate conditions, the Ti-PGMs would momentarily fluidize however would settle immediately.

Chapter 7 . Bioprocess validation considerations of biomaterials used in cell therapy manufacturing

One of the major challenges facing commercialization of cell therapies is the ability to translate protocols from the lab bench to closed, controlled bioreactors to deliver a consistent quality product in a reproducible fashion. This is a necessary step to meet scale up requirements to treat large numbers of patients. Furthermore, maintaining critical product attributes such as biologic identity and function requires great control, hence validation of the processes needs to meet regulatory standards.

The ultimate goal of the work carried out in this thesis would be to create a controlled system which could deliver personalized units of tissue engineered bone for defects of different sizes using microspheres and cells assembled into personalised geometries using custom-made moulds. The strategy to develop customised material will need to be explored further by understanding whether cell expansion and differentiation can be achieved in a sequential process within a mould effectively.

The application of tissue engineering to treat bone defects requires a balance between technical feasibility of the cell culture process and the economic drivers to minimize cost and maximize value. From the materials perspective, the material properties need to be adequate to provide the cells with an appropriate biophysical environment to deliver a product fit for purpose. While the science and engineering around developing a biomaterial play a crucial part in its success, knowledge of relevant regulations, standards and the required validation assessments are essential.

Regulatory guidance for biomaterials and medical product development focuses primarily on safety and efficacy. The US Food and Drug Administration (FDA)

and the Medicines and Healthcare Products Regulatory Agency (MHRA) aims to evaluate the risks associated with the medical entity regarding its proposed use, with biocompatibility being an area within the safety category that must be shown. The biomaterial's intended use correlates directly to the types of tests that need to be performed.

The International Organization for Standards (ISO) have developed specific areas of ISO 10993 which clarifies the necessity to understand 'the potential biological risk arising from the use of medical devices'. The guidelines understand that biological hazards are 'wide and complex' and that adverse interactions caused by certain material may not be a problem when interacting with other materials. Furthermore, it highlights the required biological tests that are required to evaluate the material, where commonly used materials, known as reference materials provide the basis for comparison and benchmarking for novel biomaterials. Additionally, the ability of a biomaterial to be sterilized significantly impacts on the ease with which to create a safe product that can be commercialised. With this research focusing on cell-based therapies, sterile processing environments need to be established to minimise the risk of disease transmission via pathogens to acceptable levels. Therefore, fully characterising biocompatibility and having a simple sterilization procedure, while ensuring performance criteria are met during product development, will ease the regulation process.

The ability of a biomaterial to carry out what it claims to do needs to be demonstrated, hence the correct type of tests need to be chosen to evaluate performance characteristics. Many of the tests that can be used to evaluate biomaterials, including phosphate glasses, have been identified by organizations like the American Society for Testing and Materials (ASTM) and ISO. Further tests to demonstrate efficacy and safety could include animal testing. Having implanted the cell-microcarrier clusters in to the chosen animal model (mouse/rat), appropriate tests should be chosen based on species and specific outcome measures such as local tissue regeneration and reactive immune responses. Testing on areas in an animal that correlate directly to the target area

for treatment in a human is important as the different anatomy and physiology to humans can be challenging.

While good manufacturing practice (GMP) addresses the manufacturing aspect of product development, it is important to consider the cell therapy lifecycle. Therefore, GMP should consider premarketing activities such as design and development, manufacturing, process validation and quality control, whilst also considering post-marketing activities. If the Advanced Therapy Medicinal Product (ATMP) is then granted approval, the product is available on the market and is continuously regulated by the FDA.

References

- ABOU NEEL, E. A., CHRZANOWSKI, W. & KNOWLES, J. C. 2008. Effect of increasing titanium dioxide content on bulk and surface properties of phosphate-based glasses. *Acta Biomater*, 4, 523-34.
- ABOU NEEL, E. A., CHRZANOWSKI, W., VALAPPIL, S. P., O'DELL, L. A., PICKUP, D. M., SMITH, M. E., NEWPORT, R. J. & KNOWLES, J. C. 2009a. Doping of a high calcium oxide metaphosphate glass with titanium dioxide. *Journal of Non-Crystalline Solids*, 355, 991-1000.
- ABOU NEEL, E. A. & KNOWLES, J. C. 2008. Physical and biocompatibility studies of novel titanium dioxide doped phosphate-based glasses for bone tissue engineering applications. *J Mater Sci Mater Med*, 19, 377-86.
- ABOU NEEL, E. A., MIZOGUCHI, T., ITO, M., BITAR, M., SALIH, V. & KNOWLES, J. C. 2007. In vitro bioactivity and gene expression by cells cultured on titanium dioxide doped phosphate-based glasses. *Biomaterials*, 28, 2967-77.
- ABOU NEEL, E. A., PICKUP, D. M., VALAPPIL, S. P., NEWPORT, R. J. & KNOWLES, J. C. 2009b. Bioactive functional materials: a perspective on phosphate-based glasses. *Journal of Materials Chemistry*, 19, 690-701.
- ABRANCHES, E., BEKMAN, E., HENRIQUE, D. & CABRAL, J. M. 2007. Expansion of mouse embryonic stem cells on microcarriers. *Biotechnology and Bioengineering*, 96, 1211-21.
- AHMED, I., LEWIS, M., OLSEN, I. & KNOWLES, J. C. 2004a. Phosphate glasses for tissue engineering: Part 1. Processing and characterisation of a ternary-based P₂O₅-CaO-Na₂O glass system. *Biomaterials*, 25, 491-9.
- AHMED, I., LEWIS, M., OLSEN, I. & KNOWLES, J. C. 2004b. Phosphate glasses for tissue engineering: Part 2. Processing and characterisation of a ternary-based P₂O₅-CaO-Na₂O glass fibre system. *Biomaterials*, 25, 501-7.
- AHMED, I., LEWIS, M. P., NAZHAT, S. N. & KNOWLES, J. C. 2005a. Quantification of anion and cation release from a range of ternary phosphate-based glasses with fixed 45 mol% P₂O₅. *Journal of Biomaterials Applications*, 20, 65-80.
- AHMED, I., LEWIS, M. P., NAZHAT, S. N. & KNOWLES, J. C. 2005b. Quantification of anion and cation release from a range of ternary

phosphate-based glasses with fixed 45 mol% P₂O₅. *J Biomater Appl*, 20, 65-80.

- AHMED, I., PARSONS, A. J., RUDD, C. D., NAZHAT, S. N., KNOWLES, J. C., GUERRY, P. & SMITH, M. E. 2008. Comparison of phosphate-based glasses in the range 50P₂O₅-(50-x)CaO-xNa₂O prepared using different precursors. *Glass Technology: European Journal of Glass Science and Technology Part A*, 49, 63-72.
- ALVAREZ, J. I., ROSS, F. P., ATHANASOU, N. A., BLAIR, H. C., GREENFIELD, E. M. & TEITELBAUM, S. L. 1992. Osteoclast precursors circulate in avian blood. *Calcified Tissue International*, 51, 48-53.
- ANSELME, K. 2000. Osteoblast adhesion on biomaterials. *Biomaterials*, 21, 667-81.
- ARCOS, D. & VALLET-REGÍ, M. 2010. Sol-gel silica-based biomaterials and bone tissue regeneration. *Acta Biomaterialia*, 6, 2874-2888.
- ARINZEH, T. L., TRAN, T., MCALARY, J. & DACULSI, G. 2005. A comparative study of biphasic calcium phosphate ceramics for human mesenchymal stem-cell-induced bone formation. *Biomaterials*, 26, 3631-3638.
- ARVIDSON, K., ABDALLAH, B. M., APPEGATE, L. A., BALDINI, N., CENNI, E., GOMEZ-BARRENA, E., GRANCHI, D., KASSEM, M., KONTTINEN, Y. T., MUSTAFA, K., PIOLETTI, D. P., SILLAT, T. & FINNE-WISTRAND, A. 2011. Bone regeneration and stem cells. *J Cell Mol Med*, 15, 718-46.
- AUBIN, J. E., LIU, F., MALAVAL, L. & GUPTA, A. K. 1995. Osteoblast and chondroblast differentiation. *Bone*, 17, S77-S83.
- AUGST, A., MAROLT, D., FREED, L. E., VEPARI, C., MEINEL, L., FARLEY, M., FAJARDO, R., PATEL, N., GRAY, M., KAPLAN, D. L. & VUNJAK-NOVAKOVIC, G. 2008. Effects of chondrogenic and osteogenic regulatory factors on composite constructs grown using human mesenchymal stem cells, silk scaffolds and bioreactors. *J R Soc Interface*, 5, 929-39.
- BALUYOT, E. S. & HARTFORD, C. G. 1996. Comparison of polyphosphate analysis by ion chromatography and by modified end-group titration. *Journal of Chromatography A*, 739, 217-222.
- BANCROFT, G. N., SIKAVITSAS, V. I., VAN DEN DOLDER, J., SHEFFIELD, T. L., AMBROSE, C. G., JANSEN, J. A. & MIKOS, A. G. 2002. Fluid flow increases mineralized matrix deposition in 3D perfusion culture of marrow

- stromal osteoblasts in a dose-dependent manner. *Proc Natl Acad Sci U S A*, 99, 12600-5.
- BARRERE, F., MAHMOOD, T. A., DE GROOT, K. & VAN BLITTERSWIJK, C. A. 2008. Advanced biomaterials for skeletal tissue regeneration: Instructive and smart functions. *Materials Science & Engineering R-Reports*, 59, 38-71.
- BARRIAS, C. C., RIBEIRO, C. C., LAMGHARI, M., SÁ MIRANDA, C. & BARBOSA, M. A. 2005. Proliferation, activity, and osteogenic differentiation of bone marrow stromal cells cultured on calcium titanium phosphate microspheres. *Journal of Biomedical Materials Research - Part A*, 72, 57-66.
- BENGHUZZI, H., PUCKETT, A., TUCCI, M. & ROBERTS, B. 1999. Bioceramics surface modification by means of osteoclasts in culture. *Biomed Sci Instrum*, 35, 321-6.
- BHUMIRATANA, S. & VUNJAK-NOVAKOVIC, G. 2012. Concise review: personalized human bone grafts for reconstructing head and face. *Stem Cells Transl Med*, 1, 64-9.
- BI, Y., STUELLEN, C. H., KILTS, T., WADHWA, S., IOZZO, R. V., ROBEY, P. G., CHEN, X. D. & YOUNG, M. F. 2005. Extracellular matrix proteoglycans control the fate of bone marrow stromal cells. *J Biol Chem*, 280, 30481-9.
- BIERBAUM, S., HINTZE, V. & SCHARNWEBER, D. 2012. Functionalization of biomaterial surfaces using artificial extracellular matrices. *Biomatter*, 2, 132-141.
- BILODEAU, K. & MANTOVANI, D. 2006. Bioreactors for tissue engineering: focus on mechanical constraints. A comparative review. *Tissue Engineering*, 12, 2367-83.
- BLAIR, H. C., KAHN, A. J., CROUCH, E. C., JEFFREY, J. J. & TEITELBAUM, S. L. 1986. Isolated osteoclasts resorb the organic and inorganic components of bone. *The Journal of Cell Biology*, 102, 1164-1172.
- BLAIR, H. C., TEITELBAUM, S. L., GHISELLI, R. & GLUCK, S. 1989. Osteoclastic bone resorption by a polarized vacuolar proton pump. *Science*, 245, 855-7.

- BOHNER, M., LOOSLI, Y., BAROUD, G. & LACROIX, D. 2011. Commentary: Deciphering the link between architecture and biological response of a bone graft substitute. *Acta Biomater*, 7, 478-84.
- BOONRUNGSIMAN, S., GENTLEMAN, E., CARZANIGA, R., EVANS, N. D., MCCOMB, D. W., PORTER, A. E. & STEVENS, M. M. 2012. The role of intracellular calcium phosphate in osteoblast-mediated bone apatite formation. *Proceedings of the National Academy of Sciences of the United States of America*, 109, 14170-14175.
- BOSE, S., FIELDING, G., TARAFDER, S. & BANDYOPADHYAY, A. 2013. Trace element doping in calcium phosphate ceramics to Understand osteogenesis and angiogenesis. *Trends in biotechnology*, 31, 10.1016/j.tibtech.2013.06.005.
- BOTCHWEY, E. A., POLLACK, S. R., LEVINE, E. M. & LAURENCIN, C. T. 2001. Bone tissue engineering in a rotating bioreactor using a microcarrier matrix system. *J Biomed Mater Res*, 55, 242-53.
- BOYLE, W. J., SIMONET, W. S. & LACEY, D. L. 2003. Osteoclast differentiation and activation. *Nature*, 423, 337-342.
- BRAUER, D. S., RUSSEL, C., LI, W. & HABELITZ, S. 2006. Effect of degradation rates of resorbable phosphate invert glasses on in vitro osteoblast proliferation. *J Biomed Mater Res A*, 77, 213-9.
- BRINDLEY, D., MOORTHY, K., LEE, J.-H., MASON, C., KIM, H.-W. & WALL, I. 2011. Bioprocess Forces and Their Impact on Cell Behavior: Implications for Bone Regeneration Therapy. *Journal of Tissue Engineering*, 2.
- BROW, R. K. 2000. Review: the structure of simple phosphate glasses. *Journal of Non-Crystalline Solids*, 263–264, 1-28.
- BROW, R. K., TALLANT, D. R., WARREN, W., MCINTYRE, A. & DAY, D. 1997. Spectroscopic studies of the structure of titanophosphate and calcium titanophosphate glasses. *Physics and chemistry of glasses*, 38, 300-306.
- BÜCHS, J. 2001. Introduction to advantages and problems of shaken cultures. *Biochemical Engineering Journal*, 7, 91-98.
- BUCHS, J., MAIER, U., MILBRADT, C. & ZOELS, B. 2000. Power consumption in shaking flasks on rotary shaking machines: II. Nondimensional description of specific power consumption and flow regimes in unbaffled flasks at elevated liquid viscosity. *Biotechnol Bioeng*, 68, 594-601.

- BUCKWALTER, J. A., GLIMCHER, M. J., COOPER, R. R. & RECKER, R. 1996a. Bone biology .1. Structure, blood supply, cells, matrix, and mineralization. *Instructional Course Lectures, Vol 45, 1996, 45, 371-386.*
- BUCKWALTER, J. A., GLIMCHER, M. J., COOPER, R. R. & RECKER, R. 1996b. Bone biology .2. Formation, form, modeling, remodeling, and regulation of cell function. *Instructional Course Lectures, Vol 45, 1996, 45, 387-399.*
- BUNE, A. J., HAYMAN, A. R., EVANS, M. J. & COX, T. M. 2001. Mice lacking tartrate-resistant acid phosphatase (Acp 5) have disordered macrophage inflammatory responses and reduced clearance of the pathogen, *Staphylococcus aureus*. *Immunology, 102, 103-13.*
- BUNKER, B. C., ARNOLD, G. W. & WILDER, J. A. 1984. Phosphate glass dissolution in aqueous solutions. *Journal of Non-Crystalline Solids, 64, 291-316.*
- BURNIE, J., GILCHRIST, T., DUFF, S. R., DRAKE, C. F., HARDING, N. G. & MALCOLM, A. J. 1981. Controlled release glasses (C.R.G.) for biomedical uses. *Biomaterials, 2, 244-6.*
- BUTLER, W. T. 1989. The nature and significance of osteopontin. *Connect Tissue Res, 23, 123-36.*
- CHAMBERS, T. J. & FULLER, K. 2011. How are osteoclasts induced to resorb bone? *Annals of the New York Academy of Sciences, 1240, 1-6.*
- CHAO, P. H., GRAYSON, W. & VUNJAK-NOVAKOVIC, G. 2007. Engineering cartilage and bone using human mesenchymal stem cells. *Journal of Orthopaedic Science, 12, 398-404.*
- CHAROONPATRAPONG-PANYAYONG, K., SHAH, R., YANG, J. P., ALVAREZ, M., PAVALKO, F. M., GERARD-O'RILEY, R., ROBLING, A. G., TEMPLETON, E. & BIDWELL, J. P. 2007. Nmp4/CIZ contributes to fluid shear stress induced MMP-13 gene induction in osteoblasts. *Journal of Cellular Biochemistry, 102, 1202-1213.*
- CHELLAPPA, M., ANJANEYULU, U., MANIVASAGAM, G. & VIJAYALAKSHMI, U. 2015. Preparation and evaluation of the cytotoxic nature of TiO₂ nanoparticles by direct contact method. *International Journal of Nanomedicine, 10, 31-41.*
- CHEN, A. K. L., REUVENY, S. & OH, S. K. W. 2013. Application of human mesenchymal and pluripotent stem cell microcarrier cultures in cellular

- therapy: Achievements and future direction. *Biotechnology Advances*, 31, 1032-1046.
- CHERRY, R. S. & PAPOUTSAKIS, E. T. 1988. Physical mechanisms of cell damage in microcarrier cell culture bioreactors. *Biotechnol Bioeng*, 32, 1001-14.
- CHICK, W. L., LIKE, A. A. & LAURIS, V. 1975. Beta Cell-Culture on Synthetic Capillaries - Artificial Endocrine Pancreas. *Science*, 187, 847-849.
- CHRZANOWSKI, W., KONDYURIN, A., LEE, J. H., LORD, M. S., BILEK, M. M. & KIM, H.-W. 2012. Biointerface: protein enhanced stem cells binding to implant surface. *Journal of Materials Science: Materials in Medicine*, 23, 2203-2215.
- CLARKE, B. 2008. Normal bone anatomy and physiology. *Clin J Am Soc Nephrol*, 3 Suppl 3, S131-9.
- CLOVER, J. & GOWEN, M. 1994. Are MG-63 and HOS TE85 human osteosarcoma cell lines representative models of the osteoblastic phenotype? *Bone*, 15, 585-591.
- COOL, S. M. & NURCOMBE, V. 2005. Substrate induction of osteogenesis from marrow-derived mesenchymal precursors. *Stem Cells Dev*, 14, 632-42.
- D.F.WILLIAMS 1999. *The Williams Dictionary of Biomaterials*, Liverpool University Press.
- DALBY, M. J., GADEGAARD, N. & OREFFO, R. O. C. 2014. Harnessing nanotopography and integrin-matrix interactions to influence stem cell fate. *Nat Mater*, 13, 558-569.
- DAVIES, J. E. 1996. In vitro modeling of the bone/implant interface. *The Anatomical Record*, 245, 426-445.
- DECKERS, M. M., VAN BEZOOIJEN, R. L., VAN DER HORST, G., HOOGENDAM, J., VAN DER BENT, C., PAPAPOULOS, S. E. & LOWIK, C. W. 2002. Bone morphogenetic proteins stimulate angiogenesis through osteoblast-derived vascular endothelial growth factor A. *Endocrinology*, 143, 1545-53.
- DEL VALLE, L. J., NAVARRO, M., SEPULCRE, F., GINEBRA, M. P. & PLANELL, J. 2003. Growth and differentiation of osteogenic cells on calcium phosphate glasses. *European biophysics journal with biophysics letters*.

- DEUTSCH, E. R. & GULDBERG, R. E. 2010. Stem cell-synthesized extracellular matrix for bone repair. *Journal of Materials Chemistry*, 20, 8942-8951.
- DIAS, A. G., LOPES, M. A., TRIGO CABRAL, A. T., SANTOS, J. D. & FERNANDES, M. H. 2005. In vitro studies of calcium phosphate glass ceramics with different solubility with the use of human bone marrow cells. *J Biomed Mater Res A*, 74, 347-55.
- DODDABALLAPUR, A., MICHALIK, K. M., MANAVSKI, Y., LUCAS, T., HOUTKOOPE, R. H., YOU, X., CHEN, W., ZEIHNER, A. M., POTENTE, M., DIMMELER, S. & BOON, R. A. 2015. Laminar shear stress inhibits endothelial cell metabolism via KLF2-mediated repression of PFKFB3. *Arterioscler Thromb Vasc Biol*, 35, 137-45.
- DOMINICI, M., LE BLANC, K., MUELLER, I., SLAPER-CORTENBACH, I., MARINI, F., KRAUSE, D., DEANS, R., KEATING, A., PROCKOP, D. & HORWITZ, E. 2006. Minimal criteria for defining multipotent mesenchymal stromal cells. The International Society for Cellular Therapy position statement. *Cytotherapy*, 8, 315-7.
- DONZELLI, E., SALVADE, A., MIMO, P., VIGANO, M., MORRONE, M., PAPAGNA, R., CARINI, F., ZAOPO, A., MILOSO, M., BALDONI, M. & TREDICI, G. 2007. Mesenchymal stem cells cultured on a collagen scaffold: In vitro osteogenic differentiation. *Arch Oral Biol*, 52, 64-73.
- DOS SANTOS, F., CAMPBELL, A., FERNANDES-PLATZGUMMER, A., ANDRADE, P. Z., GIMBLE, J. M., WEN, Y., BOUCHER, S., VEMURI, M. C., DA SILVA, C. L. & CABRAL, J. M. S. 2014. A xenogeneic-free bioreactor system for the clinical-scale expansion of human mesenchymal stem/stromal cells. *Biotechnology and Bioengineering*, 111, 1116-1127.
- DU, Y., LO, E., ALI, S. & KHADEMHOSEINI, A. 2008. Directed assembly of cell-laden microgels for fabrication of 3D tissue constructs. *Proceedings of the National Academy of Sciences of the United States of America*, 105, 9522-9527.
- DUONG, L. T. & RODAN, G. A. 2001. Regulation of Osteoclast Formation and Function*. *Reviews in Endocrine and Metabolic Disorders*, 2, 95-104.
- EFFAH KAUFMANN, E. A., DUCHEYNE, P. & SHAPIRO, I. M. 2000. Evaluation of osteoblast response to porous bioactive glass (45S5) substrates by RT-PCR analysis. *Tissue Eng*, 6, 19-28.

- EIBES, G., DOS SANTOS, F., ANDRADE, P. Z., BOURA, J. S., ABECASIS, M. M., DA SILVA, C. L. & CABRAL, J. M. 2010. Maximizing the ex vivo expansion of human mesenchymal stem cells using a microcarrier-based stirred culture system. *J Biotechnol*, 146, 194-7.
- ELBATAL, H. A., KHALIL, E. M. A. & HAMDY, Y. M. 2009. In vitro behavior of bioactive phosphate glass–ceramics from the system P₂O₅–Na₂O–CaO containing titania. *Ceramics International*, 35, 1195-1204.
- ENGLER, A. J., SEN, S., SWEENEY, H. L. & DISCHER, D. E. 2006. Matrix elasticity directs stem cell lineage specification. *Cell*, 126, 677-89.
- FOK, E. Y. & ZANDSTRA, P. W. 2005. Shear-controlled single-step mouse embryonic stem cell expansion and embryoid body-based differentiation. *Stem Cells*, 23, 1333-42.
- FROHLICH, M., GRAYSON, W. L., MAROLT, D., GIMBLE, J. M., KREGAR-VELIKONJA, N. & VUNJAK-NOVAKOVIC, G. 2010. Bone Grafts Engineered from Human Adipose-Derived Stem Cells in Perfusion Bioreactor Culture. *Tissue Engineering Part A*, 16, 179-189.
- FROUM, S. J., WEINBERG, M. A. & TARNOW, D. 1998. Comparison of bioactive glass synthetic bone graft particles and open debridement in the treatment of human periodontal defects. A clinical study. *J Periodontol*, 69, 698-709.
- FUJIBAYASHI, S., NEO, M., KIM, H. M., KOKUBO, T. & NAKAMURA, T. 2004. Osteoinduction of porous bioactive titanium metal. *Biomaterials*, 25, 443-50.
- GAO, H., TAN, T. & WANG, D. 2004. Dissolution mechanism and release kinetics of phosphate controlled release glasses in aqueous medium. *J Control Release*, 96, 29-36.
- GAYATHRI DEVI, A. V., RAJENDRAN, V. & RAJENDRAN, N. 2010. Structure, solubility and bioactivity in TiO₂-doped phosphate-based bioglasses and glass-ceramics. *Materials Chemistry and Physics*, 124, 312-318.
- GERSTENFELD, L. C., CHO, T. J., KON, T., AIZAWA, T., TSAY, A., FITCH, J., BARNES, G. L., GRAVES, D. T. & EINHORN, T. A. 2003a. Impaired fracture healing in the absence of TNF- α signaling: The role of TNF- α in endochondral cartilage resorption. *Journal of Bone and Mineral Research*, 18, 1584-1592.

- GERSTENFELD, L. C., CULLINANE, D. M., BARNES, G. L., GRAVES, D. T. & EINHORN, T. A. 2003b. Fracture healing as a post-natal developmental process: Molecular, spatial, and temporal aspects of its regulation. *Journal of Cellular Biochemistry*, 88, 873-884.
- GILBERTSON, J. A., SEN, A., BEHIE, L. A. & KALLOS, M. S. 2006. Scaled-up production of mammalian neural precursor cell aggregates in computer-controlled suspension bioreactors. *Biotechnology and Bioengineering*, 94, 783-92.
- GOH, T. K., ZHANG, Z. Y., CHEN, A. K., REUVENY, S., CHOOLANI, M., CHAN, J. K. & OH, S. K. 2013. Microcarrier culture for efficient expansion and osteogenic differentiation of human fetal mesenchymal stem cells. *Biores Open Access*, 2, 84-97.
- GOSAIN, A. K., SONG, L., RIORDAN, P., AMARANTE, M. T., NAGY, P. G., WILSON, C. R., TOTH, J. M. & RICCI, J. L. 2002. A 1-year study of osteoinduction in hydroxyapatite-derived biomaterials in an adult sheep model: part I. *Plastic and Reconstructive Surgery*, 109, 619-30.
- GOUGH, J. E., JONES, J. R. & HENCH, L. L. 2004. Nodule formation and mineralisation of human primary osteoblasts cultured on a porous bioactive glass scaffold. *Biomaterials*, 25, 2039-46.
- GRANÉLI, C., THORFVE, A., RUETSCHI, U., BRISBY, H., THOMSEN, P., LINDAHL, A. & KARLSSON, C. 2014. Novel markers of osteogenic and adipogenic differentiation of human bone marrow stromal cells identified using a quantitative proteomics approach. *Stem Cell Research*, 12, 153-165.
- GRAYSON, W. L., BHUMIRATANA, S., CANNIZZARO, C., CHAO, P. H. G., LENNON, D. P., CAPLAN, A. I. & VUNJAK-NOVAKOVIC, G. 2008. Effects of Initial Seeding Density and Fluid Perfusion Rate on Formation of Tissue-Engineered Bone. *Tissue Engineering Part A*, 14, 1809-1820.
- GRAYSON, W. L., ZHAO, F., BUNNELL, B. & MA, T. 2007. Hypoxia enhances proliferation and tissue formation of human mesenchymal stem cells. *Biochem Biophys Res Commun*, 358, 948-53.
- GRELLIER, M., BAREILLE, R., BOURGET, C. & AMEDEE, J. 2009. Responsiveness of human bone marrow stromal cells to shear stress. *J Tissue Eng Regen Med*, 3, 302-9.

- GUDA, T., WALKER, J. A., SINGLETON, B., HERNANDEZ, J., OH, D. S., APPLEFORD, M. R., ONG, J. L. & WENKE, J. C. 2014. Hydroxyapatite scaffold pore architecture effects in large bone defects in vivo. *J Biomater Appl*, 28, 1016-27.
- GUEDES, J. C., PARK, J. H., LAKHKAR, N. J., KIM, H. W., KNOWLES, J. C. & WALL, I. B. 2012. TiO₂-doped phosphate glass microcarriers: A stable bioactive substrate for expansion of adherent mammalian cells. *J Biomater Appl*.
- HABIBOVIC, P., YUAN, H. P., VAN DEN DOEL, M., SEES, T. M., VAN BLITTERSWIJK, C. A. & DE GROOT, K. 2006. Relevance of osteoinductive biomaterials in critical-sized orthotopic defect. *Journal of Orthopaedic Research*, 24, 867-876.
- HADLEY, K. B., NEWMAN, S. M. & HUNT, J. R. 2010. Dietary zinc reduces osteoclast resorption activities and increases markers of osteoblast differentiation, matrix maturation, and mineralization in the long bones of growing rats. *J Nutr Biochem*, 21, 297-303.
- HARLE, J., KIM, H.-W., MORDAN, N., KNOWLES, J. C. & SALIH, V. 2006. Initial responses of human osteoblasts to sol-gel modified titanium with hydroxyapatite and titania composition. *Acta Biomaterialia*, 2, 547-556.
- HARVESTINE, J. N., VOLLMER, N. L., HO, S. S., ZIKRY, C. A., LEE, M. A. & LEACH, J. K. 2016. Extracellular Matrix-Coated Composite Scaffolds Promote Mesenchymal Stem Cell Persistence and Osteogenesis. *Biomacromolecules*, 17, 3524-3531.
- HAYASHIBARA, T., HIRAGA, T., SUGITA, A., WANG, L., HATA, K., OOSHIMA, T. & YONEDA, T. 2007. Regulation of osteoclast differentiation and function by phosphate: potential role of osteoclasts in the skeletal abnormalities in hypophosphatemic conditions. *J Bone Miner Res*, 22, 1743-51.
- HAYMAN, E. G., PIERSCHBACHER, M. D., SUZUKI, S. & RUOSLAHTI, E. 1985. Vitronectin--a major cell attachment-promoting protein in fetal bovine serum. *Exp Cell Res*, 160, 245-58.
- HEIKKILA, J. T., KUKKONEN, J., AHO, A. J., MOISANDER, S., KYIRONEN, T. & MATTILA, K. 2011. Bioactive glass granules: a suitable bone substitute material in the operative treatment of depressed lateral tibial plateau

- fractures: a prospective, randomized 1 year follow-up study. *J Mater Sci Mater Med*, 22, 1073-80.
- HEINEMANN, C., HEINEMANN, S., WORCH, H. & HANKE, T. 2011. Development of an osteoblast/osteoclast co-culture derived by human bone marrow stromal cells and human monocytes for biomaterials testing. *Eur Cell Mater*, 21, 80-93.
- HENCH, L. L. 1991. Bioceramics: From Concept to Clinic. *Journal of the American Ceramic Society*, 74, 1487-1510.
- HENCH, L. L. 1998. Biomaterials: a forecast for the future. *Biomaterials*, 19, 1419-1423.
- HIDALGO-BASTIDA, L. A. & CARTMELL, S. H. 2010. Mesenchymal stem cells, osteoblasts and extracellular matrix proteins: enhancing cell adhesion and differentiation for bone tissue engineering. *Tissue Eng Part B Rev*, 16, 405-12.
- HILLSLEY, M. V. & FRANGOS, J. A. 1997. Alkaline phosphatase in osteoblasts is down-regulated by pulsatile fluid flow. *Calcif Tissue Int*, 60, 48-53.
- HONG, S. J., YU, H. S. & KIM, H. W. 2009. Tissue engineering polymeric microcarriers with macroporous morphology and bone-bioactive surface. *Macromol Biosci*, 9, 639-45.
- HORST, M., MILLERET, V., NOTZLI, S., MADDURI, S., SULSER, T., GOBET, R. & EBERLI, D. 2014. Increased porosity of electrospun hybrid scaffolds improved bladder tissue regeneration. *J Biomed Mater Res A*, 102, 2116-24.
- HOWARD, G. A., TURNER, R. T., PUZAS, J. E., NICHOLS, F. & BAYLINK, D. J. 1983. Bone cells on microcarrier spheres. *JAMA*, 249, 258-9.
- HUANG, W., YANG, S., SHAO, J. & LI, Y.-P. 2007. Signaling and transcriptional regulation in osteoblast commitment and differentiation. *Frontiers in bioscience : a journal and virtual library*, 12, 3068-3092.
- HUANG, Y., JIA, X., BAI, K., GONG, X. & FAN, Y. 2010. Effect of fluid shear stress on cardiomyogenic differentiation of rat bone marrow mesenchymal stem cells. *Arch Med Res*, 41, 497-505.
- HUDGENS, J. J., BROW, R. K., TALLANT, D. R. & MARTIN, S. W. 1998. Raman spectroscopy study of the structure of lithium and sodium ultraphosphate glasses. *Journal of Non-Crystalline Solids*, 223, 21-31.

- IM, G. I., SHIN, Y. W. & LEE, K. B. 2005. Do adipose tissue-derived mesenchymal stem cells have the same osteogenic and chondrogenic potential as bone marrow-derived cells? *Osteoarthritis Cartilage*, 13, 845-53.
- JANNING, C., WILLBOLD, E., VOGT, C., NELLESEN, J., MEYER-LINDENBERG, A., WINDHAGEN, H., THOREY, F. & WITTE, F. 2010. Magnesium hydroxide temporarily enhancing osteoblast activity and decreasing the osteoclast number in peri-implant bone remodelling. *Acta Biomater*, 6, 1861-8.
- JIANG, G. L., WHITE, C. R., STEVENS, H. Y. & FRANGOS, J. A. 2002. Temporal gradients in shear stimulate osteoblastic proliferation via ERK1/2 and retinoblastoma protein. *Am J Physiol Endocrinol Metab*, 283, E383-9.
- JIN, C.-Y., ZHU, B.-S., WANG, X.-F. & LU, Q.-H. 2008. Cytotoxicity of Titanium Dioxide Nanoparticles in Mouse Fibroblast Cells. *Chemical Research in Toxicology*, 21, 1871-1877.
- JING, D., SUNIL, N., PUNREDDY, S., AYSOLA, M., KEHOE, D., MURREL, J., ROOK, M. & NISS, K. 2013. Growth kinetics of human mesenchymal stem cells in a 3-L single-use, stirred-tank bioreactor. *BioPharm International*, 26, 28-38.
- JOHNSON, D. L., MCALLISTER, T. N. & FRANGOS, J. A. 1996. Fluid flow stimulates rapid and continuous release of nitric oxide in osteoblasts. *Am J Physiol*, 271, E205-8.
- JONES, A. C., ARNS, C. H., HUTMACHER, D. W., MILTHORPE, B. K., SHEPPARD, A. P. & KNACKSTEDT, M. A. 2009. The correlation of pore morphology, interconnectivity and physical properties of 3D ceramic scaffolds with bone ingrowth. *Biomaterials*, 30, 1440-51.
- JONES, J. R. 2013. Review of bioactive glass: from Hench to hybrids. *Acta Biomater*, 9, 4457-86.
- JURDIC, P., SALTEL, F., CHABADEL, A. & DESTAING, O. 2006. Podosome and sealing zone: specificity of the osteoclast model. *Eur J Cell Biol*, 85, 195-202.
- KANG, M., BOLDBAATAR, K., LEE, E.-J., PEREZ, R. A. & KIM, H.-W. 2014. Enhanced bone regeneration on the fusion protein tethered scaffolds. *Frontiers in Bioengineering and Biotechnology*.

- KAPUR, S., BAYLINK, D. J. & LAU, K. H. 2003. Fluid flow shear stress stimulates human osteoblast proliferation and differentiation through multiple interacting and competing signal transduction pathways. *Bone*, 32, 241-51.
- KASPER, G., GLAESER, J. D., GEISLER, S., ODE, A., TUISCHER, J., MATZIOLIS, G., PERKA, C. & DUDA, G. N. 2007. Matrix metalloprotease activity is an essential link between mechanical stimulus and mesenchymal stem cell behavior. *Stem Cells*, 25, 1985-1994.
- KASUGA, T., SAWADA, M., NOGAMI, M. & ABE, Y. 1999. Bioactive ceramics prepared by sintering and crystallization of calcium phosphate invert glasses. *Biomaterials*, 20, 1415-20.
- KELM, J. M., DJONOV, V., ITTNER, L. M., FLURI, D., BORN, W., HOERSTRUP, S. P. & FUSSENEGGER, M. 2006. Design of custom-shaped vascularized tissues using microtissue spheroids as minimal building units. *Tissue Engineering*, 12, 2151-2160.
- KHOR, S. F., TALIB, Z. A., DAUD, W. M. & SIDEK, H. A. A. 2011. Degradation study on ternary zinc magnesium phosphate glasses. *Journal of Materials Science*, 46, 7895.
- KIANI, A., LAKHKAR, N. J., SALIH, V., SMITH, M. E., HANNA, J. V., NEWPORT, R. J., PICKUP, D. M. & KNOWLES, J. C. 2012. Titanium-containing bioactive phosphate glasses. *Philos Trans A Math Phys Eng Sci*, 370, 1352-75.
- KING, J. A. & MILLER, W. M. 2007. Bioreactor development for stem cell expansion and controlled differentiation. *Curr Opin Chem Biol*, 11, 394-8.
- KLEIN-NULEND, J., SEMEINS, C. M. & BURGER, E. H. 1996. Prostaglandin mediated modulation of transforming growth factor-beta metabolism in primary mouse osteoblastic cells in vitro. *J Cell Physiol*, 168, 1-7.
- KLEIN-NULEND, J., VAN DER PLAS, A., SEMEINS, C. M., AJUBI, N. E., FRANGOS, J. A., NIJWEIDE, P. J. & BURGER, E. H. 1995. Sensitivity of osteocytes to biomechanical stress in vitro. *Faseb Journal*, 9, 441-5.
- KLEINHANS, C., SCHMID, F. F., SCHMID, F. V. & KLUGER, P. J. 2015. Comparison of osteoclastogenesis and resorption activity of human osteoclasts on tissue culture polystyrene and on natural extracellular bone matrix in 2D and 3D. *J Biotechnol*, 205, 101-10.

- KNOWLES, J. C. 2003. Phosphate based glasses for biomedical applications. *Journal of Materials Chemistry*, 13, 2395-2401.
- KOKUBO, T., KIM, H.-M., KAWASHITA, M. & NAKAMURA, T. 2004. REVIEW Bioactive metals: preparation and properties. *Journal of Materials Science: Materials in Medicine*, 15, 99-107.
- KOKUBO, T. & TAKADAMA, H. 2006. How useful is SBF in predicting in vivo bone bioactivity? *Biomaterials*, 27, 2907-2915.
- KÖLLMER, M., BUHRMAN, J. S., ZHANG, Y. & GEMEINHART, R. A. 2013. Markers Are Shared Between Adipogenic and Osteogenic Differentiated Mesenchymal Stem Cells. *Journal of developmental biology and tissue engineering*, 5, 18-25.
- KREIDL, N. J. & WEYL, W. A. 1941. PHOSPHATES IN CERAMIC WARE: IV, PHOSPHATE GLASSES*. *Journal of the American Ceramic Society*, 24, 372-378.
- KREKE, M. R. & GOLDSTEIN, A. S. 2004. Hydrodynamic shear stimulates osteocalcin expression but not proliferation of bone marrow stromal cells. *Tissue Eng*, 10, 780-8.
- KREKE, M. R., HUCKLE, W. R. & GOLDSTEIN, A. S. 2005. Fluid flow stimulates expression of osteopontin and bone sialoprotein by bone marrow stromal cells in a temporally dependent manner. *Bone*, 36, 1047-55.
- KRUYT, M. C., DHERT, W. J. A., YUAN, H. P., WILSON, C. E., VAN BLITTERSWIJK, C. A., VERBOUT, A. J. & DE BRUIJN, J. D. 2004. Bone tissue engineering in a critical size defect compared to ectopic implantations in the goat. *Journal of Orthopaedic Research*, 22, 544-551.
- KUCERA, T., URBAN, K. & RAGKOU, S. 2012. Healing of cavitary bone defects. *European Journal of Orthopaedic Surgery & Traumatology*, 22, 123-128.
- LACEY, D. L., TIMMS, E., TAN, H. L., KELLEY, M. J., DUNSTAN, C. R., BURGESS, T., ELLIOTT, R., COLOMBERO, A., ELLIOTT, G., SCULLY, S., HSU, H., SULLIVAN, J., HAWKINS, N., DAVY, E., CAPPARELLI, C., ELI, A., QIAN, Y. X., KAUFMAN, S., SAROSI, I., SHALHOUB, V., SENALDI, G., GUO, J., DELANEY, J. & BOYLE, W. J. 1998. Osteoprotegerin ligand is a cytokine that regulates osteoclast differentiation and activation. *Cell*, 93, 165-76.

- LAHANN, J., BALCELLS, M., LU, H., RODON, T., JENSEN, K. F. & LANGER, R. 2003. Reactive polymer coatings: a first step toward surface engineering of microfluidic devices. *Anal Chem*, 75, 2117-22.
- LAKHKAR, N. J., M DAY, R., KIM, H.-W., LUDKA, K., MORDAN, N. J., SALIH, V. & KNOWLES, J. C. 2015a. Titanium phosphate glass microcarriers induce enhanced osteogenic cell proliferation and human mesenchymal stem cell protein expression. *Journal of Tissue Engineering*, 6, 2041731415617741.
- LAKHKAR, N. J., PARK, J.-H., MORDAN, N. J., SALIH, V., WALL, I. B., KIM, H.-W., KING, S. P., HANNA, J. V., MARTIN, R. A., ADDISON, O., MOSSELMANS, J. F. W. & KNOWLES, J. C. 2012a. Titanium phosphate glass microspheres for bone tissue engineering. *Acta Biomaterialia*, 8, 4181-4190.
- LAKHKAR, N. J., PARK, J. H., MORDAN, N. J., SALIH, V., WALL, I. B., KIM, H. W., KING, S. P., HANNA, J. V., MARTIN, R. A., ADDISON, O., MOSSELMANS, J. F. & KNOWLES, J. C. 2012b. Titanium phosphate glass microspheres for bone tissue engineering. *Acta Biomater*, 8, 4181-90.
- LAKHKAR, N. J., PETICONE, C., DE SILVA-THOMPSON, D., WALL, I. B., SALIH, V. & KNOWLES, J. C. 2015b. CHAPTER 5 Titanium Phosphate Glass Microspheres as Microcarriers for In Vitro Bone Cell Tissue Engineering. *Biointerfaces: Where Material Meets Biology*. The Royal Society of Chemistry.
- LANGER, R. & VACANTI, J. P. 1993. Tissue Engineering. *Science*, 260, 920-926.
- LAVENUS, S., BERREUR, M., TRICHET, V., PILET, P., LOUARN, G. & LAYROLLE, P. 2011. Adhesion and osteogenic differentiation of human mesenchymal stem cells on titanium nanopores. *Eur Cell Mater*, 22, 84-96; discussion 96.
- LAVENUS, S., RICQUIER, J. C., LOUARN, G. & LAYROLLE, P. 2010. Cell interaction with nanopatterned surface of implants. *Nanomedicine (Lond)*, 5, 937-47.
- LEE, J. H., PARK, J.-H., YUN, Y.-R., JANG, J.-H., LEE, E.-J., CHRZANOWSKI, W., WALL, I. B. & KIM, H.-W. 2013. Tethering bi-functional protein onto

- mineralized polymer scaffolds to regulate mesenchymal stem cell behaviors for bone regeneration. *Journal of Materials Chemistry B*, 1, 2731-2741.
- LEE, K. Y., PARK, M., KIM, H. M., LIM, Y. J., CHUN, H. J., KIM, H. & MOON, S. H. 2006. Ceramic bioactivity: progresses, challenges and perspectives. *Biomed Mater*, 1, R31-7.
- LEEUWENBURGH, S., LAYROLLE, P., BARRERE, F., DE BRUIJN, J., SCHOONMAN, J., VAN BLITTERSWIJK, C. A. & DE GROOT, K. 2001. Osteoclastic resorption of biomimetic calcium phosphate coatings in vitro. *J Biomed Mater Res*, 56, 208-15.
- LI, Y. J., BATRA, N. N., YOU, L. D., MEIER, S. C., COE, I. A., YELLOWLEY, C. E. & JACOBS, C. R. 2004. Oscillatory fluid flow affects human marrow stromal cell proliferation and differentiation. *Journal of Orthopaedic Research*, 22, 1283-1289.
- LIAN, J. B. & STEIN, G. S. 1992. Concepts of Osteoblast Growth and Differentiation - Basis for Modulation of Bone Cell-Development and Tissue Formation. *Critical Reviews in Oral Biology & Medicine*, 3, 269-305.
- LIM, K. T., HEXIU, J., KIM, J., SEONWOO, H., CHOUNG, P.-H. & CHUNG, J. H. 2014. Synergistic Effects of Orbital Shear Stress on In Vitro Growth and Osteogenic Differentiation of Human Alveolar Bone-Derived Mesenchymal Stem Cells. *BioMed Research International*, 2014, 18.
- LIN, T. M., TSAI, J. L., LIN, S. D., LAI, C. S. & CHANG, C. C. 2005. Accelerated growth and prolonged lifespan of adipose tissue-derived human mesenchymal stem cells in a medium using reduced calcium and antioxidants. *Stem Cells Dev*, 14, 92-102.
- LIU, Y. K., LU, Q. Z., PEI, R., JI, H. J., ZHOU, G. S., ZHAO, X. L., TANG, R. K. & ZHANG, M. 2009. The effect of extracellular calcium and inorganic phosphate on the growth and osteogenic differentiation of mesenchymal stem cells in vitro: implication for bone tissue engineering. *Biomed Mater*, 4, 025004.
- LJUNGGREN, J. & HAGGSTROM, L. 1994. Catabolic control of hybridoma cells by glucose and glutamine limited fed batch cultures. *Biotechnol Bioeng*, 44, 808-18.

- LUCACEL, R. C., MAIER, M. & SIMON, V. 2010. Structural and in vitro characterization of TiO₂-CaO-P₂O₅ bioglasses. *Journal of Non-Crystalline Solids*, 356, 2869-2874.
- MAGAN, A. & RIPAMONTI, U. 1996. Geometry of porous hydroxyapatite implants influences osteogenesis in baboons (*Papio ursinus*). *J Craniofac Surg*, 7, 71-8.
- MAJD, H., QUINN, T. M., WIPFF, P. J. & HINZ, B. 2011. Dynamic expansion culture for mesenchymal stem cells. *Methods Mol Biol*, 698, 175-88.
- MALDA, J. & FRONDOZA, C. G. 2006. Microcarriers in the engineering of cartilage and bone. *Trends Biotechnol*, 24, 299-304.
- MARASINGHE, G., KARABULUT, M. & RAY, C. The Structure of Iron Phosphate Glasses: A Novel Medium for the Disposal of High Level Nuclear Waste. APS March Meeting Abstracts, 1997.
- MARIE, P. J. 2005. Strontium ranelate: a novel mode of action optimizing bone formation and resorption. *Osteoporosis International*, 16, S7-S10.
- MAROLT, D., KNEZEVIC, M. & NOVAKOVIC, G. V. 2010. Bone tissue engineering with human stem cells. *Stem Cell Research & Therapy*, 1.
- MARTIN, Y., ELDARDIRI, M., LAWRENCE-WATT, D. J. & SHARPE, J. R. 2011. Microcarriers and their potential in tissue regeneration. *Tissue Engineering - Part B: Reviews*, 17, 71-80.
- MARTIN, Y. & VERMETTE, P. 2005. Bioreactors for tissue mass culture: Design, characterization, and recent advances. *Biomaterials*, 26, 7481-7503.
- MATTILA, P. K. & LAPPALAINEN, P. 2008. Filopodia: molecular architecture and cellular functions. *Nat Rev Mol Cell Biol*, 9, 446-454.
- MCBEATH, R., PIRONE, D. M., NELSON, C. M., BHADRIRAJU, K. & CHEN, C. S. 2004. Cell shape, cytoskeletal tension, and RhoA regulate stem cell lineage commitment. *Dev Cell*, 6, 483-95.
- MCCULLEN, S. D., ZHAN, J., ONORATO, M. L., BERNACKI, S. H. & LOBOA, E. G. 2010. Effect of varied ionic calcium on human adipose-derived stem cell mineralization. *Tissue Eng Part A*, 16, 1971-81.
- MOHSENY, A. B., MACHADO, I., CAI, Y., SCHAEFER, K.-L., SERRA, M., HOGENDOORN, P. C. W., LLOMBART-BOSCH, A. & CLETON-JANSEN, A.-M. 2011. Functional characterization of osteosarcoma cell lines

provides representative models to study the human disease. *Lab Invest*, 91, 1195-1205.

MONCHAU, F., LEFEVRE, A., DESCAMPS, M., BELQUIN-MYRDYCZ, A., LAFFARGUE, P. & HILDEBRAND, H. F. 2002. In vitro studies of human and rat osteoclast activity on hydroxyapatite, beta-tricalcium phosphate, calcium carbonate. *Biomol Eng*, 19, 143-52.

MONEM, A. S., ELBATAL, H. A., KHALIL, E. M., AZOOZ, M. A. & HAMDY, Y. M. 2008. In vivo behavior of bioactive phosphate glass-ceramics from the system P₂O₅-Na₂O-CaO containing TiO₂. *J Mater Sci Mater Med*, 19, 1097-108.

MORONI, L. & VAN BLITTERSWIJK, C. A. 2006. Biomaterials: converge and regenerate. *Nat Mater*, 5, 437-8.

MOTT, J. D. & WERB, Z. 2004. Regulation of matrix biology by matrix metalloproteinases. *Current Opinion in Cell Biology*, 16, 558-564.

MOURSI, A. M., GLOBUS, R. K. & DAMSKY, C. H. 1997. Interactions between integrin receptors and fibronectin are required for calvarial osteoblast differentiation in vitro. *J Cell Sci*, 110 (Pt 18), 2187-96.

NAKAMURA, S., MATSUMOTO, T., SASAKI, J., EGUSA, H., LEE, K. Y., NAKANO, T., SOHMURA, T. & NAKAHIRA, A. 2010. Effect of calcium ion concentrations on osteogenic differentiation and hematopoietic stem cell niche-related protein expression in osteoblasts. *Tissue Eng Part A*, 16, 2467-73.

NAKAYAMA, T., MIZOGUCHI, T., UEHARA, S., YAMASHITA, T., KAWAHARA, I., KOBAYASHI, Y., MORIYAMA, Y., KURIHARA, S., SAHARA, N., OZAWA, H., UDAGAWA, N. & TAKAHASHI, N. 2011. Polarized osteoclasts put marks of tartrate-resistant acid phosphatase on dentin slices — A simple method for identifying polarized osteoclasts. *Bone*, 49, 1331-1339.

NAUMAN, E. A., SATCHER, R. L., KEAVENY, T. M., HALLORAN, B. P. & BIKLE, D. D. 2001. Osteoblasts respond to pulsatile fluid flow with short-term increases in PGE(2) but no change in mineralization. *J Appl Physiol* (1985), 90, 1849-54.

NAVARRO, M., GINEBRA, M.-P., CLÉMENT, J., SALVADOR, M., GLORIA, A. & PLANELL, J. A. 2003. Physicochemical Degradation of Titania-Stabilized

- Soluble Phosphate Glasses for Medical Applications. *Journal of the American Ceramic Society*, 86, 1345-1352.
- NIENOW, A. W., RAFIQ, Q. A., COOPMAN, K. & HEWITT, C. J. 2014. A potentially scalable method for the harvesting of hMSCs from microcarriers. *Biochemical Engineering Journal*, 85, 79-88.
- NOH, Y. K., DU, P., KIM, I. G., KO, J., KIM, S. W. & PARK, K. 2016. Polymer mesh scaffold combined with cell-derived ECM for osteogenesis of human mesenchymal stem cells. *Biomaterials Research*, 20, 6.
- O'BRIEN, F. J. 2011. Biomaterials & scaffolds for tissue engineering. *Materials Today*, 14, 88-95.
- OH, S. K. W., CHEN, A. K., MOK, Y., CHEN, X., LIM, U. M., CHIN, A., CHOO, A. B. H. & REUVENY, S. 2009. Long-term microcarrier suspension cultures of human embryonic stem cells. *Stem Cell Research*, 2, 219-230.
- OLIVEIRA, P. H., DA SILVA, C. L. & CABRAL, J. M. 2014. Concise review: Genomic instability in human stem cells: current status and future challenges. *Stem Cells*, 32, 2824-32.
- OLMOS, E., LOUBIERE, K., MARTIN, C., DELAPLACE, G. & MARC, A. 2015. Critical agitation for microcarrier suspension in orbital shaken bioreactors: Experimental study and dimensional analysis. *Chemical Engineering Science*, 122, 545-554.
- ONTIVEROS, C. & MCCABE, L. R. 2003. Simulated microgravity suppresses osteoblast phenotype, Runx2 levels and AP-1 transactivation. *J Cell Biochem*, 88, 427-37.
- ORRISS, I. R. & ARNETT, T. R. 2012. Rodent osteoclast cultures. *Methods Mol Biol*, 816, 103-17.
- OSTROWSKI, N., LEE, B., HONG, D., ENICK, P. N., ROY, A. & KUMTA, P. N. 2015. Synthesis, Osteoblast, and Osteoclast Viability of Amorphous and Crystalline Tri-Magnesium Phosphate. *ACS Biomaterials Science & Engineering*, 1, 52-63.
- OVERSTREET, M., SOHRABI, A., POLOTSKY, A., HUNGERFORD, D. S. & FRONDOZA, C. G. 2003. Collagen microcarrier spinner culture promotes osteoblast proliferation and synthesis of matrix proteins. *In Vitro Cell Dev Biol Anim*, 39, 228-34.

- PANOSKALTSIS, N., MANTALARIS, A. & WU, J. H. 2005. Engineering a mimicry of bone marrow tissue ex vivo. *J Biosci Bioeng*, 100, 28-35.
- PAPOUTSAKIS, E. T. 1991. Fluid-mechanical damage of animal cells in bioreactors. *Trends Biotechnol*, 9, 427-37.
- PARK, J. H., PEREZ, R. A., JIN, G. Z., CHOI, S. J., KIM, H. W. & WALL, I. B. 2013. Microcarriers Designed for Cell Culture and Tissue Engineering of Bone. *Tissue Eng Part B Rev*.
- PARMAR, N., AHMADI, R. & DAY, R. M. 2015. A Novel Method for Differentiation of Human Mesenchymal Stem Cells into Smooth Muscle-Like Cells on Clinically Deliverable Thermally Induced Phase Separation Microspheres. *Tissue Engineering. Part C, Methods*, 21, 404-412.
- PARRINGTON, J. & TUNN, R. 2014. Ca(2+) signals, NAADP and two-pore channels: role in cellular differentiation. *Acta Physiol (Oxf)*, 211, 285-96.
- PELTOLA, M., AITASALO, K., SUONPAA, J., VARPULA, M. & YLI-URPO, A. 2006. Bioactive glass S53P4 in frontal sinus obliteration: a long-term clinical experience. *Head Neck*, 28, 834-41.
- PENOLAZZI, L., MAZZITELLI, S., VECCHIATINI, R., TORREGGIANI, E., LAMBERTINI, E., JOHNSON, S., BADYLAK, S. F., PIVA, R. & NASTRUZZI, C. 2012. Human mesenchymal stem cells seeded on extracellular matrix-scaffold: viability and osteogenic potential. *J Cell Physiol*, 227, 857-66.
- PÉREZ, R. A., WON, J.-E., KNOWLES, J. C. & KIM, H.-W. 2013. Naturally and synthetic smart composite biomaterials for tissue regeneration. *Advanced Drug Delivery Reviews*, 65, 471-496.
- PERNA, K., KOSKI, I., MATTILA, K., GULLICHSEN, E., HEIKKILA, J., AHO, A. & LINDFORS, N. 2011. Bioactive glass S53P4 and autograft bone in treatment of depressed tibial plateau fractures - a prospective randomized 11-year follow-up. *J Long Term Eff Med Implants*, 21, 139-48.
- PHILLIPS, A. M. 2005. Overview of the fracture healing cascade. *Injury*, 36, S5-S7.
- PICKUP, D. M., AHMED, I., GUERRY, P., KNOWLES, J. C., SMITH, M. E. & NEWPORT, R. J. 2007. The structure of phosphate glass biomaterials from neutron diffraction and ³¹P nuclear magnetic resonance data. *Journal of Physics: Condensed Matter*, 19, 415116.

- PIERALISI, I., RODRIGUEZ, G., MICHELETTI, M., PAGLIANTI, A. & DUCCI, A. 2016. Microcarriers' suspension and flow dynamics in orbitally shaken bioreactors. *Chemical Engineering Research and Design*, 108, 198-209.
- PINERO, G. J., FARACH-CARSON, M. C., DEVOLL, R. E., AUBIN, J. E., BRUNN, J. C. & BUTLER, W. T. 1995. Bone matrix proteins in osteogenesis and remodelling in the neonatal rat mandible as studied by immunolocalization of osteopontin, bone sialoprotein, α 2HS-glycoprotein and alkaline phosphatase. *Archives of Oral Biology*, 40, 145-155.
- PITTENGER, M. F., MACKAY, A. M., BECK, S. C., JAISWAL, R. K., DOUGLAS, R., MOSCA, J. D., MOORMAN, M. A., SIMONETTI, D. W., CRAIG, S. & MARSHAK, D. R. 1999. Multilineage potential of adult human mesenchymal stem cells. *Science*, 284, 143-147.
- POLO-CORRALES, L., LATORRE-ESTEVEZ, M. & RAMIREZ-VICK, J. E. 2014. Scaffold Design for Bone Regeneration. *Journal of nanoscience and nanotechnology*, 14, 15-56.
- POSER, L., MATTHYS, R., SCHAWALDER, P., PEARCE, S., ALINI, M. & ZEITER, S. 2014. A Standardized Critical Size Defect Model in Normal and Osteoporotic Rats to Evaluate Bone Tissue Engineered Constructs. *BioMed Research International*, 2014, 5.
- QIU, Q. Q., DUCHEYNE, P. & AYYASWAMY, P. S. 1999. Fabrication, characterization and evaluation of bioceramic hollow microspheres used as microcarriers for 3-D bone tissue formation in rotating bioreactors. *Biomaterials*, 20, 989-1001.
- QUINN, J. M., NEALE, S., FUJIKAWA, Y., MCGEE, J. O. & ATHANASOU, N. A. 1998. Human osteoclast formation from blood monocytes, peritoneal macrophages, and bone marrow cells. *Calcif Tissue Int*, 62, 527-31.
- RAFIQ, Q. A., BROSANAN, K. M., COOPMAN, K., NIENOW, A. W. & HEWITT, C. J. 2013. Culture of human mesenchymal stem cells on microcarriers in a 5 l stirred-tank bioreactor. *Biotechnology Letters*, 35, 1233-1245.
- REICH, K. M., GAY, C. V. & FRANGOS, J. A. 1990. Fluid shear stress as a mediator of osteoblast cyclic adenosine monophosphate production. *J Cell Physiol*, 143, 100-4.

- RICHARDSON, J. F., HARKER, J. H. & BACKHURST, J. R. 2002a. CHAPTER 4 - Flow of Fluids through Granular Beds and Packed Columns. *Chemical Engineering (Fifth Edition)*. Oxford: Butterworth-Heinemann.
- RICHARDSON, J. F., HARKER, J. H. & BACKHURST, J. R. 2002b. CHAPTER 6 - Fluidisation. *Chemical Engineering (Fifth Edition)*. Oxford: Butterworth-Heinemann.
- RIEMAN, D. J., MCCLUNG, H. A., DODDS, R. A., HWANG, S. M., HOLMES, M. W., JAMES, I. E., DRAKE, F. H. & GOWEN, M. 2001. Biosynthesis and processing of cathepsin K in cultured human osteoclasts. *Bone*, 28, 282-9.
- RODRIGUES, C. A., FERNANDES, T. G., DIOGO, M. M., DA SILVA, C. L. & CABRAL, J. M. 2011. Stem cell cultivation in bioreactors. *Biotechnol Adv*, 29, 815-29.
- ROY, M. & BOSE, S. 2012. Osteoclastogenesis and osteoclastic resorption of tricalcium phosphate: Effect of strontium and magnesium doping. *Journal of Biomedical Materials Research Part A*, 100A, 2450-2461.
- RUBIN, J., RUBIN, C. & JACOBS, C. R. 2006. Molecular pathways mediating mechanical signaling in bone. *Gene*, 367, 1-16.
- RUNNING, J. A. & BANSAL, K. 2016. Oxygen transfer rates in shaken culture vessels from Fernbach flasks to microtiter plates. *Biotechnology and Bioengineering*, 113, 1729-1735.
- RUST, K. R., SINGLETON, G. T., WILSON, J. & ANTONELLI, P. J. 1996. Bioglass middle ear prosthesis: long-term results. *Am J Otol*, 17, 371-4.
- SALASZNYK, R. M., WILLIAMS, W. A., BOSKEY, A., BATORSKY, A. & PLOPPER, G. E. 2004. Adhesion to Vitronectin and Collagen I Promotes Osteogenic Differentiation of Human Mesenchymal Stem Cells. *J Biomed Biotechnol*, 2004, 24-34.
- SALTEL, F., DESTAING, O., BARD, F., EICHERT, D. & JURDIC, P. 2004. Apatite-mediated actin dynamics in resorbing osteoclasts. *Molecular Biology of the Cell*, 15, 5231-5241.
- SARGENT, C. Y., BERGUIG, G. Y., KINNEY, M. A., HIATT, L. A., CARPENEDO, R. L., BERSON, R. E. & MCDEVITT, T. C. 2010. Hydrodynamic modulation of embryonic stem cell differentiation by rotary orbital suspension culture. *Biotechnol Bioeng*, 105, 611-26.

- SAUTIER, J. M., NEFUSSI, J. R. & FOREST, N. 1992. Mineralization and bone formation on microcarrier beads with isolated rat calvaria cell population. *Calcif Tissue Int*, 50, 527-32.
- SCHEPERS, E. J. & DUCHEYNE, P. 1997. Bioactive glass particles of narrow size range for the treatment of oral bone defects: a 1-24 month experiment with several materials and particle sizes and size ranges. *J Oral Rehabil*, 24, 171-81.
- SCHILLING, A. F., LINHART, W., FILKE, S., GEBAUER, M., SCHINKE, T., RUEGER, J. M. & AMLING, M. 2004. Resorbability of bone substitute biomaterials by human osteoclasts. *Biomaterials*, 25, 3963-72.
- SCHMITZ, J. P. & HOLLINGER, J. O. 1986. The Critical Size Defect as an Experimental-Model for Craniomandibulofacial Nonunions. *Clin Orthop Relat Res*, 299-308.
- SCHNEIDER, R. K., PUELLEN, A., KRAMANN, R., RAUPACH, K., BORNEMANN, J., KNUECHEL, R., PEREZ-BOUZA, A. & NEUSS, S. 2010. The osteogenic differentiation of adult bone marrow and perinatal umbilical mesenchymal stem cells and matrix remodelling in three-dimensional collagen scaffolds. *Biomaterials*, 31, 467-80.
- SCHOP, D., JANSSEN, F. W., BORGART, E., DE BRUIJN, J. D. & VAN DIJKHUIZEN-RADERSMA, R. 2008. Expansion of mesenchymal stem cells using a microcarrier-based cultivation system: growth and metabolism. *Journal of Tissue Engineering and Regenerative Medicine*, 2, 126-135.
- SCHOP, D., JANSSEN, F. W., VAN RIJN, L. D., FERNANDES, H., BLOEM, R. M., DE BRUIJN, J. D. & VAN DIJKHUIZEN-RADERSMA, R. 2009. Growth, metabolism, and growth inhibitors of mesenchymal stem cells. *Tissue Eng Part A*, 15, 1877-86.
- SCHWAB, E. H., HALBIG, M., GLENSKE, K., WAGNER, A. S., WENISCH, S. & CAVALCANTI-ADAM, E. A. 2013. Distinct effects of RGD-glycoproteins on Integrin-mediated adhesion and osteogenic differentiation of human mesenchymal stem cells. *Int J Med Sci*, 10, 1846-59.
- SHARP, L. A., LEE, Y. W. & GOLDSTEIN, A. S. 2009. Effect of low-frequency pulsatile flow on expression of osteoblastic genes by bone marrow stromal cells. *Ann Biomed Eng*, 37, 445-53.

- SHIN, S.-H., PUREVDORJ, O., CASTANO, O., PLANELL, J. A. & KIM, H.-W. 2012. A short review: Recent advances in electrospinning for bone tissue regeneration. *Journal of Tissue Engineering*, 3, 2041731412443530.
- SHIRAI, Y., YOSHIMURA, Y., YAWAKA, Y., HASEGAWA, T., KIKUIRI, T., TAKEYAMA, S., MATSUMOTO, A. & OGUCHI, H. 1999. Effect of Extracellular Calcium Concentrations on Osteoclast Differentiation in Vitro. *Biochemical and Biophysical Research Communications*, 265, 484-488.
- SIDDIQUEE, K. & SHA, M. 2013. Microcarrier-Based Expansion of Adipose-Derived Mesenchymal Stem Cells in Shake Flasks. *Bioprocessing Journal* 12, 32-8.
- SIKAVITSAS, V. I., BANCROFT, G. N. & MIKOS, A. G. 2002. Formation of three-dimensional cell/polymer constructs for bone tissue engineering in a spinner flask and a rotating wall vessel bioreactor. *Journal of Biomedical Materials Research*, 62, 136-148.
- SIKAVITSAS, V. I., TEMENOFF, J. S. & MIKOS, A. G. 2001. Biomaterials and bone mechanotransduction. *Biomaterials*, 22, 2581-2593.
- SIKAVITSAS, V. I., VAN DEN DOLDER, J., BANCROFT, G. N., JANSEN, J. A. & MIKOS, A. G. 2003. Influence of the in vitro culture period on the in vivo performance of cell/titanium bone tissue-engineered constructs using a rat cranial critical size defect model. *Journal of Biomedical Materials Research Part A*, 67A, 944-951.
- SILVER, I. A., MURRILLS, R. J. & ETHERINGTON, D. J. 1988. Microelectrode studies on the acid microenvironment beneath adherent macrophages and osteoclasts. *Exp Cell Res*, 175, 266-76.
- SITTICHOCKECHAIWUT, A., SCUTT, A. M., RYAN, A. J., BONEWALD, L. F. & REILLY, G. C. 2009. Use of rapidly mineralising osteoblasts and short periods of mechanical loading to accelerate matrix maturation in 3D scaffolds. *Bone*, 44, 822-829.
- STANLEY, H. R., HALL, M. B., CLARK, A. E., KING, C. J., 3RD, HENCH, L. L. & BERTE, J. J. 1997. Using 45S5 bioglass cones as endosseous ridge maintenance implants to prevent alveolar ridge resorption: a 5-year evaluation. *Int J Oral Maxillofac Implants*, 12, 95-105.
- STROBER, W. 2001. Trypan blue exclusion test of cell viability. *Curr Protoc Immunol*, Appendix 3, Appendix 3B.

- TAKEYAMA, S., YOSHIMURA, Y., DEYAMA, Y., SUGAWARA, Y., FUKUDA, H. & MATSUMOTO, A. 2001. Phosphate Decreases Osteoclastogenesis in Coculture of Osteoblast and Bone Marrow. *Biochemical and Biophysical Research Communications*, 282, 798-802.
- TANG, J. S., CHAO, C. F. & AU, M. K. 1994. Growth and metabolism of cultured bone cells using microcarrier and monolayer techniques. *Clin Orthop Relat Res*, 254-8.
- TAT, S. K., PELLETIER, J. P., MINEAU, F., CARON, J. & MARTEL-PELLETIER, J. 2011. Strontium ranelate inhibits key factors affecting bone remodeling in human osteoarthritic subchondral bone osteoblasts. *Bone*, 49, 559-67.
- TAVASSOLI, M. 1986. Medical Problems of Space-Flight. *American Journal of Medicine*, 81, 850-854.
- TAYLOR, J. C., CUFF, S. E., LEGER, J. P., MORRA, A. & ANDERSON, G. I. 2002. In vitro osteoclast resorption of bone substitute biomaterials used for implant site augmentation: a pilot study. *Int J Oral Maxillofac Implants*, 17, 321-30.
- TEITELBAUM, S. L. 2007. Osteoclasts: What do they do and how do they do it? *American Journal of Pathology*, 170, 427-435.
- TEITELBAUM, S. L. & ROSS, F. P. 2003. Genetic regulation of osteoclast development and function. *Nat Rev Genet*, 4, 638-649.
- TEITELBAUM, S. L., TONDRAVI, M. M. & ROSS, F. P. 1997. Osteoclasts, macrophages, and the molecular mechanisms of bone resorption. *Journal of Leukocyte Biology*, 61, 381-388.
- TENENBAUM, H. C. & HEERSCHKE, J. N. M. 1982. Differentiation of osteoblasts and formation of mineralized bone in vitro. *Calcified Tissue International*, 34, 76-79.
- THOMAS, J. M., CHAKRABORTY, A., SHARP, M. K. & BERSON, R. E. 2011. Spatial and temporal resolution of shear in an orbiting petri dish. *Biotechnol Prog*, 27, 460-5.
- TISSOT, S., FARHAT, M., HACKER, D. L., ANDERLEI, T., KÜHNER, M., COMNINELLIS, C. & WURM, F. 2010. Determination of a scale-up factor from mixing time studies in orbitally shaken bioreactors. *Biochemical Engineering Journal*, 52, 181-186.

- TROUNCE, I., SCHMIEDEL, J., YEN, H. C., HOSSEINI, S., BROWN, M. D., OLSON, J. J. & WALLACE, D. C. 2000. Cloning of neuronal mtDNA variants in cultured cells by synaptosome fusion with mtDNA-less cells. *Nucleic Acids Research*, 28, 2164-2170.
- TRUONG, Y. B., GLATTAUER, V., BRIGGS, K. L., ZAPPE, S. & RAMSHAW, J. A. M. 2012. Collagen-based layer-by-layer coating on electrospun polymer scaffolds. *Biomaterials*, 33, 9198-9204.
- TSIRIDIS, E., UPADHYAY, N. & GIANNOUDIS, P. 2007. Molecular aspects of fracture healing: which are the important molecules? *Injury*, 38 Suppl 1, S11-25.
- TURUNEN, T., PELTOLA, J., YLI-URPO, A. & HAPPONEN, R. P. 2004. Bioactive glass granules as a bone adjunctive material in maxillary sinus floor augmentation. *Clin Oral Implants Res*, 15, 135-41.
- VAANANEN, H. K. & HARKONEN, P. L. 1996. Estrogen and bone metabolism. *Maturitas*, 23 Suppl, S65-9.
- VAANANEN, H. K., ZHAO, H., MULARI, M. & HALLEEN, J. M. 2000. The cell biology of osteoclast function. *J Cell Sci*, 113 (Pt 3), 377-81.
- VAN DER STOK, J., VAN LIESHOUT, E. M., EL-MASSOUDI, Y., VAN KRALINGEN, G. H. & PATKA, P. 2011. Bone substitutes in the Netherlands - a systematic literature review. *Acta Biomater*, 7, 739-50.
- VELASCO, V., GRUENTHAL, M., ZUSSTONE, E., THOMAS, J. M. D., BERSON, R. E., KEYNTON, R. S. & WILLIAMS, S. J. 2016. An orbital shear platform for real-time, in vitro endothelium characterization. *Biotechnology and Bioengineering*, 113, 1336-1344.
- VISSE, R. & NAGASE, H. 2003. Matrix Metalloproteinases and Tissue Inhibitors of Metalloproteinases. *Structure, Function, and Biochemistry*, 92, 827-839.
- VITALE-BROVARONE, C., NOVAJRA, G., MILANESE, D., LOUSTEAU, J. & KNOWLES, J. C. 2011. Novel phosphate glasses with different amounts of TiO₂ for biomedical applications Dissolution tests and proof of concept of fibre drawing. *Materials Science & Engineering C-Materials for Biological Applications*, 31, 434-442.
- VOLKMER, E., DROSSE, I., OTTO, S., STANGELMAYER, A., STENGELE, M., KALLUKALAM, B. C., MUTSCHLER, W. & SCHIEKER, M. 2008. Hypoxia

- in static and dynamic 3D culture systems for tissue engineering of bone. *Tissue Engineering Part A*, 14, 1331-1340.
- WAGNER, W., BORK, S., LEPPERDINGER, G., JOUSSEN, S., MA, N., STRUNK, D. & KOCH, C. 2010. How to track cellular aging of mesenchymal stromal cells? *Aging*, 2, 224-230.
- WALL, I., DONOS, N., CARLQVIST, K., JONES, F. & BRETT, P. 2009. Modified titanium surfaces promote accelerated osteogenic differentiation of mesenchymal stromal cells in vitro. *Bone*, 45, 17-26.
- WANG, T. W., WU, H. C., WANG, H. Y., LIN, F. H. & SUN, J. S. 2009. Regulation of adult human mesenchymal stem cells into osteogenic and chondrogenic lineages by different bioreactor systems. *Journal of Biomedical Materials Research Part A*, 88, 935-46.
- WEHELIYE, W., YIANNESKIS, M. & DUCCI, A. 2013. On the fluid dynamics of shaken bioreactors-flow characterization and transition. *AIChE Journal*, 59, 334-344.
- WEI, X., YANG, X., HAN, Z.-P., QU, F.-F., SHAO, L. & SHI, Y.-F. 2013. Mesenchymal stem cells: a new trend for cell therapy. *Acta Pharmacol Sin*, 34, 747-754.
- WEINER, S. & WAGNER, H. D. 1998. The material bone: Structure mechanical function relations. *Annual Review of Materials Science*, 28, 271-298.
- WILSON, S. R., PETERS, C., SAFTIG, P. & BRÖMME, D. 2009. Cathepsin K Activity-dependent Regulation of Osteoclast Actin Ring Formation and Bone Resorption. *The Journal of Biological Chemistry*, 284, 2584-2592.
- WINTER, G. D. & SIMPSON, B. T. 1969. Heterotopic Bone Formed in a Synthetic Sponge in Skin of Young Pigs. *Nature*, 223, 88-&.
- WITTRANT, Y., GORIN, Y., WOODRUFF, K., HORN, D., ABBOUD, H. E., MOHAN, S. & ABBOUD-WERNER, S. L. 2008. High D(+)glucose concentration inhibits RANKL-induced osteoclastogenesis. *Bone*, 42, 1122-1130.
- XIA, L., KILB, J., WEX, H., LI, Z., LIPYANSKY, A., BREUIL, V., STEIN, L., PALMER, J. T., DEMPSTER, D. W. & BRÖMME, D. 1999. Localization of Rat Cathepsin K in Osteoclasts and Resorption Pits: Inhibition of Bone Resorption and Cathepsin K-Activity by Peptidyl Vinyl Sulfones. *Biological Chemistry*.

- XYNOS, I. D., EDGAR, A. J., BUTTERY, L. D. K., HENCH, L. L. & POLAK, J. M. 2001. Gene-expression profiling of human osteoblasts following treatment with the ionic products of Bioglass® 45S5 dissolution. *Journal of Biomedical Materials Research*, 55, 151-157.
- YAMAGUCHI, M. & WEITZMANN, M. N. 2011. Zinc stimulates osteoblastogenesis and suppresses osteoclastogenesis by antagonizing NF-kappaB activation. *Mol Cell Biochem*, 355, 179-86.
- YATES, A. J., OREFFO, R. O. C., MAYOR, K. & MUNDY, G. R. 1991. Inhibition of bone resorption by inorganic phosphate is mediated by both reduced osteoclast formation and decreased activity of mature osteoclasts. *Journal of Bone and Mineral Research*, 6, 473-478.
- YEATTS, A. B. & FISHER, J. P. 2011. Bone tissue engineering bioreactors: dynamic culture and the influence of shear stress. *Bone*, 48, 171-81.
- YEATTS, A. B., GEIBEL, E. M., FEARS, F. F. & FISHER, J. P. 2012. Human mesenchymal stem cell position within scaffolds influences cell fate during dynamic culture. *Biotechnology and Bioengineering*, 109, 2381-91.
- YOU, J., REILLY, G. C., ZHEN, X., YELLOWLEY, C. E., CHEN, Q., DONAHUE, H. J. & JACOBS, C. R. 2001. Osteopontin gene regulation by oscillatory fluid flow via intracellular calcium mobilization and activation of mitogen-activated protein kinase in MC3T3-E1 osteoblasts. *J Biol Chem*, 276, 13365-71.
- YOUREK, G., MCCORMICK, S. M., MAO, J. J. & REILLY, G. C. 2010. Shear stress induces osteogenic differentiation of human mesenchymal stem cells. *Regenerative medicine*, 5, 713-724.
- ZAYZAFOON, M., GATHINGS, W. E. & MCDONALD, J. M. 2004. Modeled microgravity inhibits osteogenic differentiation of human mesenchymal stem cells and increases adipogenesis. *Endocrinology*, 145, 2421-32.
- ZHANG, H., LAMPING, S. R., PICKERING, S. C. R., LYE, G. J. & SHAMLOU, P. A. 2008. Engineering characterisation of a single well from 24-well and 96-well microtitre plates. *Biochemical Engineering Journal*, 40, 138-149.
- ZHANG, H., WILLIAMS-DALSON, W., KESHAVARZ-MOORE, E. & SHAMLOU, P. A. 2005. Computational-fluid-dynamics (CFD) analysis of mixing and gas-liquid mass transfer in shake flasks. *Biotechnology and Applied Biochemistry*, 41, 1-8.

- ZHANG, X., BÜRKI, C.-A., STETTLER, M., DE SANCTIS, D., PERRONE, M., DISCACCIATI, M., PAROLINI, N., DEJESUS, M., HACKER, D. L., QUARTERONI, A. & WURM, F. M. 2009. Efficient oxygen transfer by surface aeration in shaken cylindrical containers for mammalian cell cultivation at volumetric scales up to 1000 L. *Biochemical Engineering Journal*, 45, 41-47.
- ZHANG, Y. & SANTOS, J. D. 2001. Microstructural characterization and in vitro apatite formation in CaO–P₂O₅–TiO₂–MgO–Na₂O glass-ceramics. *Journal of the European Ceramic Society*, 21, 169-175.
- ZHENG, Q., DU, J., XIA, Z., ZENG, H., LI, S., YAN, Y. & CHEN, F. 1998. Biodegradation of tricalcium phosphate ceramics by osteoclasts. *J Tongji Med Univ*, 18, 257-61.
- ZOHAR, R., CHEIFETZ, S., MCCULLOCH, C. A. G. & SODEK, J. 1998. Analysis of intracellular osteopontin as a marker of osteoblastic cell differentiation and mesenchymal cell migration. *European Journal of Oral Sciences*, 106, 401-407.

Appendix

A.1 Geometrical characteristics and calculated Fr_c and N_c (using minimum and maximum operating conditions) using 96-well microplates.

Variable		Value	Unit
Well Inner Diameter	d_i	6.4×10^{-3}	m
Orbital Diameter	d_o	1×10^{-2}	m
Liquid Volume (min)	V_{min}	1.5×10^{-7}	m^3
Liquid Volume (max)	V_{max}	1.6×10^{-7}	m^3
Critical Froude Number (min)	Fr_{cmin}	0.65	
Critical Froude Number (max)	Fr_{cmax}	0.70	
Critical Speed (min)	N_{cmin}	340	min^{-1}
Critical Speed (max)	N_{cmax}	350	min^{-1}

A.2 Geometrical characteristics and calculated Fr_c and N_c (using minimum and maximum operating conditions) using an 125ml Erlenmeyer flask.

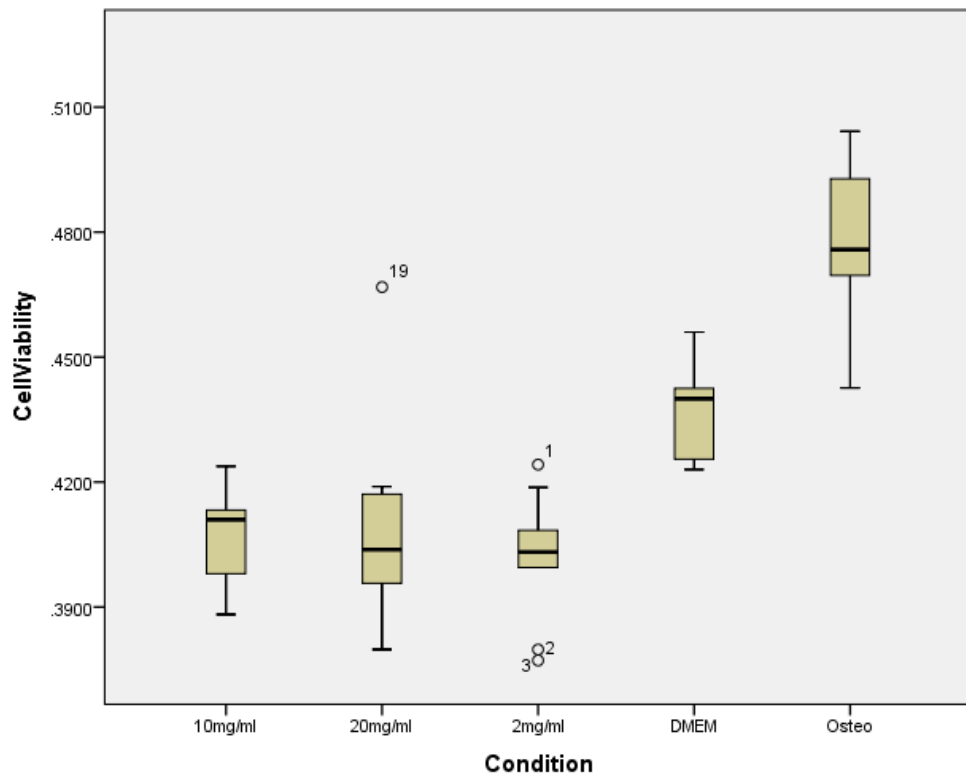
Variable		Value	Unit
Flask Inner Diameter	d_i	6.6×10^{-2}	m
Orbital Diameter	d_o	1.0×10^{-2}	m
Non-Dimensional Fluid Height	h_L/d_i	0.51	
Orbital to Flask Diameter Ratio	d_o/d	0.15	
Flask Maximum Working Volume	V_L	8×10^{-5}	m^3
Relative Density	ρ^*	2.6	
Particle to Vessel Diameter Ratio	d_p/d	1.29×10^{-3}	
Suspension Froude	Fr_s	0.58	
Suspension speed	N_s	320	min^{-1}

A.3 Geometrical/Physical characteristics and calculated Ga and flowrate to achieve Ti-PGM suspension

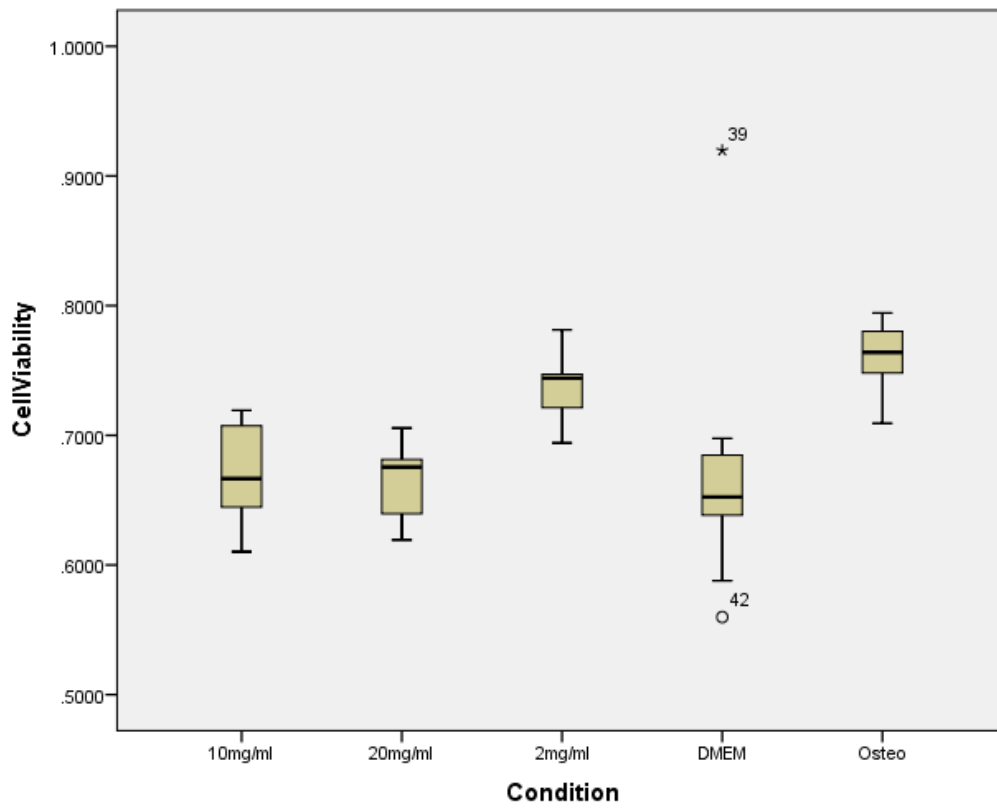
Variable		Value	Unit
Particle Diameter	d_i	6.6×10^{-2}	m
Relative Density	ρ^*	2.6	
Voidage corresponding to Minimum Fluidising Velocity	e_{mf}	0.4	
Galileo Number	Ga	12.06	
Reynolds Number at the Minimum Fluidising Velocity	Re_{mf}	0.02×10^{-2}	
Volumetric Flowrate at the Minimum Fluidising Velocity	Q_{mf}	7×10^{-8}	m^3/s

A.4 Box-and-whisker plots required for bar charts presented in Chapter 3

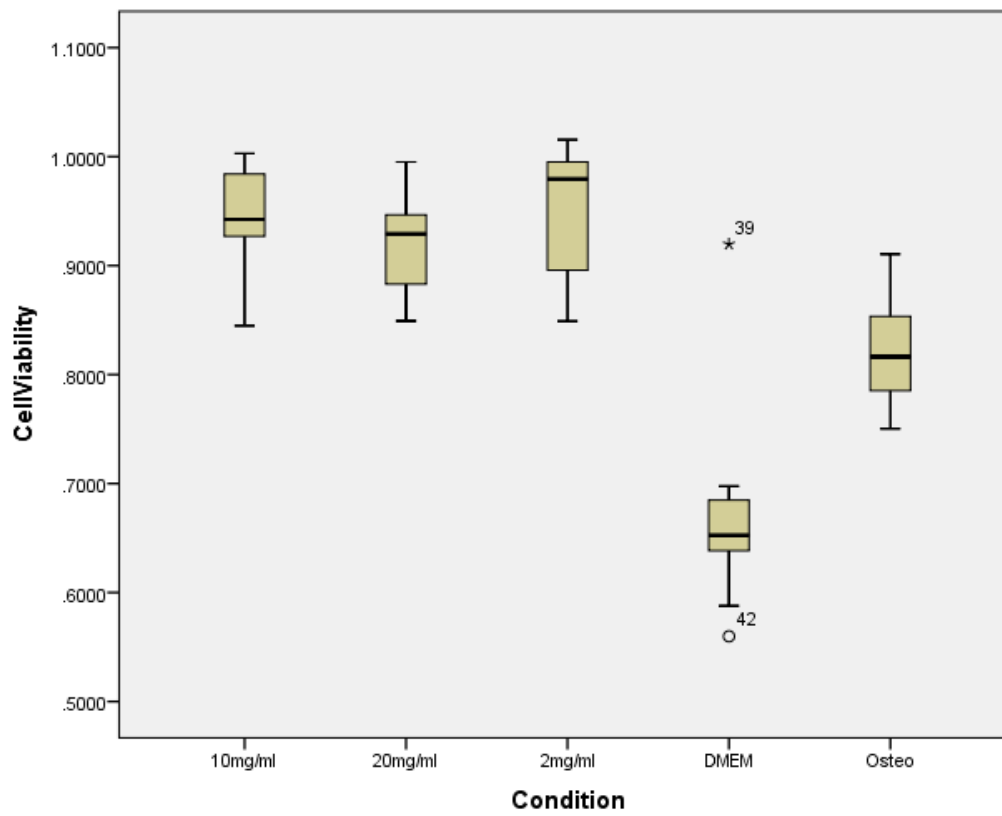
(a)



(b)



(c)



(d)

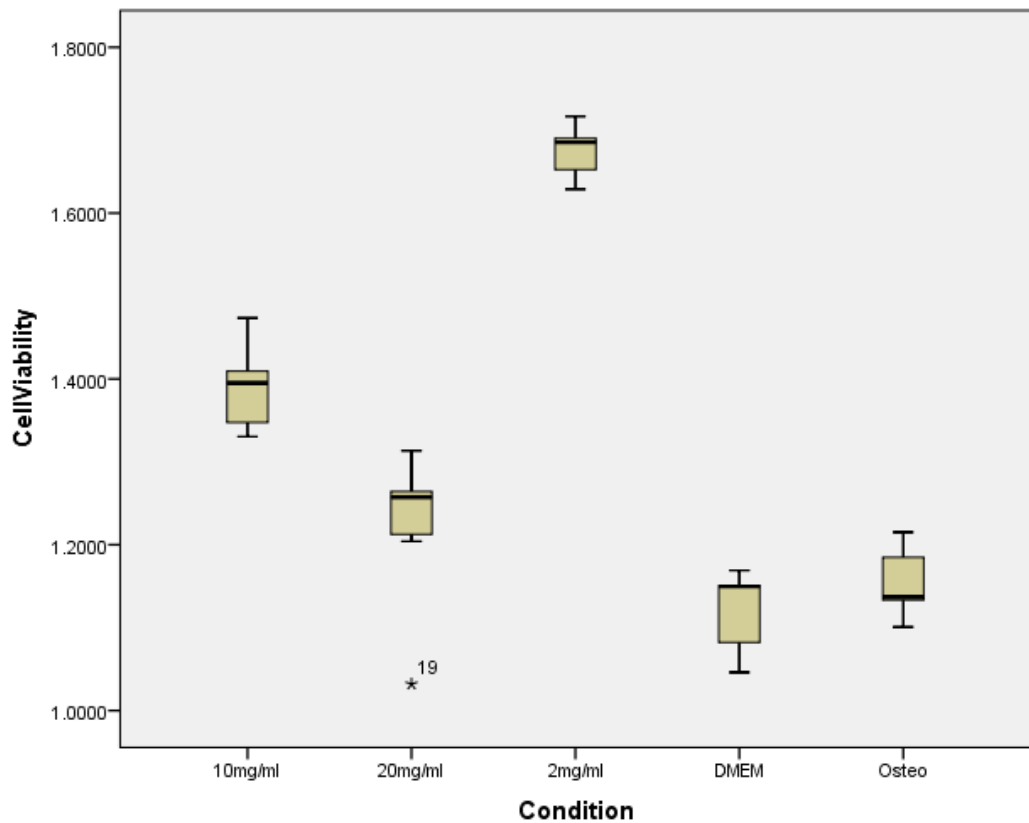


Figure A.1. Box-and-whisker plots representing the results of a CCK-8 assay to quantify hBM-MSC proliferation, cultured in different types of conditioned media (Ti-conditioned media (2 mg/ml,10mg/ml and 20mg/ml), DMEM and osteogenic media in Nunclon™ flat bottomed tissue culture 96-well microplates on days a) 1, b) 3 c) 5 and 7. Note that circles indicate outliers (values more than the interquartile range) while asterisks indicate extreme outliers (values more than three times the interquartile range).

A.5 List of conferences

1. **Tissue Engineering and Regenerative Medicine International Society Asia-Pacific Annual Conference (TERMIS-AP) Daegu, Korea.**
September 24-27, 2014.
Scalable Production of Tissue Engineered Microunits for Bone Regeneration Using Bioactive Glass Microspheres and Dynamic Culture Conditions (Oral Presentation)
2. **Scale-up and Manufacturing of Cell-based Therapies V, Engineering Conference International (ECI). San Diego, USA.**
January 18-22, 2015.
Scalable Production of Tissue Engineered Microunits for Bone Regeneration Using Bioactive Glass Microspheres and Dynamic Culture Conditions (Poster presentation)
3. **Tissue and Cell Engineering Society Annual Conference (TCES)**
July 4-6 2016
Scalable Production of Tissue Engineered Microunits for Bone Regeneration Using Bioactive Glass Microspheres and Dynamic Culture Conditions (Poster presentation)

A.6 List of publications

1. Lakhkar NJ, Peticone C, **De Silva-Thompson D**, Wall IB, Salih V, Knowles JC (2014) Titanium phosphate glass microspheres as microcarriers for *in vitro* bone cell tissue engineering. In *Biointerfaces: Where Material Meets Biology*. RSC Publishing
2. Peticone C, **De Silva-Thompson D**, Owens G, Hae-Won Kim, Micheletti M, Knowles J, Wall I (2017) Towards modular bone tissue engineering using Ti–Co-doped phosphate glass microspheres: cytocompatibility and dynamic culture studies. *Journal of Biomaterials Applications* Vol 32, Issue 3, pp. 295 – 310
3. Wall, I., **De Silva-Thompson, D.**, Peticone, C. and Perez, R. (2016) Industrial translation requirements for manufacture of stem cell–derived and tissue-engineered products. *Tissue Engineering and Regeneration in Dentistry: Current Strategies* John Wiley & Sons